Dissertation

Towards restoring the protein degradation pathway(s) in Hutchinson-Gilford progeria syndrome (HGPS)

Diana Gabriel

Fakultät für Medizin
Lehrstuhl Epigenetik der Hautalterung

Towards restoring the protein degradation pathway(s) in Hutchinson-Gilford progeria syndrome (HGPS)

Diana Gabriel

Vollständiger Abdruck der von der Fakultät für Medizin der Technischen Universität München zur Erlangung des akademischen Grades eines Doktors der Naturwissenschaften (Dr. rer. nat.) genehmigten Dissertation.

Vorsitzende(r): Prof. Dr. Carsten Schmidt-Weber

Prüfer der Dissertation:

1. Prof. Dr. Karima Djabali
2. Prof. Dr. Bernhard Küster
3. Prof. Dr. Angelika Noegel

Die Dissertation wurde am 27.06.2016 bei der Technischen Universität München eingereicht und durch die Fakultät für Medizin am 17.05.2017 angenommen.

Publication list

Sections of this thesis can be found in the following publications:

1. Gabriel, D., Roedl, D., Gordon, L. B. & Djabali, K. Sulforaphane enhances progerin clearance in Hutchinson-Gilford progeria fibroblasts. *Aging Cell* **14**, 78-91, doi:10.1111/acel.12300 (2015).

→ used mainly (but not exclusively) in Section 4.1, 4.2, 5.1, 5.2

2. Gabriel, D., Gordon, L. B. & Djabali, K. Temsirolimus Partially Rescues the Hutchinson-Gilford Progeria Cellular Phenotype. *PLoS One* **11**, e0168988, doi:10.1371/journal.pone.0168988 (2016).

→ used mainly (but not exclusively) in Section 4.6, 5.6

3. Gabriel, D., Shafry, D. D., Gordon, L. B. & Djabali, K. Intermittent treatment with farnesyltransferase inhibitor and sulforaphane improves cellular homeostasis in Hutchinson-Gilford progeria fibroblasts. *Oncotarget* **8**, 64809-64826, doi:10.18632/oncotarget.19363 (2017).

→ used mainly (but not exclusively) in Section 4.3, 5.3

Acknowledgement

I did it! This exciting journey reaches its end. I really enjoyed my research, had ups and downs and learned a lot. I finally succeeded, which would never have happened without the help, support, guidance, and friendship of many different people. It is time to say how much I appreciated all these people, their work, and actions.

First of all, I would like to thank my supervisor Prof. Karima Djabali. Thank you for giving me the opportunity to join your lab and for guiding me through all the years of hard work. I appreciate your vast knowledge and skills in many areas, as well as your assistance in writing reports, papers, and grants. Without your expertise I wouldn't have learned so much. Your maddening attention to detail drove me to finally learn to prioritize and focus on what is important. Even small changes can make a huge difference between a good and a bad therapeutic. In the end you taught me how to think and criticize my own work, and simply to do good research. I will never forget our first trip to Luxembourg! Thanks for everything!

Special thanks to my second advisor Prof. Bernhard Küster for being a member of my committee, for your advice, and suggestions.

Many thanks to Prof. WenChieh Chen for being my mentor and your encouraging way of thinking about my research.

Thanks to the Progeria Research Foundation who financially supported my research and the amazing scientific meetings that broadened my knowledge about progeria.

Further, I want to thank the members of my group.
Veronika, when we first met we knew immediately that we have the same lose screw in our head. We helped each other to understand logical (and not so logical) results of our experiments or how we could improve them to make them more logical ;) We became very close and spent not only time during the work together but also met in our free time. We supported each other in many ways and I am going to miss our crazy discussions and road trips. Thank you for your friendship, believe, and trust!
Leithe and LuXiang, thanks for also spending time on the weekend in the lab. It helped me a lot not to feel lonesome :) Thanks for all the discussions which broadened my knowledge in many ways.
Many thanks also to Daniela Rödl who initiated my whole thesis. Without her I wouldn't have started my thesis in this lab. Thanks for your support during the whole years we spent together and these were quite some (8 years!!!). That you are no longer there is a huge loss! I will always remember you as the funny and positive person you were!
I also would like to thank the "not-so-close-member" of the group Christian. Our evenings in a pub or at the Christkindl market were always cheerful and boozy. I am going to miss our Kicker death matches in the evening.

This thesis would not have been possible without the support of my family. My parents were always there for me when I needed them. They believed in me and made me feel well. My brother and sisters helped me a lot by just being on the phone and listening. Your advices couldn't have been more different though. ;) You all just have been there for me and you would have come immediately if I would have said something. Any thanks would not be enough.

Last but not least, to Marcel, thank you for being there for me and supporting me. I guess it wasn't easy to handle my different moods during the thesis. By just letting me talk about everything you helped me to keep going even though we sometimes had different opinions. You made me feel strong, clever, and accepted me as the person I am. Thanks for always being there for me!

Table of Contents

List of Abbreviations

%	Percentage
(p)4EBP1	(Phosphorylated) eukaryotic initiation factor 4E-binding protein 1
(p)S6RP	(Phosphorylated) S6 ribosomal protein
*p	Significance value
°C	Celsius
µl	Micro liter
µM	Micro molar
53BP1	Tumor protein p53 binding protein 1
A	Ampere
AMC	7-Amino-4-methylcoumarin
AMPK	Adenosine monophosphate-activated protein kinase
ATM	Ataxia telangiectasia mutated
ATP	Adenosine triphosphate
Bag 1/2/3	BAG family molecular chaperone regulator 1/2/3
bp	Base pair
BrU	5-Bromouracil
BSA	Bovine serum albumin
CAAX	C= cysteine, A= aliphatic amino acid, X= variable
cAMP	Cyclic adenosine monophosphate
CDK	Cyclin dependent kinase
CHAPS	3-[(3-Cholamidopropyl)-dimethylammonio]-1-propane sulfonate
C.I.	Confidence interval
CMT2B1	Charcot-Marie-Tooth type
CPD	Cumulative population doubling
Cq	Chloroquine
DCF(DA)	2', 7' –dichlorofluorescin (diacetate)
DCM	Dilated Cardiomyopathy
DDX1	ATP-dependent RNA helicase
DMSO	Dimethyl sulfoxide
DTT	Dithiothreitol
E1	Ubiquitin-activating enzyme
E2	Ubiquitin-conjugating enzyme
E3	Ubiquitin ligase
EDMD	Emery-Dreifuss muscular dystrophy
FBS	Fetal bovine serum
FHL1	Four and a half LIM-domain
Fors	Forskolin
FPLD	Familial partial lipodystrophy
FTI	Farnesyl transferase inhibitor

HCl	Hydrochloric acid
HEPES	2-[4-(2-hydroxyethyl)piperazin-1-yl]ethanesulfonic acid
HGPS	Hutchinson-Gilford Progeria Syndrome
HP 1	Heterochromatin 1
HRP	Horseradish peroxidase
Hsp	Heat shock protein
ICMT	Protein-S-isoprenylcysteine O-methyltransferase
IEF	Isoelectric focusing
IGF1R	Insulin-like growth factor
IPG	Immobilized pH gradient
ITC	Isothiocyanate
KCl	Potassium chloride
Keap1	Kelch-Like ECH-Associated Protein 1
KOH	Potassium hydroxide
LAP2α	Lamina-associated polypeptide 2α
LC3B-I/II	Light chain 3 protein B I/II
LGMD-1B	Limb-girdle muscular dystrophy 1B
LMNA	Lamin A gene
M	Molar
mA	Milliampere
MAD	Mandibuloacral disease
MALDI	Matrix-assisted laser desorption/ionization
MDC	Monodansylcadaverine
MEF	Mouse embryonic fibroblast
mg	Milligram
MG132	Carbobenzoxy-L-leucyl-L-leucyl-L-leucinal
$MgCl_2$	Magnesium chloride
ml	Milliliter
mM	Millimolar
mRNA	Messenger ribonucleic acid
MS	Mass spectra
mTOR	Mammalian target of rapamycin
mTORC1	mTOR complex 1
MW	Molecular weight
NCBInr	National Center for Biotechnology Information non-redundant
NEF	Nuclear envelope transmembrane
nm	Nanometer
Nrf2	Nuclear factor erythroid 2–related factor 2
Nup414	Nuclear pore protein 414
PAGE	Polyacrylamide gel electrophoresis
PBS	Phosphate buffered saline

PCR	Polymerase chain reaction
PGC1α	Peroxisome proliferator-activated receptor gamma coactivator 1-alpha
PKA	Protein kinase A
PPD	Population doubling
PSMC2	26S protease regulatory subunit 7
PVDF	polyvinylidene fluoride
ROS	Reactive oxygen species
S.D.	Standard deviation
S/F	SFN/Forskolin
S/T	SFN/Temsirolimus
S+F	SFN+FTI
S6K1	S6 kinase 1
SDS	Sodium dodecyl sulfate
SFN	Sulforaphane
Sirt1	Sirtuin 1
Suc	Sucrose
SUN	Sad1 and UNC84 Domain Containing
TBS	Tris buffered saline
Tem	Temsirolimus
T_m	Melting temperature
TOF	Time of flight
UPS	Ubiquitin-proteasome system
V, Vhr	Volt, Volt/Hour
WB	Western blot
ZMPESTE24	Zinc metalloproteinase Ste 24

Table 1: Abbreviation of the Amino acids used in this thesis.

Amino acid	**3-Letter**	**1-Letter**
Cysteine	Cys	C
Isoleucine	Ile	I
Methionine	Met	M
Serine	Ser	S

List of Figures

List of Tables

Abstract

The Hutchinson-Gilford progeria syndrome (HGPS, OMIM 176670) is a rare premature aging disorder associated with hair loss, stunted growth, and weight loss in childhood.[1] Myocardial infarction or stroke lead to an early death of 14.7 years.[1] In 90 % of cases, HGPS is linked to a mutation in exon 11 of the lamin A gene (GGC>GGT, G608G). This generates a novel cleavage site resulting in a 50 amino acid deletion at the carboxy-terminal tail of prelamin A.[2] The deletion removes the ZMPSTE24 cleavage site from the lamin A processing pathway, resulting in a persistent farnesylation of the protein, which is called progerin.[3,4] Consequently, progerin is tightly anchored to the nuclear envelope, causing nuclear blebbing, heterochromatin disorganization, and DNA double-strand break (DSB) accumulation.[1,5,6] Attempts to reverse the HGPS cellular phenotype have identified farnesyltransferase inhibitors (FTI), statins or isoprenylcysteine carboxyl methyl-transferase (ICMT) inhibitors. By inhibiting the farnesyl attachment to progerin, FTIs reversed some of the phenotypic changes in HGPS cells.[7-10] Three clinical trials with HGPS children have used the drugs mentioned above.[1] FTI successfully improved vascular stiffness, bone structure, and the audiological status of the children.[11] However, FTI showed inevitable side effects *in vitro* e.g. donut-shaped nuclei, lamin B disruption, prelamin A accumulation, and no improvements of DNA damage and cell growth.[12-14]

In this study, proteomic analysis by 2D-gelelectrophoresis identified a mechanistic link underlying progerin accumulation in the HGPS nucleome, which was interconnected to the protein degradation pathways, autophagy and proteasome. Based on this, compounds that can boost progerin degradation will ameliorate the HGPS cellular phenotype. One of them is sulforaphane (SFN), which induces autophagy, proteasome activity, and antioxidant response by activating Nrf2-Keap1 signaling pathway.[15-18] SFN improved proteostasis and mitochondrial function, as well as reducing progerin and DNA damage levels of HGPS cells. Furthermore, autophagy and proteasome activity can be activated via different upstream signaling pathways, which could have an impact on restoring the HGPS cellular phenotype. For this, forskolin has been tested to modulate Sirt1, AMPK, and cAMP signaling pathways to induce autophagy, mitochondrial biogenesis, and proteasome activity, respectively.[19-29] Forskolin reversed all tested HGPS hallmarks including DNA damage, mitochondrial dysfunction, and progerin accumulation. Forskolin showed similar positive effects as SFN even though these compounds act on different signaling pathways. Both SFN and

forskolin could be considered as candidate drugs for future therapeutics for HGPS children and other age-related disorders.

A phase I clinical trial with FTI in combination with the rapamycin analog (rapalog) everolimus has been initiated in 2016. However, studies regarding the efficacy and side effects of such a combination are absent. Therefore, it has been tested whether future therapies involving drug combinations further ameliorate the HGPS cellular phenotype. Within this project, FTI has been used to block the farnesylation process and SFN to activate the Nrf2-Keap1 signaling pathway. The identification of a novel treatment regimen with FTI and SFN showed the highest clearance of progerin, abolished the negative side effects of FTI, and ameliorated mitochondrial function and DNA damage in HGPS fibroblasts. This novel regimen could be highly considered for HGPS treatment.

Rapamycin activates autophagy through the specific inhibition of the mTOR signaling pathway. Hence, rapamycin is an obvious candidate and has proven to reverse the HGPS cellular phenotype.[30,31] However, rapamycin is difficult to utilize clinically and harbors high toxicity. The analysis of a FDA approved rapalog that is less toxic and available for intravenous injection has been undertaken. By using temsirolimus (Tem), the efficacy of rapalogs has been further assessed regarding proteostasis, DNA damage, and - for the first time - mitochondrial function. Tem partially rescued the HGPS cellular phenotype by reducing progerin via autophagy. Given that mTOR is crucial for mitochondrial biogenesis, mitochondrial dysfunction of HGPS was not ameliorated by Tem.[32] This suggests that future therapeutic strategies should identify drug combinations and treatment regimens that target all dysfunctionalities of HGPS cells.

In sum, this study identified the significant impact of progerin expression on HGPS proteostasis. A crucial function that cells need to maintain to remain viable. Several strategies to rescue this important function has been undertaken by targeting different signaling pathways implicated in the maintenance of proteostasis including Nrf2 by SFN, AMPK by forskolin, and mTor by Tem. One of these strategies might hold some hope in future treatment of HGPS and possibly other age-related conditions.

1 Introduction

1.1 Aging

Aging is one of the most complex and multi-dimensional processes that affects all organisms from yeast to human. Molecules, cells and tissues start to accumulate damage over time, resulting in loss of function and increased vulnerability to disease, ultimately leading to death.[33] Aging is one of the most important demographic megatrends with implications for all aspects of our societies. A more aged society is inevitable since health and quality conditions of elderly people have improved and new insights into age-related diseases have been achieved.[34] However, the molecular mechanisms underlying physiological aging are not entirely understood. Many theories have been proposed to explain the process and cause of aging. Modern biological theories of human aging fall into two main categories, namely (1) programmed or (2) damage and error theories. The programmed theories depend on changes in gene expression that affect the system for maintenance, repair and defense response such as failures in the conserved insulin/IGF-1 signaling pathway or dysregulated immune response. The error theories emphasize environmental conditions that induce cumulative DNA damage at various stages of the cell, such as DNA polymerase errors, telomere shortening, mitochondrial free radical damage, and stem cell depletion.[35] Endogenously, DNA damage is caused by radiation (UV, X-ray or gamma-rays), toxins, chemicals, and viruses. Intrinsically, our own metabolism produces reactive oxygen species (ROS) in the mitochondria as a side product, inducing the damage of macromolecules and structures of the cells. All theories ultimately lead to the notion that DNA damage accumulation contributes to aging via genomic instability, senescence, and cancer.

Research of aging ranges from deciphering of the mechanism to understanding the different roles of extrinsic and intrinsic causes of senescence. Any biological change could affect the lifespan of humans and their hormones, enzymes, and genes implicated in age-related disorders. Models to understand the physiology and genetic of aging are cells and organisms that do not age or age quickly. No signs of aging were found in bacteria, yeast, and the clones of many plants as they propagate vegetatively, i.e. through division of a mother cell in two totipotent daughter cells. Human beings age and live 70 to 80 years, although they can also suffer from premature aging. Genetic diseases that accelerate senescence are called progeriod syndromes or progeria and

serve to identify specific genes and factors that influence life span in humans.[36] Progeriod syndromes are classified into two classes: (1) unimodal and (2) segmental. Unimodal progeriod syndromes show one predominant aspect of the normal aging phenotype such as Alzheimer's disease. By contrast, segmental progeriod syndromes display multiple aspects of the aging phenotype that affect several but not all tissues e.g. Werner's syndrome and Hutchinson-Gilford progeria syndrome (HGPS).[37] Studies of HGPS have not only provided insights into the disease' cellular mechanisms but also physiological aging.

1.2 Hutchinson-Gilford progeria syndrome

The Hutchinson-Gilford progeria syndrome is an extremely rare genetic disorder affecting the skin, musculoskeletal, and vasculature systems. Signs of progeria were first described in 1886 by Jonathan Hutchinson, who reported a 6-year-old male patient whose overall appearance was similar to an old man. Independently in 1887, Hastings Gilford depicted a second patient with similar clinical findings. HGPS has an incidence of one per 4 to 8 million life births. Today, 124 cases of living patients in over 40 countries are identified.[38-40]

Phenotypic features of HGPS children are not present at birth and in early infancy, but start to develop at 12 to 24 months after birth (Fig. 1).[38,39] During their life, children start to develop classical HGPS symptoms at different stages starting from failure of thrive at the age of 1 to alopecia, skeletal abnormalities (stiffness of joints, low bone density), loss of subcutaneous fat, and mid-facial cyanosis at the age of 2-3. HGPS children present growth retardation and a reduced rate of weight gain.[38,39] Progeria signs also include the lack of ear lobes, conductive hearing loss, aged-looking skin, dystrophic fingernails and toenails, prominent eyes, and a high-pitched voice.[39]

However, HGPS individuals are normal regarding their motor and mental development. The immune system, wound healing, and brain function are not affected in HGPS. In these children, the tumor rate is not increased.[41]

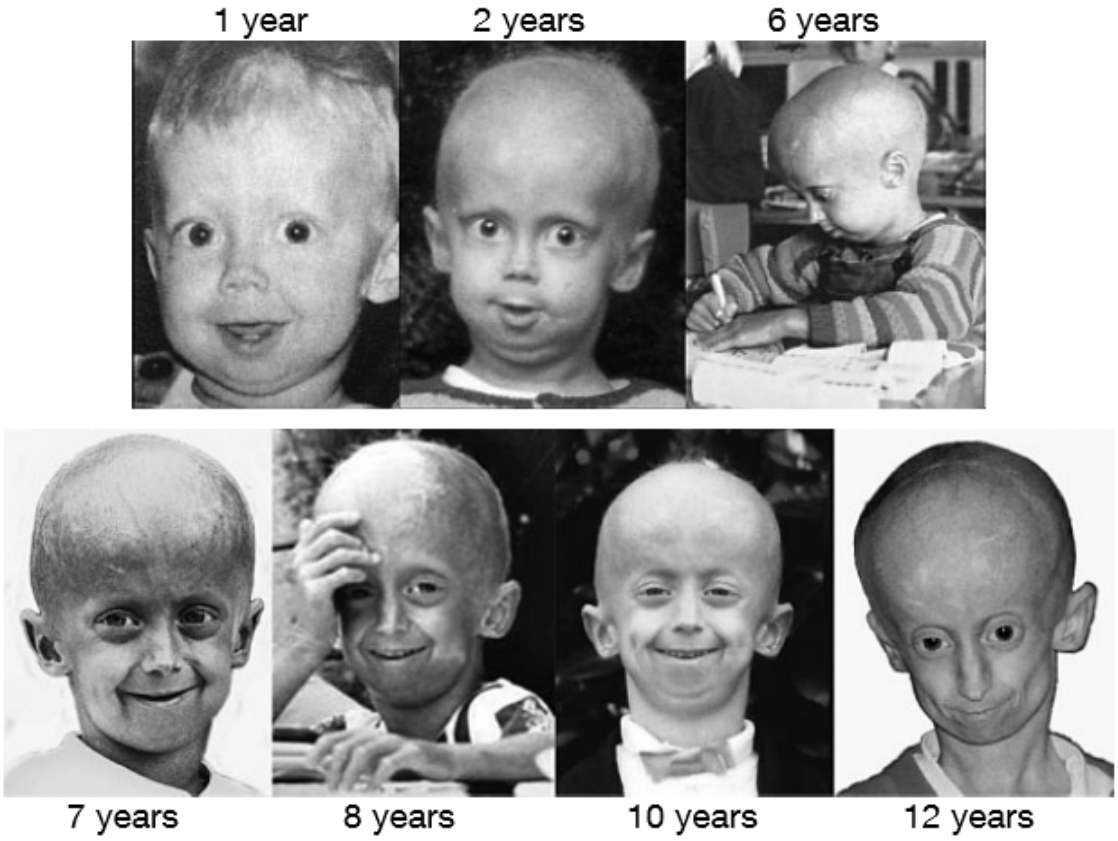

Figure 1: Progress of the HGPS disease of a Dutch child. At the age of one year, he does not show typical HGPS symptoms. The disease onset is between 12 and 24 months.[38] [modified figure from Hennekam, 2006]

Early death of most HGPS cases is caused by accelerated atherosclerosis of the carotid and coronary arteries such as angina, congestive heart failure, myocardial infarction, and stroke.[39] The average life expectancy in HGPS is 13.5 years.[38,40]

These clinical phenotypes and a genotype analysis led to the diagnosis of HGPS. The most common HGPS genotype is a G608G mutation in the lamin A gene (*LMNA*).[38,39,41-43]

1.2.1 Molecular basis of HGPS

While *LMNA* exons 1-10 encode lamin A and lamin C, exons 11 and 12 specifically encode the carboxy-terminal tail of lamin A. The most common LMNA mutation occurs in exon 11 at nucleotide position 1824. This mutation involves a C → T substitution (cytosine to thymine), also known as G608G transition. This leads to an activation of a cryptic splice donor site, resulting in a 150-base pair deletion. The translated protein is 50 amino acid shorter than the lamin A protein and is called progerin (Fig. 2). Progerin and its incorrect processing is the cause of HGPS.

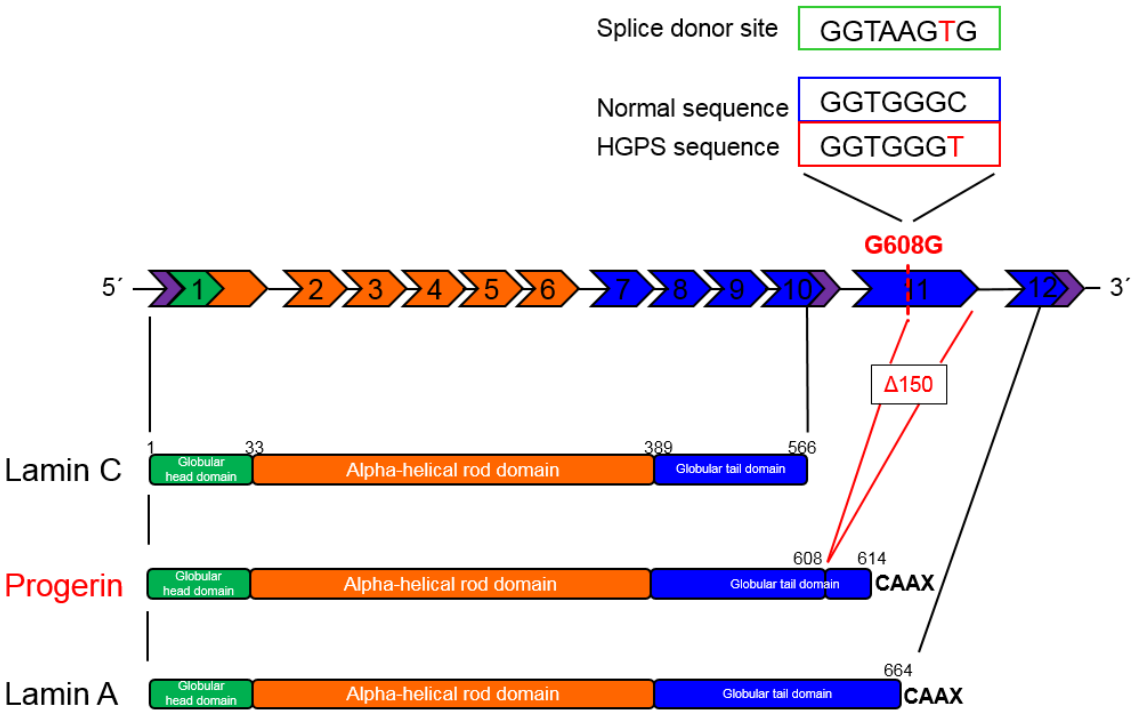

Figure 2: Mutation of HGPS in the lamin A gene. Schematic representation of the lamin A gene with its 12 exons encoding for lamin A and lamin C. While exon 1-10 encodes for lamin C, exon 1-12 encodes for lamin A with a terminal CAAX box. The HGPS mutation occurs within exon 11 (c.1824C>T, p.G608G), leading to a novel cryptic splice site. Consequently, 150 nucleotides (Δ150) are deleted from the lamin A mRNA, resulting in 50 missing amino acids within the protein that is called progerin. Untranslated regions are displayed in purple.

The parents' DNA does not carry the lamin A mutation of HGPS indicated by ex-screening analysis. The HGPS patient carries a heterogeneous and de novo point mutation in lamin A gene. These findings suggest that the mutation in lamin A gene must have occurred in the germline cells.[44,45]

1.2.2 Cellular phenotype of HGPS

The progerin protein acts in a dominant-negative manner to prevent the normal assembly of nuclear lamins into the nuclear lamina. In contrast to lamin A, progerin is tightly anchored to the nuclear envelope due to its farnesylation residue. This emphasizes abnormal nuclear blebbing and aberrant nuclear shapes of HGPS nuclei.[14,44] The truncated nuclear lamina leads to aberrant incorporation and localization of lamina-associated proteins (e.g. emerin, LAP2α) to the nuclear envelope. Thus, the disorganization may contribute to an observed loss of peripheral heterochromatin and clustering of the nuclear pore complexes in HGPS.[5,46] This leads to the disorganization of numerous transcription factors.[47] These effects might be responsible for the mis-regulated gene expression profiles and impaired DNA damage response in HGPS.[48,49] For this, HGPS cells exhibit an elevated steady-state level of DNA DSB compared to wild-type fibroblasts. DSBs are caused by progerin-induced nuclear structural irregularities.[50] HGPS nuclei also harbor progerin accumulation, reduced lamin B and LAP2, and abnormal lamin localization.[5,48] Worsening of the HGPS phenotype is clearly shown by the formation of nuclear introflections and enlargement of nuclei, as well as progressive loss of peripheral heterochromatin.[46] The severity of nuclear architecture defects and higher progerin accumulation correlate with patient age.

Progerin also forms insoluble cytoplasmic aggregates during mitosis and nuclei disassembly. This interferes with chromosome segregation, causing binucleated cells.[51]

These findings reveal that progerin is one cause of premature aging and cellular senescence (Fig. 3). Many HGPS features were found in physiological aging.

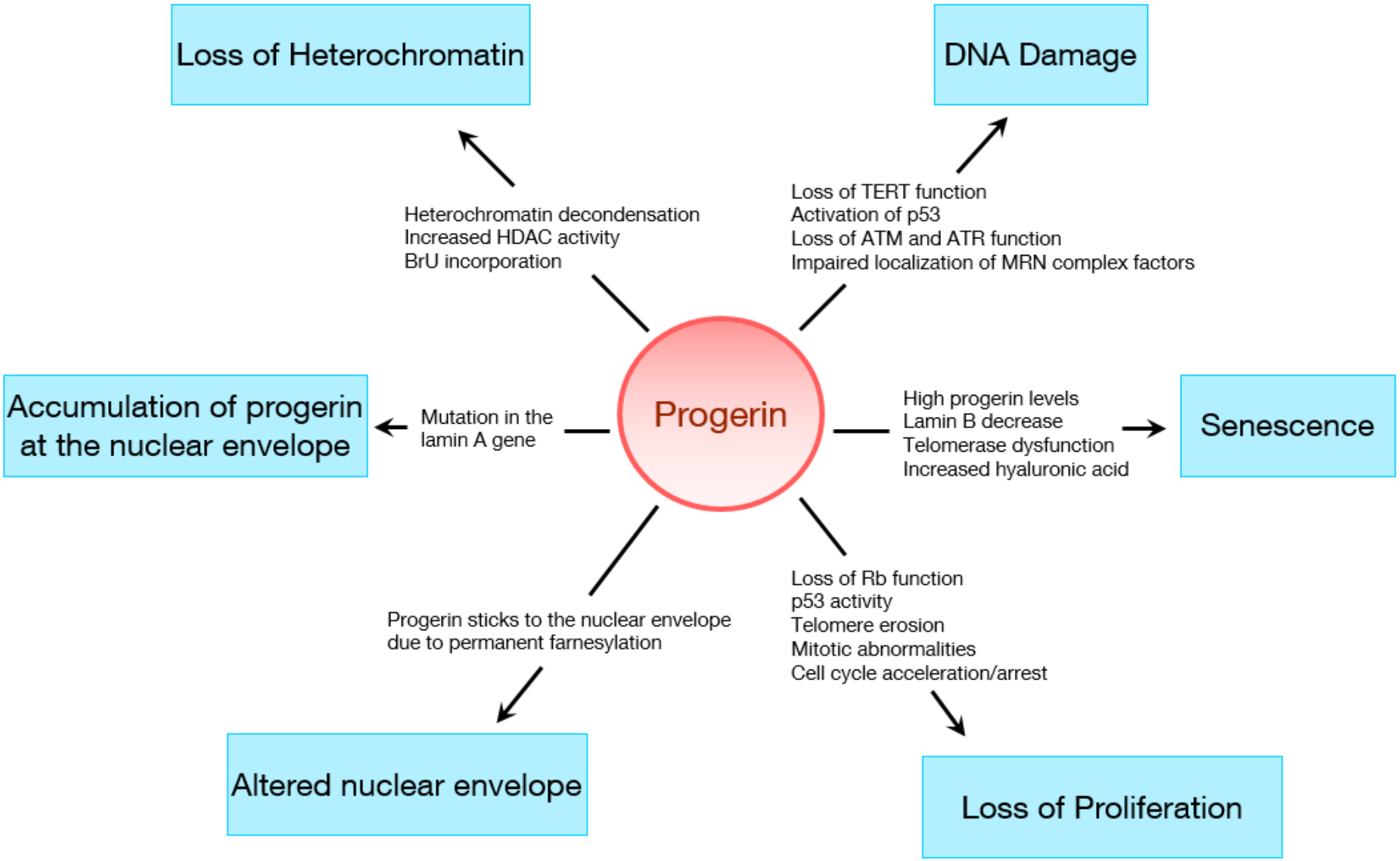

Figure 3: Impact of progerin on the cells. Progerin acts on different cellular function causing premature aging and cellular senescence.[6,46,50,52]

1.3 Lamins

Eriksson (2003) identified mutations in the lamin A gene as being responsible for the HGPS.[2,53]

Nuclear lamins were initially identified as the major component of the nuclear lamina which is a proteinaceous layer between the chromatin and the inner nuclear membrane.[54] From sequencing of the lamin cDNA, Lenz-Bohme et al. (1997) revealed that the nuclear lamins belong to the intermediate supergene family and were classified as the type V intermediate family. [55] Intermediate filaments have a well-defined conserved domain structure consisting of a variable NH_2-terminal globular head domain, a central α-helical rod comprising 4 coiled-coil domains, and a globular COOH-terminal tail domain (Fig. 2).[56] All domains are known to be involved in the lamin assembly.[57] The rod domain interacts with other lamins while the tail domain binds to chromatin, lamina-associated polypeptide 2, and emerin.[58] The C-terminal tail domain contains a structural Ig-fold domain and a nuclear localization signal.[59] Analysis of genomic sequences indicates that nuclear lamins are the progenitors of all intermediate filaments.[60]

Vertebrates have three lamin genes (*LMNA*, *LMNB1*, *LMNB2*) encoding at least 7 different isoforms.[61] The *LMNA* (lamin A) gene is localized on the human chromosome 1q21.2 and encodes the A-type lamins, lamin A and lamin C.[62,63] *LMNB1* encodes for lamin B1 and is located on chromosome 5q23.3-q31.1, while the *LMNB2* gene encodes for lamin B2 and lamin B3 and is located on chromosome 19p13.3. A-type lamins are known to be developmentally regulated. They are expressed in differentiated cells, while B-type lamins are expressed at all developmental stages.[64,65]

1.3.1 Posttranslational Modifications of the lamin proteins

Lamins A, B1, and B2 are expressed as prelamins that require extensive posttranslational modifications of their carboxy-terminal CAAX (Cysteine-Aliphatic-Aliphatic-any Amino Acid, Cys-Ser-Ile-Met in prelamin A) box to become mature lamins (Fig. 4).[66] The CAAX motif triggers three sequential enzymatic modifications.[67] The first modification step is the farnesylation of the cysteine of the CAAX motif by farnesyltransferase. The farnesylated modification is important but not sufficient for targeting and anchoring the protein to the inner nuclear membrane.[68] The next prelamin A modification is the cleavage of the last 15 C-terminal amino acids (-AAX), including the farnesyl group. This process requires the enzyme ZMPSTE24 (Zinc metalloprotease related to the STE24 homolog in yeast, FACE1 – farnesylated-proteins converting enzyme).[69] A methyl esterification is the next maturation step of the carboxy-terminal cysteine performed by isoprenylcysteine carboxyl methyltransferase (ICMT). Finally, ZMPSTE24 catalyzes a second proteolytic cleavage to remove another 15 amino acids at the C-terminus. This results in the production of mature lamin A lacking the carboxy-terminal farnesyl and carboxymethyl modifications. The enzymes required for modifying the carboxy-terminus of the lamins are present in the inner nuclear membrane and endoplasmic reticulum membranes. However prelamin A is processed in the nucleus due to their rapid transport into the nucleus after translation, which takes place in the cytoplasm.[14, 67]

In HGPS, the G608G mutation activates a novel cryptic splice site that deletes 150 nucleotides on the prelamin A mRNA. The translated prelamin A does not contain the second important recognition site for the ZMPSTE24 enzyme (RSYLLG). This absence leads to a permanently farnesylated and carboxy-methylated lamin A protein as the cleavage by ZMPSTE24 cannot occur. The truncated lamin A protein is produced in HGPS and is referred to as progerin (farnesylated prelamin AΔ50, lamin AΔ50).

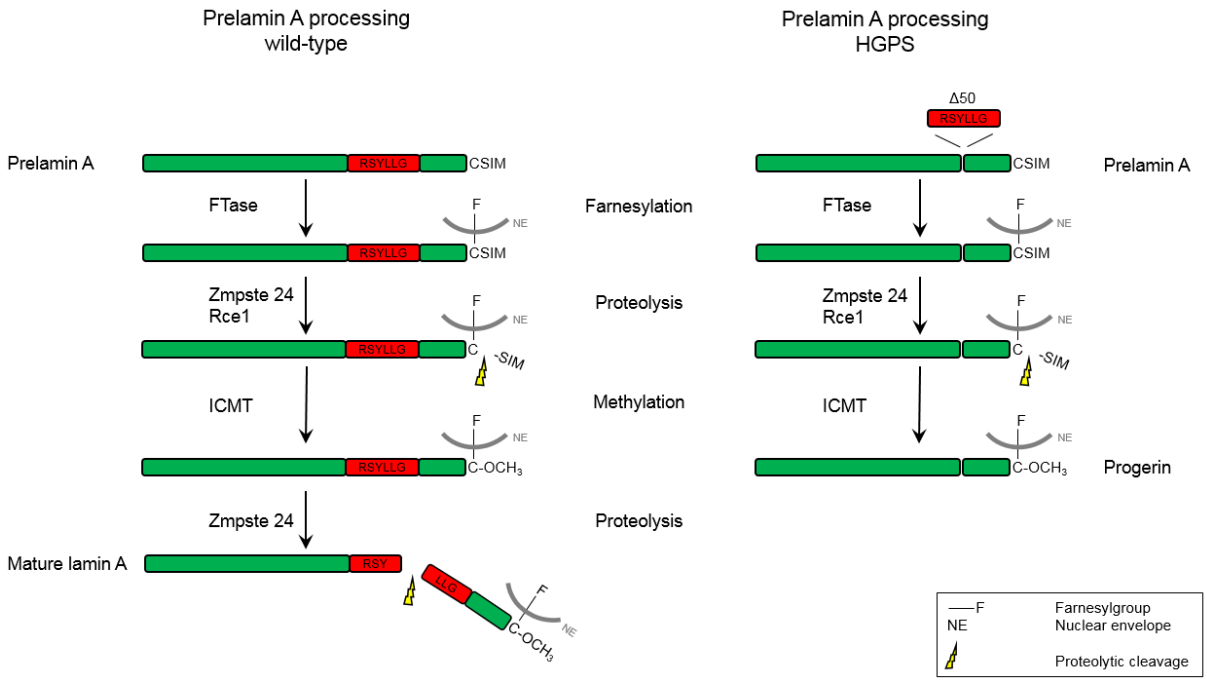

Figure 4: Post-translational processing of prelamin A. The wild-type or normal processing of prelamin A is shown on the left-hand side. The process contains 4 steps from prelamin A to mature lamin A. In HGPS (right-hand side) the recognition site RYSLLG for ZMPSTE24 is missing, resulting in a stop of the maturation process after step 3. Thus, the lamin AΔ50 protein stays remains permanently farnesylated and carboxy-methylated and is known as progerin.

1.3.2 The lamin network

The nuclear envelope separates the cytoplasm from the nucleus and comprises the outer nuclear membrane (ONM) and the inner nuclear membrane (INM), separated by the perinuclear space (PNS).[70] Cytoplasm and nucleus are connected through nuclear pore complexes (NPC), which regulate the macromolecular trafficking across the nuclear envelope.[71] The outer nuclear membrane comprises ER proteins and ribosomes, whereas the inner nuclear membrane has its own set of integral membrane proteins. Most of these proteins interact with the nuclear lamina, which is underlying the INM (Fig. 5).[70]

The nuclear lamina is a filamentous meshwork built up from A- and B-type lamins and nuclear lamin-associated proteins. Lamins have important anchorage functions for nuclear envelope transmembrane (NET) proteins such as lamin B receptor (LBR), lamin-associated polypeptide 1/2, emerin, and MAN1.[14,44,56,57] They are essential for organizing peripheral chromatin, which is linked to gene expression control.[72] Lamins

organize the cytoskeleton as they localize NPC within the nuclear envelope.[14,56,73-75] Lamin A and C interact with SUN and nesprin proteins to form the LINC complex, which links the nucleoskeleton to the cytoskeleton. Depletion of A-type lamins leads to abnormalities in nuclear architecture and mislocalization of integral membrane proteins of the INM.[74] The absence of lamin A and lamin C from the nuclear envelope was correlated with mislocalization of emerin to the endoplasmic reticulum.[76] Such cells are often characterized by an increased deformability, misshapen nuclei, and reduced mechanical stiffness and viability when subjected to mechanical strain. [73,75] Emerin is also known to interact with the chromatin bridging protein barrier-to autointegration factor (BAF). Mutations in the BANF1 gene have been identified as the cause of hereditary progeriod syndromes.[77]

A-type lamins are also known to interact with the LBR, which contains a binding site for heterochromatin 1 (HP1) and anchors heterochromatin as well as the lamina to the membrane. LBR might mediate the interaction between chromatin and lamin B with implications in gene silencing.[78]

Lamins demonstrate interactions with transcription factors, chromatin remodeling complexes, and DNA replication machinery.[14,40,72,79-81] Lamins play an important role during mitosis as the assembly and disassembly of the nuclear envelope is crucial.[73] During mitosis, lamins are dephosphorylated by protein phosphatase 1 and bind to the periphery of decondensing chromosomes.[82] Dephosphorylation is required for lamin assembly during the telophase/early G1 transition.[73]

The discoveries that lamins are involved in the regulation of cell cycle progression and their different expression during development, suggest that they also function in the regulation of cell differentiation. [83]

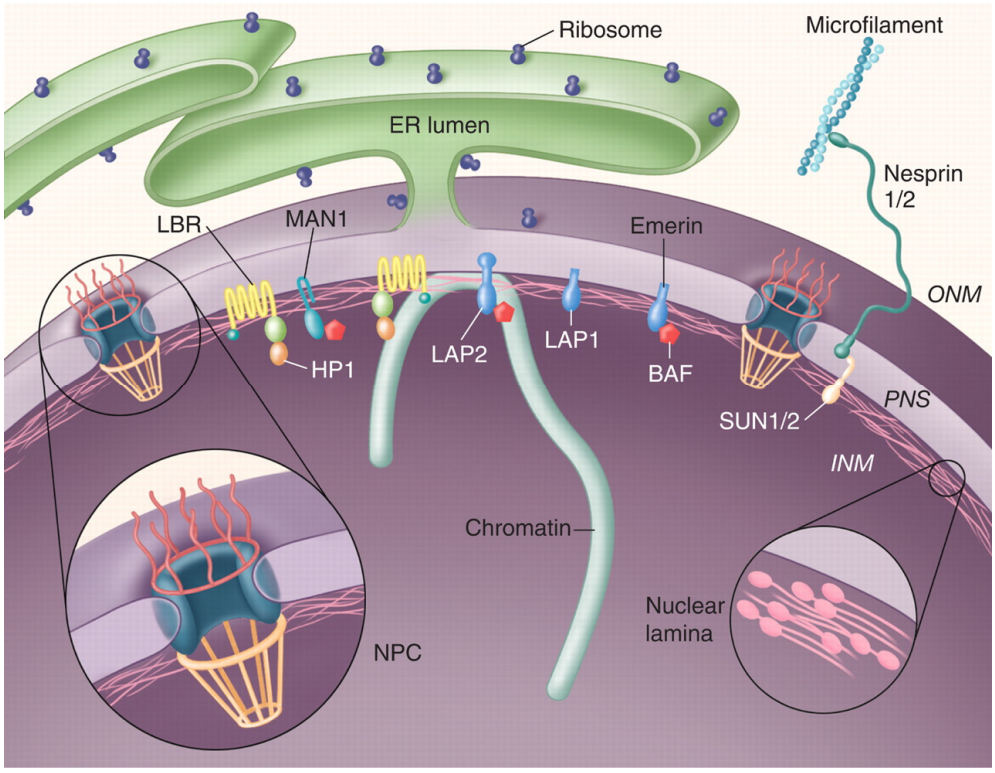

Figure 5: The network of the lamins. The nuclear lamina is composed of lamin A, C, and B and interacts with chromatin and several transmembrane proteins such as emerin, HP1, and LAP2. The lamina plays a role in NPC positioning and interact with the cytoskeleton through SUN 1/2 and nesprin 1/2.[70]

The interest in lamins has increased in the recent years due to the lamins major interaction network. Lamins were found to play essential roles in a variety of human diseases (laminopathies), including progeriod syndromes and disorders that affect muscle, adipose, bone, and neuronal tissues.

1.3.3 Lamins and genetic diseases

Mutations in the lamin genes lead to severe alterations in the stability and shape of the cell nucleus. These changes have a major impact on the organization of the components of the nuclear envelope and can impair processes like gene transcription and survival.[84]

Lamin A mutations are directly associated with a wide range of human diseases termed laminopathies.[2] These diseases were grouped into 4 classes. The first one comprises those diseases affecting striated skeletal and cardiac muscles, and includes Emery-

Dreifuss muscular dystrophy (EDMD), limb-girdle muscular dystrophy 1B (LGMD-1B), and dilated cardiomyopathy (DCM). The second group affects white fat deposition and bone turnover and includes familial partial lipodystrophy (FPLD) and mandibuloacral disease (MAD). The third group display the axonal neuropathy Charcot-Marie-Tooth type 2B1 (CMT2B1) and results in demyelination of peripheral motor nerves and is an additional sixth disease. Premature aging syndromes were added to the fourth group and include the HGPS and some cases of atypical Werner's syndrome.[85, 86]

1.3.4 Involvement of progerin in physiological aging

Mutations in the *LMNA* gene are implicated in different premature aging diseases. Premature aging features were also found in normal nuclei of elderly individuals and include changes in histone modification and increased DNA damage. In healthy individuals, the nuclear defects are caused by the sporadic use of the same cryptic splice site in lamin A. This leads to the expression of progerin whose constitutive activation causes HGPS.[87,88] The nuclear defects are caused by the prolonged presence of progerin and not due to the amount of the aberrantly spliced *LMNA* mRNA or the amount of progerin. Aged cells might be more sensitized to the presence of progerin and less able to neutralize the negative effects due to the existence of a p53-dependent checkpoint. Thus, structural abnormalities of the nuclear lamina are recognized and linked to the activation of the senescence program and terminal differentiation.[87,88]

In HGPS, progerin not only induces mitotic defects during the physiological aging process but also binucleated and giant cells, which increase with passage number. In normal fibroblasts, the bimodal distribution of progerin implicates the presence of an irreversible switch in late-passage cells activating the cryptic splice site.[51] Studies demonstrated that the cryptic splice site of lamin A could be used *in vivo* in normal individuals from human skin biopsies.[88] Progerin mRNA was detected in all skin biopsies from newborn to 90 year-old individuals and remained constant with age. The progerin protein appeared to accumulate in elderly samples specifically in primary dermal fibroblasts and terminally differentiated keratinocytes. Progerin-positive nuclei were first found near the basement membrane and started to spread throughout the

dermis with advanced age. Progerin expression *in vivo* could correspond to a terminally differentiated or senescent subpopulation.[88]

Another evidence shows that progerin is implicated in physiological aging as it plays a role in cardiovascular disease of HGPS and cardiovascular aging of unaffected elderly individuals.[41] While HGPS patients showed clear nuclear progerin staining in vascular smooth muscle cells (VSCM) and in the coronary arteries, unaffected subjects showed also progerin-positive cells as cytoplasmic punctuate staining in some cells of the coronary arteries but no staining in VSCM. This study supports the hypothesis that progerin-positive cells increases with size and advanced age in different cell types and in aging cardiovascular tissue.[41] More evidence was provided as adult stem cells in HGPS express low levels of progerin compared to non-stem cells. This means that progerin-expressing cells *in vivo* can correspond to a subpopulation of terminally differentiated cells or senescent cells.[89]

The cause of increasing progerin expression in normal aging has recently been specified. While HGPS subjects showed a mutation in exon 11 of the lamin A gene, healthy aged subjects showed that telomere damage had a causative role activating the cryptic splice site. Thus, progerin expression was activated in a telomere-dependent cellular senescence during cell aging *in vitro*. The proposed mechanism in senescent cells demonstrates progressive telomere shortening concomitant with activation of p53. This leads to global alternative splicing including progerin expression which in turn contributes to senescence.[90]

In sum, progerin is one cause of premature aging and cellular senescence. Researchers plan to continue exploring the mechanisms of HGPS, which might help learning more about cardiovascular diseases that occurs during the normal aging process.[11,91] Thus, elderly individuals might benefit from finding new therapeutic avenues for children with HGPS.

1.4 Possible therapies of HGPS

In 2012, researchers discovered the first-ever treatment of progeria. Basic research was performed in the last ten years to find possibilities for elongating the life of the affected children. Children show improvement in one or more areas of their condition after the first-ever progeria clinical drug trial. This proves that the farnesyl transferase inhibitor drug lonafarnib is the first known, effective treatment for children with progeria.[11]

1.4.1 Farnesyltransferase inhibitors (FTI)

Finding the gene for progeria was the key element to this entire avenue of possible therapies. Basic research on prelamin A and lamin A provided the understanding that FTIs may be a viable treatment for progeria. FTIs were first tested on progeria cells and subsequently on progeria mice.[91]

The farnesyl group of progeria cells remains attached at the mutated prelamin A protein leading to a permanent link to the nuclear envelope. FTIs function by inhibiting the attachment of the farnesyl molecule onto progerin in the first place, thus “neutralizing” the damaging properties of progerin and restoring the nucleus to a more normal state (Fig. 6, Table 2).[91] FTI treatment led to a significant increase of soluble progerin in the mitotic cytoplasm.[51,92-94]

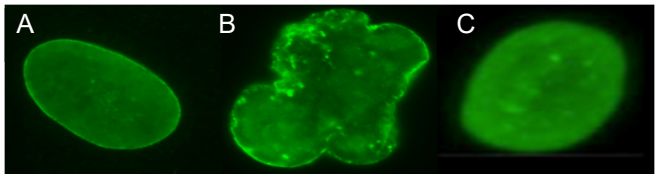

Figure 6: Immunofluorescence staining of skin cells with FTI. (A) Normal skin cell, (B) Progeria skin cell, and (C) Progeria skin cell after FTI treatment.[93]

FIT treatment of fibroblasts reversed gene expression defects. Retinoblastoma was identified as a key factor in HGPS pathogenesis and its modulation could ameliorate premature aging and possibly complications of physiological aging.[95]

Table 2: Treatment of HGPS with FTIs *in vitro*.[51,92-95]

Syndrome	FTI	Dose	Reduction of misshaped nuclei
HGPS (G608)	PB-43	7d, 2.5 µM	11.2-14.6 %
HGPS (R644C)	PB-43	7d, 2.5 µM	5.7 %
HGPS (G608G)	Lonafanrib	72h, 0.5-2 µM	20-30 %
HGPS (G608G)	PD169541	72h, 100 nM	33 %
HGPS (G608G)	Lonafarnib	72h, 1.5 µM	25 %

Nuclear-shape abnormalities and heterochromatin organization may also be rescued by FTI treatment, followed by a chromatin-modifying drug. Reversal of the nuclear defects is related to lowering of the progerin level in drug-treated samples and elicits recovery of the ribonucleoprotein staining pattern.[46]

Nevertheless, FTI was the first possible drug treatment for HGPS children and it promised to reverse the cellular phenotype of HGPS nuclei. For this, FTIs were tested in progeria mice. In progeria mice, disease symptoms were prevented by FTI treatment. Yang et al. (2008) created a knock-in mouse experiment expressing non-farnesylated progerin ($Lmna^{nHG/+}$). Aside from a cysteine-to-serine substitution in the CAAX motif, $Lmna^{nHG/+}$ mice were genetically identical to the original mouse model $Lmna^{HG/+}$. The absence of progerin farnesylation in $Lmna^{HG/+}$ cells was verified with metabolic labeling experiments. The $Lmna^{nHG/+}$ mice developed the same spectrum of disease phenotypes as found in $Lmna^{HG/+}$ mice. The important message of this study is that non-farnesylated progerin is still toxic. Nonetheless, the extent of the disease phenotypes in $Lmna^{HG/+}$ mice was milder than in $Lmna^{HG/+}$ mice, and mouse embryonic fibroblasts (MEFs) contained less misshapen nuclei. A possible explanation of the milder phenotypes is lower steady-state levels of progerin in $Lmna^{nHG/+}$. Treatment of $Lmna^{HG/+}$ MEFs with FTI reduced the progerin levels. $Lmna^{nHG/+}$ mice still developed severe disease phenotypes even though progerin farnesylation was absent.[96]

Studies from Varela et al. (2008) demonstrated that both prelamin A and progerin undergo alternative prenylation by geranylgeranyltransferase in the setting of farnesyltransferase inhibition. This could explain the low efficiency of FTIs in ameliorating the phenotypes of progeriod mouse models.[97] Hence, two additional compounds have been implicated in clinical trial studies (Table 3). Bisphosphonates have been used to block geranylgeranylation (Zoledronic acid) whereas statins (Pravastatin) have been used to block prenylation.[97]

Fong et al. (2004) tested the efficacy of FTI in ZMPSTE24-deficient mice. This progeria mouse model resembles HGPS in sharing phenotypes like retarded growth, alopecia, dental abnormalities, micrognathia, osteolytic lesions in bones, and osteoporosis. The FTI-treated mice exhibit improved body weight, grip strength, bone integrity, and percent survival at 20 weeks of age. These results suggest that FTIs may have beneficial effects in human with progeria.[98]

To date, five clinical trials have been performed for treatment of HGPS with FTIs and its combination with bisphosphonates and statins (Table 3). All of the studies use the age groups child/adult/senior and are not double-blind (no placebo).

Table 3: Clinical trials of FTIs in HGPS patients.

Conditions	Start	End	Intervention	Phase	Number of children enrolled
Progeria	10/2004		Clinical study		15
Progeria, HGPS	5/2007	10/2009	Lonafarnib	II	28
HGPS	10/2008	3/2013	Zoledronic Acid, Pravastatin	II	15
Progeria	3/2009	4/2009	Lonafarnib, Zoledronic Acid	II	5
Progeria	8/2009	2/2012	Lonafarnib, Zoledronic Acid, Pravastatin	II	45

One of the clinical trials recently led to the first results.[11] Lonafarnib has not only proven effective for cancer but also for progeria. Twenty-eight children from 16 countries participated in the 2 ½ year drug trial, representing 75 % of known progeria cases worldwide at the time when the trial began. Every child showed improvement in one or more of four HGPS characteristics. The first primary outcome was that the children gain weight. Improvements of the bone structure and better hearing was also observed. Most importantly, the flexibility of blood vessels was increased. This was a breakthrough for children, since heart attack or stroke (cardiovascular disease) are the causes of death in HGPS. However, a statement is not possible concerning whether a two-year treatment period delayed strokes, heart attacks or increased longevity.[11]

In contrast to the positive effects of FTI, evidence raises that FTI induces severe consequences for the nuclei.

FTI has recently been shown to disrupt the lamin B 1/2 processing and localization.[13] A- and B-type lamins form separate, but interacting, networks in the nucleus. Depletion of lamin B1 can affect the remaining lamin B2 and lamin A/C network. This means that some disease phenotypes ascribed to dysfunction of lamin A, may be mediated through changes in the lamin B network. B-type lamins are important for cell proliferation and organ development. Changes in one lamin network by FTI will automatically affect the other lamin network leading to mechanisms that induces other progeriod symptoms. In addition, treatment with FTI led to a rapid cell cycle arrest that induces senescence in proliferating cells.[13]

Treatment with FTI also mediated spindle defects and donut-shaped nuclei.[12] Thus, nuclei divided abnormally and became aneuploid.[12] Moreover, FTI could not reduce the accumulated DSBs in HGPS cells. This suggests that DNA damage accumulation and misshapen nuclei are probably two unrelated phenotypes caused by prelamin A accumulation in HGPS. Strategies for treatment of HGPS need to combine elimination of DNA damage accumulation as well as normalization of nuclear morphology.[6] Research for new treatments of progeria has to be conducted. Small compounds have recently cleared progerin and ameliorated the diseases' phenotype via the activation of the protein degradation pathways.[30,99] The two major protein degradation pathways are autophagy and ubiquitin-proteasome system.[100]

1.4.2 The Autophagy Pathway – Rapamycin

Autophagy encompasses the different routes that cells use to deliver unnecessary or dysfunctional cytoplasmic substrates to lysosomes for protein degradation. These include macroautophagy, chaperone-mediated autophagy, and microautophagy.[101] Autophagy comprises two key steps: 1) formation of autophagosomes that capture the substrates; and 2) fusion of autophagosomes and lysosomes to form autolysosomes in which the autophagic content is degraded.[102-105] The membrane trafficking processes in autophagy are controlled by autophagy-related genes (ATGs) and signaling lipid phospatidylinositol-3-phosphate that recruits effector proteins to the autophagic vacuoles.[102-105] Signals for the autophagosome formation are regulated by the mammalian target of rapamycin (mTOR). mTOR is inhibited under starvation conditions, and this contributes to autophagy.[101,106] Factors that activate or inhibit mTOR are insulin-like growth factor (IGF1R), GTPases, p53, adenosine monophosphate-activated protein kinase (AMPK). This leads to an activation or inhibition of autophagy (Fig. 7).[24,107-111]

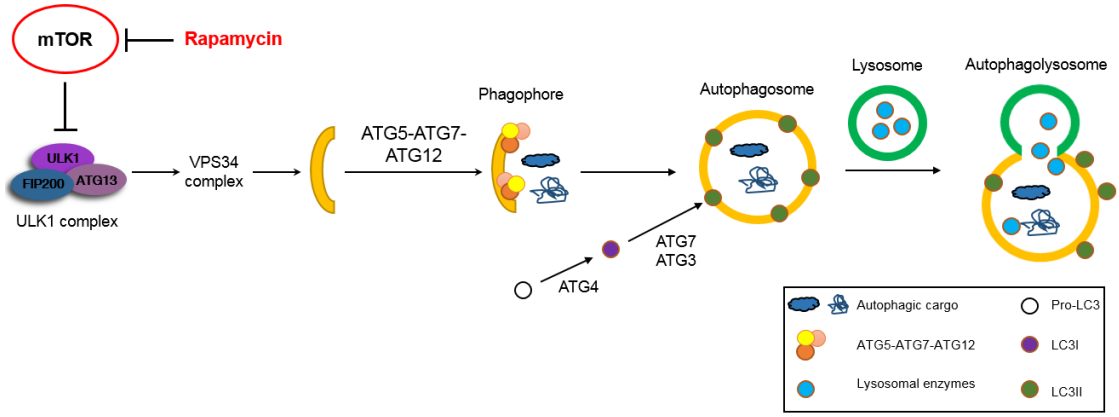

Figure 7: Inhibition of autophagy by mTOR. Inhibition of mTOR leads to activation of ULK1 complex, which leads to VSP34 activation through phosphorylation and phagophore formation. Induction of autophagy is controlled by autophagy-related (Atg) gene products. Atg control autophagosome formation through Atg5-Atg7-Atg 12 (ULK complex) and LC3-II complexes. Pro-LC3 is cleaved Atg4 protease to generate the cytosolic LC3-I. LC3-I is conjugated to phosphatidylethanolamine (PE) that requires Atg7 and Atg3. The lipidated form of LC3, known as LC3-II, is attached to the autophagosome membrane. The autophagosome subsequently fuses with the lysosome to form an autolysosome which degrades the internal contents. Formation of the ULK complex is blocked by mTOR and thus, autophagic cargo is not degraded. Rapamycin inhibits the mTOR signaling pathway activating the autophagy machinery. [112,113]

Emerging evidence has shown that impairment of autophagy has been linked to degenerative disease and carcinogenesis.[102,114] Autophagy is a predominantly cytoprotective process affecting the liver, heart, nervous system, and kidney.[101,106,115-118] Autophagy has a prominent role in determining the life span of model organisms. Reduced autophagy has been associated with accelerated aging.[119] Induction of autophagy is proposed as an attractive therapeutic strategy for diseases in which an increased protein degradation capacity is beneficial. Thus, a number of molecule-based autophagy inducers (incl. drugs in clinical use) or natural products have been identified.[102,120-122]

Cao et al. (2011) investigated the effect of the drug rapamycin on cultured HGPS fibroblasts.[30] The FTI lonafarnib is a relatively cytotoxic agent with gastrointestinal and hematological dose-limiting toxicities in cancer patients.[123] Rapamycin, a non-toxic drug is an attractive option for progeria children.

Rapamycin cleared progerin, prevents nuclear abnormalities (nuclear blebbing), and delayed replicative senescence. Rapamycin induced the clearance of progerin through the autophagy pathway by inhibiting the mTOR pathway.[30] Rapamycin slowed the progression of cellular senescence as less β-Gal-positive cells were detected at day 60.[30] In further detail, rapamycin suppresses the geroconversion (conversion from quiescence to senescence) by progerin clearance.[123] A senescent phenotype can be linked to hyper-active growth-promoting and nutrient-sensing pathways such as mTOR. Activated mTOR drives the senescent morphology when the cell cycle is arrested. [30,123] Rapamycin and upstream inhibitors of mTOR inhibit geroconversion in premature and physiological aging.[124,125] The cellular life span was extended by the rapamycin inhibition of the TOR pathway.[30]

Furthermore, rapamycin prevents atherosclerosis in animal models of accelerated atherosclerosis. It prevents atherosclerotic restenosis in humans by increasing lipolysis and simultaneously reducing the lipid entry into tissues.[126,127]

Rapamycin is a clinically approved, non-toxic drug, which is already used in transplant patients and in children with TSC syndrome.[123] The positive effects of rapamycin in cells proved the drug for usage in future mouse models.

Nevertheless, the negative side effects of rapamycin should be considered before applying to HGPS individuals. Rapamycin induces gastrointestinal symptoms, edema, infection, delayed wound healing, high cholesterol and triglyceride levels, anemia, and

interstitial pneumonitis.[31] Moreover, rapamycin showed only diminishing effects on mammalian aging rates. While a number of aging phenotypes were improved by rapamycin (cancer potential, immune system); myocardial pathology, arterial degeneration, and DNA damage - among others - were not measurably altered. This indicates only a direct influence of rapamycin on these traits and not slowing down aging.[128]

For this purpose, it will be important to identify safer analogs of rapamycin for chronic treatments in humans to minimize toxicity and further improve the cellular phenotype.

1.4.3 Ubiquitin – Proteasome Pathway (UPS)

The UPS contributes to the maintenance of cellular homeostasis and protein quality control. It also functions as a regulator of many cellular processes, including proliferation, cell cycling, gene transcription, apoptosis, antioxidant responses, and immune reactions.[129,130]

Proteasomes are multi-sub-unit complexes comprising the 20S proteolytic core particle and 19S regulatory core complex. Proteolysis is performed by three subunits, which have caspase-like (β1), trypsin-like (β2), and chymotrypsin-like (β5) activites.[131] At present, little is known about the importance of each proteasomal activity *in vivo*. The clearance of defect proteins involves several steps by the ubiquitin-proteasome system, whereby a chain of activated ubiquitin monomers is covalently linked to lysine residues of the target protein in an ATP-dependent manner. The process is initiated by the action of ubiquitin-activating enzymes (E1), ubiquitin-conjugating enzymes (E2), and ubiquitin ligases (E3). E1 activates and transfers ubiquitin to the carrier protein E2. E2 presents ubiquitin to E3, whereby the latter binds to the target protein. Thus, E3 interacts with E2 to covalently attach the ubiquitin to the target protein. This process is carried at least 4 times, creating a polyubiquitin chain. The ubiquitin chain serves as a recognition signal by the proteasome (Fig. 8).[132-135]

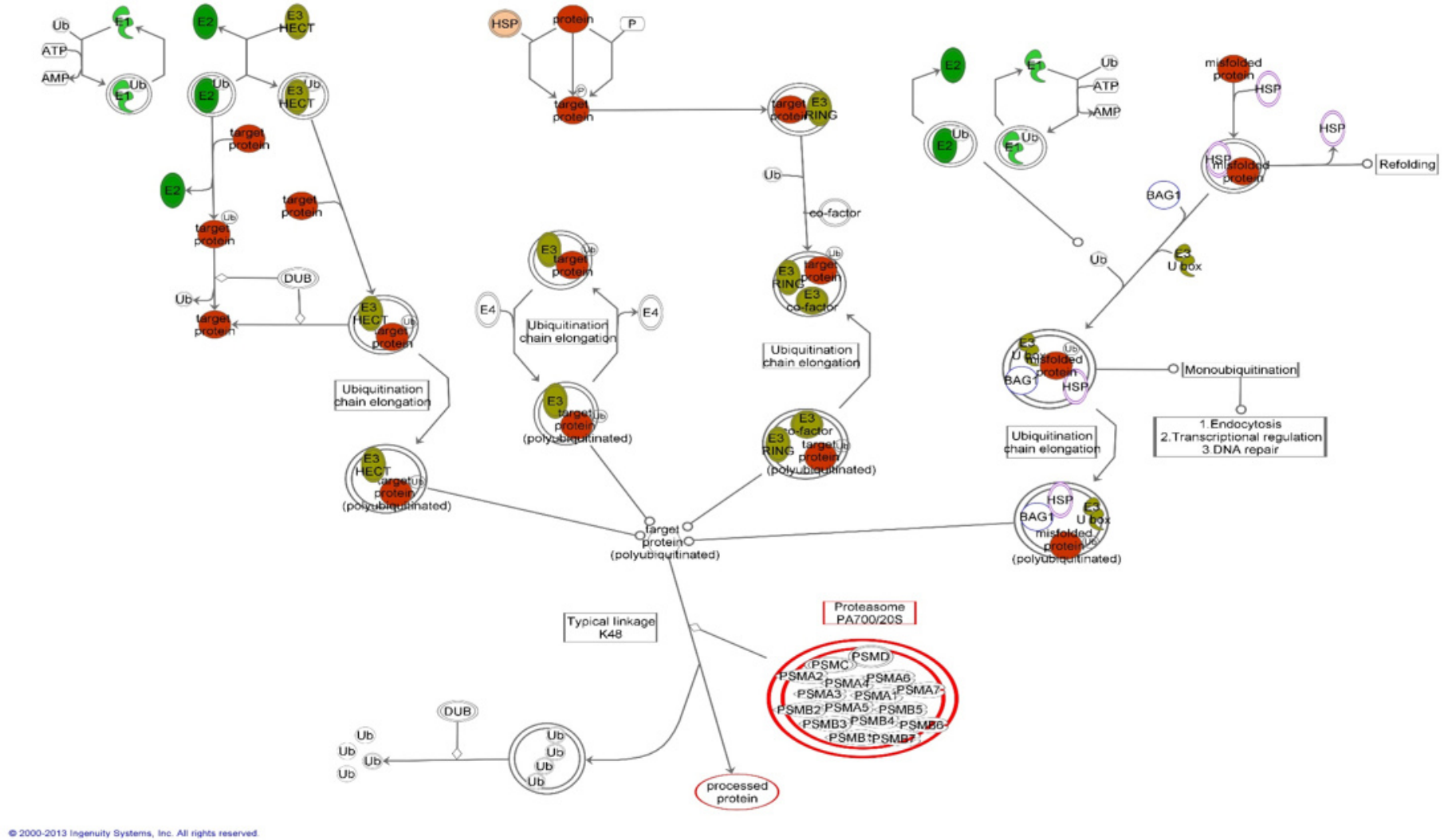

Figure 8: Protein Ubiquitination Pathway. E1 hydrolyzes ATP and adenylates a ubiquitin molecule, which is subsequently transferred to the E1-active site. A second ubiquitin is added and the complex is transferred to E2. E3 recognizes the specific protein to be ubiquitinated and catalyzes transfer of ubiquitin from E2 to the target protein. A target protein must be labeled with at least 4 ubiquitin molecules before it is recognized by the proteasome.[132]

The proteasome has emerged as an attractive target for cancer therapy. Bortezomib was the first proteasome inhibitor. It encouraged anti-tumor activity in preclinical studies and clinical trials.[133,136]

Evidence is mounting to support the central hypothesis that proteasome functional insufficiency represents a common pathological phenomenon in heart disease. However, pharmacological inhibition of the proteasome is implicated as a potential therapeutic strategy to intervene pressure-overload cardiac hypertrophy, viral myocarditis, doxorubicin cardiotoxicity, and perhaps myocardial ischemic injury. It exists a multitude of unexplained inconsistencies and controversies between the two possibilities of the proteasome impact, which may eventually be clarified.[137]

Proteasome dysfunction might also be involved in Alzheimer disease. The age-dependent decrease of the proteasomal activity might lead to the accumulation of Aβ and tau. The proteasome activity was reduced by 50 % in primary neurons isolated from APP transgenic mice compared to neurons of wild-type mice. Additionally, the proteasomal activity is further reduced once Aβ and tau aggregate. Proteasome activity was normalized in APP mutated neurons to wild-type levels when treated with γ-secretase inhibitor.[138,139]

Recent studies showed a marked decrease in the 20S proteasome activity by *in vitro* assays of substantia nigra extracts from Parkinson's disease brains.[140,141] Spillantini et al. (2003) observed a 55 % reduction in the proteasomal chymotrypsin-like activity in the substantia nigra. These results suggest structural and functional impairments of the ubiquitin-proteasome system in sporadic Parkinson's disease.[141,142]

Physiologically, the proteasomal activity decreases with age.[143,144] A decline in proteasome function is assumed to contribute to the development of age-related pathology and to aging process itself.[145] This hypothesis was proven by mouse hepatocytes, which undergo premature senescence due to disassembly of the 20S proteasome.[146] Furthermore, reduced 26S proteasome activity was shown to shorten life span and enhance the development of neurodegenerative phenotypes in Drosophila.[143] Tomaru et al. (2012) provided the evidence that a reduced chymotrypsin-like activity shorten the life span of mice. The diminished activity accumulated ubiquitinated and oxidized proteins. The results suggest that reduced proteasomal activity accelerates the aging process and enhances the development of age-related pathology.[130] The lower proteasomal activity of dermal fibroblasts from elderly people is attended by a reduction of the proteasomal catalytic subunits PSMB5

and PSMB6 and an accumulation of oxidized and ubiquitinated proteins.[147] A lentiviral gene transfer restored the proteasomal activity and decreased the accumulation of oxidized and ubiquitinated proteins. This delayed the senescence in dermal fibroblast from elderly people.[147]

HGPS analysis revealed a decrease in overall caspase-like proteasome activity and in the levels of two the active proteolytic β5- and β7-complex subunits.[148] The HGPS cells showed higher ROS than age-matched controls. Increased ROS levels induced higher levels of mitochondrial superoxide dismutase (SOD).[148]

The list of proteins is long that are involved in the ubiquitin-proteasome system. The substrate recognition and processing by the UPS require a close cooperation with molecular chaperones.[149] Chaperones are defined by their ability to recognize non-native conformations of other proteins. They are suited to distinguish between native and abnormal proteins during substrate selection.[149]

However, further studies are necessary to address the molecular mechanisms underlying an age-related decrease in proteasomal activity and identify specific substrate proteins and the altered expression involved in the development of age-related diseases. Such studies may provide a new approach to the prevention and treatment of age-related diseases.

2 Aim of the thesis

Several studies have shown that cells or mouse models of HGPS treated with FTI, statins or ICMT inhibitor could reverse some of the phenotypic changes of these cells or tissues.[7-10] Three clinical trials involving children with HGPS have been initiated with the drugs mentioned above and revealed positive effects of FTI. However, recent evidence indicates negative side effects of the FTI treatment, which require further mechanistic studies to determine the causes of the phenotypic changes occurring in HGPS cells and hopefully find ways to target these defects.[12,13]

The main objective of this thesis is to understand the molecular mechanisms that are triggered by the accumulation of progerin at the nuclear envelope in HGPS cells. Proteomic analysis allows the identification of differentially expressed proteins in HGPS cells to determine their functional relationships to signaling pathways to prioritize specific targets for testing new therapeutic strategies. It is hypothesized that in particular the protein degradation pathways in HGPS are altered and that therapeutics should reverse this defect to normalize the HGPS cellular phenotype.

To test this hypothesis this work investigates the following aims:

1) To dissect how progerin impacts the nuclear compartment of HGPS cells and triggers premature senescence. To understand the mechanistic defects underlying HGPS, a proteome analysis of dermal fibroblasts from progeria patients in comparison to fibroblasts from control individuals was performed. The focus was on the nuclear compartment as progerin accumulates in this compartment. Protein profiling using 2D DIGE gel electrophoresis coupled with mass spectrometry was performed to identify changes in the nuclear proteome. Bioinformatic analyses of the protein list found to be altered in the nuclear compartment in HGPS cells could be interconnected to a molecular network regulating the protein degradation pathways.

2) To determine new therapeutics derived from signaling pathway-based investigations, and establish the criteria of reversibility of cellular dysfunctions. Based upon the result of the 2D-DIGE proteomics, enhancers of the protein degradation pathways were analyzed. Autophagy and UPS can be activated via different upstream signaling pathways, which might impact the reversibility of HGPS cellular dysfunction. For this, two novel drugs, sulforaphane and forskolin, have been identified that can enhance the protein degradation pathways via different signaling

pathway targets. Sulforaphane activates protein degradation via Nrf2-Keap1 signaling pathway, forskolin enhances protein degradation via Sirt1 and AMPK signaling pathway. Furthermore, these drugs provide a low toxicity and side effects profile, and exhibit antioxidant properties. They are tested in control and HGPS cells and analyzed by several biochemical assays such as proteostasis levels and Western blotting.

3) To define a rapamycin analog with a more favorable pharmacokinetic profile, and study the impact of this rapalog on mitochondrial function. Rapamycin is known as a specific inhibitor of the mTOR signaling pathway. The inhibition of mTOR activates the protein degradation via autophagy.[30] Therefore rapamycin has been an obvious candidate, proving to improve HGPS cellular phenotype *in vitro*.[30] However, due to its high toxicity, the analysis of a rapalog that is FDA approved, less toxic, and available for intravenous injection has been undertaken to determine the extent to which it rescues HGPS cellular phenotype. This study further assesses the efficacy of rapamycin analogs by using temsirolimus.[150] Moreover, mTOR is known to play a crucial role for mitochondrial biogenesis.[32] This is the first report investigating the effect of rapamycin analogs on mitochondrial function. It is hypothesized that therapeutics need to target diverse signaling pathways to reverse the HGPS cellular phenotype than only activating protein degradation pathways. Temsirolimus is tested in control and HGPS cells and analyzed by several biochemical assays to examine proteostasis, mitochondrial function, DNA damage, nuclear morphology and others.

4) To investigate potential future therapy involving drug combinations on the HGPS cellular phenotype. Today, the HGPS children that are enrolled in the PRF clinical trial are treated with FTI. This treatment showed improvements in vascular stiffness, bone structure, and audiological status of the children.[11] FTI inhibits the farnesylation of progerin thereby preventing its incorporation into the nuclear envelope.[93] To test novel potential treatments that could ameliorate further the disease condition, search for additional candidate drugs for combination with FTI are underway. In April 2016, a phase I clinical trial with rapamycin analog everolimus in combination with FTI has been initiated. However, the efficacy and potential side effects of the combination *in vitro* are unknown.

In this study, the effect of such a treatment regimen has been tested *in vitro* by using FTI in combination with sulforaphane to determine the extent to which HGPS cellular phenotype can be restored. While FTI blocks the farnesylation pathway, sulforaphane enhances autophagy and mitochondria function via activation of Nrf1-Keap1 signaling.

This is the first study testing the effect of a drug combination. This regimen could open a completely new avenue for further drug testing of HGPS. A new application scheme and fast evaluation will be provided within this study, which allows rapid testing of new drug combinations. After verifying a beneficial drug sequence, control and HGPS cells are treated in combination and analyzed for proteostasis, mitochondrial function, and DNA damage response.

The outcome of these studies may significantly improve the recovery of HGPS children. Two novel drugs, sulforaphane and forskolin, and a drug combination, SFN and FTI, have been identified as candidate drugs for treatment of HGPS disease.
With the knowledge of this study, other age-related diseases such as Parkinson's and Alzheimer's disease could benefit from these therapeutic strategies. Indeed both age-related diseases exhibit similar functional defects as observed in HGPS condition, in particular alteration in proteostasis and mitochondria dysfunction.
The approach of 2D-gelelectrophoresis allows the rapid identification of defective signaling pathways, which is important for the screening for diseases with abnormal protein accumulations.

3 Materials and Methods

3.1 Materials

The following items were used for experimental procedures and cell culture.

3.1.1 Equipment

Table 4: Technical Equipment.

Device	Manufacturer
Axio Imager D2	Zeiss
Axiovert 40CFL	Zeiss
Balance Cp 4202 S	Sartorius
Biofuge fresco	Thermo Scientific
CASY Cell Counter	Roche
Certomat BS-1	Sartorius
Chemi-Doc MP Imaging System	BioRad
FLUOstar Omega	BMG Labtech
HeraSafe	Thermo Scientific
Incubator	Binder
InoLab pH 720	WTW
Mastercycler DNA Engine Thermal cycler PCR	Eppendorf
Mini Gel cell / Mini Trans-Blot cell	BioRad
Multifuge 3S-R+	Thermo Scientific
Nano Drop Spectrometer ND-1000	PeqLab
Power Pac Universal / HC	Bio-Rad
Real-time PCR MX3000P	Stratagene
Rocking platform	VWR
Sonifier 250	Branson
Thermomixer comfort	Eppendorf
Universal Hood II	BioRad
Vortex Genie-2	VWR

3.1.2 Consumables

Table 5: Consumables.

Name	Manufacturer
3.5, 6, 10 cm tissue culture dish	Falcon
4-20 % Mini-Protean TGX Precast Gel	BioRad
Eppendorf tubes (1.5, 2 ml)	Eppendorf
IPG strips	GE Healthcare
Luminunc 96- well plates white	Thermo Scientific
Membrane high-bond ECL (nitrocellulose)	Amersham
Microscope slides superfrost plus	Thermo Scientific
Mini Transblot filterpaper	BioRad
Polypropylen conical tubes (15, 50 ml)	Falcon
Serological pipets (1, 2, 5, 10, 25 ml)	Sarstedt
Superslip coverslips	Fisher Scientific
Tip one pipet tips (10, 20, 200, 1000 µl)	Starlab
Zip-tip C18	Millipore

3.1.3 Reagents

Table 6: Reagents.

Name	Manufacturer
0.25 % Trypsin EDTA	Invitrogen
2-Mercaptoethanol	BioRad
7-Amino-4-methylcoumarin	Sigma Aldrich
Agarose ultrapure	BioRad
Dapi Vectashield mounting medium	Vector Inc.
DEPC treated water	Invitrogen
Destreak solution	GE Healthcare
Dimethylformamide	Merck
DMEM (1x) GlutaMax 4.5 g/l D-glucose+pyruvate	Gibco
Dodecyl sulfate sodium salt (SDS)	Merck

Ethanol	Roth
Ethidium bromide	Sigma Aldrich
Fetal bovine serum (FBS)	Invitrogen
Forskolin	Sigma Aldrich
D-(+)-Galactose	Sigma Aldrich
Gentamycin (10 mg/ml)	Invitrogen
Glutamine (200 mM)	Invitrogen
Glycine	Sigma Aldrich
HEPES	Sigma Aldrich
2x Laemmli Buffer	BioRad
L-Sulforaphane	Sigma Aldrich
Magnesium chloride	Sigma Aldrich
Matrix solution	Agilent Technologies
Methanol	Roth
Modified porcine trypsin protease	Promega
Penicillin-Streptomycine (5,000 U/ml)	Invitrogen
Phosphate-buffered saline (PBS)	Invitrogen
Ponceau S	Sigma Aldrich
Potassium chloride	Fisher Scientific
Precision Plus protein standards (dual color)	BioRad
Sodium chloride	Merck
Sodium hydroxide	Merck
Sso Fast Eva Green Supermix	BioRad
Sucrose	Sigma Aldrich
Temsirolimus	Sigma Aldrich
Triton X-100	Sigma Aldrich
Trizma base	Sigma Aldrich
Tween 20	Sigma Aldrich
Urea	Sigma Aldrich

3.1.4 Kits

Table 7: Kits.

Name	Manufacturer
20S Proteasome Assay	Cayman Chemicals
Autophagy/Cytotoxicity Dual Staining	Cayman Chemicals
CellTiter-Glo Luminescent Cell Viability Assay	Promega
CellTox Green Cytotoxicity Assay	Promega
Clarity Western ECL substrate	BioRad
DCFDA - Cellular ROS Detection Assay	Abcam
Omniscript RT Kit	Qiagen
Oxygen Consumption/Glycolysis Dual Assay	Cayman Chemicals
QIAshredder Kit	Qiagen
RNeasy Mini Kit	Qiagen
Total ROS/Superoxide Detection Kit	EnzoLifescience

3.1.5 Antibodies

Table 8: Primary Antibodies.

Antibody	Species	IF	WB	Supplier	Order Number
Anti-53BP1	rabbit	1:2000	1:10000	Bethyl Lab.	A300-272A
Anti-pAMPKα	rabbit	1:100	1:1000	Cell signaling	2539
Anti-Beta-Actin	mouse	-	1:10000	Sigma Aldrich	A1978
Anti-Beta-Tubulin	mouse	-	1:1000	Sigma Aldrich	T8328
Anti-FHL1	rabbit	1:100	1:1000	Santa Cruz	sc-8017
Anti-H2A.X	mouse	1:250	-	Millipore	JBW301
Anti-HDJ-2	mouse	-	1:5000	Abcam	ab3089
Anti-HP1-γ	mouse	1:100	1:3000	Millipore	mab3450
Anti-Hsp27	mouse	-	1:3000	Abcam	ab2790
Anti-Lamin A	rabbit	1:500	-	Sigma Aldrich	L1293
Anti-Lamin A	mouse	1:500	-	Abcam	ab8980
Anti-Lamin A/C	mouse	-	1:5000	Thermo Fisher	mab636

Anti-Lamin A/C [151]	rabbit	-	1:5000	N. Chaudhary	-
Anti-Lamin A/C H110	rabbit	-	1:3000	Santa Cruz	sc-20681
Anti-Lamin B1	goat	1:60	1:500	Santa Cruz	sc-6217
Anti-Lap2α	rabbit	1:500	-	ImmuQuest	IQ175
Anti-LC3B	rabbit	-	1:20000	Sigma Aldrich	L7543
Anti-MTCO2	rabbit	1:250	1:5000	Abcam	ab79393
Anti-NPC [414]	mouse	1:500	-	Abcam	ab50008
Anti-PGC1α	rabbit	1:70	1:700	Santa Cruz	sc-13067
Anti-Prelamin A	goat	1:300	1:3000	Santa Cruz	sc-6214
Anti-Progerin	mouse	1:300	-	Enzo Lifesc.	ALX-804-662-R200
Anti-Progerin (S5) [88]	rabbit	1:1	1:2.5	K. Djabali	-
Anti-Proteasome 20S	mouse	-	1:5000	Abcam	ab22665
Anti-Sirt1	rabbit	1:100	1:3000	Abcam	ab32441
Anti-Rad51	rabbit	1:300	1:1000	Novus Biolog.	NBP2-32622
Anti-Ubiquitin	mouse	-	1:2000	Santa Cruz	sc-8017
p-E4BP1	rabbit	1:100	1:1000	Cell Signaling	9459
p-S6RP	rabbit	1:200	1:2000	Cell Signaling	2211

Table 9: Secondary Antibodies.

Antibody	**Species**	**Dilution**	**Supplier**	**Order Number**
α-mouse-Alexa Fluor 488	donkey	1:750	Invitrogen	A21202
α-rabbit- Alexa Fluor 488	donkey	1:750	Invitrogen	A21206
α-mouse- Alexa Fluor 555	donkey	1:750	Invitrogen	A31570
α-rabbit- Alexa Fluor 555	donkey	1:750	Invitrogen	A31572
α-goat- Alexa Fluor 555	donkey	1:750	Invitrogen	A11055
α-mouse-HRP	goat	1:5000	Jackson ImmunoResearch	115-035-003
α-goat-HRP	donkey	1:5000	Jackson ImmunoResearch	705-035-003
α-rabbit-HRP	goat	1:5000	Jackson ImmunoResearch	111-035-003

3.1.6 DNA Oligonucleotides

Table 10: List of oligonucleotides used for real-time PCR and qPCR.

Primer	Primer sequence
STUB1 fw	5'-CTGCTGTTGGACTGTGGACT-3'
STUB1 rev	5'-CTCGTGCTCACGGATTTTAT-3'
BAG3 fw	5'-GGAGTGCTGAAAGTGGAAGC-3'
BAG3 rev	5'-CTGGACTTGACCTGGGACAT-3'
BAG2 fw	5'-GCTTTGAGAGAAGCAGCAAC-3'
BAG2 rev	5'-GCTGGGGGTTTCTAATTGTT-3'
BAG1 fw	5'-AGCAATGAGAAGCACGACCT-3'
BAG1 rev	5'-GAAGTGCACCATGGAGAGGAG-3'
Hsp27 fw	5'-GTCCCTGGATGTCAACCACT-3'
Hsp27 rev	5'-GACAGGGAGGAGGAAACTTG-3'
Hsp70 fw	5'-GCTCTTTGCTGCTTCACTTC-3'
Hsp70 rev	5'-AGGTGGCAGTGTTGATTCAT-3'
Hsp90a fw	5'-GTCTAGTTGACCGTTCCGCA-3'
Hsp90a rev	5'-GAGGAGGCACCCTCAAGTTC-3'
Hsp90b fw	5'-GAAGTGCACCATGGAGAGGAG-3'
Hsp90b rev	5'-GCGAATCTTGTCCAAGGCATC-3'
LMNA/C fw	5'-GCAAAGTGCGTGAGGAGTTT-3'
LMNA/C rev	5'-GAGTTCAGCAGAGCCTCCAG-3'
Progerin fw	5'-ACTGCAGCAGCTCGGGG-3'
Progerin rev	5'-TCTGGGGGCTCTGGGC-3'
LMNA fw	5'-GTGAGTACAACCTGCGCTCG-3'
LMNA rev	5'-GAGTGACCGTGACACTGGAG-3'
GAPDH fw	5'-CTCTGCTCCTCCTGTTCGAC-3'
GAPDH rev	5'-TTAAAAGCAGCCCTGGTGAC-3'

3.1.7 Cell culture media

The following media were prepared under sterile conditions according to the recipes below.

Table 11: Cell culture medium-Fibroblast growth medium containing glucose.

Fibroblast growth medium containing glucose	
DMEM (high glucose)	500 ml
FBS	75 ml (15 %)
Gentamicin	2.5 ml (0.5 %)
Penicillin-Streptomycin	5 ml (1 %)
Glutamine	5 ml (1 %)

Table 12: Cell culture medium-Fibroblast growth medium containing galactose.

Fibroblast growth medium containing galactose	
DMEM (no glucose)	500 ml
FBS	75 ml (15 %)
Gentamicin	2.5 ml (0.5 %)
Penicillin-Streptomycin	5 ml (1 %)
Glutamine	5 ml (1 %)
Sodium pyruvate	5.75 ml (1.0 mM)
Galactose	1.035 g (10 mM)

Table 13: Cell culture medium-Freezing medium.

Freezing medium	
FBS	9 ml
DMSO	1 ml

3.1.8 Buffers

Table 14: TBS buffer.

10x TBS buffer	
Trizma	60.55 g
Sodium chloride	87.66 g
Milli-Q water	Ad 1 l

Table 15: TBS-Tween and PBS-Tween.

1x TBS-T and PBS-T	
10 x TBS/ 10x PBS	100 ml
Milli-Q water	900 ml
Tween 20	500 µl

Table 16: Blocking buffer for Immunofluorescence.

Blocking buffer for Immunofluorescence	
FBS	7.5 ml (15 %)
Tween 20	150 µl
PBS	Ad 50 ml

Table 17: 2x2-D sample buffer.

2x2-D sample buffer	
Urea	8 M
CHAPS	4 %
DTT	20 mg/ml
Pharmalytes	2 %
Bromphenol blue	Trace amount

Table 18: Buffer A.

Buffer A	
Hepes/KOH (pH 7.9)	10 mM
Magnesium chloride	1.5 mM
Potassium chloride	10 mM
DTT	0.5 mM
Protease inhibitor cocktail	
Phosphatase inhibitor cocktail	

Table 19: Buffer B.

Buffer B	
Trizma (pH 7.5)	10 mM
Magnesium chloride	3.3 mM
sucrose	0.25 mM

Table 20: Buffer X.

Buffer X	
Trizma (pH 8.0)	70 mM
Triton-X 100	0.045 % v/v

Table 21: Equilibration buffer-1.

Equilibration buffer-1	
Trizma (pH 8.8)	50 mM
Urea	6 M
Glycerol	30 %
SDS	2 %
DTT	10 mg/ml
Bromphenol blue	Trace amount

Table 22: Equilibration buffer-2.

Equilibration buffer-2	
Trizma (pH 8.8)	50 mM
Urea	6 M
Glycerol	30 %
SDS	2 %
Iodacetamide	45 mg/ml
Bromphenol blue	Trace amount

Table 23: Lysis buffer for nuclei preparation.

Lysis buffer for nuclei preparation	
Trizma (pH 8.8)	30 mM
Urea	7 M
Thiourea	2 M
CHAPS	4 %

Table 24: Rehydration buffer.

Rehydration buffer	
DTT	20 mg/ml
Urea	7 M
Thiourea	2 M
CHAPS	4 %
Pharmalytes	1 %
Bromphenol blue	Trace amount

Table 25: 10x SDS gel running buffer.

10x SDS gel running buffer	
Glycine	144 g (1.92 M)
Trizma	30 g (0.248 M)
SDS	10 g (1 %)
Milli-Q water	Ad 1 l

Table 26: Western blot transfer buffer.

Western blot transfer buffer	
Glycine	11.3 g (150 mM)
Trizma	2.42 g (20 mM)
MeOH	200 ml (20 %)
SDS	1 g (0.1 %)
Milli-Q water	Ad 1 l

Table 27: Sample Laemmli buffer.

Sample Laemmli buffer	
2x Laemmli buffer	950 µl
2-Mercaptoethanol	50 µl
Proteinase inhibitor cocktail	10 µl
200 mM PMSF	5 µl

Table 28: Milk buffer.

Sample Laemmli buffer	
Milk powder (non-fat)	0.6 g
Tween-20	150 µl
PBS	Ad 50 ml

3.2 Cell culture and Drug treatments

Dermal fibroblasts from subjects with HGPS were obtained from the Progeria Research Foundation Cell and Tissue Bank. The following fibroblast strains were used: HGADFN003 (M, age 2), HGADFN127 (f, age 4), HGADFN155 (f, age 1), HAGDFN164 (f, age 5), HGADFN188 (f, age 2), and HGADFN178 (f, age 6).

Age-matched control fibroblasts from young skin were obtained from the Coriell Institute for Medical Research (Camden, NJ). The following control strains were used: GMO1651C (f, age 13), GMO3348E (m, age 10), GMO3349C (m, age 10), GMO323B (m, age 11), and GMO8398A (m, age 8).

Adherent cultured cells were grown in 10 cm cell culture dishes in an incubator with 5 % CO_2 and 37°C in fibroblast growth medium. To keep the cells in the logarithmic growth phase, cells were passaged according to their doubling time by splitting. For this, cells were washed with PBS and incubated with 1.5 ml 0.25 % trypsin for 10 minutes. Trypsinized cells were resuspended in 6.5 ml fresh DMEM medium and collected by centrifugation at 1,000 x g for 5 minutes. After centrifugation, the medium was removed and the cells were seeded in 8 ml of fibroblast growth medium and splitted according to the planned experiments.

Cells were treated as indicated in the following table.

Table 29: Final concentration of Compounds used in experiments.

Compound	Concentration
L-Sulforaphane (SFN)	1.0 µM
	2.0 µM
	3.0 µM
Temsirolimus (Tem)	1.0 µM
Forskolin (Fors)	2.5 µM
Farnesyltransferase inhibitor (FTI)	0.0625 µM
	0.25 µM
	0.5 µM
	1.0 µM
	1.5 µM

To every treatment, mock-treated cells containing the vehicle (DMSO) were carried along. Unless otherwise stated, cells were grown in Fibroblasts growth medium containing glucose.
Wild-type and progerin mouse fibroblasts harboring the G609G mutation were kindly provided by Prof. Carlos Lòpez-Otin (Biochemistry and Molecular Biology, Universidad de Oviedo). Cells were cultured as stated for human fibroblasts and treated with sulforaphane only.

3.3 One-dimensional gel electrophoresis

3.3.1 SDS-gel electrophoresis

Sodium dodecyl sulfate polyacrylamide gel electrophoresis (SDS-PAGE) is a technique to separate proteins according to their electrophoretic mobility. The samples of a SDS-gel electrophoresis have identical charge per unit due to binding of SDS. This interaction results in fractionation by size.[152]
For SDS-PAGE under reducing conditions, gel solution with 30 % acrylamide in the resolving part was prepared using an acrylamide/bisacrylamide solution. Precast gels were purchased from BioRad with a concentration of 4-20 %.
Freshly harvested cell pellets of mock-treated and drug-treated fibroblasts were collected and washed with PBS. For the isolation of proteins Laemmli-sample buffer was added in a ratio of 100 µl to 1 x 10^6 cells. The probes were heated 3 times for 5 minutes at 95 °C. Protein concentrations were determined by using the Dotblot quantification of 2 µl drops of samples and a dilution series of BSA standard. Samples were adjusted to 30 µg and loaded on the gel. A molecular weight standard was loaded as a running control. The gel was run at a constant voltage of 210 V.

3.3.2 Western blot analyses

Tobwin et al. developed the Western blot method in 1979. This method is an analytical technique used to detect specific proteins in a given sample of tissue homogenate or extract with poly- or monoclonal antibodies.[153]
Electrophoretic transfer of proteins from polyacrylamide gels to a polyvinylidene fluoride (PVDF) membrane was performed by use of a wet blot apparatus. Transfer was carried out for 1.5 hours at 400 mA at room temperature. After the transfer, the membrane was stained with Ponceau-S in order to verify the transfer efficiency. The Ponceau-S was removed from the membrane by using PBS and the membrane was directly used for protein detection.

3.3.3 Detection of transferred proteins with specific antibodies

The detection of the proteins is called immunodetection, which uses the principle of antigen-antibody interactions. An antigen-specific primary antibody binds at the epitope of the antigen, which is fixed on the membrane. Another secondary antibody in turn binds a specific region of the primary antibody. The secondary antibody is labeled with an enzyme e.g. HRP (horseradish peroxidase). This enzyme catalyzes the conversion of luminol to its oxidized form. The chemiluminescence of the oxidized form can be detected.[153]
For protein detection with antibodies, the activated membrane was incubated in milk buffer over night at 4 °C or 1h at room temperature. Then, the membrane was incubated with the primary antibody (Table 8). To remove unbound antibody, the membrane was washed with PBS-T and subsequently, incubated with the secondary antibody conjugated to horse radish peroxidase (HRP) at room temperature (Table 9). After washing the membrane in PBS-T, protein bands were visualized with ECL substrate (luminol and hydrogen peroxide) by ChemiDoc MP and Image Lab software. Relevant bands were analyzed and normalized to internal b-actin.

3.4 Two-dimensional gel electrophoresis

3.4.1 Nuclei Preparation

Control and HGPS cells in growth phase were collected in parallel, and washed in PBS 3 times. The cells were pelleted by centrifugation (1,900 x g, 10 minutes). On average, 10^7 cells were used for this approach. Each 10^7 cells were resuspended in 5 ml of buffer A (10 mM Hepes/KOH pH 7.9, 1.5 mM $MgCl_2$, 10 mM KCl, 0.5 mM DTT supplemented with protease inhibitor and phosphatase inhibitor cocktails), incubated for ten minutes on ice, and then broken with 12-15 strokes in a tight dounce homogenizer. The fractionation steps were carried at 4 °C. The crude nuclear (pellet) and cytoplasmic (supernatant) fractions were isolated by centrifugation at 800 x g for 10 minutes and 4 °C. The pellet was resuspended in 10 ml of buffer B containing 10 mM Tris/HCl pH 7.5, 3.3 mM $MgCl_2$ and 0.25 M sucrose and centrifuged for 5 minutes at 1,000 rpm. The resulting pellet was resuspended in 2.5 ml of 10 mM $MgCl_2$ and 0.25 M sucrose, layered over a 2.5 ml of 0.5 mM $MgCl_2$, and 0.35 M sucrose. The solution was pelleted by centrifugation at 2,500 rpm for 10 minutes. That pellet was correspond to the purified nuclei preparation and was verified by microscopy. Nuclei pellets were analyzed two by two. One control and one HGPS nuclei pellet were resuspended in two-dimensional lysis buffer (30 mM Tris-HCl, pH 8.8, 7 M urea, 2 M thiourea, and 4 % CHAPS) at a concentration between 4-6 mg/ml. The mixture was sonicated at 4°C followed by shaking for 30 minutes at room temperature. The samples were centrifuged for 30 minutes at 14,000 rpm, and the supernatant was collected. Protein concentration was measured using the Bradford assay.

3.4.2 Protein determination by Bradford Assay

The Bradford protein assay is a spectroscopic analytical procedure used to measure the concentration of protein in a solution. It is based on an absorbance shift of the dye Comassie Brilliant Blue G-250 under acid conditions when a redder form of the dye is converted into a bluer form on binding to the protein.[68]

The 5 x Bradford Reagent was diluted in the ratio of 4:1 with water and run through a gravity filter. The standards were created from BSA stock (1 mg/ml) to give a standard curve from 0-1 mg/ml. Therefore, the amounts of BSA and buffer were used as written in Table 30.

Table 30: Preparation of the standards.

Sample	BSA amount [µl]	Buffer amount [µl]
Sample #1 (0.0 mg/ml)	0	30
Sample #2 (0.2 mg/ml)	6	24
Sample #3 (0.4 mg/ml)	12	18
Sample #4 (0.6 mg/ml)	18	12
Sample #5 (0.8 mg/ml)	24	6
Sample #6 (1.0 mg/ml)	30	0

The standards were plate in a 96-well plate in triplicates (10 µl per well) as well as the protein samples. 200 µl of diluted Bradford reagent was added to each well, and let stand for 5 minutes. The plate was set into the ELISA-reader and measured at 595 nm. The standard curve and the data from Bradford were used to determinate unknown protein concentration.

3.4.3 Two-dimensional gel electrophoresis

The analysis of the proteome as the final level of gene expression started out with techniques based on 2-D gel electrophoresis as introduced by O'Farrell and Klose (1975). 2-D gels may separate up to 10,000 protein spots on one gel.[154]
High-resolution 2-D gel electrophoresis can reveal virtually all proteins present in a cell or tissue at any given time, including those with posttranslational modifications and rapid turnover rates.[82]
The 2-D gel electrophoresis is a technique that combines first-dimension isoelectric focusing in a polyacrylamide gel with a pH gradient and a high concentration of urea with a second-dimension separation on SDS polyacrylamide gels. In the first dimension, the proteins are separated according to their charges (pI), and in the second dimension according to their molecular weight (MW). Starting materials, such

as cell lysates or tissue extract, can be applied to gels directly and fractionated with high resolution. The separated proteins are embedded in the matrix where they can be detected with high sensitivity.[82]

3.4.3.1 CyDye labeling

For each sample, 30 µg of protein was mixed with 200 pmol CyDy2 or Cy3 and kept in the dark on ice for 30 minutes. The labelling reaction was stopped by adding 10 mM lysine to each sample, and incubating in the dark on ice for an additional 15 minutes. The labelled samples were mixed together. 2 x 2-D Sample buffer, destreak solution, and rehydration buffer were added to a final volume of 260 µl. The samples were mixed well and spun down before loading onto the strip holder.

3.4.3.2 Isoelectric focusing and SDS-PAGE

After loading the labeled samples to pH 3-10 linear IPG strips, the isoelectric focusing (IEF) was run for 12 hours rehydration at 20 °C, followed by 500 V for 1,000 VHr, 1,000 V for 2,000 VHr, and 8,000 V for 24,000 VHr. Upon finishing the IEF, the IPG strips will incubated in freshly made equilibration buffer-1 for 15 minutes with gentle shaking. Then the strips were rinsed in freshly made equilibration buffer-2 for 10 minutes with gentle shaking. Next, the IPG strips were rinsed in SDS-gel running buffer before transferring into 12 % SDS-gels (18 × 16 cm) followed by sealing with 0.5 % Agarose in SDS- polyacrylamide gel electrophoresis (SDS-PAGE) running buffer. The SDS-gels were run at 15 °C until the dye front ran out of the gels.

3.4.3.3 Image scan and data analysis

Gel images were scanned immediately following the SDS-PAGE using Typhoon TRIO (Amersham BioSciences) of Cy2, and Cy3 labeled protein images by excitation at 488, 532, and 633 nm, respectively, and emission at 520, 590, and 680 nm, respectively, at a spatial resolution of 100 µm. The scanned images were then analyzed by Image Quant software Version 6.0 (Amersham BioSciences), followed by in-gel analysis using DeCyder software Version 6.0 (Amersham BioSciences). The DeCyder spot detection algorithm calculated ratio (volume of a spot from the secondary image/volume of the corresponding spot from the primary image), and a threshold of 1.5-fold change were set.

3.4.3.4 Protein identification by mass spectrometry

Spot picking and Trypsin digestion: The spots of interest were picked up by Ettan Spot Picker (Amersham BioSciences) based on the in-gel analysis and spot picking design by DeCyder software. The gel spots were washed a few times, then digested in-gel with modified porcine trypsin protease (Trypsin Gold, Promega). The digested tryptic peptides were desalted by Zip-tip C18 (Millipore), and peptides were elute from the Zip-tip with 0.5 µl of Matrix solution (Agilent Technologies) and spotted on the matrix-assisted laser desorption/ionization (MALDI) plate (model ABI 01-192-6-AB). MALDI-time of flight (TOF; MS) and TOF/TOF (tandem MS/MS) was performed on an ABI 4700 mass spectrometer (Applied Biosystems). MALDI-TOF mass spectra was acquired in reflection-positive ion mode, averaging 4,300 laser shots per spectrum. TOF/TOF tandem MS fragmentation spectra was acquired for each sample, averaging 4300 laser shots per fragmentation spectrum on each of the ten most abundant ions present in each sample (excluding trypsin autolytic peptides and other known background ions). Both of the resulting peptide mass and the associated fragmentation spectra were submitted to GPS Explorer version 3.5 equipped with MASCOT search engine (Matrix Science) to search the database of National Center for Biotechnology Information non-redundant (NCBInr). The parameters were set at 800-4000 Da to create the “peak list.” Searches were performed without constraining protein molecular weight or isoelectric point, with variable carbamidomethylation of cysteine and

oxidation of methionine residues, and with one missed cleavage allowed in the search parameters. Mass tolerance was set at 0.3 Da and 100 ppm. Candidates with either protein score confidence interval (C.I.) % or Ion C.I. % greater than 95 will consider significant.

3.4.3.5 Bioinformatic research

The identified proteins that are involved in the proteostasis of a cell were analyzed by UniProt, Ingenuity, and NCBI. For this, involved pathways of the proteins were analyzed, designed, and combined in order to find differences or similarities between control and HGPS cells.

3.5 Measurement of proteasome activity in fibroblasts

The ubiquitin-proteasome pathway is the major proteolytic system in the cytosol of eukaryotic cells. The proteasome catalyzes the selective degradation of short-lived regulatory proteins and the rapid elimination of proteins with abnormal conformation. The proteasome complex is known as the 26S proteasome and contains one 20S core particle structure and two 19S regulatory caps. The 20S proteasome is the catalytic core of the proteasome complex, and is responsible for the breakdown of key proteins involved with apoptosis, DNA repair, endocytosis, and cell cycle control.[133] The multicatalytic 20S proteasome has three peptidase activities (trypsin-like, chymotrypsin-like, and peptidylglutamyl-peptide hydrolyzing).[155]

Treated and mock-treated cells were harvested and counted using CASY cell counting technology. The pellets were washed and seeded by a density of $1x10^5$ cells in 96-well plate. The cells were allowed to attach overnight. For cell lysis, 100 µl of Lysis buffer were added and the cells were incubated with the Lysis buffer for 30 minutes. The solution was centrifuged at 1,000 x g for 10 minutes. 90 µl of the Lysate were transferred to a new well and 10 µl of AMC-conjugated chymotrypsin substrate (2.5 µmol) were added. The plates were incubated for 1h at 37 °C. Each cell line was done in duplicates or triplicates. To each of these wells, 10 µl of AMC-conjugated chymotrypsin substrate were added. The fluorescent intensity of each well (excitation

= 360 nm, emission = 480 nm) was read immediately, after 1 hour of incubation at 37 °C with FLUOstar Omega.

3.6 Autophagy measurements in fibroblasts

The intensity levels of autophagic vacuoles in fibroblasts were measured using an Autophagy/Cytotoxicity Dual Staining Kit. Mock-treated and drug-treated cells were treated for the desired period, harvested, and equal amounts were seeded on a 96-well plate in triplicates. Cells were allowed to attach at 37 °C in their corresponding medium. Plates were centrifuged and the medium was aspirated. Monodansylcadaverine was added to the wells at a ratio of 1:1,000 in a final volume of 100 µl. The plates were incubated at 37 °C for 10 minutes. Then, the cells were washed with Assay buffer. 100 µl of Assay buffer were added to the wells before measuring the autophagic vacuole intensity (Excitation=335 nm, Emission=512 nm).

3.7 Cell toxicity measurements of fibroblasts

Cytotoxicity was determined using a CellTox^{TM} Green Kit. Cells were seeded in 96-well plate at a density of 6000 cells per well. The plate was incubated for the desired exposure period of 5 hours, 24 hours, and 48 hours with DMSO, SFN, Tem, and Fors. CellTox^{TM} Green Reagent was prepared according to the manufacturer's instruction of the Endpoint Method (1:500). 100 µl of the Reagent were added to the wells and the plate was mixed for one minute in an orbital shaker. Afterwards, the plate was incubate for at least 15 minutes at room temperature shielded from light. Fluorescence was measured at an excitation of 485-500 nm and an emission of 520-530 nm.

3.8 Population doublings (PPD)/Cumulative population doublings (CPD) determination

Cells were seeded in triplicates at a density of variable cell amounts per 10cm-dish. Cells were cultivated for the desired period in DMEM high glucose medium containing the vehicle DMSO or the drugs. After the growth period, cells were harvested, and the number of cells was measured with a CASY® Cell Counter. PPDs were determined using the formula: n=3.32 (log (cells harvested) - log (cells seeded)), where n= the final PPD number at the end of a given subculture. CPDs were determined using the following formula: n= 3.32 (log (cells harvested) – log (cells seeded)) + X, where n= the final CPD number at the end of a given subculture and X= former CPD as described previously.[95]

3.9 Measurement of reactive oxygen species (ROS) in fibroblasts

Reactive oxygen species were measured using the DCFDA cellular ROS Detection Assay Kit. Mock-treated and drug-treated cells were seeded in a 96-well plate at a density of 32,000 cells per well in their corresponding medium. Cells were allowed to attach overnight. Then, cells were washed with 1x PBS and incubated with 25 µM DCFDA for 45 minutes at 37 °C. The reagent was removed and the cells were washed with 1x PBS. After addition of 100 µl of 1x buffer solution to the wells, fluorescence was measured at Ex485 nm/Em535 nm.

3.10 Measurement of intracellular ATP content in fibroblasts

The intracellular ATP content of mock-treated and treated fibroblast cells was measured using a CellTiter Glo Luminescent Cell Viability Kit. Cells were incubated for the desired period in vehicle-containing (DMSO) or drug-containing medium. Then, cells were harvested and seeded in equal densities (32,000 cells) in a 96-well plate in triplicates. Cells were allowed to attach at 37 °C overnight in their corresponding medium. The plates were equilibrated at room temperature for 30 minutes, centrifuged, and the medium was aspirated. Afterwards, 100 µl of CellTiter Glo reagent was added

to the wells. The plates were mixed for two minutes in an orbital shaker, followed by a 10-minute incubation. An ATP standard was prepared and added to unused wells in triplicates. The luminescence intensity was measured.

3.11 Measurement of Mitotoxicity in fibroblasts

Cells were cultured in either glucose or galactose medium supplemented with 1.0 µM temsirolimus. For the measurement, cells were treated for 2h with galactose ± temsirolimus and compared to mock-treated cells in glucose medium. Cells in glucose medium supplemented with temsirolimus were carried along. After treatment, measurement were performed using a Mitochondrial ToxGlo Assay from Promega. For this, cells were seeded at a density of 10,000 cells per well in a 96-well plate format. Cells were allowed to attach over night at 37 °C before the treatment was carried out. To measure cytotoxicity, cells were incubated with a bis-AAF-R110 substrate for 30 min at 37 °C before the fluorescence was measured. The same plate was used afterwards for measuring the intracellular ATP content. Thus, substrate was added to the wells and mixed for 5 min. Luminescence signal was measured.

3.12 Measurement of total ROS and superoxide in fibroblasts

For fluorescence microscopy, cells were splitted directly on to coverslips and treated with the test compounds or the vehicle. On the day of the experiment, the medium was replaced with fresh medium. A ROS inhibitor (N-acetyl-L-cysteine) was added 30 minutes before Induction. For induction, ROS/Superoxide Detection solution was added at the same volume. Coverslips were incubated at 37 °C for 30 min. After 20 minutes, ROS production was induced with pyocyanin and allowed to incubate for another 10 minutes at 37 °C. Then, coverslips were washed and covered with 1x washing buffer. Fluorescence was detected at Ex/Em: 490/525nm (green, ROS) and Ex/Em: 550/620nm (orange, superoxide).

For fluorescence microplate assays, cells were cultured in normal medium and medium containing the vehicle or test compound. The day before the experiment, cells were seeded in a 96-well clear bottom/black wall plate at a density of 20.000 cells/well.

Cells were allowed to attach over night at 37 °C. Then, cells were washed and treated according manufacturer's instructions for negative and positive control. 100 µl of ROS/Superoxide detection solution were added and incubated for 60 minutes at 37 °C. Plate was read (bottom reading) with FLUOStar and standard fluorescein (488/520nm) and rhodamine (550/610nm) filter sets.

3.13 Measurement of Oxygen Consumption and Glycolysis in fibroblasts

Oxygen consumption and glycolysis levels of mock-treated and treated fibroblast cells were measured using an Oxygen Consumption/Glycolysis Dual Assay Kit. Cells were incubated for the desired period in mock-treated or drug-treated medium. Then, cells were harvested and seeded in equal densities in a 96-well plate in triplicates. Cells were allowed to attach at 37 °C overnight in their corresponding medium. For oxygen consumption, 10 µl MitoXpress Solution were added to the wells and overlaid with 100 µl HS Mineral Oil. The fluorescence intensity was measured at 37 °C at Ex/Em: 380±20nm/650±20nm. For glycolysis, a new 96-well plate was used and to every well 90 µl of Assay buffer was added. Next, 10 µl of the samples from the oxygen consumption plate was transferred to the new plate and 100 µl of Reaction solution was added. The plate was incubated with gentle agitation for 30 minutes at room temperature. The absorbance was read at 490nm with FLUOStar.

3.14 Measurement of MAPK and PI3K signaling pathway activity

The activity of MAPK and PI3K signaling pathways was measured using Muse PI3K/MAPK Dual Pathway Activation Kit. Control and HGPS cells were mock-treated or 2.5 µM forskolin-treated for different time periods. Then, cells were collected and washes with PBS. Cells were resuspended with 50 µl 1x Assay buffer per 100,000 cells. Equal parts of Fixation buffer were added to the cell suspension and mixed by gently pipetting followed by 10 minutes incubation on ice. Cells were centrifuged and the supernatant was discarded. Permeabilization buffer was added to the cells for 10 minutes on ice. Cells were centrifuged and the permeabilization buffer was replaced

by 90 µl Assay buffer per 100,000 cells. Subsequently, 10 µl antibody working cocktail were added for 30 minutes in the dark at room temperature. Antibody solution contained anti-phospho-ERK1/2 and anti-phospho-Akt. Following incubation step, 100 µl Assay buffer were added before the samples were centrifuged and the supernatant was discarded. Samples were measured with the Muse Cell Analyzer.

3.15 Immunocytochemistry

Mock-treated and drug-treated fibroblast cells were grown directly on coverslips. Cells were fixed in ice-cold methanol at -20 °C for 10 minutes. Cells were permeabilized with 0.3 % Triton X-100, followed by blocking with 5 % FBS in PBS. Then, cells were incubated for 2 hours with primary antibodies (Table 8) and for 1 hour with secondary antibodies (Table 9), separated by washing steps. Samples were counterstained with Dapi Vectashield mounting medium. Time-matched images were acquired using an Axioplan fluorescence microscope.

3.16 Real-time and reverse transcription Polymerase Chain Reaction (PCR)

PCR was developed by Kary Mullis in 1983. PCR is a laboratory technique which is used to amplify, detect and quantify targeted DNA molecules.[156] The quantity of the DNA can be an absolute number of copies or a relative amount when normalized to additional genes. Non-specific fluorescent dyes e.g. SYBR green intercalate with any double-stranded DNA which allows the detection of the genes. The key feature is that the amplified DNA is detected as the reaction progresses in real time whereas the product of PCR is detected at its end (reverse transcription). [157,158]

3.16.1 RNA Isolation

Fibroblasts were grown until they reached a confluency of 90 %. Cells were collected, washed with PBS, and RNA was isolated with the RNeasy Mini Kit. Cells were disrupted by adding 600 µl of buffer RLT (containing β-Mercaptoethanol). The solution was transferred directly into a QIAshredder spin column, and centrifuged for 2 min at full speed. One Volume of 70 % Ethanol was added to each homogenized lysate. 700 µl of each sample were transferred to an RNeasy spin column and centrifuged. Afterwards, 700 µl of buffer RW1 and 500 µl buffer RPE (twice) were added to the RNeasy spin column with centrifugation steps in between. The RNeasy spin column was placed on a new tube and 30 µl of RNAse-free water were added. A last centrifugation step was performed to elute the RNA. RNA amount was measured using NanoDrop. RNA was stored at -80 °C until use.

3.16.2 cDNA synthesis

Fibroblast-cDNA was synthesized out of total cellular RNA by using Omniscript Reverse Transcriptase. Briefly, 2 µg RNA, 2 µl 10x reaction buffer, 2 µl 10 mM dNTP-Mix, 2 µl Oligo-dT-primer, 1 µl RNAse-Inhibitor, and 1 µl reverse transcriptase were mixed together and filled up to a volume of 20 µl with DEPC water. The following cDNA synthesis was performed at 37 °C for 1 hour with the Thermocycler assuming a final cDNA concentration of 50 ng/µl.

3.16.4 Reverse transcription PCR

Primers were designed using Primer3 (http://frodo.wi.mit.edu/cgibin/primer3/primer3_www.cgi). The efficiency of primers were tested by using reverse transcription PCR (RT-PCR). The list of genes that were validated by RT-PCR and their corresponding primers are shown in Table 10.
For the approach, Taq DNA polymerase Kit from Qiagen was used. For this, 2 µl 10x buffer, 2 µl 25 mM $MgCl_2$, 0.4 µl 10 mM dNTP, 0.1 µl Taq-polymerase were mixed and filled with DEPC water to a final volume of 16 µl. Then, 1 µl 1 µM forward primer, 1 µl

1 µM reverse primer, and 2 µl of cDNA were added to the sample. The reaction was performed by using the Thermocycler and the following program (Table 31).

Table 31: Reaction cycle of reverse transcription PCR for primer testing.

Cycles	Time	Temperature
1x	15 min	95 °C
50x	10 sec	95 °C
	45 sec	T_m (primer specific)
	30 sec	72 °C
1x	10 min	72 °C

To analyze the PCR product, a 1.5 % agarose gel was prepared with high purity agarose, 0.4 % EtBr and 1xTBE buffer. To 20 µl of the reaction samples, 6 µl of Orange-G were added. Thereafter, 12 µl of the samples were added to the lanes and a 100 bp marker was also loaded. The gel was run at 180V until the loading front reaches the end of the gel.
If the amplicon was not detectable with the given T_m of the primers, Gradient-PCR were performed. In this approach, T_m was variable within a 4 °C variation. The best T_m was chosen according to the best amplicon signal in the gel.

3.16.3 Real-time PCR

Real-time PCR reactions contained Power SYBR Green PCR mastermix (Applied Biosystems), 300 nM of each primer (Table 10), and 100 ng of template in a 20 µl reaction volume. Amplification was carried out using the Mx3000P Real-Time PCR Detection System (Stratagene) with an initial denaturation at 95°C for two minutes followed by 40 cycles at 95 °C for 35 seconds, 59-60 °C for 20 seconds, and 70 °C for 30 seconds. Three experiments were performed for each assay in which the samples were run in triplicate. GAPDH was used as an endogenous control and quantification was performed using the relative quantification method where the real-time PCR signal of the experimental RNA was measured in relation to the signal of the control. The 2(ΔΔCT) method was used to calculate relative changes in gene expression.[159]

3.17 Statistical Analyses

The results are presented as the mean ± S.D. Comparisons were performed using Student's T-Test. A p-value≤0.05 was considered statistically significant.

4 Results

At the beginning of this project, proteomic analysis of HGPS fibroblasts has been barely performed. Drug interventions have been chosen according to their ability of farnesylation inhibition and longevity increase. However, a direct link to the HGPS signaling pathways was missing. Within this project, the impact of progerin on the nucleoproteome has been identified. This allows the identification of defective signaling pathways by using a novel approach of HGPS proteomic analysis. In order to identify altered nuclear protein expressions, a 2D-gelelctrophoresis was performed of isolated nuclear proteins of control and HGPS fibroblasts followed by mass spectroscopy. Bioinformatic analysis allowed the connection of these proteins to signaling pathways. The data were verified by proteostasis assays, Western blot, and real-time PCR.

4.1 Basic analysis of control and HGPS fibroblast cells

4.1.1 Proteomic analysis of HGPS nuclei

As major cellular alterations occur in the nucleus, nuclear HGPS protein extracts were quantitatively compared to normal dermal fibroblasts using two-dimensional difference gel electrophoresis (2D-DIGE) followed by mass spectroscopy of selected protein spots (Fig. 9).

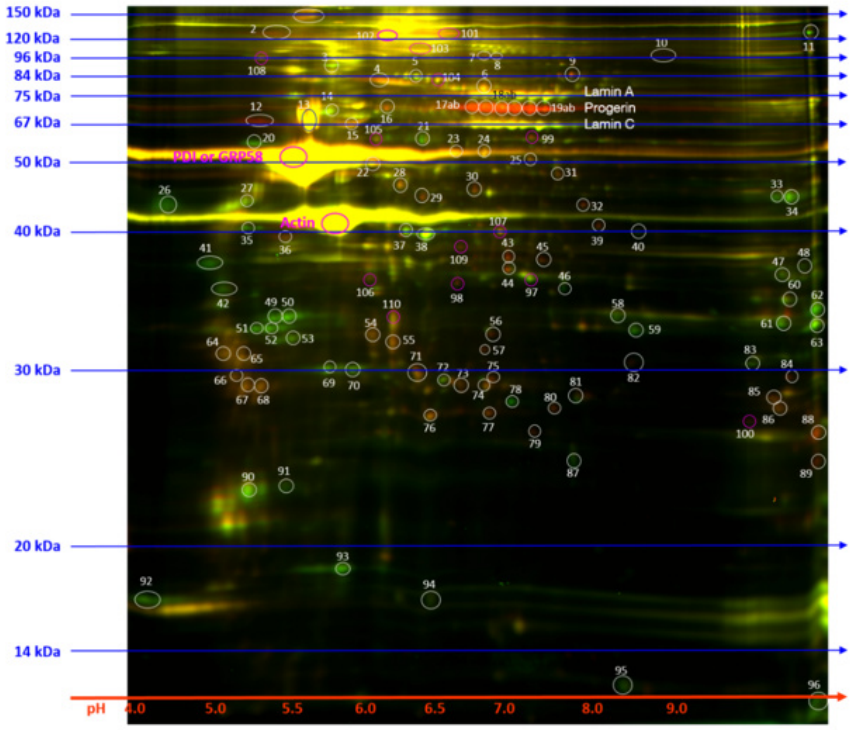

Figure 9: 2D-DIGE analysis of the nuclear proteome in HGPS fibroblasts. HGPS and normal fibroblast nuclei were labeled with CyDye DIGE fluors. Both samples were simultaneously separated on a single 2D gel, using IEF with a linear pH 3–10 IPG strip in the first dimension followed by a 12 % SDS-PAGE in the second dimension. After electrophoresis, the gel was scanned using a Typhoon image scanner. ImageQuant software was used to generate the presented image data. The control nuclei preparation (GMO3349C) is labeled in green, and the HGPS nuclei preparation (HGADFN127) is labeled in red; the merged image corresponds to the overlay of both samples. Representative gel image is shown.

Proteins are shown in red that have a higher expression in HGPS fibroblasts, proteins with higher expression in control fibroblasts are shown in green. Equally expressed proteins appear yellow.

An average of 1,000 protein spots was detected on gels and almost 114 spots were found to be changed by more than 1.5-fold in HGPS nuclei by comparison to control nuclei. The 40 most significantly altered protein spots were identified by peptide mass-fingerprint analysis. Tandem mass spectroscopy fragmentation spectra were acquired for each of the ten most abundant ions present in each protein spot that were submitted for a search to identify proteins from the NCBInr database. Candidates were considered significant when they showed a protein score confidence interval (C.I.) % or Ion C.I. % greater than 95.

The most altered proteins were found to be spots 17-19a/b (Fig. 9). These spots were highly represented in HGPS nuclei showing 10- to 20-fold increase by comparison to normal nuclei. Mass spectroscopy revealed the spots as the progerin protein, the disease-causing lamin A variant responsible for HGPS. As expected, the progerin spots migrated between lamin A (spot 111 to 112) and lamin C (spots 113 to 114) as indicated in figure 10.

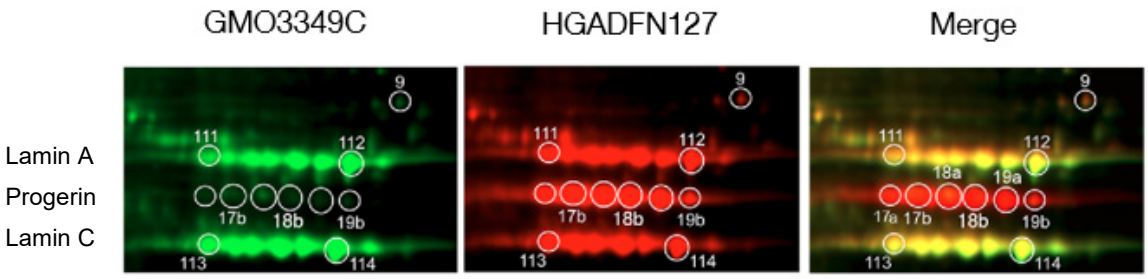

Figure 10: Enlarged gel images of the 2D-DIGE analysis. Images correspond to enlarged gel images that indicate the positions of A-type lamin protein spots as indicated. The control nuclei preparation (GMO3349C) is labeled in green, and the HGPS nuclei preparation (HGADFN127) is labeled in red; the merged image corresponds to the overlay of both samples.

Several protein spots were found in a linear rage according to their isoelectric point due to the different post-translationally modified isoforms of lamin A and C. Lamin A and C were expressed similar in HGPS and normal nuclei and for this, are shown in yellow on the merged image of the gel (Fig. 10). Progerin spots were abundant and detected primarily in HGPS nuclei. However, progerin was detected in normal nuclei preparation as relatively weaker spots at position 17a,b and 18a. This provides the first proteomic evidence of the presence of progerin in normal nuclei (Fig. 10).
Collectively, analyses of the HGPS nucleome indicate that progerin protein spots are biomarkers of HGPS. 2D-DIGE demonstrates that trace amount of progerin were detectable in normal nuclei.

4.1.2 Proteins are differentially represented in HGPS nucleosome

From two independent 2D-DIGE analyses, 75 proteins spots were identified by MS and 28 proteins were found to be differentially represented in both studies (Table 32).

Table 32: Proteins identified via 2D-DIGE by mass spectroscopy. Two independent 2D-DIGE revealed 28 proteins that were differentially expressed in HGPS nuclei compared to control nuclei.

Proteins	Swiss Prot Nr	Fold change	Localization	Function
26S protease regulatory subunit 7 (PSMC2)	P35998	-1.44	Nucleus/Cytoplasm	Subunit of the 26S proteasome complex, involved in: degradation of proteins, hydrolysis of ATP, proliferation of cells[1]
Annexin A1	P04083	2.88	Nucleus/Cytoplasm	Is a calcium/phospholipid binding protein, responsible for: cellular development, cellular growth and proliferation, fusion of vesicles, actin cytoskeleton [1]
ATP-dependent RNA helicase (DDX1)	Q92499	2.01	Nucleus/Cytoplasm	Is a putative RNA helicase, involved in: cellular development, growth and proliferation, has exonuclease and helicase activity[1]
BAG family molecular chaperone regulator 2 (Bag2)	O95816	2.42	Nucleus/Cytoplasm	Co-Chaperone, involved in: folding of proteins, metabolism of proteins, Inhibition of Ubiquitin ligase CHIP [1,4]
Chaperone protein HSP90 beta (Hsp90b)	P08238	-1.57	Nucleus/Cytoplasm	Chaperone protein, involved in: protein folding, protein degradation [1,5]
Chromosome 14 open reading frame 166	Q549M8	1.75	Nucleus	Is a protein-coding gene, involved in: binding to RNA polymerase II, regulation of transcription [1]

Collagen, type VI, alpha 1	P12109	-2.31	Endoplasmic reticulum	Main component of connective tissue, responsible for: axon guidance, cell adhesion, extracellular matrix organization [1]
Cysteine and glycine-rich protein 1	P21291	3.56	Nucleus	Encodes LIM-domain proteins, responsible for: cellular development, cellular growth and proliferation [1]
EH-domain containing 3	Q9NZN3	-1.59	Nucleus/Cytoplasm	Is a protein-coding gene, features: binds ATP, calcium ion binding, has GTPase activity [1]
Enolase 1, (alpha)	P06733	-1.44	Nucleus/Cytoplasm	Is a glycolytic enzyme, features: DNA binding, magnesium ion binding, phosphopyruvate hydratase activity, protein binding, has transcription corepressor activity [1]
Eukaryotic translation elongation factor 2	Q9GZV4	-1.56	Nucleus/Cytoplasm	Essential factor for protein synthesis, it has GTPase activity and translation elongation factor activity [1]
Four and a half LIM domain protein 1 (FHL1)	Q13642	-3.79	Nucleus/Cytoplasm	Involved in cytoskeleton organization, cellular development, growth and proliferation, depolarization of cellular membrane, migration of vascular smooth muscle cells [1]
Guanine nucleotide-binding protein subunit beta-2-like 1	P63244	-2.64	Nucleus/Cytoplasm	Receptor for activated C kinase 1, involved in: cellular development, growth and proliferation, disruption of cell-cell contacts, positive regulation of proteasomal ubiquitin-dependent protein catabolic process [1]
Heat shock protein beta-1 (Hsp27)	P04792	-1.89	Nucleus/Cytoplasm	Chaperone, responsible for: folding of proteins, degradation of proteins, antiapoptosis, initiation of translation of mRNA, Ubiquitin binding [1,3]

Heat shock-related 70 kDa protein 2 (Hsp70)	P54652	2.68	Nucleus/Cytoplasm	Chaperone, responsible for: unfolded protein binding, refolding of proteins, dissociation and reassociation of 26S proteasome [1,2]
Lamin A/C	P02545	-	Nucleus	Component of the nuclear lamina, important role in: nuclear assembly, chromatin organization, nuclear membrane and telomere dynamics
Lamin A Variant, Progerin	P02545	10-20	Nucleus	Mutant lamin A linked to HGPS [1]
Lamin B1	P20700	-1.99	Nucleus	Nuclear membrane protein, involved in: cellular component disassembly involved in apoptotic process [1]
Leprecan-like 2	Q8IVL6	1.88	Nucleus	Extra cellular matrix organization, metal ion binding, oxidoreductase activity [1]
Mitogen-activated protein kinase 8 interacting protein 1	P45983	2.01	Nucleus/Cytoplasm	regulator of pancreatic beta-cell function, has protein kinase inhibitor activity [1]
Prolyl 4-hydroxylase subunit alpha-1	P13674	-1.55	Endoplasmic Reticulum	Key enzyme in collagen synthesis, involved in: Cellular development, growth and proliferation [1]
Protein disulfide isomerase family A, member 2	P07237	-1.13	Endoplasmic reticulum	Enzyme that binds lipids, breaks disulfide bonds, folds proteins, synthesis of cyclic GMP [1]
Pyruvate kinase, muscle	P14618	-2.21	Nucleus/Cytoplasm	Enzyme in Glycolysis, has catalytic activity, kinase activity, binds metal ion, proteins and nucleotides [1]
Ras and Rab interactor 2	Q8WYP3	-1.13	Nucleus/Cytoplasm	GTPase activator activity [1]

Serpin H1	P50454	-2.89	Endoplasmic reticulum	Chaperone protein for collagen, involved in: cellular development, growth and proliferation, extracellular matrix organization, collagen organization [1]
Transketolase	P51854	-3.5	Nucleus/Cytoplasm	Enzyme that has catalytic activity, transferase activity, transketolase activity, binds metal ion and monosaccharide [1]
Valosin-containing protein (VCP)	P55072	-2.02	Nucleus/ Endoplasmic reticulum/ Cytoplasm	Includes ATP-binding proteins, involved in: aggresome formation, protein degradation, ER stress response, proliferation of cells, proteasomal ubiquitin-dependent protein catabolic process [1]

Functional analysis of these 28 proteins revealed their functional link to at least 4 major biological categories using bioinformatic software program (Ingenuity Systems):

(1) Cytoskeleton and Actin-related proteins
(2) Collagen-associated proteins
(3) Signal transduction and Protein processing proteins
(4) Protein degradation and Chaperone proteins.

Proteins involved in protein degradation and chaperone assistance play a crucial role in cell homeostasis. Some of these proteins are molecular chaperones, namely Hsp27, Hsp70, and Hsp90, which interact with misfolded proteins and assist in their correct folding. Others include PSMC2, a 26S regulatory subunit, BAG2, and VCP that are components of the proteolytic systems and involved in the degradation and elimination of damaged proteins.

4.1.3 Proteasome activity is altered in HGPS

As protein degradation pathways were found to be affected in HGPS, the extent of proteasome alterations was determined in HGPS cells. For this, the proteasome activity was validated by comparing 4 HGPS cell strains with 4 distinct normal cell lines at early and late passages (Fig. 11).

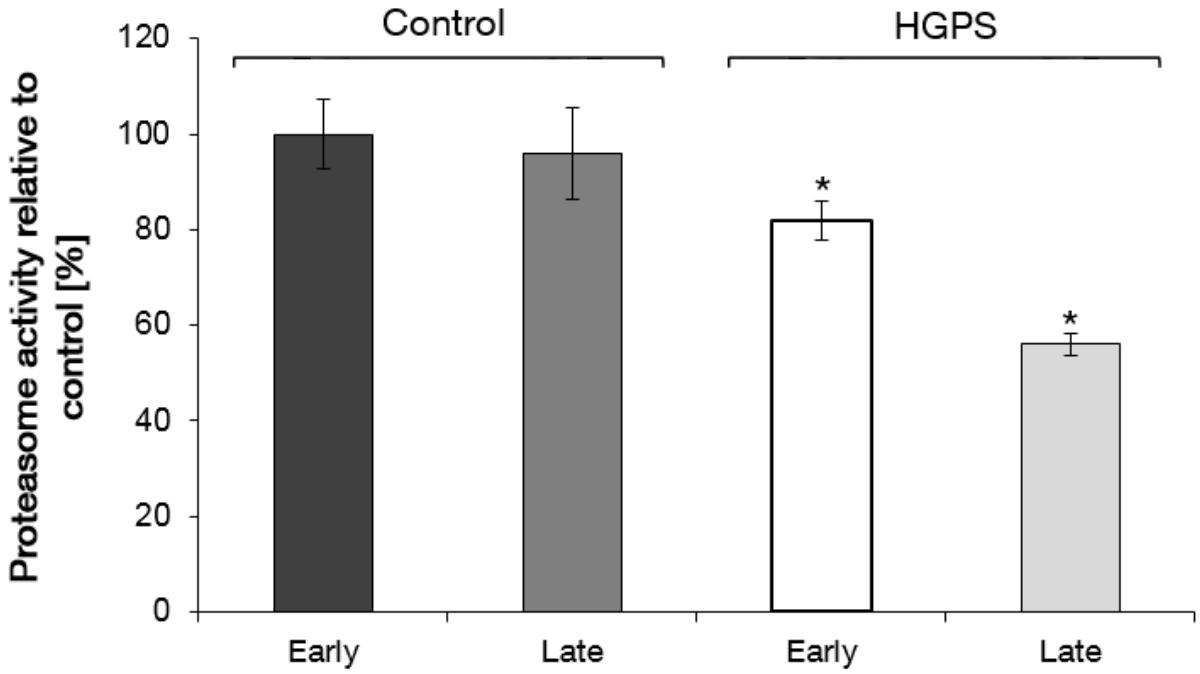

Figure 11: Proteasomal Activity of HGPS cells is reduced. Proteasome activity was defined by measuring the chymotrypsin-like proteasome activity in control and HGPS fibroblasts using Suc-LLVY-AMC as a substrate. The percentage of activity was calculated relative to early passage control cultures. Data are expressed as the mean ± S.D. (*p ≤ 0.05; n=4).

Normal cells exhibit no significant changes at early passages (< 15) compared to late passages (> 18). HGPS cells showed an average decrease in proteasome activity of 18 % at early passages and an average of 44 % in late passages relative to early passaged control cells.

The data indicate that the proteasome degradation pathway in HGPS cells is altered in an age-dependent manner.

To further analyze the extent of the alterations of proteasome proteins, gene expression profiling of these components was performed in early and late HGPS cultures compared to normal fibroblast cultures (Fig. 12 A, B).

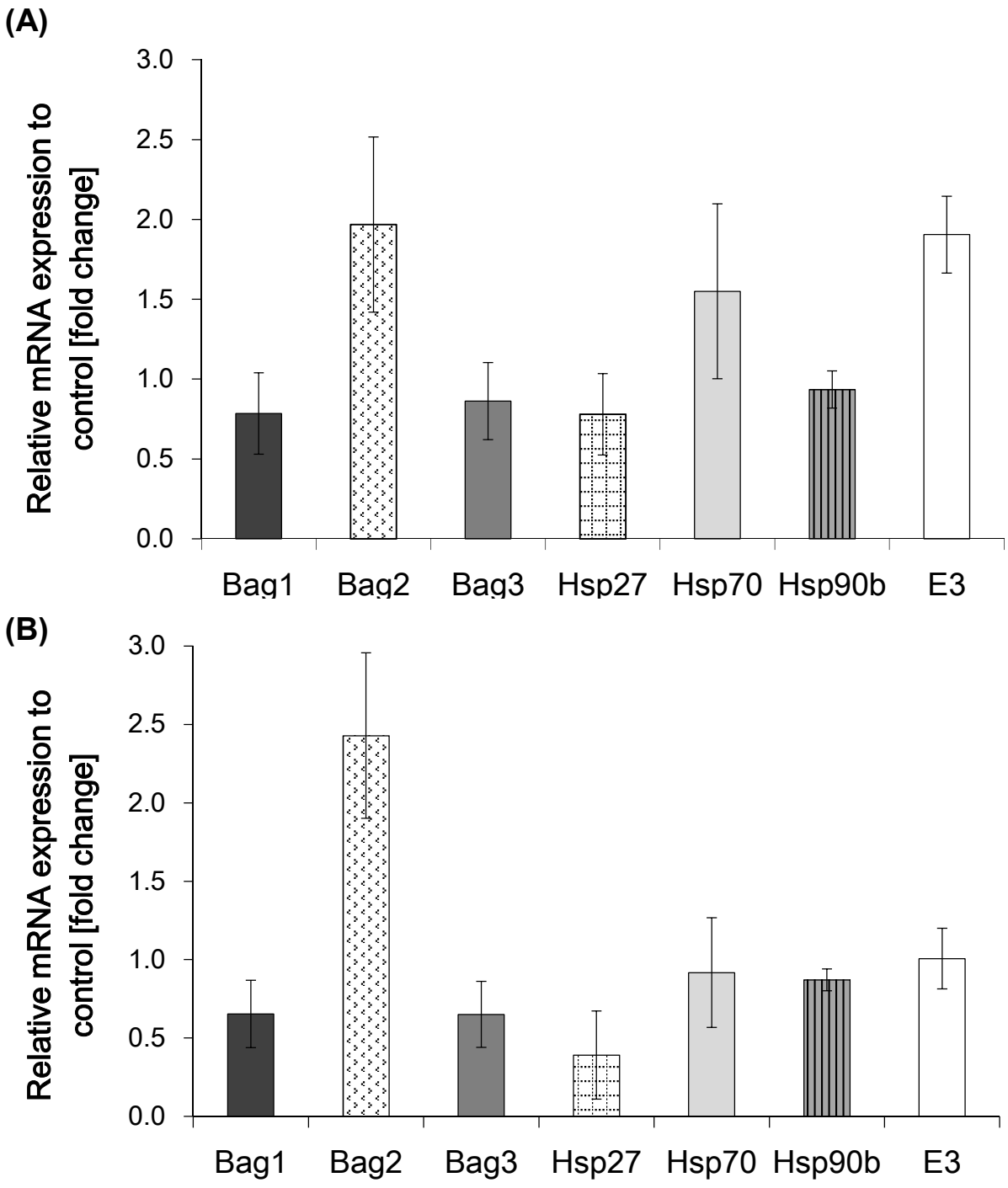

Figure 12: mRNA expression profiling of distinct proteasome proteins. Encoding mRNA levels of the indicated proteins were determined in total mRNA preparations isolated from early (<15, A) and late (> 18, B) passages control and HGPS cells by real-time PCR. All values are presented as mean ± S.D. (*p ≤ 0.05; n=4).

In accordance with the proteomics data, HGPS cells exhibit an approximately 2-fold increase in BAG2 expression levels. Significantly, BAG1 and BAG3 expression levels were reduced in HGPS cells. Moreover, Hsp27 levels and Hsp90 levels were similarly

reduced. Hsp27 was even more reduced in late HGPS cultures. Increased levels of Hsp70 were observed in HGPS cultures.

In summary, the real-time PCR data were consistent with the expression levels observed in the proteomics analyses and the changes in protein levels were more profound in late HGPS cultures.

Subsequently, Western blot analyses were performed of total protein extracts from HGPS and normal cells to further assess the protein expression levels of A-type lamins, S20 proteasome subunit C2, and Hsp27 (Fig. 13 A, B).

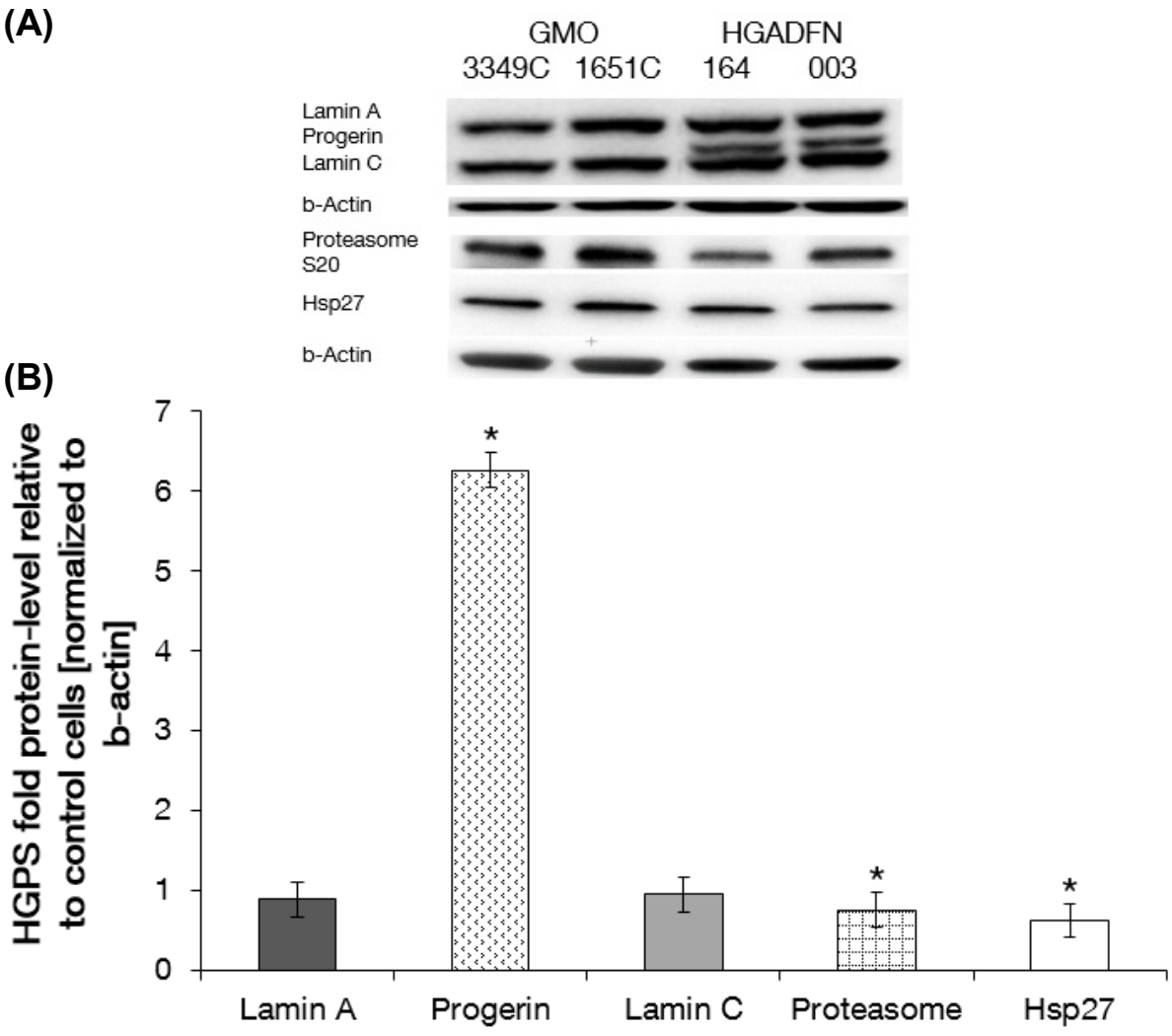

Figure 13: Western blot analyses of control cells and HGPS cells. (A) Representative Western blots of lamin A/C, progerin, proteasome subunit S20 C2, Hsp27 and b-actin in control and HGPS total cell extracts. (B) Quantifications of lamin A, lamin C, progerin, proteasome S20 C2 and Hsp27 levels normalized to b-actin are presented as the fold change relative to control cells (*p ≤ 0.05; n=3).

The expression of the A-type lamins was altered in HGPS cells as observed in the 2D-DIGE analyses. While the levels of lamin C remained constant, lamin A levels decreased and progerin levels significantly increased. Progerin was highly expressed in HGPS cells. Western blot analyses confirmed the decrease of S20 proteasome subunit C2 and Hsp27 in HGPS.

Collectively, proteasome subunits and Hsp27 were constitutively reduced in HGPS cells. HGPS nucleome analyses indicated alterations in the levels of proteins associated to the degradation systems, which served to build a schematic representation of their functional relationship (Fig. 14).

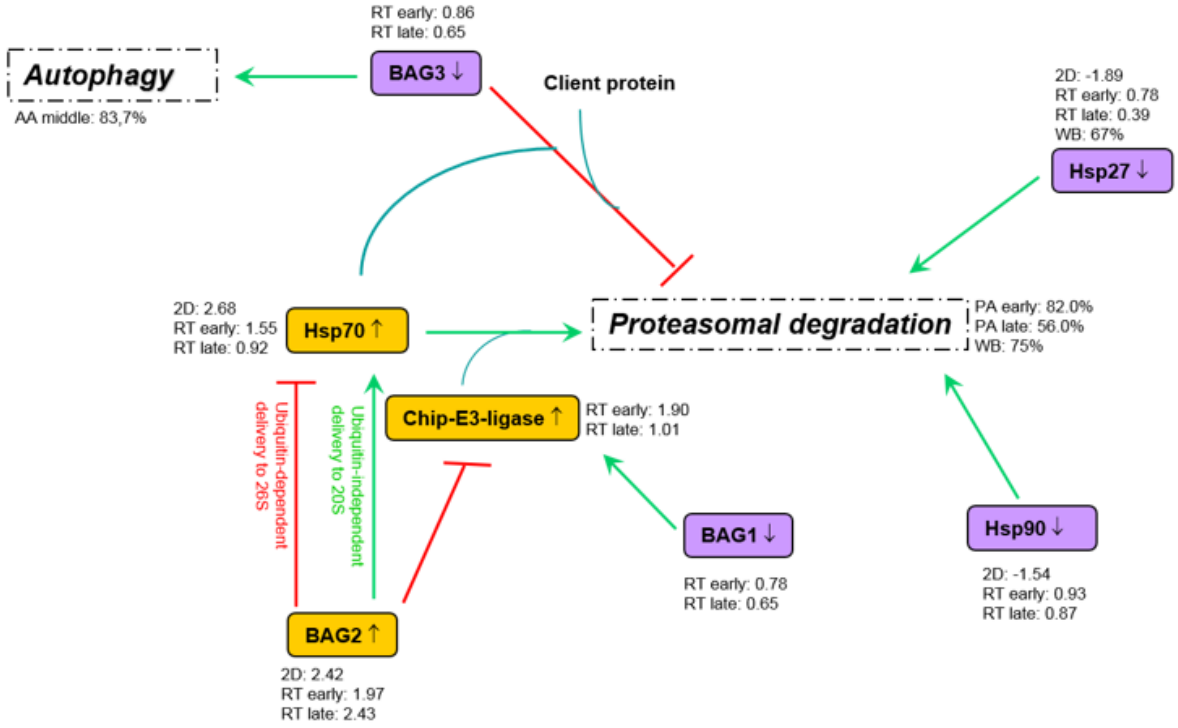

Figure 14: Schematic representation of protein alterations linked to protein degradation. The proteins identified by 2D-DIGE (BAG1, BAG2, BAG3, Chip-E3-ligase, Hsp70, Hsp90, and Hsp27) are shown. Their levels were determined by 2D-DIGE followed by mass spectra analyses (2D), real-time PCR (RT) and Western blot analyses (WB), as indicated. Proteasome activity (PA) and autophagy (AA) in HGPS cells relative to control cells are indicated. All values represent the values of HGPS cells compared to control cells.

Additionally, BAG1 and BAG3 were added to the analysis. They are regulators of proteasomal and macroautophagy pathways, respectively.[100] BAG2 is a specific inhibitor of the chaperone-associated ubiquitin E3-ligase (Chip).[160]

4.2 Improving the proteostasis in HGPS with sulforaphane (SFN)

As proteins of the degradation system were found to be reduced in HGPS fibroblasts, drug interventions that ameliorate the status of proteasome and autophagy activity were investigated. The focus was on natural occurring compounds that exert not only influence on the protein degradation pathways but also exhibit antioxidant properties. Sulforaphane was found to activate proteasome via Hsp27 and autophagy via Nrf2-Keap1 pathway (Fig. 15).[17,161]

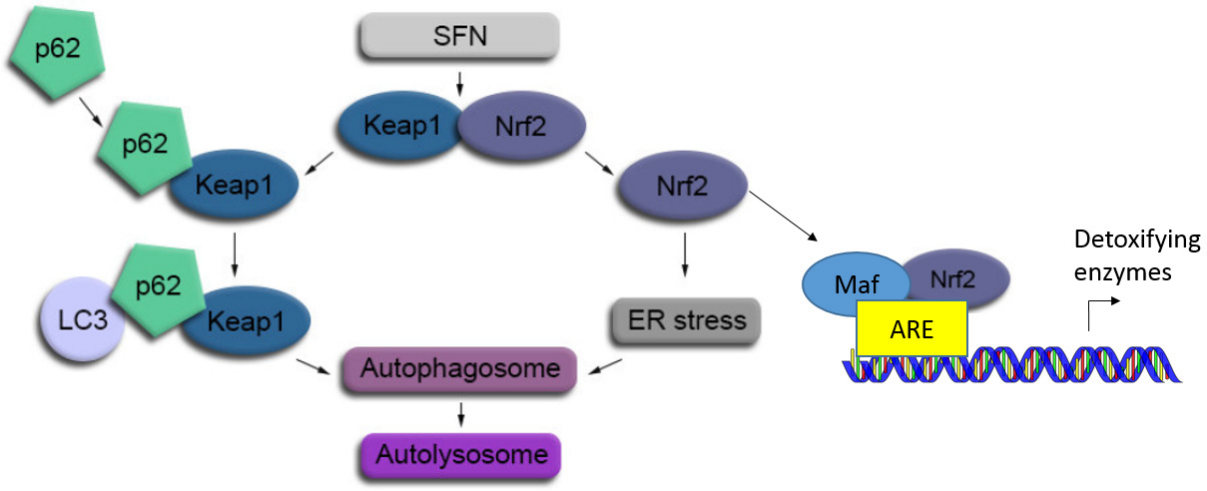

Figure 15: Activation of signaling pathways by sulforaphane. Sulforaphane regulates the autophagy via the Nrf2/ARE pathway. Uncoupled Keap1 binds to p62 which subsequently interacts with LC3. In turn, the complex interacts with lysosomes to form autolysosomes. In addition, Nrf2 can increase the production of the unfolded protein response (UPR) by endoplasmic reticulum inducing ER stress to eliminate the unfolded proteins by autolysosomes. Moreover, the induction of Nrf2 activates the transcription of antioxidant response elements (ARE).[162]

By increasing Nrf2, sulforaphane activates the transcription of antioxidant response elements and ameliorates the oxidative stress of a cell.[161] For this, SFN was tested on control and HGPS fibroblast during short and long-term treatment. The effect of SFN was analyzed by using different proteostasis assays such as proliferation rate, proteasome and autophagy measurements, progerin clearance, mitochondrial function measurements (ROS and ATP), and DNA damage response.

4.2.1 SFN enhances protein degradation in HGPS cells

Sulforaphane (1-isothiocyanato-4-methylsulphinylbutane) belongs to the isothiocyanate (ITC) group and can be derived from plants and cruciferous vegetables.[163] SFN exhibit anti-cancer and antimicrobial properties.[163] It was previously reported that SFN enhances the proteasome activity by inducing the expression of the small heat shock protein Hsp27 and the 26S proteasome subunit PSMB5.[16,17] Thus, the possibility that SFN treatment might also exert beneficial effects on HGPS cellular homeostasis was tested. First, the potential toxicity of SFN was assessed by applying different concentrations to control fibroblast cultures. The percentage of cell death and the proliferation rate of the cells was investigated (Fig. 16 A, B).

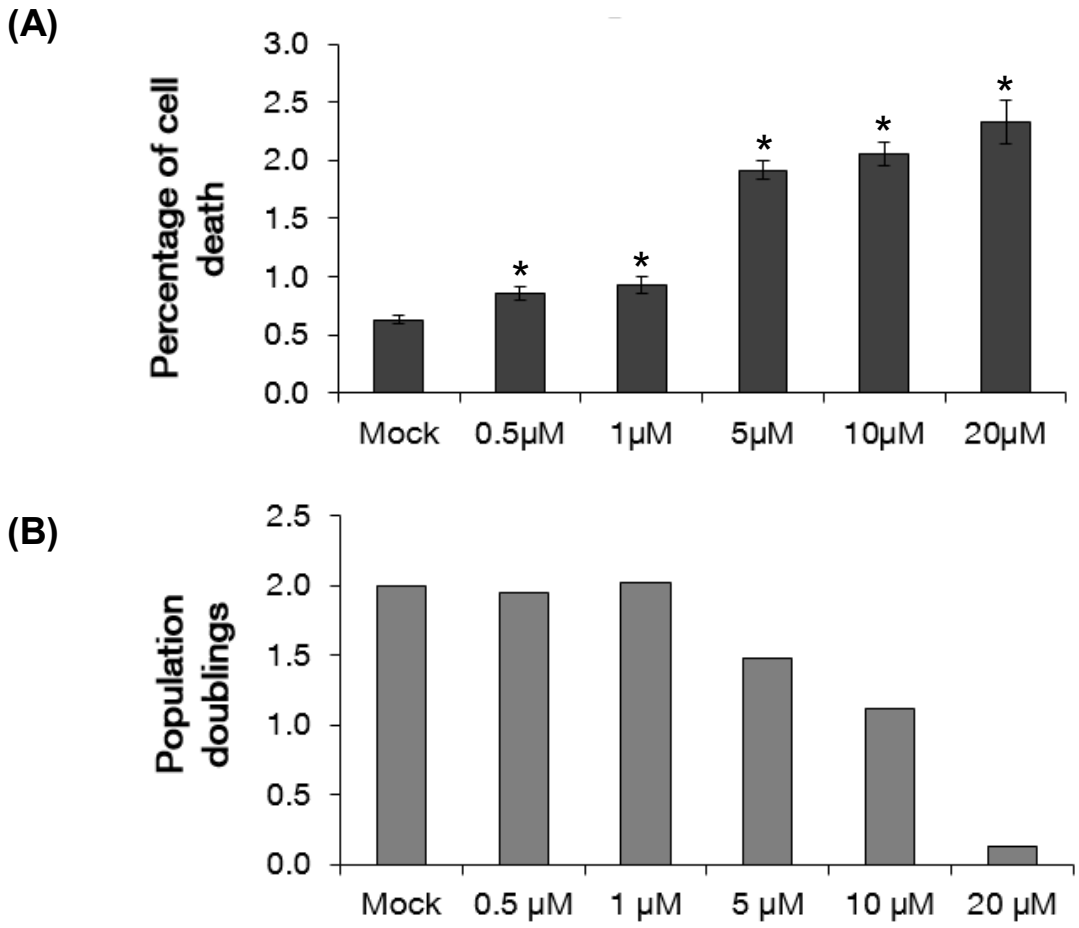

Figure 16: Celltoxicity of SFN. Cells were treated daily with SFN up to 48h. (A) Percentage of cell death after 48h of indicated SFN concentrations. Data are expressed as the fold ± S.D. relative to mock-treated cells (*$p \leq 0.05$; n=3). (B) Cell proliferation presented as population doublings after 48h at indicated SFN concentrations.

Treatment with 5 µM SFN led to greater cell death than 1 % in control cells after 48h. For this, a concentration of 1 µM SFN was chosen as it exhibits reduced cell death compared to mock-treated control cells.

For all subsequent experiments, cells were fed daily with either fresh medium supplemented with 1 µM SFN or mock-treated medium containing the vehicle (DMSO) alone.

HGPS and control cells treated with 1 µM SFN exhibit a significantly increased growth rate at day 3 compared to mock-treated counterparts (Fig. 17).

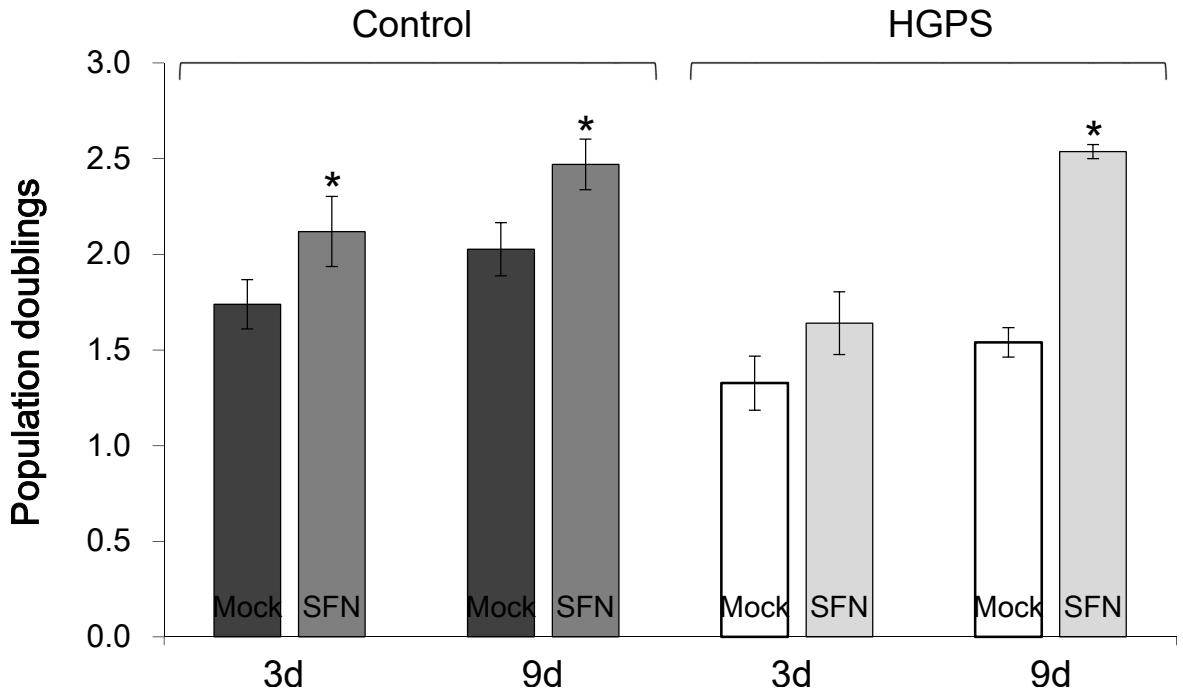

Figure 17: Cell proliferation with and without SFN. Population doubling levels were calculated as stated in the Materials and Methods relative to mock-treated counterparts. Control and HGPS cells were mock-treated (vehicle DMSO) or treated daily with 1 µM SFN for a period of 3 or 9 days (*p ≤ 0.05, n=4).

Furthermore, the proliferation defect in HGPS cells was ameliorated after 9 days of SFN treatment. These findings indicate that SFN improved the proliferation potency of normal and HGPS cell *in vitro*.

Subsequently, the effect of SFN on the proteasome activity was tested (Fig. 18).

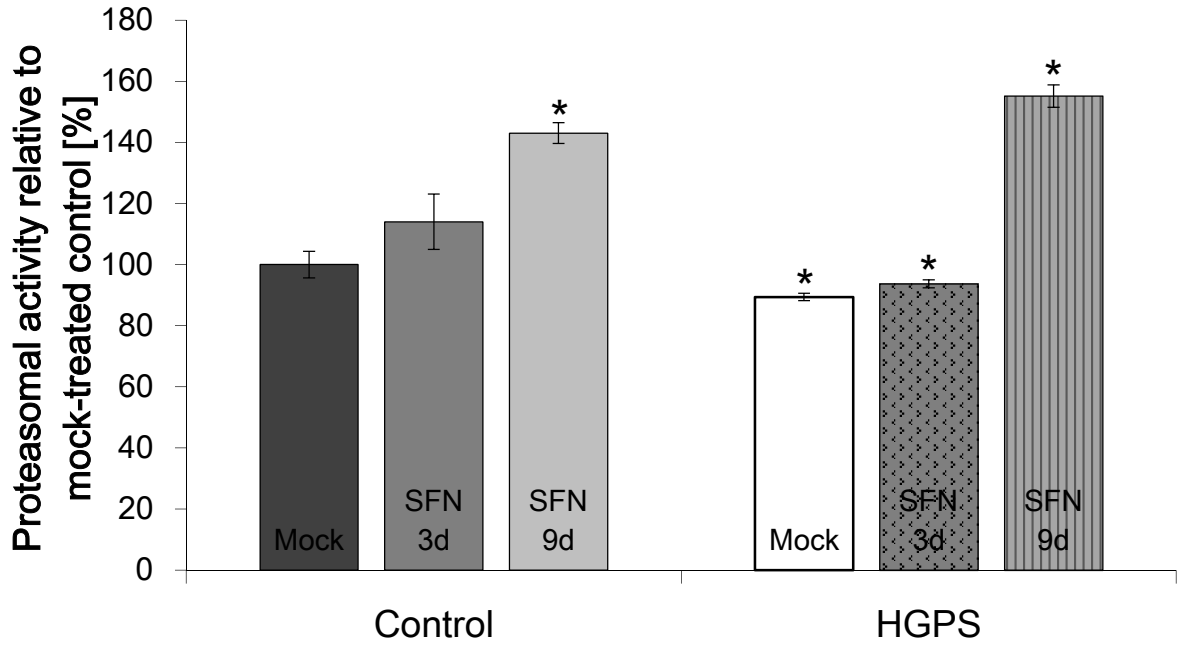

Figure 18: Proteasomal Activity after SFN treatment. Proteasome activity was determined by measuring chymotrypsin-like proteasome activity in control and HGPS fibroblasts using Suc-LLVY-AMC as a substrate. Cells were either mock-treated or treated daily with 1 µM SFN for a period of 3 or 9 days. The percentage of activity was calculated relative to the mock-treated control. Data are expressed as the mean ± S.D. (*$p \leq 0.05$; n=4).

Control cells treated with SFN demonstrated increased proteasome activity that improved with time by comparison with mock-treated controls. Mock-treated HGPS cells exhibit reduced proteasome activity compared to mock-treated control cells. SFN treatment increased the proteasome activity significantly after 9 days of treatment compared to mock-treated HGPS cells.

Cells rely on two proteolytic systems to maintain proteostasis: autophagy and the ubiquitin-proteasome system.[164] For this, an investigation whether the autophagy pathway was altered in HGPS cells was performed (Fig. 19).

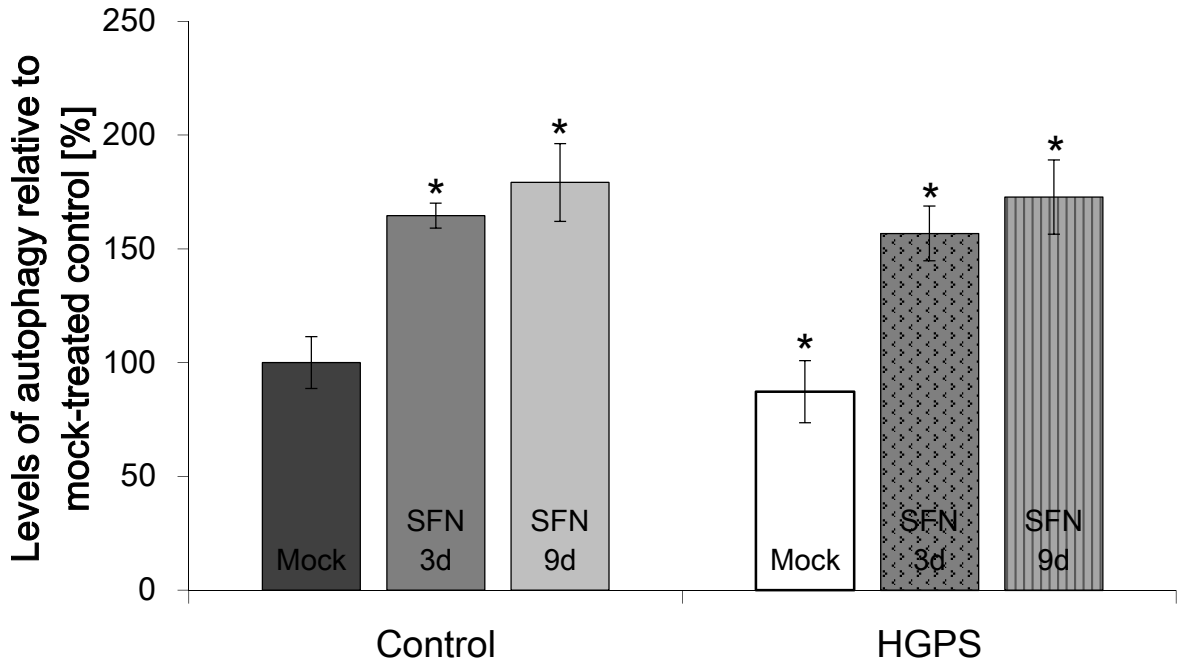

Figure 19: Autophagy levels after SFN treatment. Autophagy levels were determined in control and HGPS fibroblasts by measuring monodansylcadaverine (MDC) levels with fluorescence photometry. Cells were either mock-treated or treated daily with 1 µM SFN for a period of 3 or 9 days. The percentage of activity was calculated relative to the mock-treated control. Data are expressed as the mean ± S.D. (*$p \leq 0.05$; n=4).

Early passage HGPS cells show a 16.4 % decrease in autophagy compared to mock-treated control cells. In control cells, SFN treatment enhanced autophagy after 3 and 9 days of treatment significantly. SFN-treated HGPS cells exhibit a similar fold increase in autophagy after 3 and 9 days of treatment. These findings indicate that SFN activates and enhances the autophagy pathway in both control and HGPS cells.

Based upon the above observations, SFN appeared to boost the protein degradation systems in HGPS and control cells.

Next, a possible clearance of progerin was determined in SFN-treated HGPS cells. For this, the status of A-type lamins was investigated by performing Western blot analyses of total protein extracts derived from HGPS and control cells mock-treated or SFN-treated, as indicated in a representative image. Lamin A, lamin C and progerin signals were determined by densitometry from 3 independent Western blots. These signals were normalized to b-actin signal to correct the variability in protein sample concentration and/or uneven loading (Fig. 20 A, B).

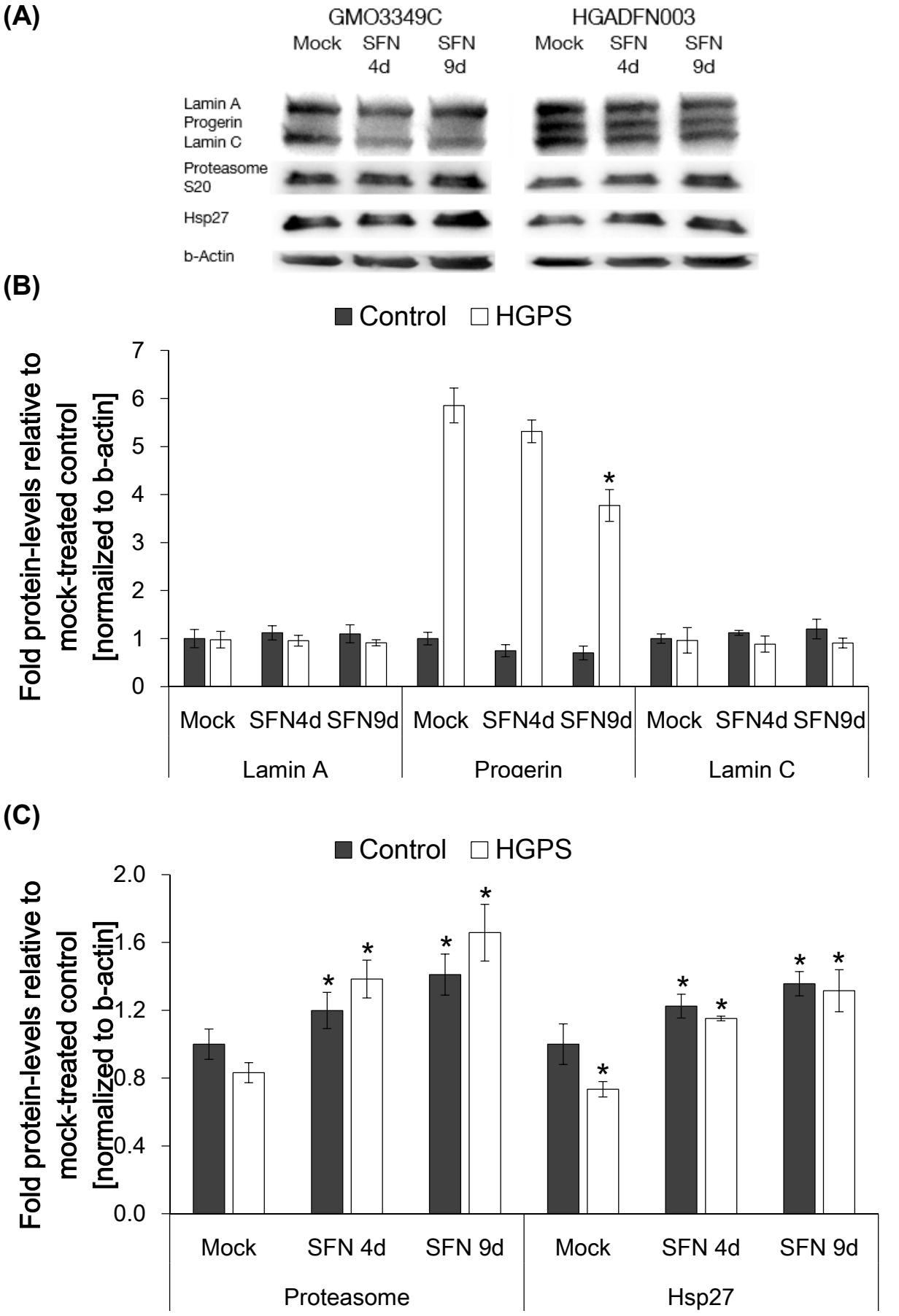
(A)
GMO3349C
HGADFN003
Mock
SFN 4d
SFN 9d
Mock
SFN 4d
SFN 9d
Lamin A
Progerin
Lamin C
Proteasome S20
Hsp27
b-Actin
(B)
Control
HGPS
Fold protein-levels relative to mock-treated control [normalized to b-actin]
0
1
2
3
4
5
6
7
Mock
SFN4d
SFN9d
Mock
SFN4d
SFN9d
Mock
SFN4d
SFN9d
Lamin A
Progerin
Lamin C
(C)
Control
HGPS
Fold protein-levels relative to mock-treated control [normalized to b-actin]
0.0
0.4
0.8
1.2
1.6
2.0
Mock
SFN 4d
SFN 9d
Mock
SFN 4d
SFN 9d
Proteasome
Hsp27

(D)

Ratio	Control Mock	Control SFN 4d	Control SFN 9d
Lamin A	49.07 ± 1.74	52.50 ± 1.42	52.88 ± 1.93
Progerin	3.45 ± 2.66	1.00 ± 2.15	1.40 ± 1.76
Lamin C	47.48 ± 4.36	46.50 ± 4.93	45.72 ± 1.77

Ratio	HGPS Mock	HGPS SFN 4d	HGPS SFN 9d
Lamin A	39.65 ± 3.78	41.44 ± 1.87	42.46 ± 3.01
Progerin	29.55 ± 4.31	25.41 ± 1.72	23.15 ± 2.79
Lamin C	30.80 ± 3.93	33.15 ± 2.18	34.39 ± 2.37

Figure 20: **Analysis of SFN treatment by Western blot.** (A) Representative Western blots of lamin A/C, progerin, proteasome subunit S20 C2, Hsp27, and b-actin of total control or HGPS cell extracts isolated from mock-treated cells or cells treated with 1μM SFN daily for 4 or 9 days. (B and C) Quantification of lamin A, lamin C, progerin, proteasome subunit S20 C2 and Hsp27 levels normalized to b-actin, and presented as the fold change relative to control cells (*p ≤ 0.05; n=3). (D) The proportions of lamin A, progerin, and lamin C within each sample were determined by Western blot with anti-lamin A/C antibody. Data are presented as the mean ±S.D. (*p ≤ 0.05; n=3).

Lamin A and lamin C levels remained unchanged in SFN-treated control and HGPS cells. Progerin signals were approximately 5-fold higher in HGPS total extracts compared with normal cell extracts. SFN treatment effectively induced progerin degradation in HGPS cells, as progerin levels were reduced by 13 % after 4 days and almost 40 % after 9 days of treatment compared to mock-treated HGPS cells. The analysis of the protein ratios revealed that SFN improves the status of lamin A and lamin C while reducing progerin by 22 % after 9 days. These data indicated that SFN enhances the clearance of progerin in HGPS cells.

To further understand the mechanisms by which SFN enhances protein degradation, the levels of the 20S proteasome subunit C2 were determined. SFN treatment induced a significant increase in the levels of the 20S C2 subunit in control and HGPS cells. Furthermore, Western blot analyses revealed an increase levels of the small heat shock protein Hsp27 in SFN-treated cells. In mock-treated HGPS cells, Hsp27 levels were reduced when compared with mock-treated-control. However, Hsp27 levels in HGPS cells increased after 4 days of SFN treatment and continued to rise after day 9. This finding was in accordance with the previously reported induction of Hsp27 protein levels after SFN treatment in HeLa and COS-1 cells.[17]

Collectively, these findings indicate that SFN induces the up-regulation of protein components involved in protein degradation pathways and thereby enhances the clearance of progerin in HGPS cells.

To determine in particular which protein degradation pathway is responsible for the clearance of progerin in SFN-treated cells, cells were treated with 1 µM SFN for 5 days and subsequently exposed for 12 hours to SFN in combination with 1 µM MG132, a proteasome inhibitor, or 25 µM chloroquine diphosphate, an inhibitor of autophagy (Fig. 21 A, B).

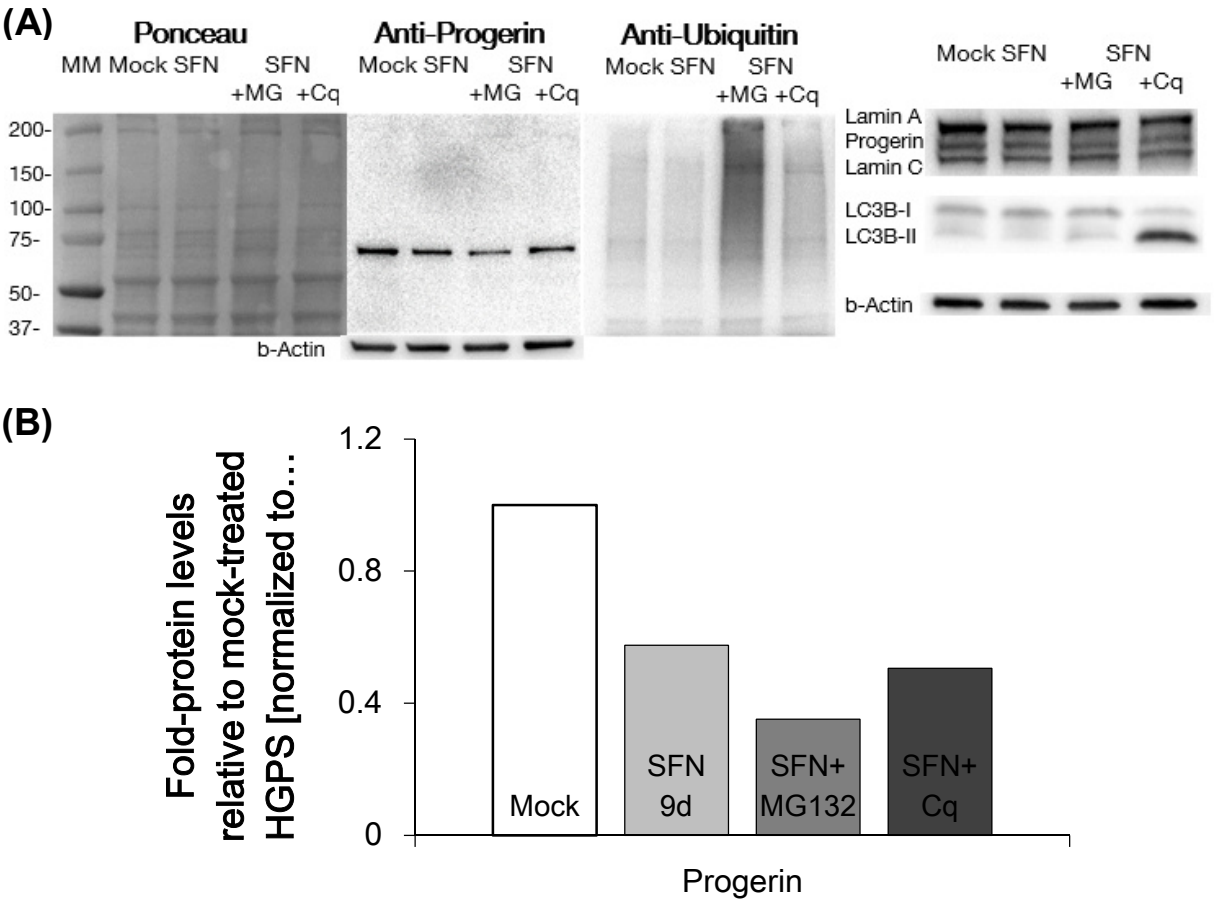

Figure 21: Western blot analyses of the protein degradation pathways after SFN treatment. (A) Representative Western blots of HGPS lysates of mock-treated cells or cells treated with SFN, SFN with MG132 or SFN with Chloroquine (Cq). Left panel: Samples were probed with antibodies specific to progerin and ubiquitin (n=3). Right panel corresponds to antibody staining against lamin A/C, LC3B-I and LC3B-II, and b-actin (n=3). (B) Quantification of progerin levels of the same cells as in (A), normalized to b-actin and presented as the fold change relative to mock-treated HGPS cells.

HGPS cells exhibit an increased amount of ubiquitinated proteins in response to MG132. Addition of chloroquine resulted in a significant increase in LC3B-II, a specific marker of autophagosome that accumulates when autophagy is inhibited.[100] LC3B-II levels were barely detectable in HGPS cells treated with SFN or MG132, indicating that autophagy remained active. Progerin levels were reduced in SFN-treated cells and slightly more in SFN-MG132 treated cells. This result indicates that autophagy was further stimulated by proteasome inhibition, as reported previously.[165] Progerin levels remained similar in cells exposed to SFN and chloroquine for 12 hours. This treatment was insufficient to induce a detectable increase in progerin levels. Collectively, these data indicate that SFN stimulates autophagy and thereby enhances progerin clearance in HGPS cells.

Previous HGPS studies have demonstrated increased levels ROS and reduced levels of ATP in HGPS cells.[148] Because SFN is known to have antioxidant properties, the possibility to ameliorate these cellular alterations was tested. In accordance with earlier studies, it was found that ROS levels were increased in early passages of HGPS cultures and appeared to decrease after 9 days of SFN treatment. A significant decrease of ROS levels was also observed in control cells after 9 days of SFN treatment (Fig. 22).

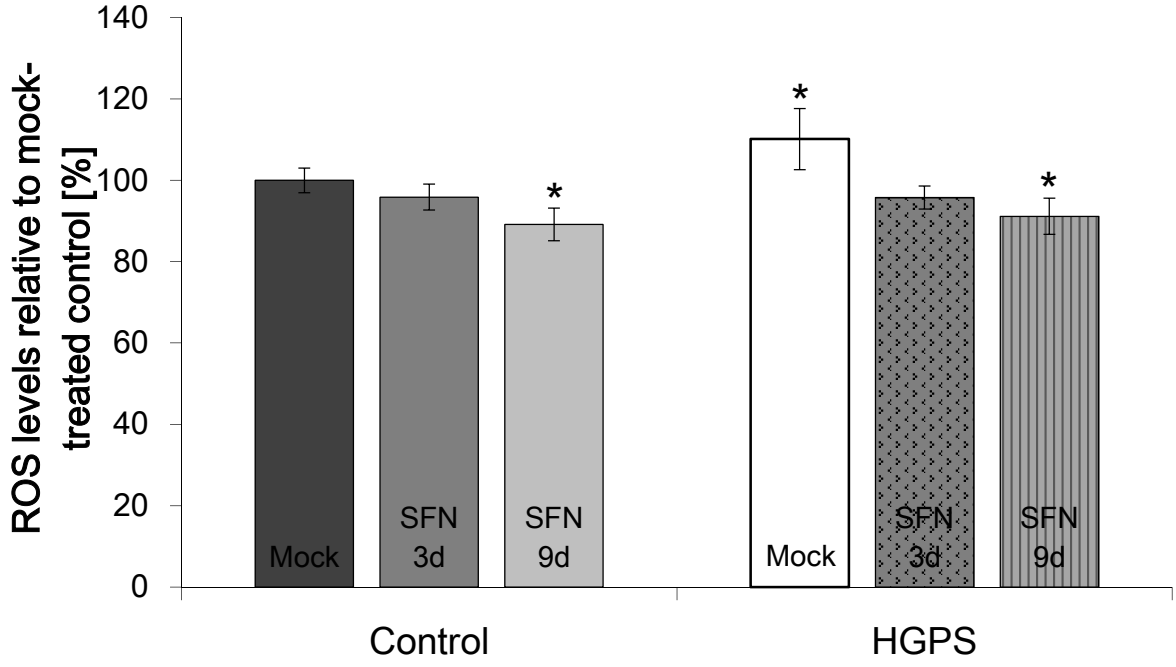

Figure 22: ROS levels after SFN treatment. Intracellular ROS levels were determined by measuring oxidized dichlorofluorescin (DCF) levels using a DCFDA cellular ROS detection assay as described in the Methods. Data represent the mean ± S.D. (*p ≤ 0.05; n=3) compared to mock-treated control.

ATP levels were significantly reduced in HGPS cells compared with normal cells (Fig. 23).

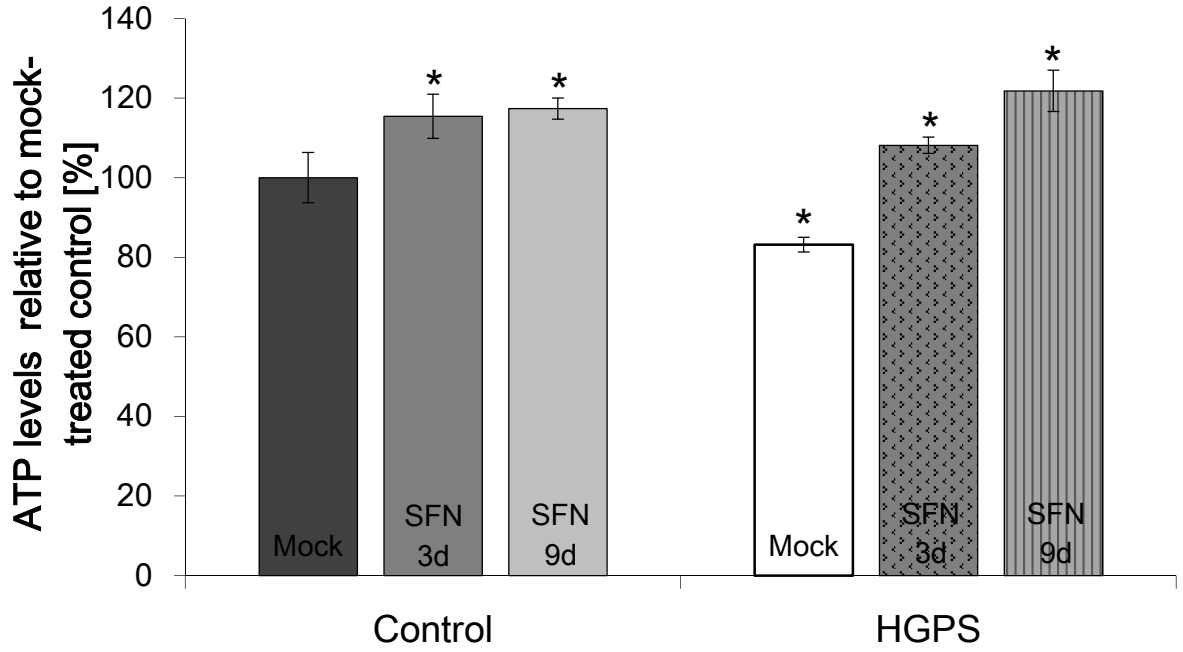

Figure 23: ATP levels of cells treated with or without SFN. Cellular ATP levels were measured using CellTiter Glo luminescence ATP assay as described in the Methods. Data are presented as the mean ± S.D. (*p ≤ 0.05; n=3) relative to mock-treated control.

SFN treatment induced a significant increase in intracellular ATP levels in control and HGPS cells. These data indicate that the antioxidant activity of SFN ameliorates the energy levels in HGPS cells.

4.2.2 SFN treatment improves nuclear alterations in HGPS fibroblasts

HGPS cells exhibit well-defined abnormalities such as nuclear envelope alterations (nuclear blebs and invagination), reduced levels of nuclear components (lamin B1 and LAP2α), and clustering of nuclear pores.[5,166] First, the impact of SFN on the nuclear shape was investigated, including analyzing nuclear blebs and invaginations.[5] SFN-treated or mock-treated cells were examined in parallel, whereby the percentage of dysmorphic nuclei were determined by direct counts (Fig. 24).

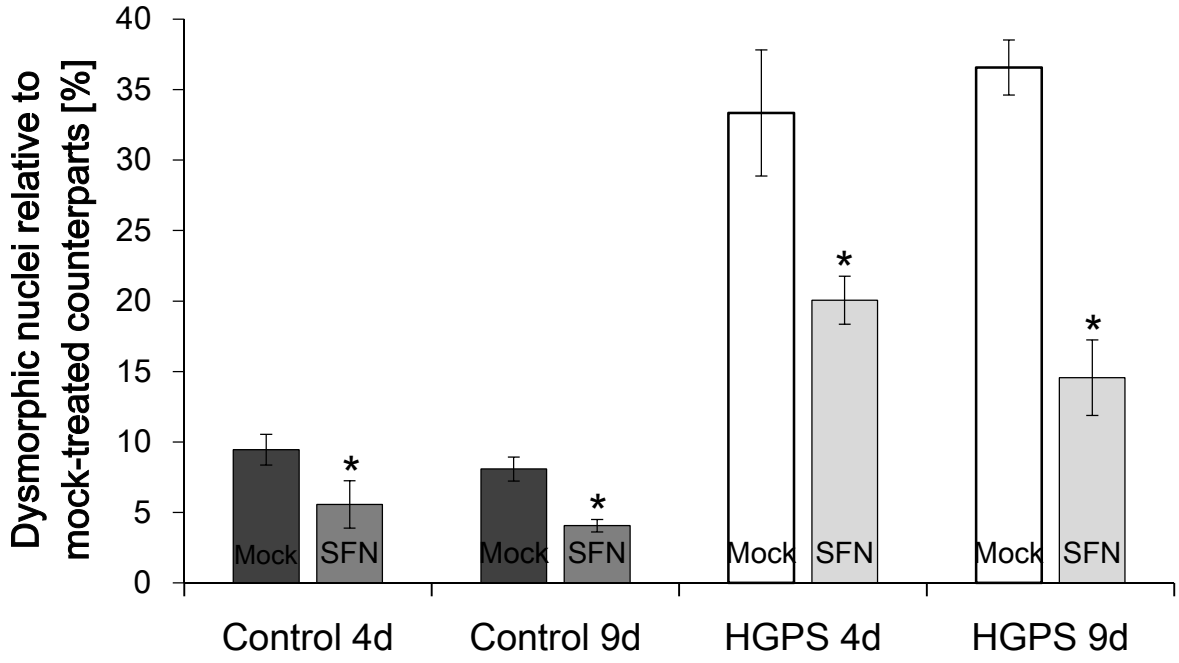

Figure 24: Dysmorphic nuclei after treatment with or without SFN. Frequency of misshapen nuclei (dysmorphic) in 3 control and 3 HGPS fibroblast lines after 4 or 9 days of treatment with either the vehicle or 1 μM SFN. The bars indicate the mean frequency of misshapen nuclei relative to mock-treated counterparts. An average of 800 nuclei were examined for each control and HGPS cell lines and treatment. Data are presented as the mean ± S.D. (*p ≤ 0.05; n=3).

SFN treatment reduced the frequency of nuclear blebbing in both control and HGPS cells after 4 days and even more after 9 days of treatment.

Next, immunochemistry analysis determined the distribution and expression of the A-type lamins and nuclear components (Fig. 25).

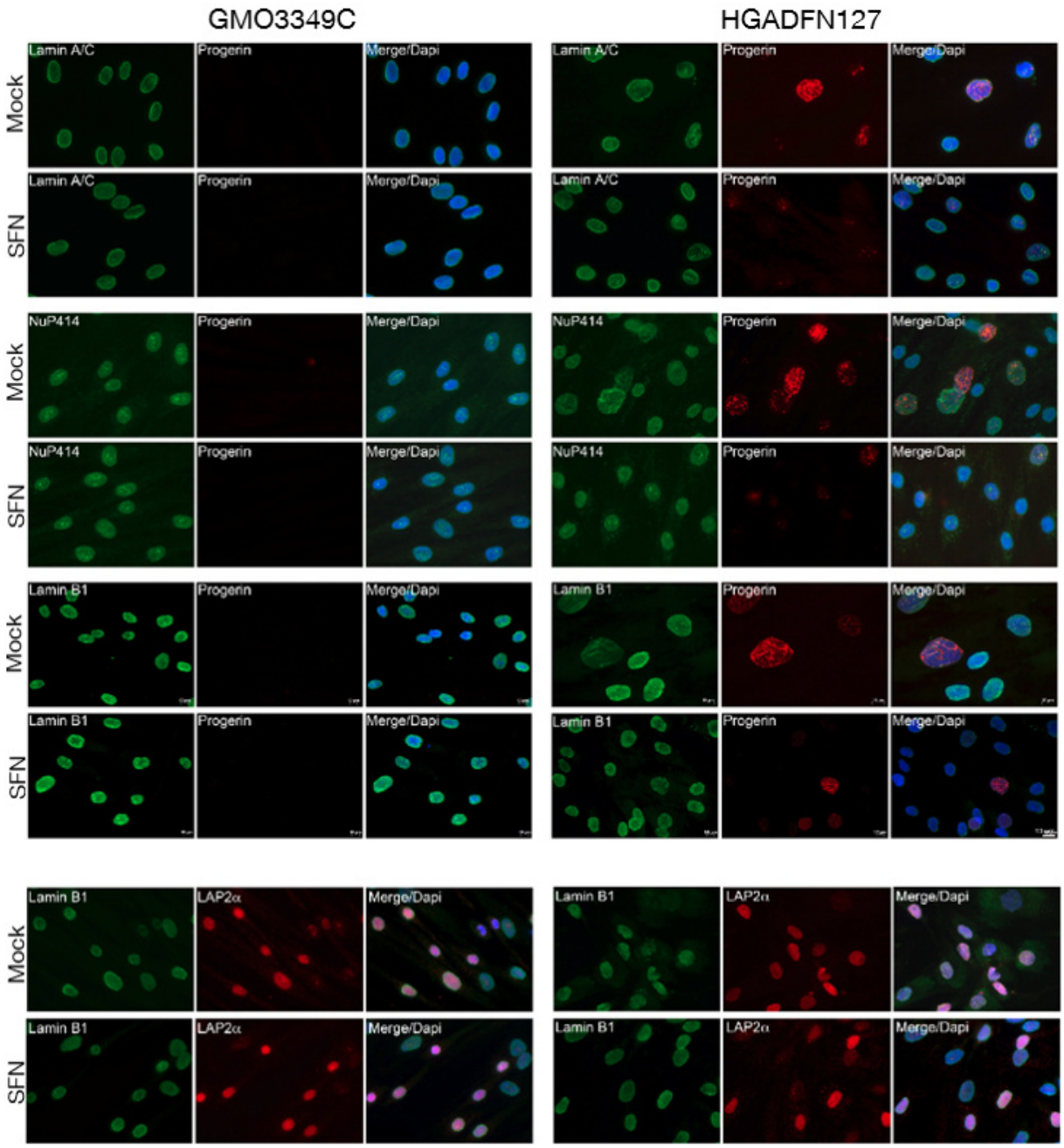

Figure 25: Immunochemistry of mock-treated or SFN-treated cells. Upper panel: Immunochemistry using antibodies directed against indicated proteins (lamin A/C, progerin, nuclear pore protein (Nup414), and lamin B1) was performed on control (GMO3349C) and HGPS (HGADFN127) cells mock-treated or SFN-treated for a period of 9 days (n=3). Lower panel: The same cells and condition as in upper panel were immunolabeled with anti-LAP2α (lamina-associated polypeptide 2α) and anti-lamin B1 antibodies. Scale bar: 10 µm.

Staining with anti-progerin antibody revealed progerin accumulation in the most dysmorphic HGPS nuclei. It is localized to the nuclear envelope with aggregated staining in some areas. Progerin staining in normal-shaped nuclei exhibit weak signals

with very few dots or foci while other nuclei exhibit no signal. In SFN-treated HGPS cultures, progerin-positive nuclei were reduced indicated by the decreased number of brightly labeled nuclei and intensity of signals compared to mock-treated HGPS cultures. The percentage of nuclei with bright progerin staining was reduced from an average of 38 % in mock-treated HGPS cultures to 15 % in SFN-treated HGPS cultures. The distribution of the nuclear pores was not altered by SFN treatment (Fig. 25, upper panel). Lamin B1 signals were very low to barely detectable in most of the dysmorphic HGPS nuclei (Fig. 25, lower panel). Bright progerin-positive HGPS nuclei were associated with weak lamin B1 staining. After SFN treatment, the number of HGPS nuclei exhibiting reduced lamin B1 signals were reduced concomitantly with a decreased number of bright progerin-positive nuclei. Low lamin B1 signals coincided with low LAP2α signals (Fig. 25, lower panel). The frequency of nuclei with low levels of lamin B1 and Lap2α staining was reduced in SFN-treated HGPS cells. These findings indicate that SFN normalized the levels of lamin B1 and Lap2α by reducing progerin levels in HGPS nuclei.

4.2.3 SFN treatment reduces the DNA damage levels of HGPS fibroblasts

Endogenous DNA damage and DNA DSBs were found to accumulate in HGPS cells with passage.[48,167] Levels of DNA damage repair factors such as 53BP1 and Rad51 were found to be altered in HGPS fibroblasts.[167,168]

For this, the basal levels of DSBs cells were determined in mock-treated and SFN-treated by staining with antibodies directed against the phosphorylated form of γH2A.X. DNA damage response of mock-treated and SFN-treated cells were analyzed by using 53BP1 and Rad 51 directed antibodies (Fig. 26 A-D).

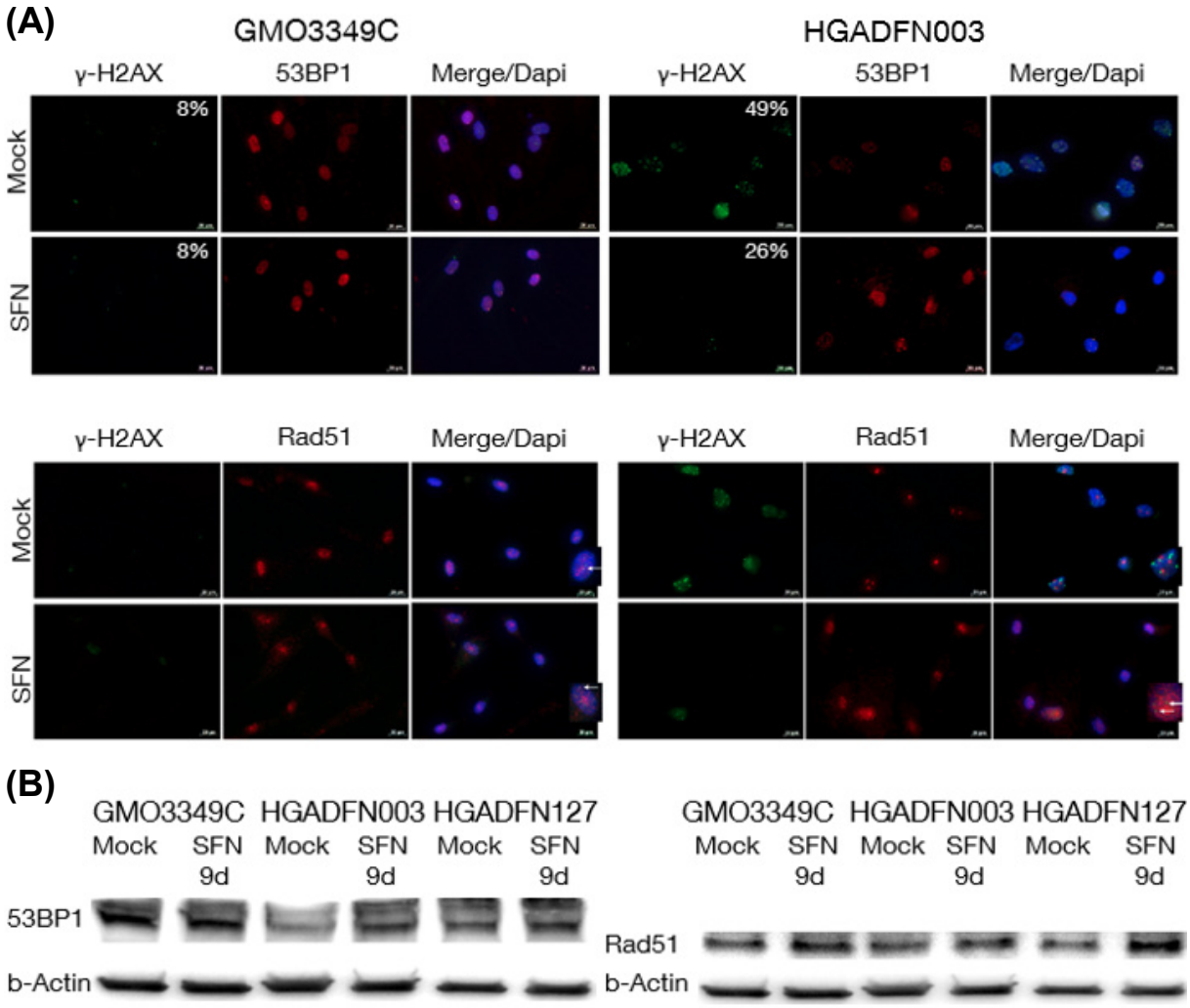
(A)
GMO3349C
HGADFN003
γ-H2AX
53BP1
Merge/Dapi
γ-H2AX
53BP1
Merge/Dapi
Mock
SFN
8%
8%
49%
26%
γ-H2AX
Rad51
Merge/Dapi
γ-H2AX
Rad51
Merge/Dapi
Mock
SFN
(B)
GMO3349C
HGADFN003
HGADFN127
GMO3349C
HGADFN003
HGADFN127
Mock
SFN 9d
Mock
SFN 9d
Mock
SFN 9d
Mock
SFN 9d
Mock
SFN 9d
Mock
SFN 9d
53BP1
b-Actin
Rad51
b-Actin
(C)
53BP1 protein-levels relative to mock-treated control [normalized to b-actin, %]
120
100
80
60
40
20
0
Mock
SFN
Mock
SFN
*
*
Control
HGPS

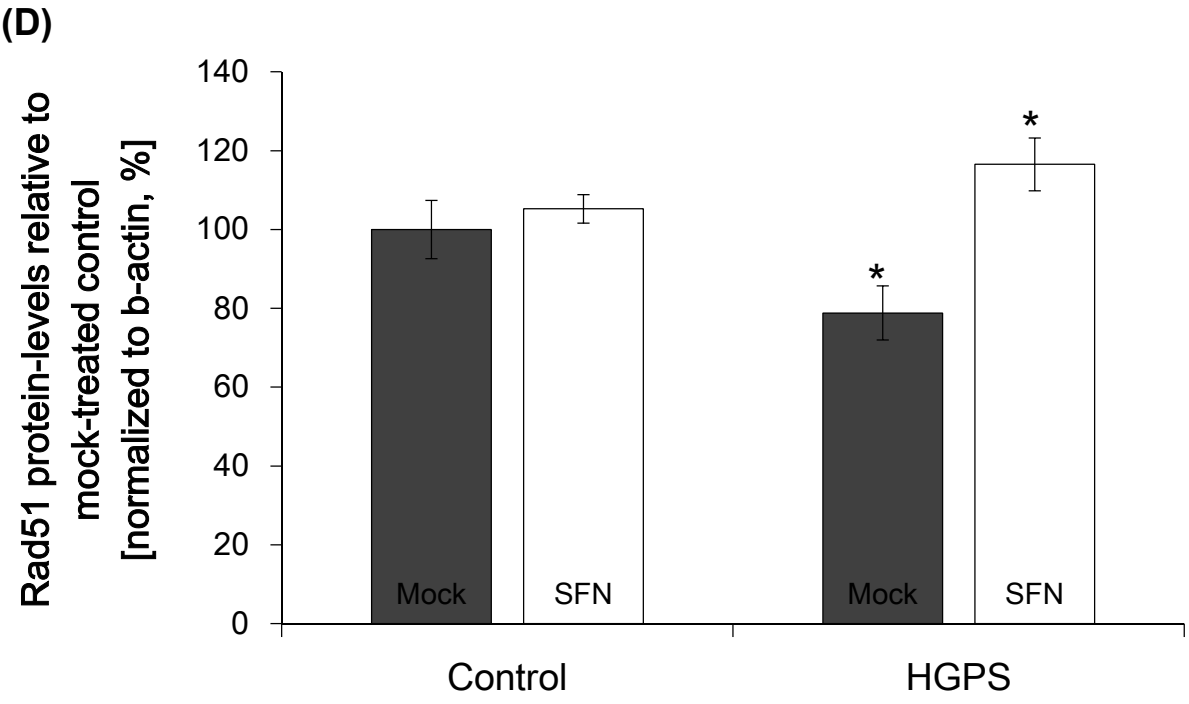

Figure 26: SFN ameliorates the levels of DNA double-strand breaks in HGPS. (A) Upper panel: Immunocytochemistry using 53BP1 and γH2A.X antibodies on control cells and HGPS cells mock-treated or treated with SFN for 9 days. Percentage of γH2A.X foci is indicated (n=4). Lower panel: Immunocytochemistry of control and HGPS cells mock-treated or SFN-treated for 9 days and stained with Rad51 and γH2A.X antibodies (n=4). Scale bar: 20 µm. (B) Western blot evaluation of 53BP1 (left) and Rad51 (right) levels of the same cells and condition as in (A). (C) Quantification of 53BP1 levels (upper panel) and Rad51 levels (lower panel) normalized to b-actin and compared to mock-treated control cells. Data are presented as the mean ± S.D. (*$p \leq 0.05$, n=4).

HGPS nuclei exhibit a significantly increased number γH2A.X foci (49 %) compared to mock-treated control cells (8 %). After SFN treatment, γH2A.X foci were reduced to 26 %. These results indicate more efficient DNA damage repair in HGPS cells in response to SFN. Consistent with these finding, the reduced levels of 53BP1 and Rad51 in mock-treated HGPS cells were found to be increased after 9 days of SFN treatment (Fig. 26 B, C) and the nuclear distribution was normalized (Fig. 26 A). 53BP1 and Rad51 were found to be co-localized with DNA damage foci of γH2A.X after SFN treatment. This indicates that SFN improved DNA damage repair in HGPS fibroblasts.

Moreover, HGPS cells show a loss of heterochromatin and reduced levels of chromatin proteins such as heterochromatin protein 1 (HP1).[5,87] Accordingly, HP1-γ levels were reduced in mock-treated HGPS cells when compared to mock-treated control cells. However, SFN restored the HP1-γ levels in HGPS as indicated by Western blot and immunocytochemistry (Fig. 27 A-C).

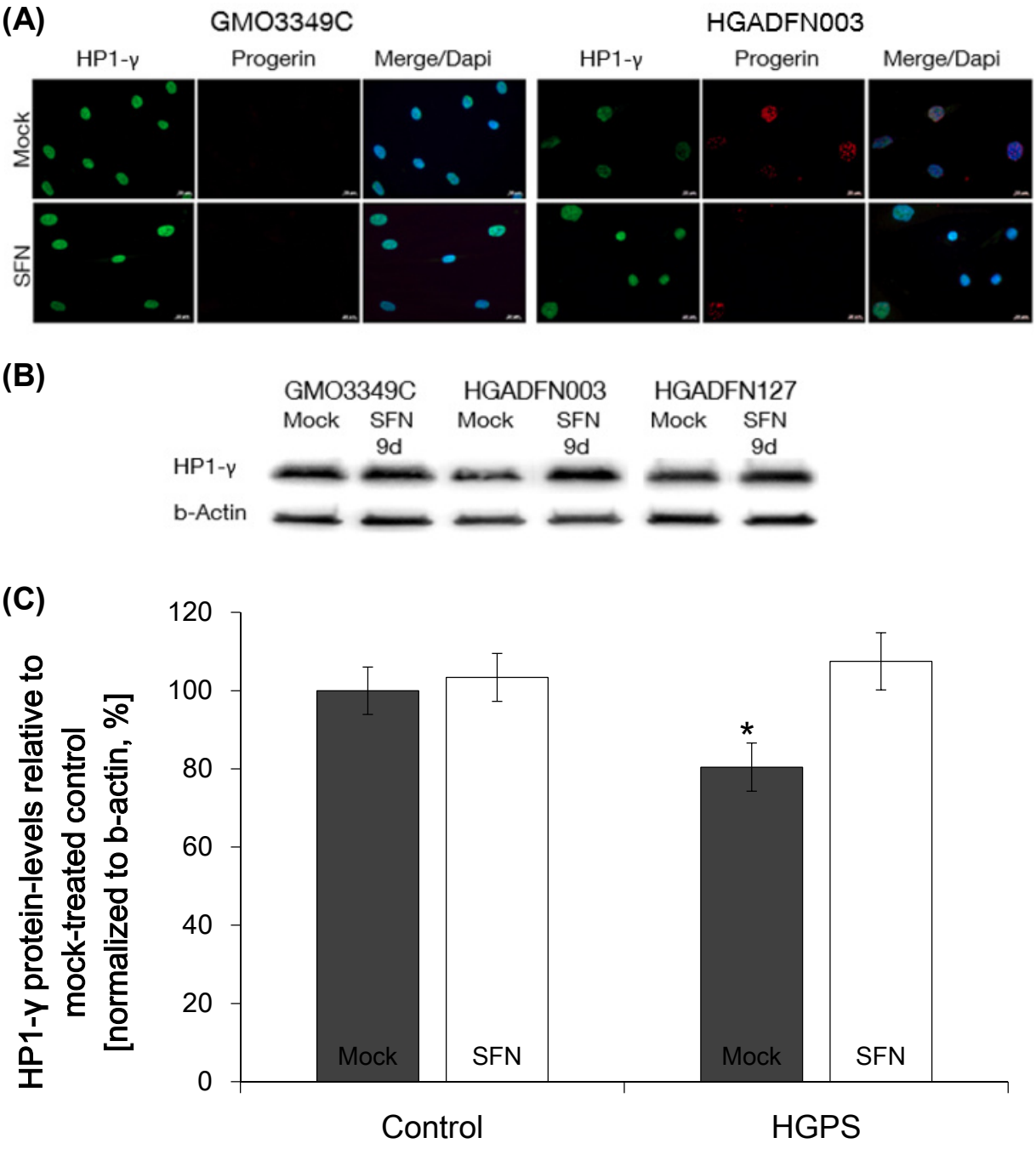

Figure 27: SFN improves heterochromatin levels in HGPS. (A) Immunocytochemistry using HP1-γ and progerin antibodies on control cells and HGPS cells mock-treated or treated with SFN for 9 days (n=4). Scale bar: 20 µm. (B) Western blot evaluation of HP1-γ levels of the same cells and condition as in (A). (C) Quantification of HP1-γ levels normalized to b-actin and compared to mock-treated control cells. Data are presented as the mean ± S.D. (*p ≤ 0.05, n=4).

4.2.4 Long-term SFN treatment further ameliorates HGPS cellular phenotype

Cultures were passaged several times and treated every other day with 1 µM SFN or vehicle for several months to test the long-term potential of SFN on HGPS and normal fibroblasts. The proliferation rates demonstrate sustained increases in growth of SFN-treated control and HGPS cells while mock-treated HGPS cells reached a growth plateau after several passages (Fig. 28 A, B).

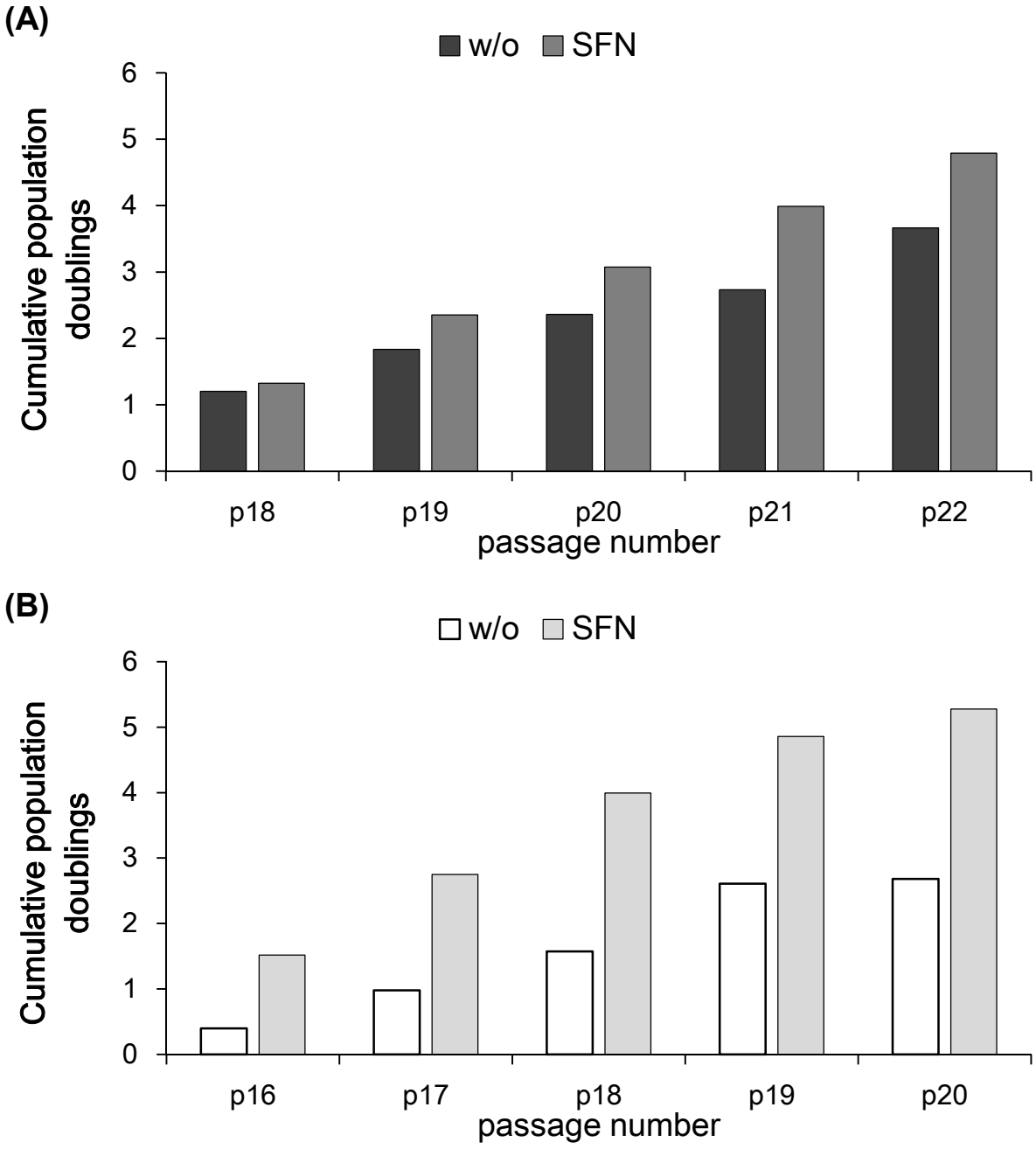

Figure 28: The proliferation rate in long-term cultures treated with SFN. (A) Long-term cultures of control and (B) HGPS cells treated with the vehicle (w/o) or 1 µM SFN. The cumulative population doublings were calculated as described in the methods.

Western blot analyses revealed a significant and sustained decrease in progerin levels during the 85 days of SFN treatment. The proportions of lamin A and C were improved while progerin levels were reduced by an average of 33 % in SFN-treated HGPS cells (Fig. 29 A, B). This indicates that SFN further ameliorates the status of the A-type lamins.

(A)

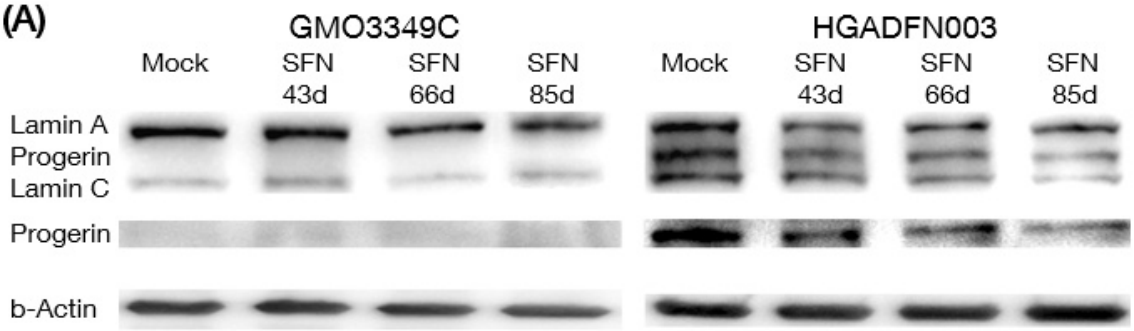

(B)

Ratio	Control Mock	Control SFN 43d	Control SFN 66d	Control SFN 85d
Lamin A	59.95 ± 1.05	62.81 ± 2.17	63.60 ± 2.32	63.77 ± 0.91
Progerin	3.64 ± 1.55	1.25 ± 2.44	1.01 ± 2.11	0.51 ± 2.46
Lamin C	36.41 ± 1.16	35.94 ± 2.44	35.39 ± 3.80	35.73 ± 1.87

Ratio	HGPS Mock	HGPS SFN 43d	HGPS SFN 66d	HGPS SFN 85d
Lamin A	38.59 ± 2.95	40.92 ± 3.49	43.51 ± 1.53	46.67 ± 1.33
Progerin	35.40 ± 1.13	28.52 ± 2.99	27.80 ± 4.29	24.59 ± 1.39
Lamin C	26.01 ± 1.70	30.56 ± 1.54	28.69 ± 1.07	28.74 ± 1.95

Figure 29: Western blot analyses of long-term SFN cultures. (A) Western blot evaluation of A-type lamins (lamin A, progerin, Lamin C) in control and HGPS cell that were mock-treated or SFN-treated every 2 days for the indicated period (a representative image is shown; n=3). Blots were probed with lamin A/C, progerin, and b-actin antibodies. (B) The proportions of the A-type lamins in each sample were examined by Western blot with an anti-lamin A/C antibody. Data represent the mean ± S.D. with respect to mock-treated control cells after values were normalized to b-actin signal (*$p \leq 0.05$; n=3).

Gene expression profiling of A-type lamins mRNA levels indicated that the overall levels remained unchanged in all conditions (Fig. 30 A, B).

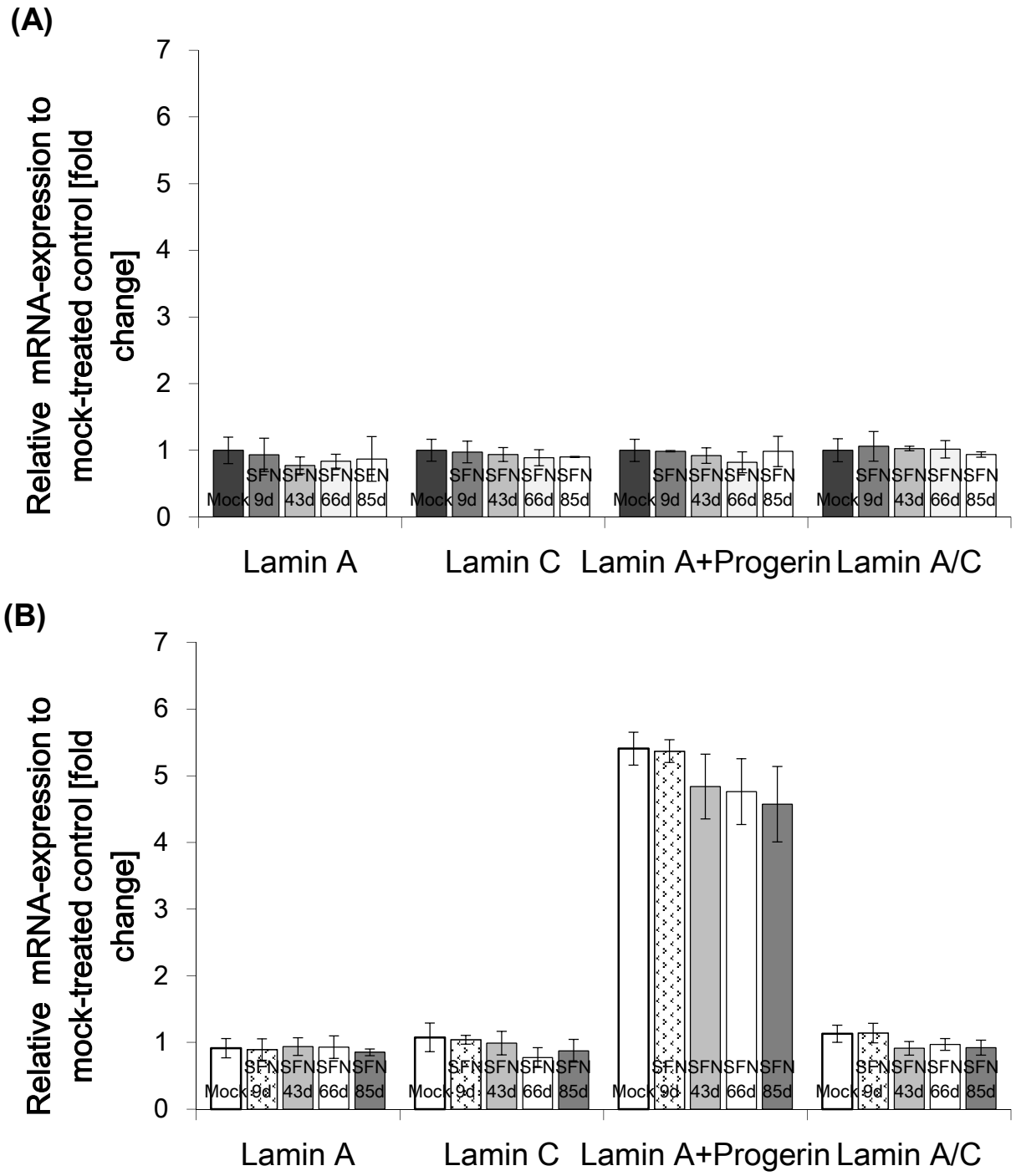

Figure 30: mRNA expression patterns in long-term SFN cultures. Encoding mRNA levels of indicated proteins were determined in total mRNA preparations isolated from control (A) and HGPS (B) cells by real-time PCR. Cells were either mock-treated with 1 µM SFN every 2 days for the indicated period. All values are presented as the mean ± S.D. (*p ≤ 0.05; n=3).

The constant progerin clearance was accompanied with a constant increase of the protein degradation pathways. Proteasome activity and autophagy levels remained high in control and HGPS cells after 85 days of SFN treatment (Fig. 31 A, B).

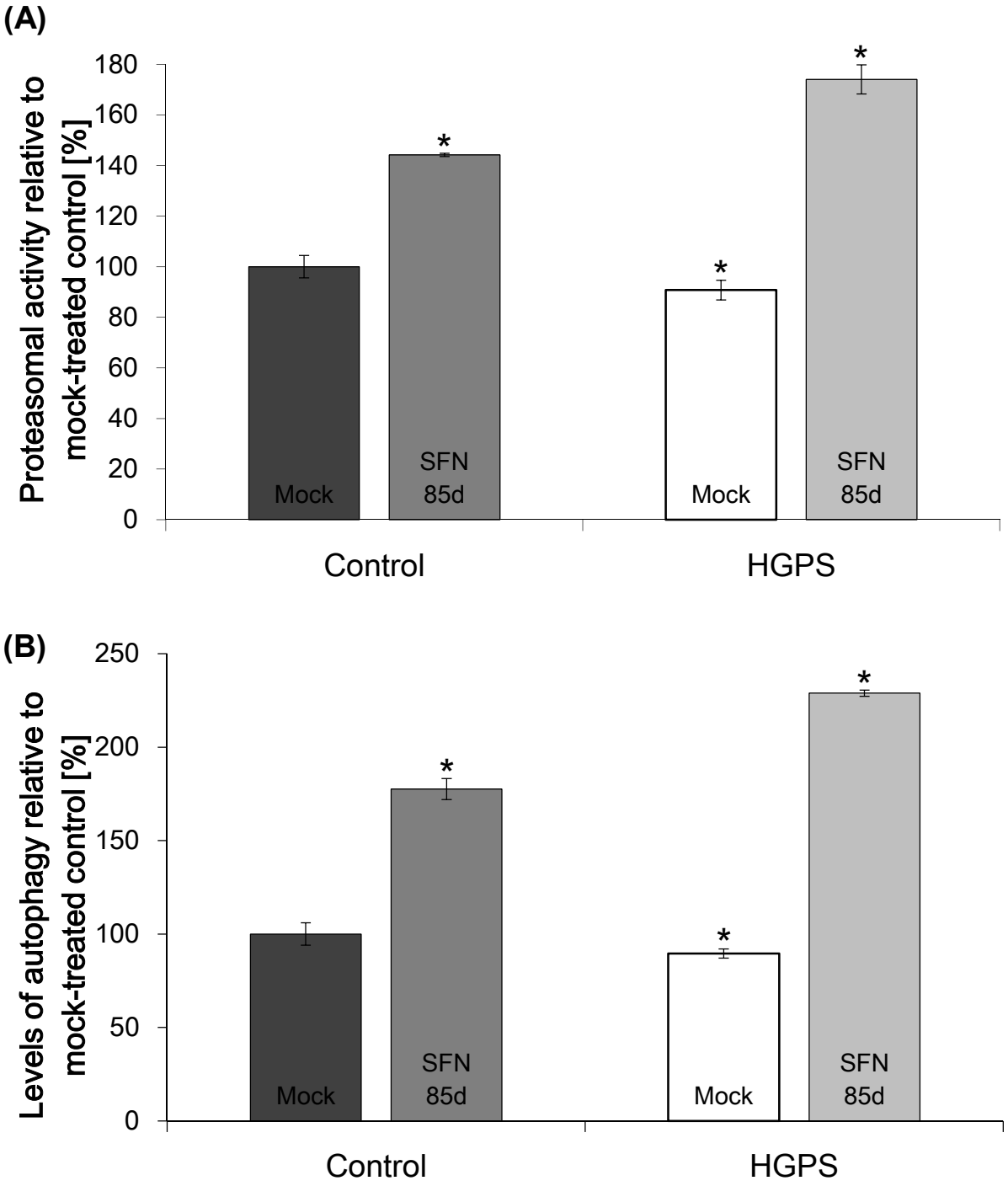

Figure 31: Protein degradation levels of fibroblasts after 85 days of SFN. (A) Proteasome activity was defined by measuring the chymotrypsin-like proteasome activity in control and HGPS cells using Suc-LLVY-AMC as a substrate. Cells were either mock-treated or treated with 1 µM SFN every 2 days for the indicated period. The percentage of proteasome activity was calculated relative to mock-treated control. Data are presented as mean ± S.D. (*p ≤ 0.05, n=3). (B) The same cells and conditions as in (A) were used to determine the autophagy by measuring monodansylcadaverine (MDC) levels by fluorescence photometry as described in the Methods. Data are expressed as the mean ± S.D. relative to mock-treated control (*p ≤ 0.05; n=3).

In sum, SFN treatment induced a constant increase in proteostasis in normal and HGPS cultures during long-term treatment. Progerin clearance remained high during the 12-weeks of treatment in HGPS cells treated with SFN.

4.3 A drug combination of SFN and FTI further ameliorates the HGPS cellular phenotype

Given that SFN reversed the HGPS cellular phenotype to a certain extent, it was investigated whether a drug combination could further improve it. By applying a drug combination, different signaling pathways could be activated in HGPS that a single drug cannot target. This would reverse more different phenotypic changes in HGPS. In particular, the blocking of farnesylation by FTI and the activation of Nrf2-Keap1 pathway by SFN were used in this study. First, the concentrations of both drugs in combination has to be determined before several proteostasis assays (proliferation rate, progerin clearance, mitochondrial function, and DNA damage response) will verify whether the combination has more beneficial effects than the single drug treatment. Specific markers for the severe side effects of FTI have to be observed e.g. prelamin A accumulation, donut-shaped nuclei, and lamin B1 disruption. Those have to be compared to the drug combination which should avoid the negative effects of FTI.

4.3.1 Determination of the drug concentrations for the use in treatment combination

As SFN exhibit beneficial effects on the HGPS phenotype, this compound was chosen for a combinatory treatment with FTI. Previous experiments (Appendix 8.1) preserved the negative effects of FTI on the HGPS phenotype when applied in combination with SFN. All these combinations led to cell death, donut-shaped nuclei, and prelamin A accumulation. Even lower concentrations of FTI and SFN induced high toxicity. For this, a concentration of single FTI and SFN treatment has to be determined at which the drugs induce high proliferation rates and autophagy.

First, the FTI concentration was assessed that was still beneficial for control and HGPS fibroblasts. FTI was applied at different concentrations for 1d before cell growth (Fig. 32 A, B), autophagy levels (Fig. 33 A, B), and prelamin A accumulation (Fig. 34) were examined.

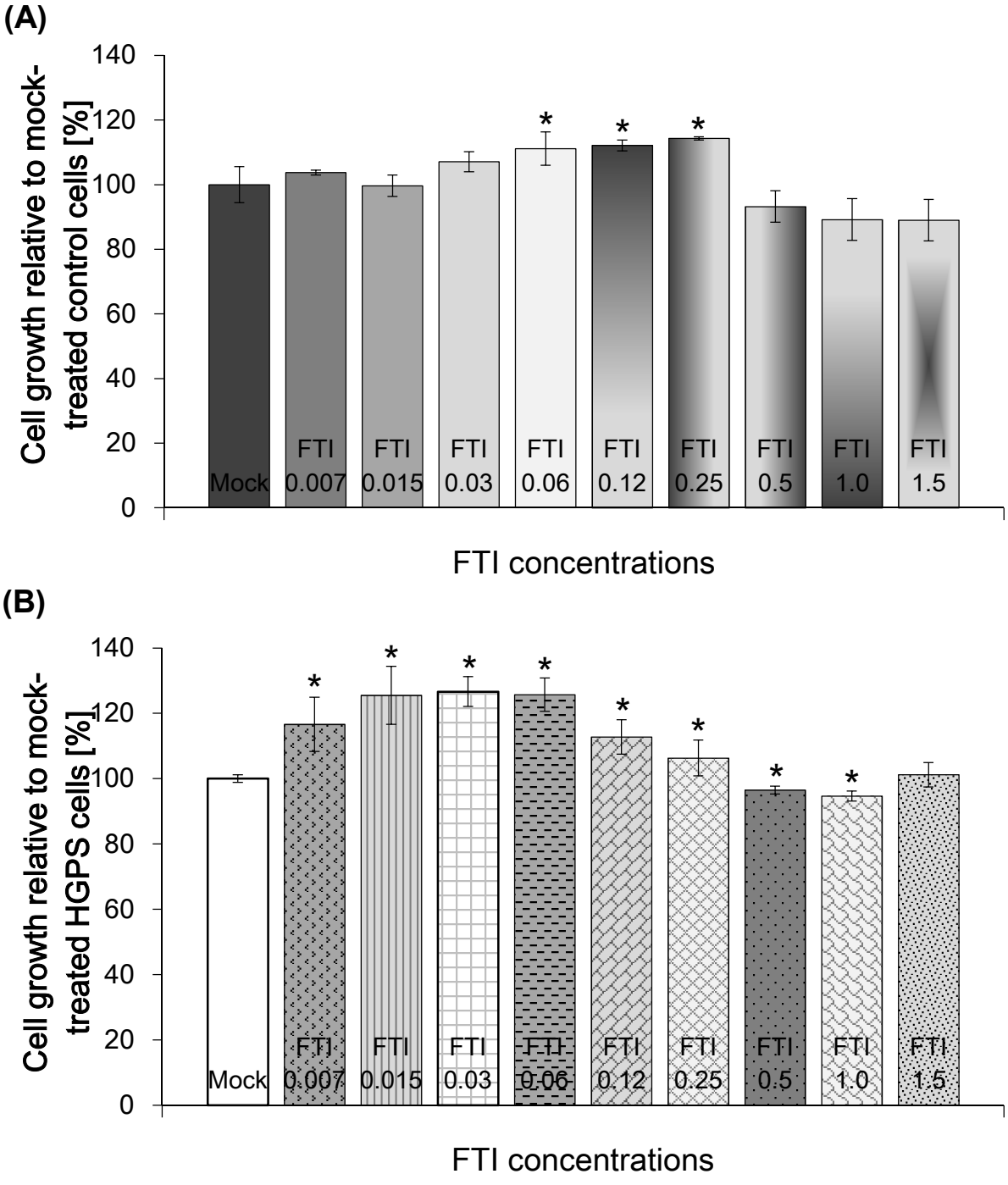

Figure 32: **Cell growth of control and HGPS fibroblasts after different FTI concentrations.** (A) Control cells were mock-treated (DMSO) or treated with different FTI concentrations FTI for 24h. Cell growth was calculated according to the cell counts and relative to mock-treated cells. Data are expressed as the mean ± S.D. (*p ≤ 0.05; n=5). (B) HGPS cells were treated and analyzed as stated in (A).

Control cells showed a sustained increase in growth rate until a concentration of 0.25 µM FTI was reached. Higher concentrations of FTI reduced the growth rate of control cells. In HGPS cells, the peak of cell growth was reached at a concentration of 0.06 µM FTI. Higher FTI concentrations showed a decrease in growth rates. Concentrations higher than 0.5 µM FTI led to cell death. Autophagy levels of control and HGPS cells were direct proportional with increased FTI concentration (Fig. 33 A, B).

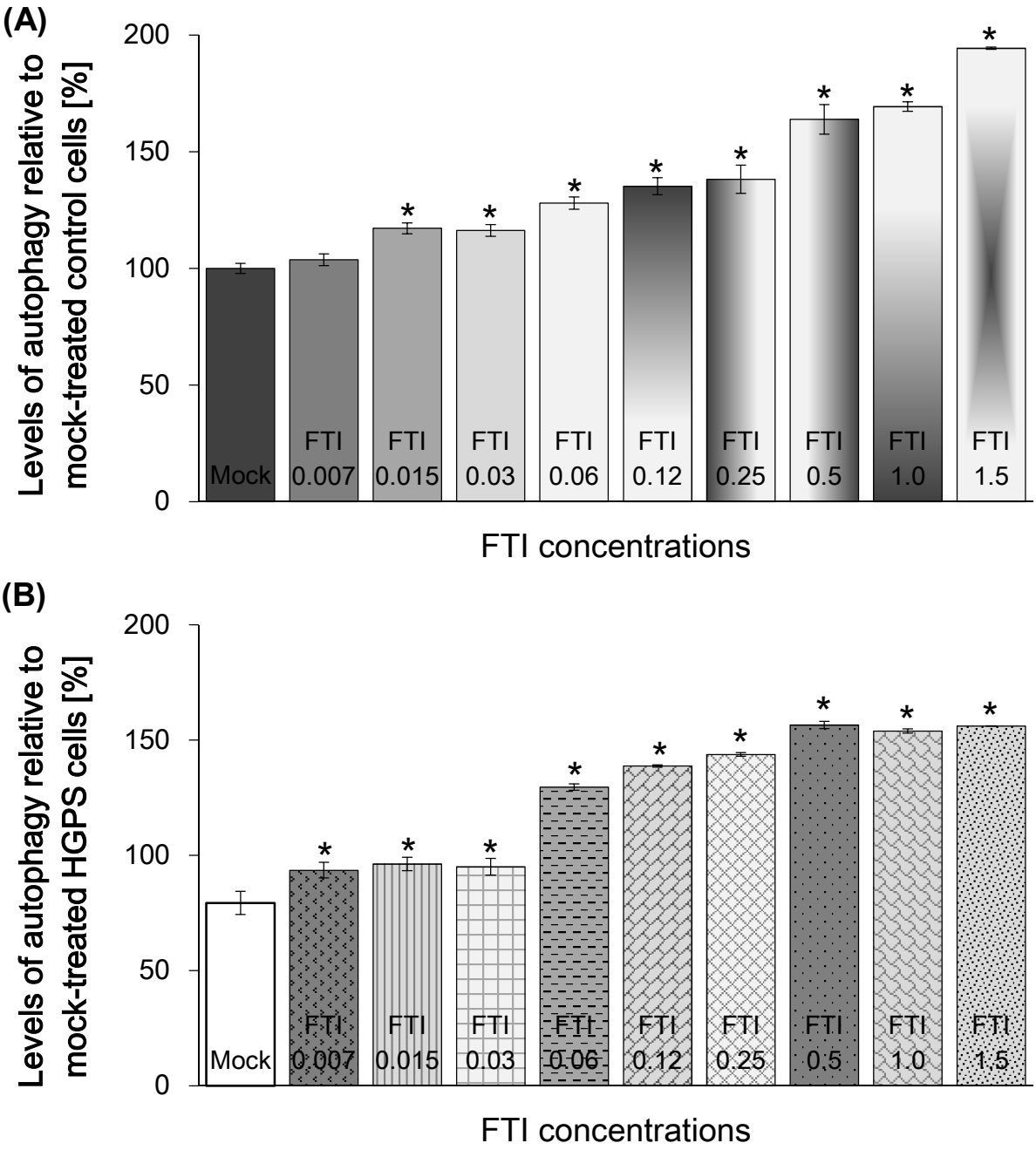

Figure 33: **Autophagy activity of different FTI concentrations.** (A and B) Autophagy activity was measured as described in the Methods section for control and HGPS cells, respectively. Cells were treated with different concentrations of FTI as indicated for 24h. The percentage of activity was calculated relative to mock-treated cells. Data are expressed as the mean ± S.D. (*p ≤ 0.05; n=5).

As mentioned, treatment with FTI leads to accumulation of non-farnesylated, full-length prelamin A, i.e. the more prelamin A accumulates the more effective the inhibition of the farnesylation by FTI. Hence, prelamin A accumulation was analyzed of HGPS fibroblasts after 1d of the indicated FTI concentrations (Fig. 34).

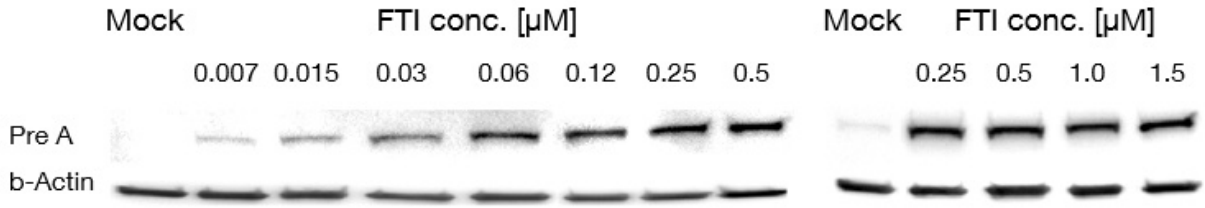

Figure 34: **Prelamin A accumulation at different FTI concentrations.** Western blot of HGPS cells mock-treated or treated with different concentrations of FTI (FTI conc.) for 24h. Blot was probed with an anti-prelamin A antibody and b-actin.

HGPS cells reached a sufficient level of prelamin A accumulation after 0.06 µM of FTI treatment. Collectively, beneficial effects were detected for 0.06 µM FTI on cell growth, autophagy, and prelamin A accumulation. For further experiments, 0.06 µM FTI was selected.

Subsequently, the effect of different SFN concentrations was observed on control and HGPS cells after 1d of treatment. SFN was investigated according autophagy induction without inducing cell death as SFN is known to clear progerin via autophagy (Fig. 35 A, B).[99]

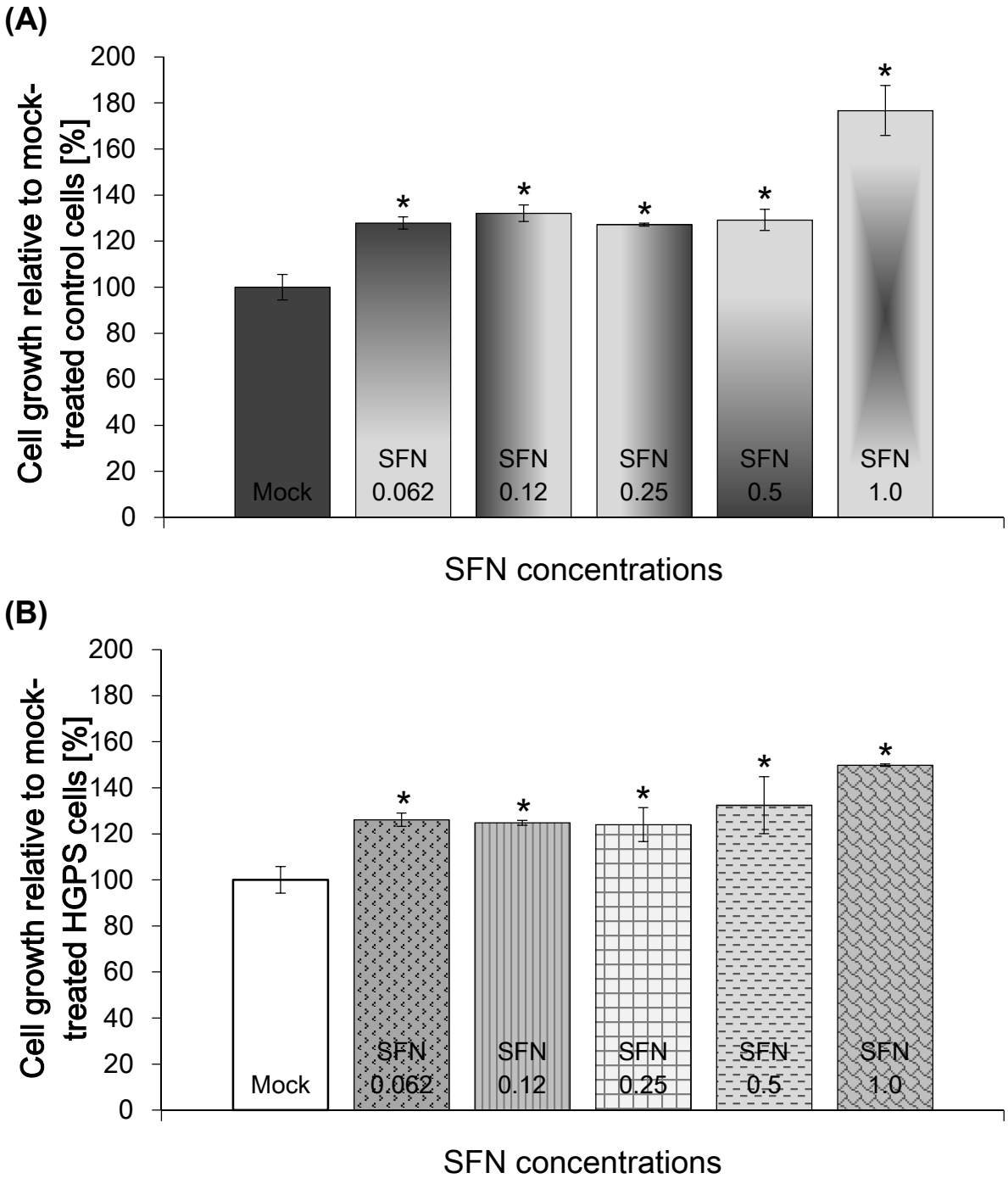

Figure 35: **Cell growth after different concentrations of SFN.** Control (A) and HGPS (B) cells were mock-treated or treated with different concentrations of SFN as indicated daily for 9 days. Cell growth was calculated according to the cell counts and relative to mock-treated cells and presented as the mean ± S.D. (*$p \leq 0.05$; n=5).

Control and HGPS cells showed an increased cell growth at any concentration of SFN. The highest growth rate was reached after 1 µM of SFN in control and HGPS cells. Autophagy levels were found to be increased at higher concentrations of SFN in control and HGPS cells (Fig. 36 A, B).

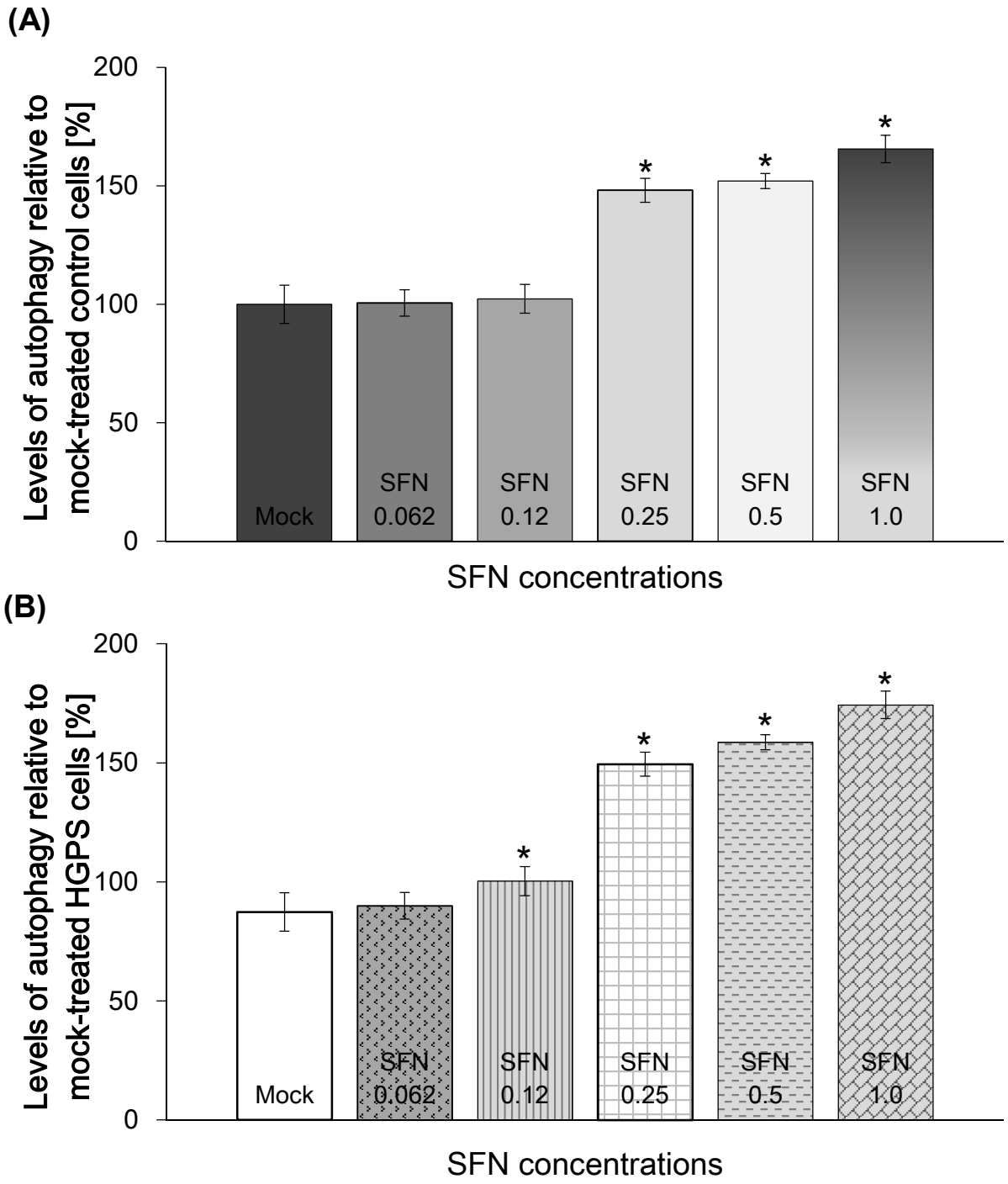

Figure 36: **Autophagy levels of different SFN concentrations.** Control (A) and HGPS (B) cells were mock-treated or treated with different concentrations of SFN as indicated daily for 9 days. Autophagy activity was determined as described in the Methods. Values were calculated relative to mock-treated cells and presented as the mean ± S.D. (*p ≤ 0.05; n=5).

Control cells showed a significant increase in autophagy levels at 0.25 µM SFN and the autophagy levels further increased with higher concentrations of SFN. Mock-treated HGPS cells exhibit lower autophagy levels when compared to control cells. SFN increased the autophagy levels of HGPS fibroblasts significantly at a

concentration of 0.25 µM. The levels of autophagy were further increased at 0.5 µM SFN and even more at 1 µM SFN. Highest autophagy levels were observed at 1 µM SFN and cells still showed increased proliferation in both control and HGPS cells. Hence, SFN was used at a concentration of 1 µM for further experiments. Previous studies showed that higher concentrations than 1 µM of SFN induced cell death.[99]
Nonetheless, how can these two drugs be combined to extract the positive properties of SFN and FTI and reverse the HGPS cellular phenotype? Preliminary data showed that simultaneous treatment of the cells with FTI and SFN is cytotoxic (Appendix 8.1). The cytotoxicity has to be avoided and another application of the drugs has to be found. It has recently been shown that HGPS cells require 3 days to reacquire their aberrant nuclear shape after FTI treatment.[169] Thus, the effect of FTI is reversible and washed away in 3 days. Taking this parameter into account allows designing a novel treatment regimen. After replacing FTI, SFN can be added for 3 days until the effect of FTI has been washed away. The positive effect of SFN within 3 days has been verified by previous studies (Chapter 4.2). This regimen comprises a cycle of treatment as follows: 0.06 µM FTI for 1d to detach progerin from the nuclear envelope, followed by 3 days of SFN treatment to enhance autophagy and antioxidant response. This treatment is hereafter referred as cycle treatment where n cycles display ((1d FTI+3 days SFN) x n) with n=number of cycles.

4.3.2 Cycle treatment induces the highest progerin clearance in HGPS

In order to analyze the efficiency of the cycle treatment, single treatment of SFN and FTI for the corresponding days were carried along. Cells were fed every day with fresh media containing the vehicle (DMSO) or the drugs. All treatments were analyzed and compared to the mock-treated control.
First, population doublings were examined after each indicated cycle (Fig. 37 A, B, C).

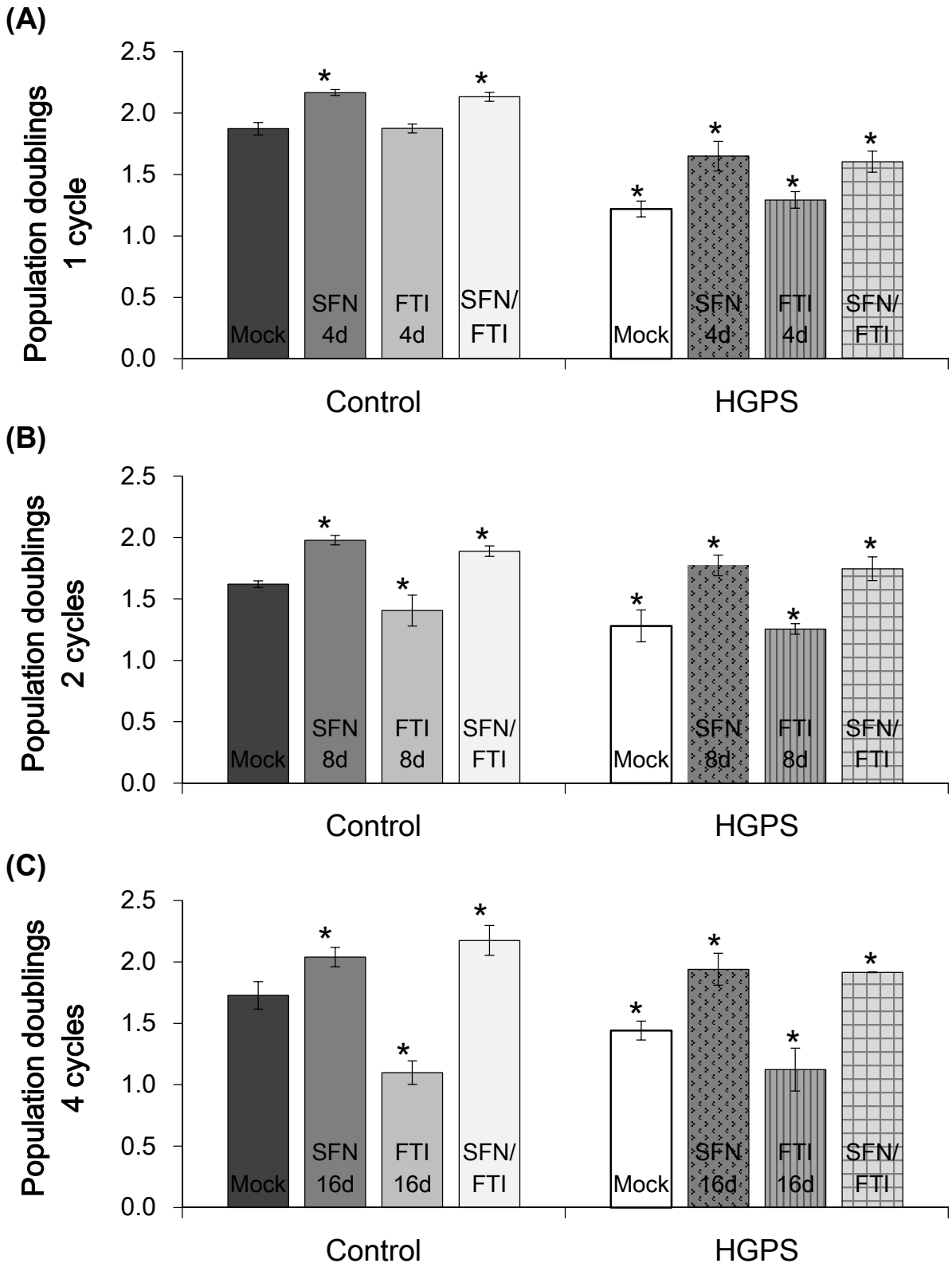

Figure 37: **Populations doublings of cycle-treated control and HGPS cells.** Population doublings were calculated as stated in Materials and Methods relative to mock-treated control for 1 cycle (A), 2 cycles (B), and 4 cycles (C). Cells were either mock-treated (vehicle DMSO) or treated with 0.06 µM FTI for 1 day followed by 3 days of 1 µM SFN treatment which corresponds to 1 cycle. Single treatment of 0.06 µM FTI and 1 µM SFN for the corresponding time duration (4 days, 8 days, and 16 days) was carried along for comparison reasons (*$p \leq 0.05$, n=5). Cells were fed in a daily manner.

While mock-treated control cells exhibit higher proliferation rates, mock-treated HGPS cells showed meager cell growth. Control cells and HGPS cells showed significantly increased proliferation after 4 days of SFN treatment or 1 cycle of SFN/FTI. FTI treatment for 4 days did not improve nor deteriorate the cell growth in control and HGPS fibroblasts. Prolonged treatment of SFN for 8 days and two cycles of SFN/FTI induced significantly higher growth rates of control and HGPS cells. The proliferation defect of HGPS cells was reversed after 8 days of SFN treatment or two cycles of SFN/FTI. While FTI treatment of 8 days induced cell death in control cells, HGPS cells were less affected by this treatment and showed the same proliferation rates as mock-treated HGPS cells. Sixteen days of SFN treatment or 4 cycles of SFN/FTI treatment further improved the cell growth in control and HGPS cells. Cell growth of FTI-treated cells was significantly reduced after 16 days of treatment. Collectively, single SFN treatment and cycle treatment reversed the proliferation defect after 8 days of treatment in HGPS fibroblasts to the same extent and led to significantly higher proliferation rates in control cells.

Autophagy induction of SFN, FTI, and SFN/FTI was tested as progerin is degraded via the autophagy system (Fig. 38 A, B, C).[10]

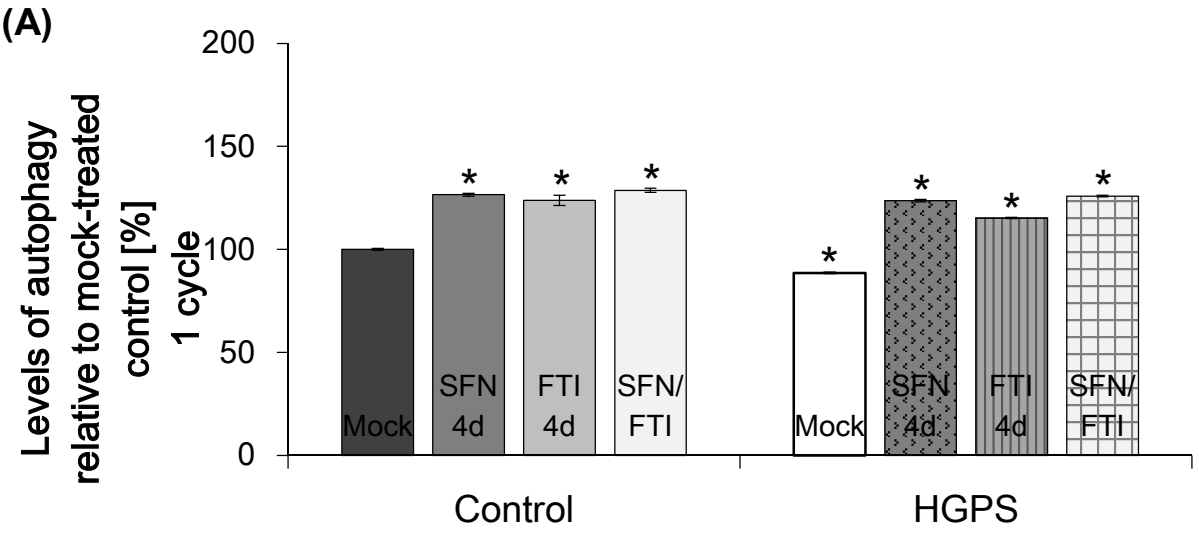

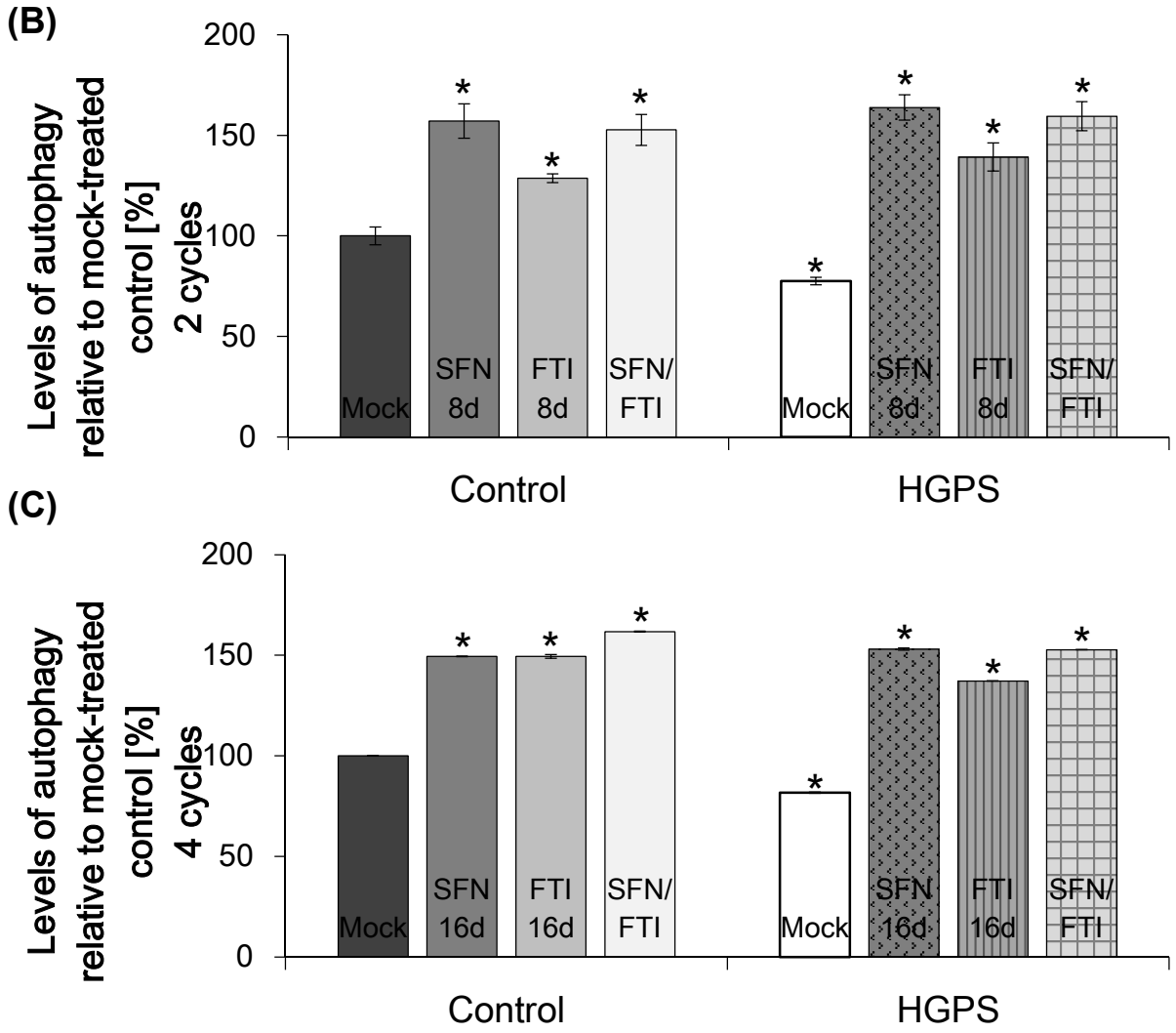

Figure 38: **Autophagy activity after cycle treatment.** Autophagy activity was measured after 1 cycle (A), 2 cycles (B), and 4 cycles (C) by using monodansylcadaverine (MDC). Control and HGPS cells were either mock-treated (vehicle DMSO) or treated with 0.06 µM FTI for 1 day followed by 3 days of 1 µM SFN treatment which corresponds to 1 cycle. Single treatment of 0.06 µM FTI and 1 µM SFN for the corresponding time (4 days, 8 days, and 16 days) was carried along for comparison reasons. Data are expressed as the mean ± S.D. relative to mock-treated control (*$p \leq 0.05$; n=5).

Autophagy levels were significantly increased in control and HGPS cells after all 3 drug treatments and even increased with time: the longer the treatment of the cells, the higher the autophagy levels became. Single SFN treatment and cycle treatment reached approximately the same autophagy levels, whereas FTI induced autophagy to a lesser extent.

Next, it was analyzed to which level the autophagy induction leads to progerin clearance in HGPS. Western blot analysis was performed and the ratios of the A-type lamins were quantified (Fig. 39 A, B, C).

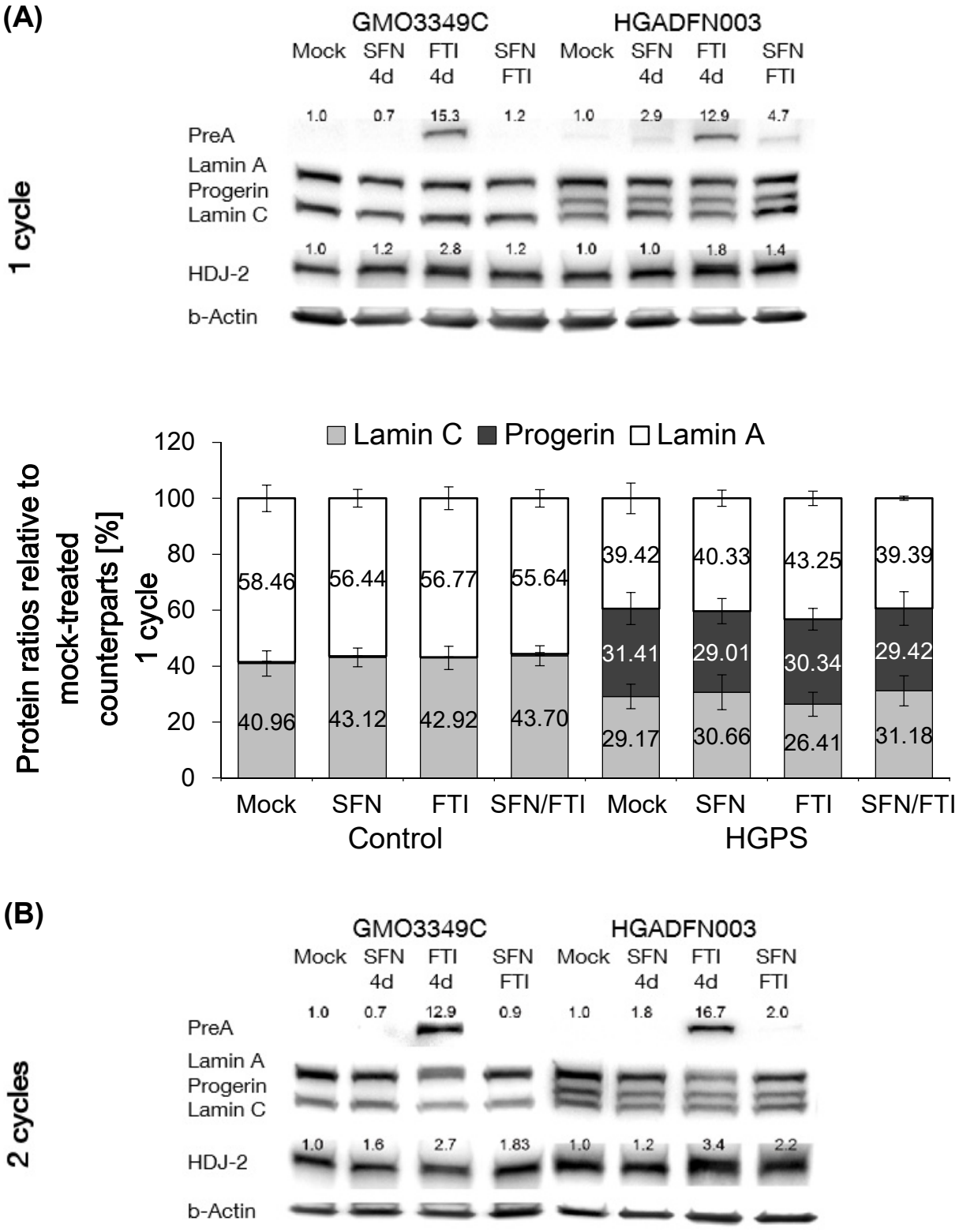

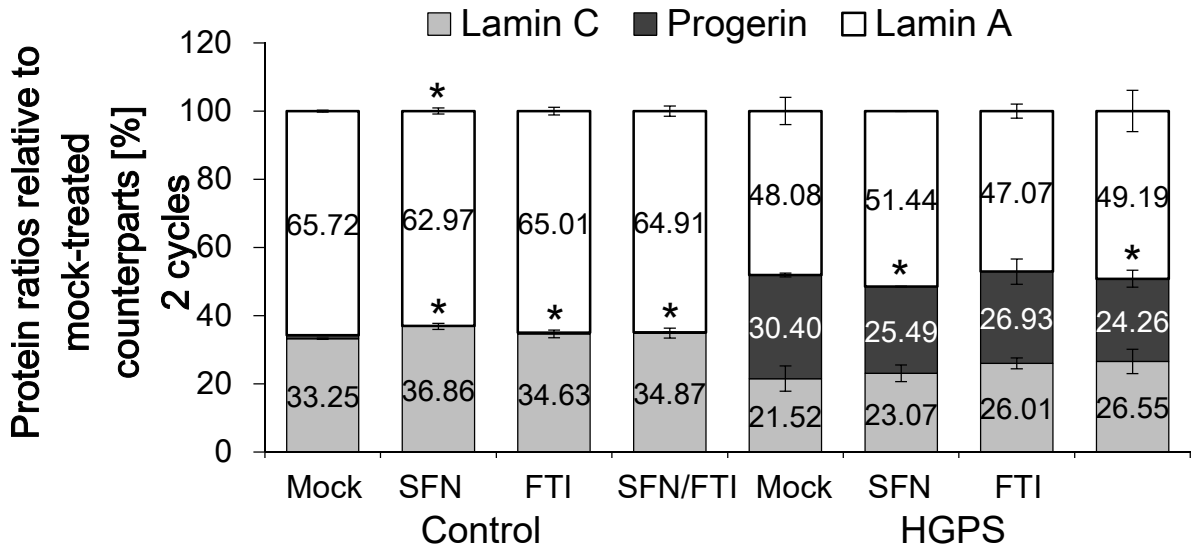
Lamin C
Progerin
Lamin A
Protein ratios relative to mock-treated counterparts [%]
2 cycles
120
100
80
60
40
20
0
65.72
62.97
65.01
64.91
48.08
51.44
47.07
49.19
33.25
36.86
34.63
34.87
30.40
25.49
26.93
24.26
21.52
23.07
26.01
26.55
Mock
SFN
FTI
SFN/FTI
Mock
SFN
FTI
Control
HGPS

(C)

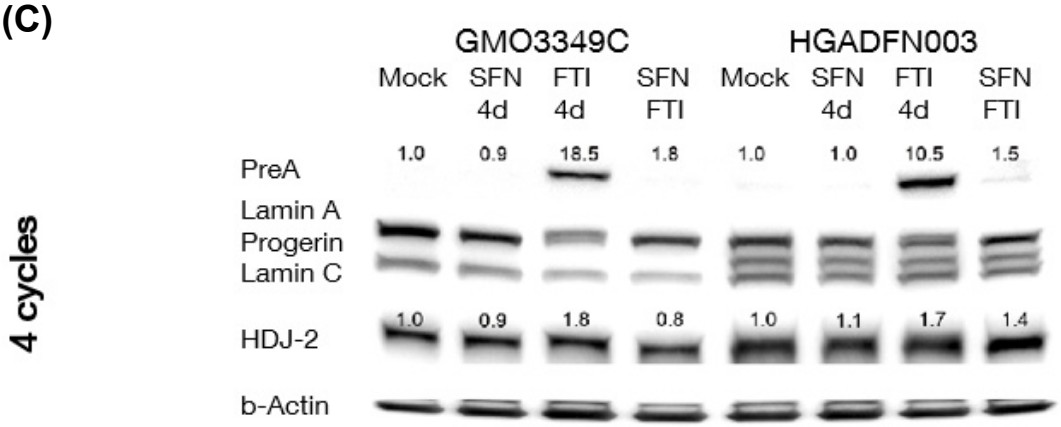
GMO3349C
HGADFN003
Mock
SFN 4d
FTI 4d
SFN FTI
Mock
SFN 4d
FTI 4d
SFN FTI
4 cycles
PreA
Lamin A
Progerin
Lamin C
HDJ-2
b-Actin
1.0
0.9
18.5
1.8
1.0
1.0
10.5
1.5
1.0
0.9
1.8
0.8
1.0
1.1
1.7
1.4

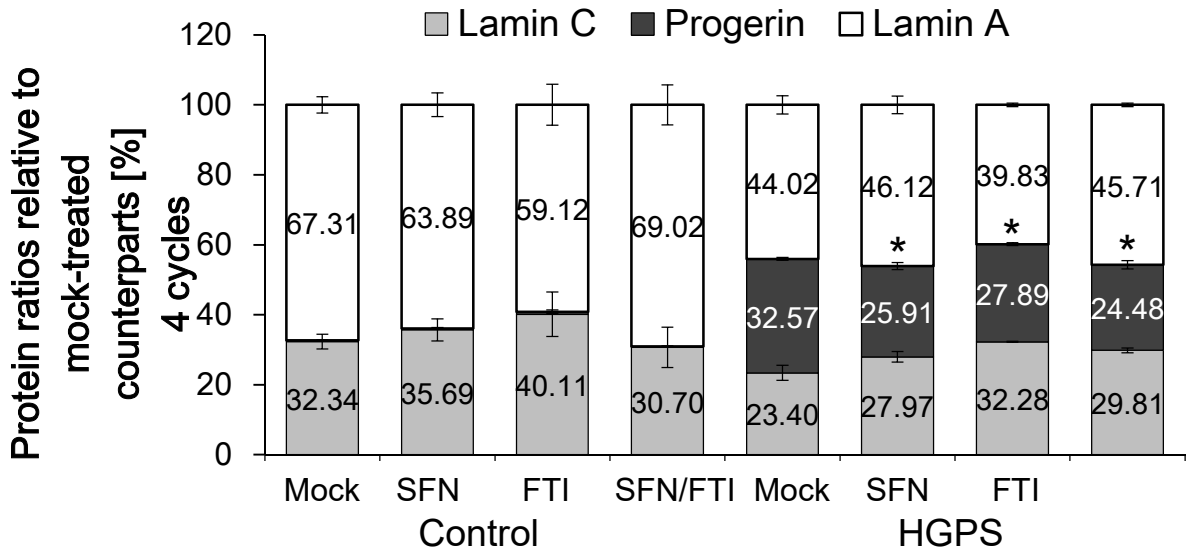

Figure 39: **Western blots and their quantification after cycle treatment.** Representative Western blots of control and HGPS fibroblasts after 1 cycle (A), 2 cycles (B), and 4 cycles (C). 1 cycle represents 1 day 0.06 µM FTI treatment followed by 3 days of 1 µM SFN. Blots were probed with prelamin A, lamin a/c, HDJ-2, and b-actin antibodies (n=4). Numbers above prelamin A and HDJ-2 bands indicate the fold-change of these proteins relative to their mock-treated counterparts. The ratios of A-type lamins were determined within each sample relative to mock-treated counterparts and analyzed by Western blot with lamin A/C antibody according to 1 cycle (A, lower panel), 2 cycles (B, lower panel), and 4 cycles (C, lower panel). Single treatment of 0.06 µM FTI and 1 µM SFN for the corresponding time (4 days, 8 days, and 16 days) was carried along for comparison reasons (*$p \leq 0.05$, n=4).

During the first cycle and single treatment of 4 days, progerin clearance was not significantly induced. SFN and cycle treatment led to a clearance of progerin by 7 % while FTI showed a clearance of 3 %. Progerin was cleared significantly by 20 % and 16 % after two cycles and 8 days of SFN, respectively. The status of the A-type lamins was ameliorated. FTI treatment for 8 days cleared progerin by 11 %. Long-term treatment of HGPS cells showed a significant reduction of progerin in all 3 drug treatments. FTI treatment for 16 days cleared progerin by 14 % while SFN induced a clearance of 20 %. The cycle treatment induced the greatest progerin clearance after only 16 days. Progerin was decreased by 25 % after 4 cycles of 1 day FTI followed by 3 days SFN. The status of the A-type lamins in SFN- and cycle-treated HGPS cells was ameliorated after 8 days and maintained during treatment.

The efficiency of FTI treatment was detected with prelamin A staining and HDJ-2 staining. Inhibition of farnesylation results in prelamin A accumulation and non-farnesylated HDJ-2 accumulation. While FTI increases both prelamin A and non-

farnesylated HDJ-2 (indicated by the numbers above each band), cycle treatment showed reduced accumulation of these proteins when compared to FTI-treated cells.

Other characteristics of HGPS cells are elevated levels of ROS and reduced levels of ATP.[148] The compound SFN has been found to reduce ROS and increase cellular ATP levels in HGPS fibroblasts.[99] By contrast, FTI induced oxidative DNA damage by ROS and significant higher ATP levels.[170-172] The potential of the cycle treatment to ameliorate ROS and ATP levels in HGPS fibroblasts was tested (Fig. 40, 41).

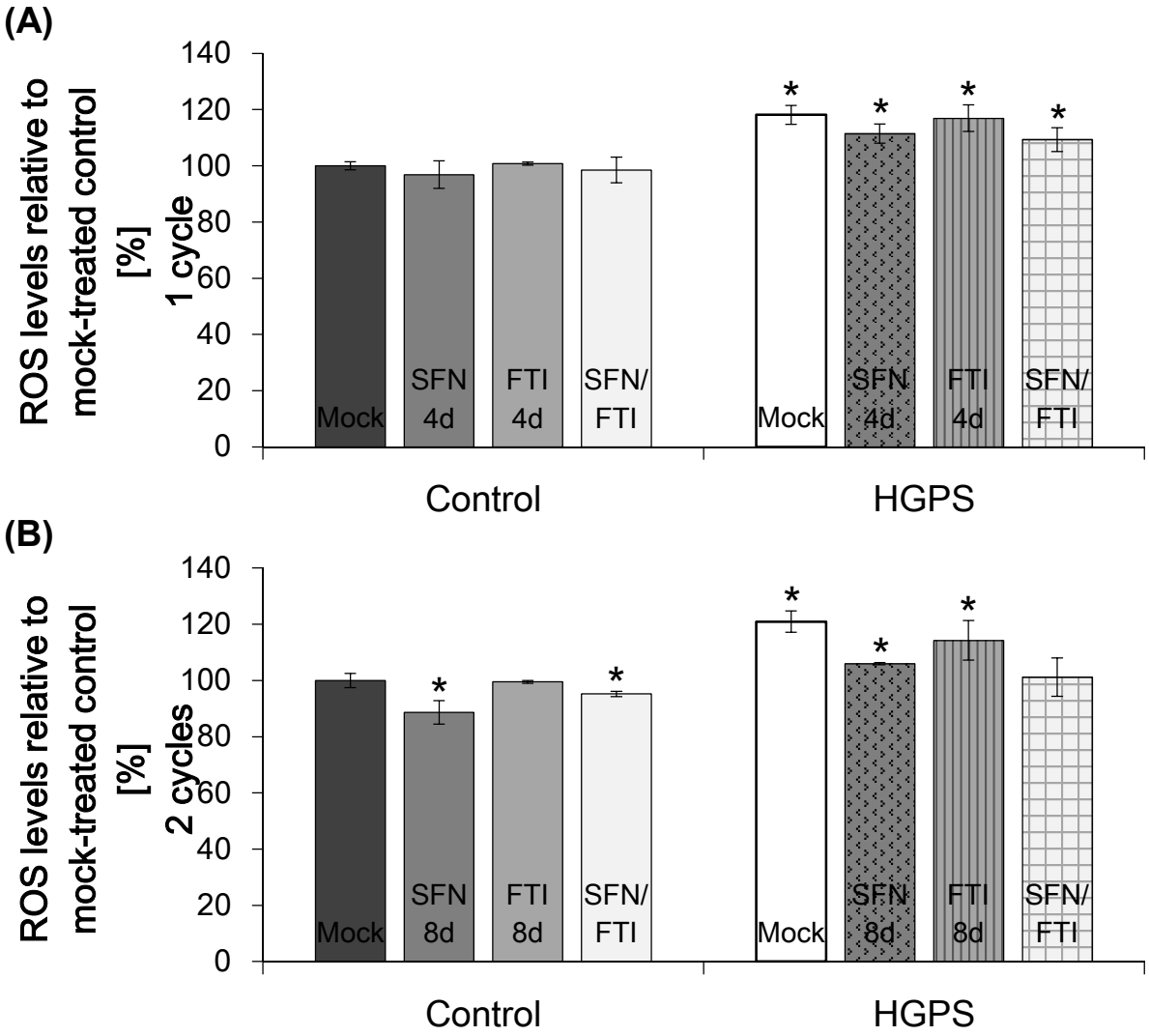

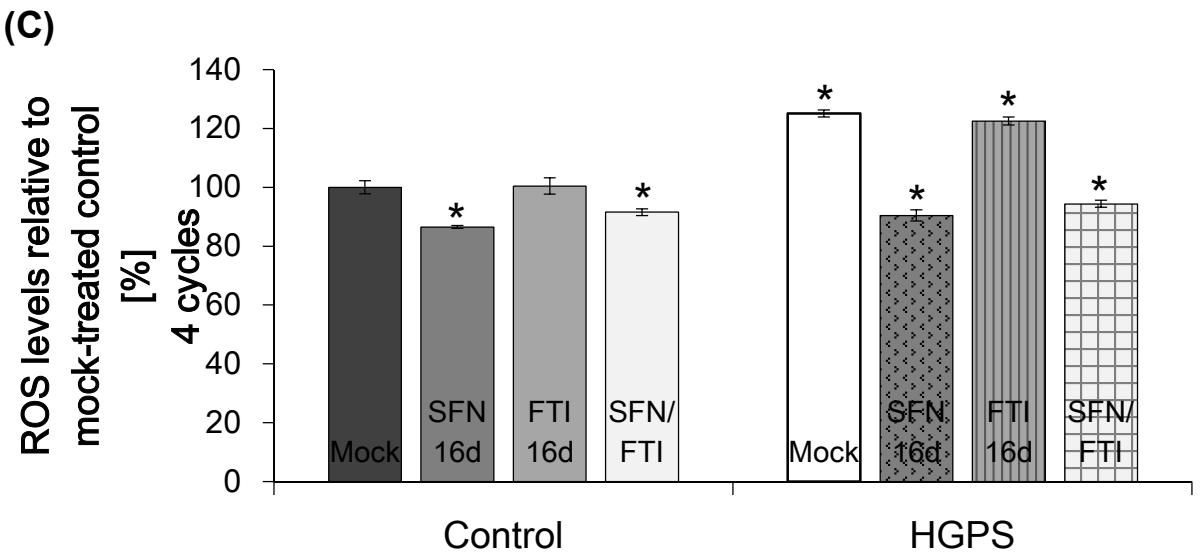

Figure 40: **Reactive oxygen species levels after cycle-treatment.** Intracellular ROS levels of mock-treated and 1 cycle (A), 2 cycles (B), and 4 cycles (C) of treated control and HGPS cells were determined by measuring oxidized dichlorofluorescin (DCF) levels as described in the Methods. Single SFN and FTI treatment were carried along for the corresponding times. Data represents the mean ± S.D. (*$p \leq 0.05$; n=5) relative to mock-treated control.

ROS levels were found to be significantly increased in HGPS cells compared to control cells (Fig. 40). While FTI treatment induced no significant change in ROS levels, SFN and cycle treatment reduced reactive oxygen species in control and HGPS fibroblasts. In HGPS, 1 cycle treatment reduced ROS levels significantly (Fig. 40 A) and ROS levels were further significantly reduced with additional cycles (Fig. 40 B, C). SFN started to significantly reduce ROS levels after 8 days of treatment in HGPS cells (Fig. 40 B). Furthermore, control cells showed significantly reduced ROS levels after 8 days of SFN treatment or two cycles (Fig. 40 B). The lower ROS levels were maintained after 16 days of SFN treatment or 4 cycles in control fibroblasts (Fig. 40 C).

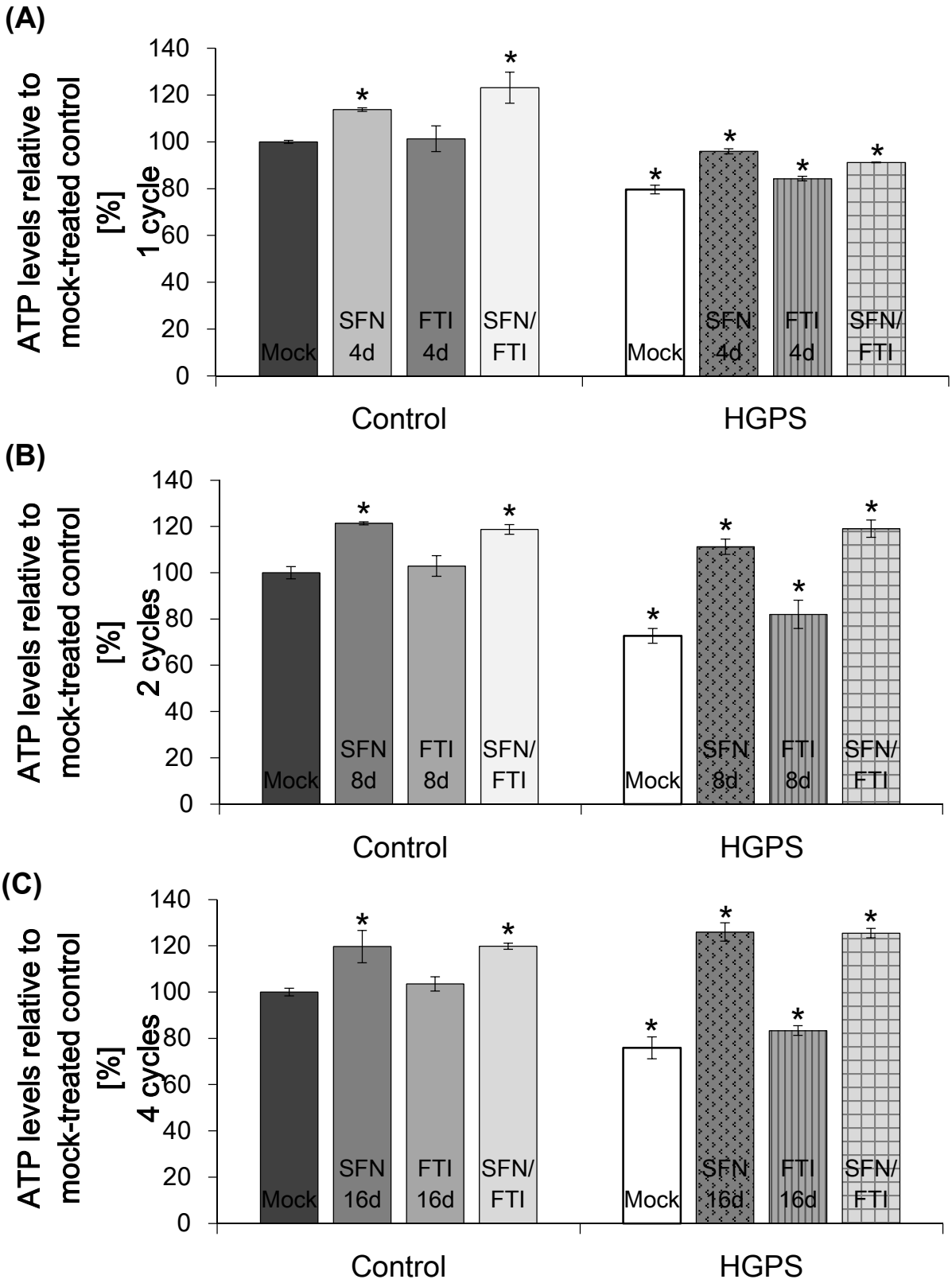

Figure 41: Cellular ATP levels of cycle-treated fibroblast cells. ATP levels of control and HGPS cells mock-treated or treated with 1 cycle (A), 2 cycle (B) or 4 cycles (C) of FTI and SFN were measured using a CellTiter Glo assay as described in the Methods. Single treatments of SFN and FTI for the corresponding days were carried along for comparison reasons. Data represents the mean ± S.D. (*$p \leq 0.05$; n=5) relative to mock-treated control cells.

HGPS cells exhibit reduced levels of cellular ATP levels and further evidence was provided that single SFN treatment increases cellular ATP levels that were further improved with time (Fig. 41 A-C). FTI treatment induced a slight increase in cellular ATP levels of control and HGPS cells even though it is not significant at day 4 and 8 (Fig. 41 A, B). ATP levels were significantly increased after 16 days of FTI treatment (Fig. 41 C). Cycle treatment showed a significant increase in cellular ATP levels after 1 cycle in control and HGPS cells (Fig. 41 A). After two cycles of treatment, ATP levels of HGPS cells were restored and were found to be even higher than mock-treated control levels (Fig. 41 B). Four cycles of SFN/FTI treatment further improved cellular ATP levels (Fig. 41 C). All cycle treatments exhibit the same increased ATP levels as single SFN treatment.

However, other regimens of cycle treatment could also ameliorate the HGPS cellular phenotype. By shortening the intervals of FTI, more progerin could be detached from the nuclear envelope and cleared by SFN via autophagy. Further experiments have been conducted to analyze whether shorter SFN treatment within the cycles could improve the HGPS cellular phenotype even more than the 1d FTI followed by 3d SFN. This cycle could be described as n cycles = ((1d FTI+2 days SFN) x n) with n=number of cycles. The data can be seen in Appendix 8.2.1.
The same experiments and concentrations were used as stated for the 1d FTI followed by 3d SFN treatment. The same positive outcome was observed for the new cycle treatment of control and HGPS cells. Single SFN and FTI treatment showed the same results as expected. Only the differences will be highlighted given that the effect of 1d FTI followed by 2d SFN was similar to 1d FTI followed by 3d SFN.
Comparing the rates of the population doublings, HGPS cells treated for 1 cycle of 1d FTI/3d SFN showed 6 % higher growth rates compared to the 1 cycle of 1d FTI/2d SFN. Two cycles of SFN/FTI showed 7 % higher growth rates than 3 cycles of 1d FTI/2d SFN and 4 cycles of SFN/FTI showed 14 % higher proliferation rates than 6 cycles of 1d FTI/2d SFN.
Autophagy levels of 1 cycle 1d FTI/3d SFN were 13 % higher than 1 cycle of 1d FTI/2d SFN. After 2 cycles of 1d FTI/3d SFN, autophagy levels were 20 % more increased and were still increased by 13 % after 4 cycles compared to 3 cycles of 1d FTI/2d SFN and 6 cycles, respectively.

Progerin clearance was 6 % higher after 4 cycles of 1d FTI/3d SFN compared to 6 cycles of 1d FTI/2d SFN.
ATP levels were reduced to a same extent in 1d FTI/3d SFN-treated HGPS cells and 1d FTI/2d SFN-treated HGPS cells whereas ROS levels were more reduced in 1 cycle of 1d FTI/3d SFN-treated HGPS cells than in 1 cycle of 1d FTI/2d SFN-treated HGPS cells (4 %). During the treatment, ROS levels were similarly reduced after 2 cycles and 3 cycles, respectively. After 4 cycles of 1d FTI/3d SFN, ROS levels were 4 % lower in HGPS cells than in 6 cycles of 1d FTI/2d SFN-treated HGPS cells.

4.3.3 Cycle treatment reverses the nuclear shape without causing FTI side effects

The nuclei of HGPS fibroblasts are characterized by nuclear envelope alterations and reduced levels of nuclear components such as lamin B1.[5,166] FTI treatment has been shown to reduce the nuclear shape abnormalities.[93] However, FTI disrupts the lamin B network, causes prelamin A accumulation and donut-shaped nuclei. [13,99,173]
These alterations were investigated by immunofluorescence after 2 cycles of 1d FTI/3d SFN (Fig. 42, 43, 44, 45). Single treatments of SFN and FTI were conducted for comparison reasons.
Staining with anti-lamin A/anti-progerin antibodies revealed that all treatments reduces the nuclear-shape alterations of HGPS fibroblasts (Fig. 42).

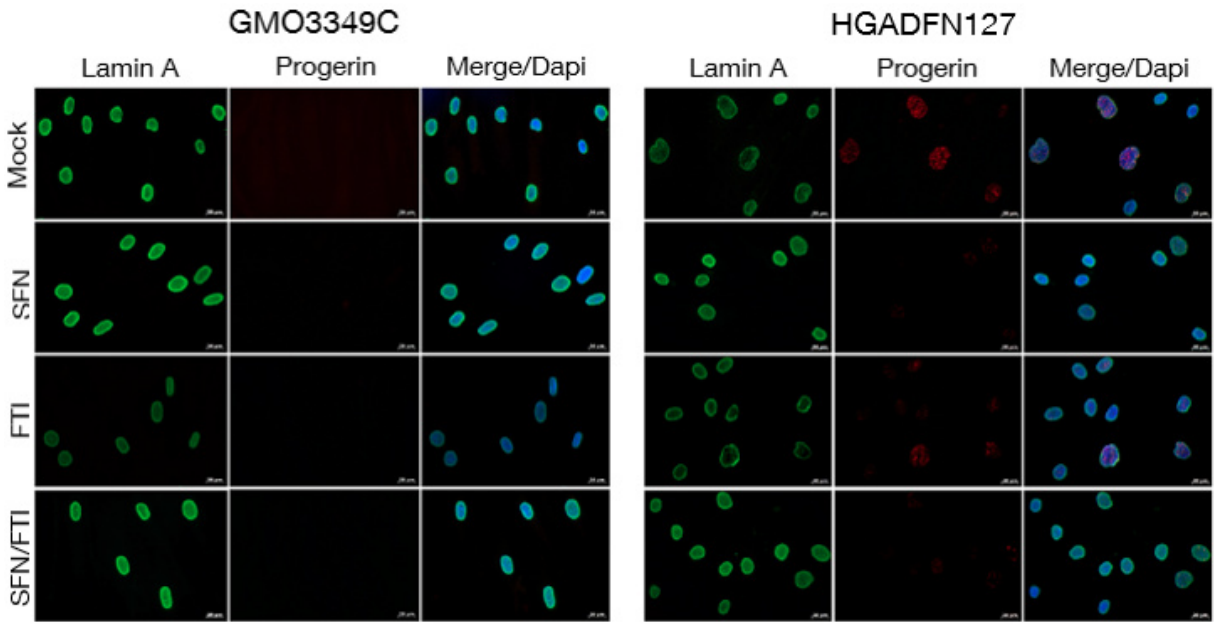

Figure 42: Nuclear shape alterations of HGPS fibroblasts after cycle treatment. Immunochemistry was performed of control (GMO3349C) and HGPS (HGADFN127) fibroblast after 2 cycles of 1 day 0.06 µM FTI and 3 days 1 µM SFN treatment using antibodies directed against indicated proteins (lamin A and progerin). Single treatment of 0.06 µM FTI and 1 µM SFN for 8 days was carried along for comparison reasons. Cells were treated daily with fresh medium. Representative images are shown (n=4). Scale-bar: 20 µm.

HGPS cells show a control-like nuclear shape that appears to be ovoid and without nuclear blebbing after SFN-, FTI-, and cycle treatment. Progerin clearance is higher in SFN- and cycle-treated HGPS cells as in FTI-treated cells. As expected, lamin A staining is weaker in FTI-treated cells than the lamin A staining of the other treatments due to the inhibition of mature lamin A processing.

In mock-treated HGPS cells, weak lamin B staining is concomitant with bright progerin staining (Fig. 43).

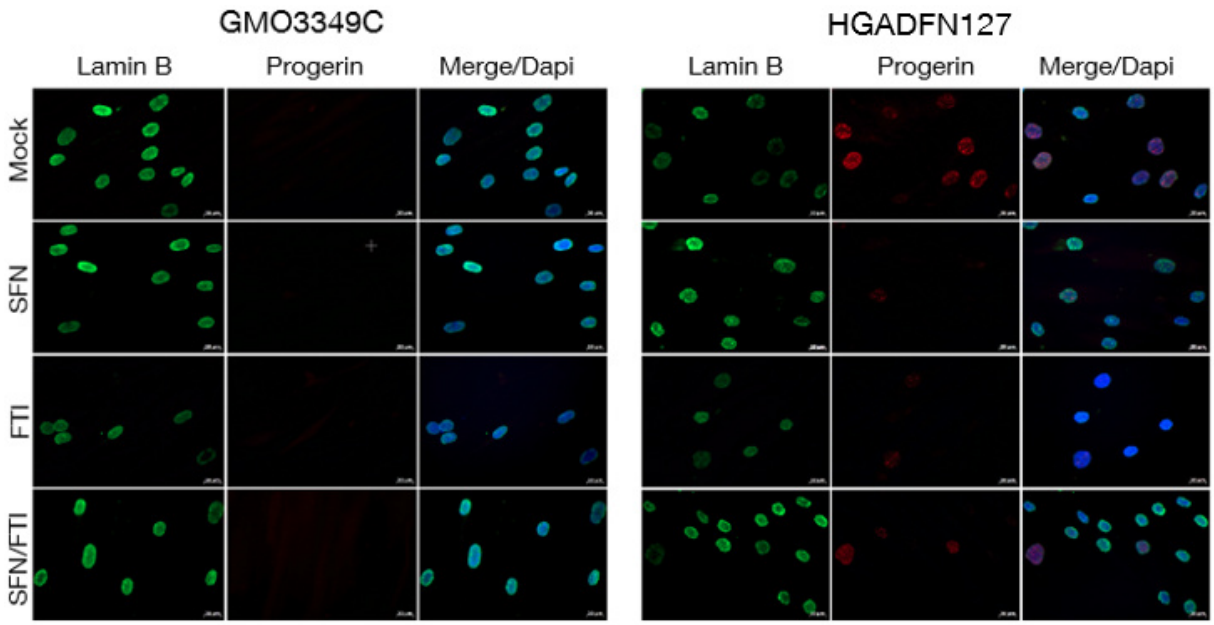

Figure 43: **Lamin B network after cycle treatment of control and HGPS cells.** Immunochemistry was performed of control (GMO3349C) and HGPS (HGADFN127) fibroblast after 2 cycles of 1 day 0.06 µM FTI and 3 days 1 µM SFN. Single treatment of 0.06 µM FTI and 1 µM SFN for 8 days was carried along for comparison reasons. Cells were treated daily with fresh medium. Antibodies directed against indicated proteins were used (lamin B1 and progerin). Representative images are shown (n=4) Scale bar: 20 µm.

In SFN-treated and cycle-treated HGPS cells, progerin levels are reduced while lamin B staining showed control-like behavior. In FTI-treated cells, lamin B appeared as weak staining, which can be explained by the fact that the farnesylation of lamin B is also inhibited by FTI.

Accumulation of prelamin A has been clearly observed after FTI treatment in control and HGPS cells while mock-treated and SFN-treated cells shows barely prelamin A (Fig. 44). The cycle treatment slightly induced prelamin A accumulation. However, the brightly labeled nuclei after FTI treatment were not observed in the cycle-treated cells.

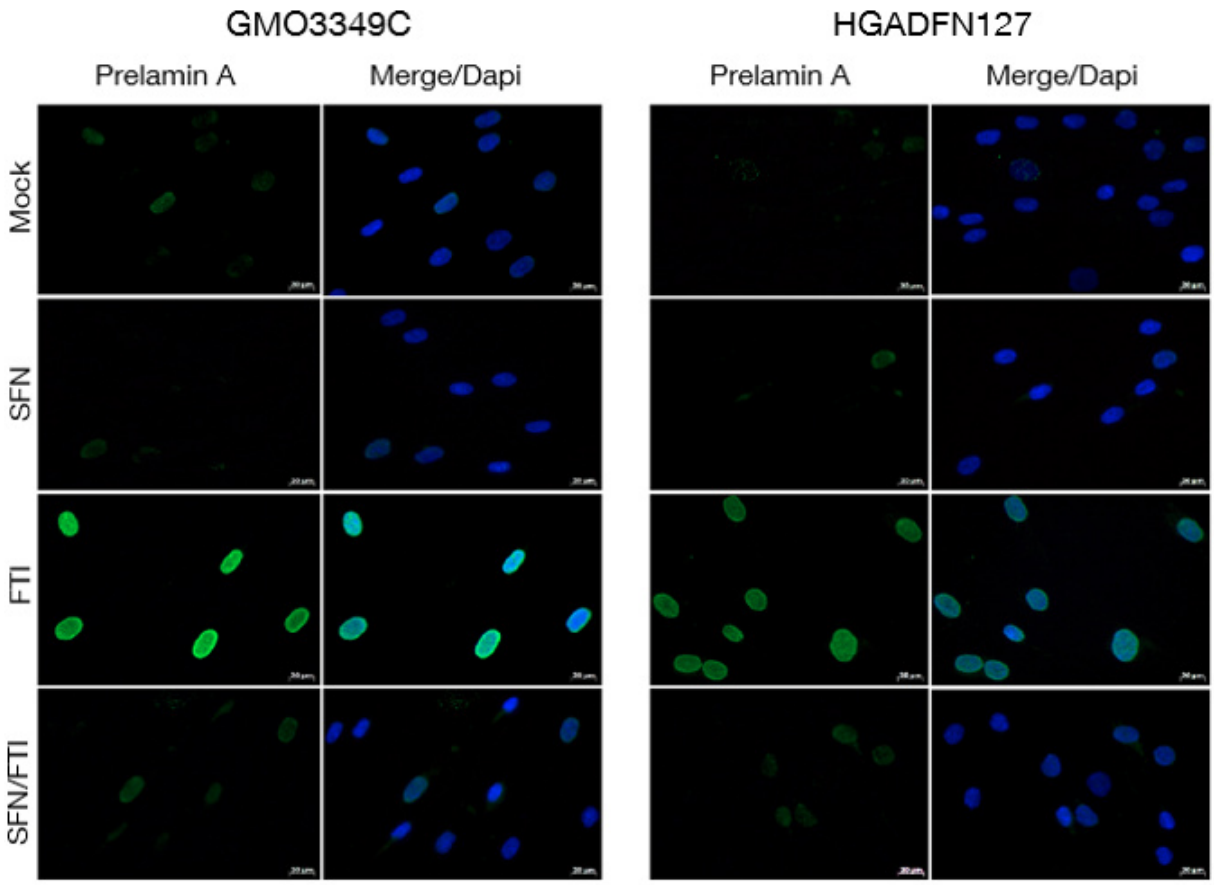

Figure 44: **Immunofluorescence of prelamin A accumulation after cycle treatment.** Immunochemistry was performed of control (GMO3349C) and HGPS (HGADFN127) fibroblast after 2 cycles of 1 day 0.06 µM FTI and 3 days 1 µM SFN. Single treatment of 0.06 µM FTI and 1 µM SFN for 8 days was carried along. Antibody directed against prelamin A was used. Representative images are shown (n=4). Scale bar: 20 µm.

The analysis of donut-shaped nuclei was performed by direct counts of the lamin A-stained nuclei (Fig. 45).

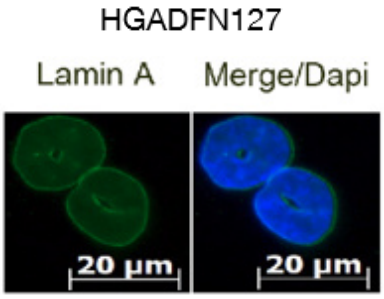

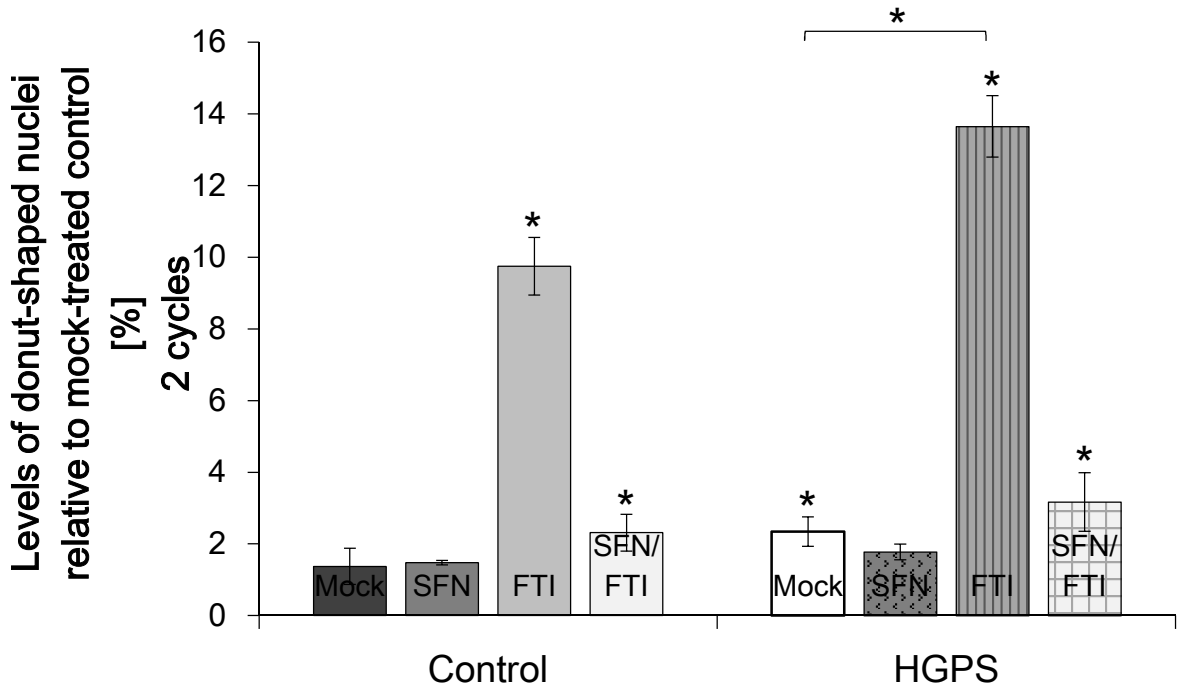

Figure 45: **Analysis of donut-shaped nuclei after cycle treatment.** Control and HGPS fibroblast after 2 cycles of 1 day 0.06 µM FTI and 3 days 1 µM SFN were used to analyze donut-shaped nuclei by direct counts of lamin A-stained nuclei. An average of 1,000 nuclei were counted. Upper panel shows donut-shaped nuclei. Lower panel shows the quantification of donut-shaped nuclei relative to mock-treated control. Data are presented as the mean ± S.D. (*p ≤ 0.05; n=3).

Mock-treated HGPS cells showed higher levels of donut-shaped nuclei compared to mock-treated control cells. Donut-shaped nuclei were also generated in control and HGPS cells after FTI treatment, which further confirmed previous studies. The levels were found to be significantly increased by 5-fold after FTI treatment compared to their mock-treated counterparts. Cycle treatment showed the tendency of donut-shaped nuclei generation but the higher levels were not significantly elevated when compared to mock-treated cells. SFN treatment showed the same levels of donut-shaped nuclei in control cells as mock-treated control cells. In HGPS, SFN reduced the levels of donut-shaped nuclei compared to mock-treated HGPS cells.

The immunofluorescence staining was also repeated with the shorter cycle treatment. Cells were treated for 3 cycles with 1d FTI followed by 2d SFN (Appendix 8.2.2). Single drug treatment with SFN and FTI for 9 days were carried along for comparison reasons. With this cycle treatment we could also detect the same beneficial effects of the nuclear shape, lamin B network and prelamin A accumulation as for the 2-cycle treatment with 1d FTI and 3d SFN. The only minor difference was found in the appearance of donut-

shape nuclei. Compared to 2 cycles of 1d FTI/3d SFN, 3 cycles of 1d FTI/2d SFN showed 3 % more donut-shaped nuclei. The induction of donut-shaped nuclei is significantly higher in the 3-cycle-treated HGPS cells (1d FTI/2d SFN) compared to mock-treated HGPS cells. By contrast, the 2 cycles of 1d FTI/3d SFN showed no significant increase in donut-shaped nuclei.

4.3.4 Cycle treatment reduces DNA damage and activates DNA damage response

HGPS fibroblasts have been shown to have a susceptibility to DNA damage due to defective DNA damage repair response.[174] DNA damage repair factors have been found to be altered in HGPS cells such as 53BP1 and Rad51.[167,168] SFN treatment has been shown to reduce the levels of DNA damage by inducing DNA damage repair response by 53BP1 and Rad51.[99] By contrast, FTI treatment did not result in reducing the frequency of DNA DSBs and damage checkpoint signaling.[6] Thus, it was tested whether the cycle treatment could reduce DNA damage in HGPS fibroblasts by the induction of DNA damage response.

Immunofluorescence staining has been performed of control and HGPS cells treated with SFN, FTI or 2 cycles of 1d FTI/3d SFN. Antibodies directed against anti-γH2A.X, anti-53BP1, and anti-Rad51 have been used. Levels of 53BP1 have been confirmed and quantified by Western blot. Direct counts of nuclei harboring the DNA damage marker H2A.X allowed the analysis whether drug treatment improves the accumulation of DNA damage (Fig. 46).

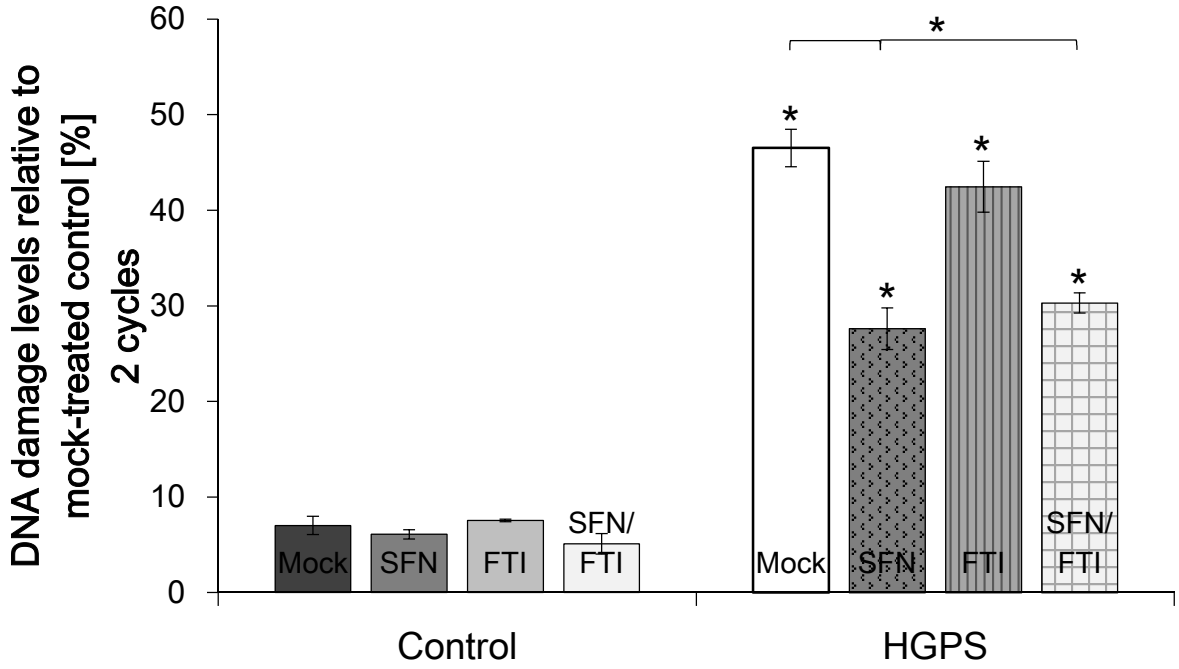

Figure 46: **Number of DNA damage foci after cycle treatment.** Analysis of DNA damage by direct counts of H2A.X-stained nuclei of control and HGPS fibroblast mock-treated or treated for 2 cycles with 1 day 0.06 µM FTI followed by 3 days 1 µM SFN. Single treatment of 0.06 µM FTI and 1 µM SFN for 8 days was carried along for comparison reasons. Cells were treated daily with fresh medium. An average of 1,000 nuclei were counted. Quantification of DNA damage levels are relative to mock-treated control. Data are presented as the mean ± S.D. (*p ≤ 0.05; n=3).

The number of HGPS nuclei harboring γH2A.X foci was 47 % on average, which was significantly higher compared to 7 % of DNA damage in control cells. Treatment with SFN led to a significant reduction of DNA damage. Control cells showed an average of 6 % of DNA damage and the DNA damage levels of HGPS were reduced significantly to 27 % after 8 days of SFN treatment. FTI did not ameliorate the levels of DNA damage in control cells and only reduced the levels in HGPS to 42 %. Two cycles of 1d FTI/3d SFN reduced the levels of DNA damage in control cells to 5 % and in HGPS cells significantly to 30 %.

The analysis of the DNA damage repair factor 53BP1 revealed that mock-treated HGPS cells exhibit lower levels compared to control cells (Fig. 47 A-C).

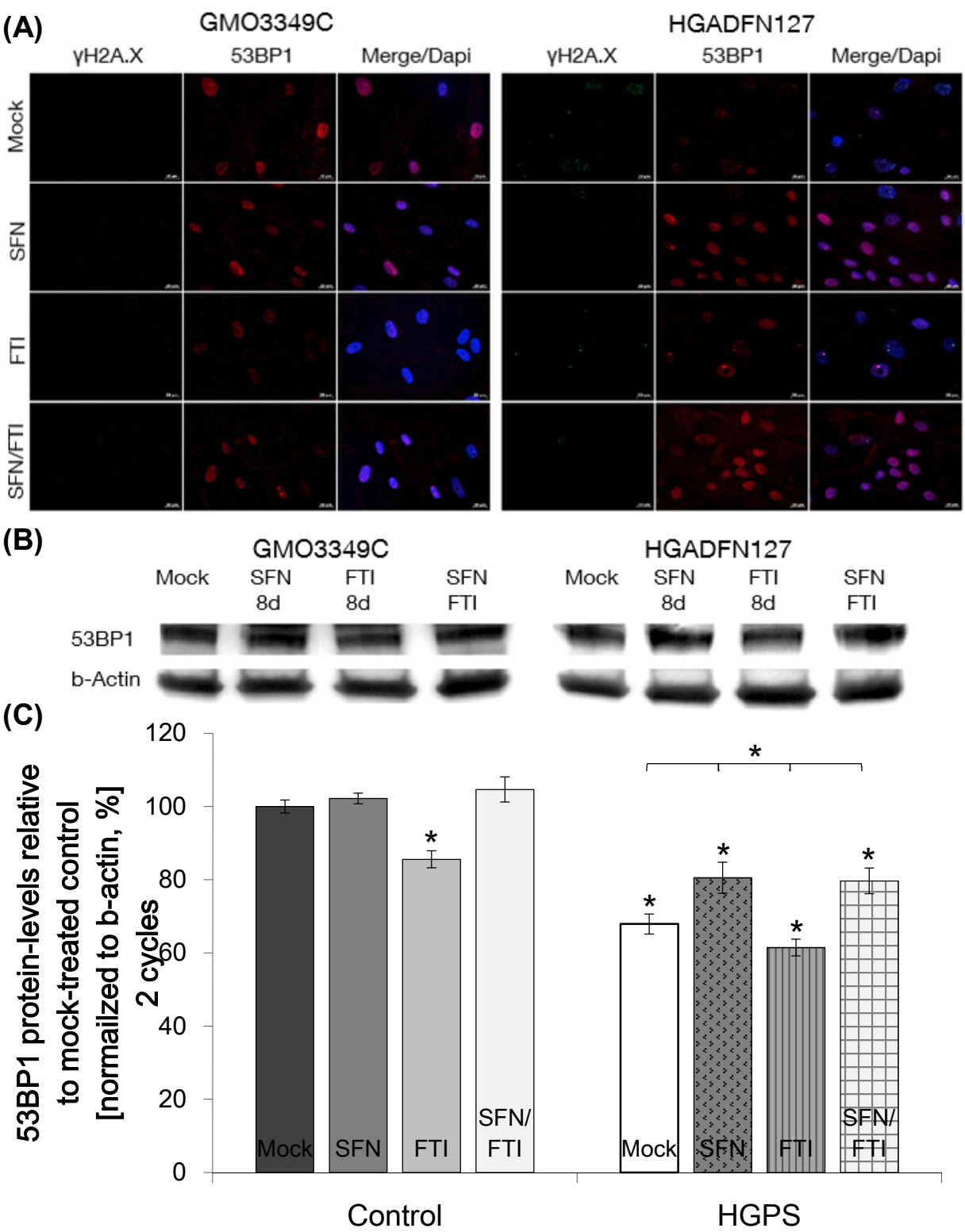

Figure 47: **Analysis of the DNA damage repair factor 53BP1 after cycle treatment.** Control (GMO3349C) and HGPS (HGADFN127) cells mock-treated or treated for 2 cycles 1d FTI/3d SFN were used for immunofluorescence staining against H2A.X and 53BP1. Single treatment of FTI and SFN for 8 days was carried along. Representative images are shown (n=4). Scale bar: 20 µm. (B) Western blot analysis of the same cells and conditions as in (A). Antibodies against 53BP1 and b-actin were used. Representative image is shown (n=3). (D) Quantification of 53BP1 levels normalized to b-actin and presented as the mean ≤ S.D. relative to mock-treated control cells (*p ≤ 0.05; n=3).

SFN as well as the cycle treatment increased the levels of 53BP1 in control and HGPS cells indicating DNA damage repair by non-homologous end joining. The distribution of 53BP1 was improved and showed homogenous staining throughout the nucleoplasm while mock-treated HGPS cells showed aggregated staining in certain areas. By contrast, FTI reduced the levels of 53BP1 and the distribution was not altered compared to mock-treated HGPS cells.

Rad51 serves as another DNA damage repair factor that activates homologous recombination. Rad51 was also investigated in this study (Fig. 48).

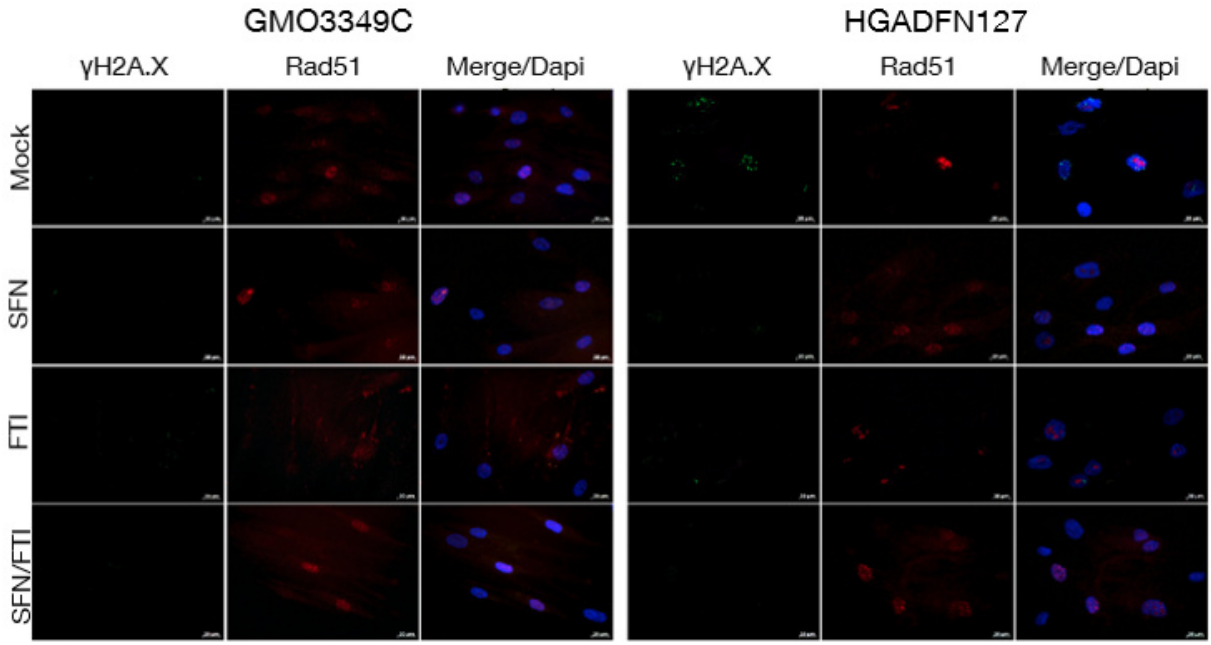

Figure 48: **Analysis of DNA damage repair factor Rad51 after cycle treatment.** Control (GMO3349C) and HGPS (HGADFN127) fibroblast mock-treated or treated for 2 cycles with 1 day 0.06 µM FTI followed by 3 days 1 µM SFN were used to perform immunochemistry with antibodies directed against H2A.X and Rad51. Single treatment of 0.06 µM FTI and 1 µM SFN for 8 days was carried along for comparison reasons. Representative images are shown (n=4). Scale bar: 20 µm.

Levels of Rad51 were found to be decreased in mock-treated HGPS cells compared to control cells. Rad51 showed accumulated staining in HGPS cells and no co-localization with γH2A.X. In SFN- and cycle-treated HGPS cells, Rad51 levels were increased and the distribution was normalized and control-like. Furthermore, Rad51 co-localized with the DNA damage marker γH2A.X. FTI treatment showed accumulated Rad51-staining and no co-localization with γH2A.X as it was also observed in mock-treated HGPS cells.

The same positive effects on DNA damage reduction and DNA damage repair response has been observed with the 3 cycles of 1d FTI followed by 2d SFN (Appendix 8.2.3). However, the reduction of DNA damage was less efficient with the 3 cycles of 1d FTI/2d SFN as 8 % more DNA damage was observed than with the 2 cycle treatment of 1d FTI/3d SFN.
In sum, SFN and cycle treatment reduced DNA damage by the activation of DNA damage repair response by raising the levels of 53BP1 and Rad51.

4.3.5 Comparison of cycle treatment with SFN and FTI single treatment

The data of the cycle treatments with the corresponding single treatments of SFN and FTI are presented in the table below. The different cellular phenotypes of HGPS fibroblasts are presented according to the treatment and duration. Values are relative to the mock-treated HGPS fibroblasts, which are indicated in red.

Table 33: Comparison of SFN, FTI, and cycle treatment regarding some HGPS characteristics.

Treatment	Duration	Progerin clearance	DNA damage	Autophagy	ROS	ATP	Donut-shaped	PPD
Mock			46 %	85 %	120 %	0.75	2.4 %	1.21
SFN	1 cycle	8 %		124 %	113 %	90 %		1.65
FTI	1 cycle	3 %		115 %	119 %	79 %		1.29
3d SFN, 1d FTI	1 cycle	6 %		125 %	111 %	86 %		1.61
2d SFN, 1d FTI	1 cycle	8 %		113 %	114 %	87 %		1.54
SFN	2 cycles	16 %	28 %	164 %	105 %	115 %	1.7 %	1.77
FTI	2 cycles	11 %	40 %	140 %	114 %	84 %	1.3 %	1.25
3d SFN, 1d FTI	2 cycles	20 %	30 %	160 %	100 %	122 %	3.1 %	1.74
2d SFN, 1d FTI	3 cycles	13 %	32 %	135 %	104 %	117 %	3.3 %	1.61
SFN	4 cycles	20 %		153 %	87 %	126 %		1.94
FTI	4 cycles	14 %		137 %	117 %	82 %		1.12
3d SFN, 1d FTI	4 cycles	25 %		153 %	90 %	126 %		1.92
2d SFN, 1d FTI	6 cycles	19 %		140 %	97 %	124 %		1.83

In sum, the cycle treatment of 1d FTI followed by 3d SFN exhibit the same positive effects on HGPS fibroblasts as single SFN treatment but induced a higher progerin clearance. While single FTI treatment showed only a progerin clearance by 14 % after 16 days, SFN and 4 cycles of 1d FTI/3d SFN induced a progerin clearance by 20 % and 25 %, respectively. The proliferation defect of HGPS, DNA damage, autophagy, ROS and ATP are restored in the cycle treatment as in SFN single treatment. The negative effect of FTI to induce donut-shaped nuclei is significantly reduced in the cycle treatment but still slightly higher as in SFN single treatment. By applying a different

duration of SFN treatment within the cycle (1d FTI/2d SFN), results are less efficient than with 1d FTI followed by 3d SFN.

4.4 SFN improves the cellular phenotype of Lmna$^{G609G/G609G}$ mouse fibroblasts

In preparation of further *in vivo* testing, it was investigated whether SFN could recapitulate the same positive effect on progeria mouse models as on human HGPS fibroblasts. Control and HGPS mouse cells were obtained from Dr. Carlos Lopez-Otin laboratory. HGPS mouse fibroblasts carry a homozygous mutation (G609G) similar to the human heterozygous mutation G608G of HGPS children.[175]

Control and HGPS mouse fibroblasts were treated every day with 1 µM SFN. The effect of 1 µM SFN was diminishing on the mouse fibroblasts (Appendix 8.3). The cells showed amelioration of progerin clearance, autophagy, and proliferation. However, this concentration did not ameliorate the mouse cellular phenotype when applied *in vivo*. A Western blot of human fibroblasts and mouse fibroblasts revealed that mouse fibroblasts express lower levels of lamin A/C (Appendix 8.3, Fig. 127). While human HGPS fibroblasts exhibit similar ratios of lamin A, progerin, and lamin C, mouse HGPS fibroblasts showed high levels of progerin and diminishing levels of lamin A. Lamin C was found to be similar to human HGPS fibroblasts.

For this, mouse fibroblasts were treated with higher concentrations of SFN. Cells were treated every day with 2, 3, and 4 µM of SFN for up to approximately 50 days. Cells were analyzed at different time points regarding their proliferation rate, protein degradation pathways, mitochondrial function, and progerin clearance.

First, cumulative population doublings were analyzed after the indicated periods (Fig. 49).

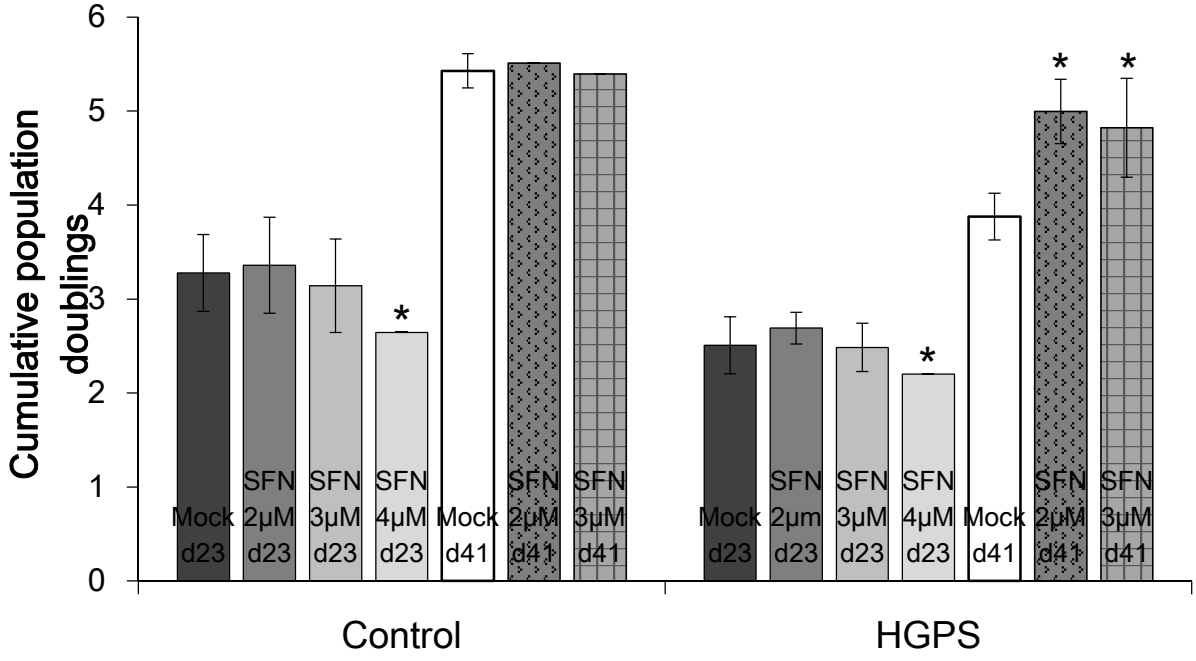

Figure 49: The proliferation rate of mouse fibroblasts after SFN treatment. Long-term cultures of control and HGPS mouse fibroblasts treated with the vehicle or different concentrations of SFN (2, 3, 4 µM) for the indicated periods (*p ≤ 0.05; n=3). The cumulative population doublings were calculated as described in the Methods relative to mock-treated counterparts.

Mock-treated control fibroblasts exhibit higher proliferation rates than the mock-treated HGPS fibroblasts. However, mock-treated HGPS fibroblasts still showed sustained increase of proliferation after 41 days of treatment. SFN treatment did not lead to an amelioration of the proliferation rates in control fibroblasts. While a concentration of 2 and 3 µM of SFN showed no effect on control fibroblasts, 4 µM of SFN led to a significant decrease of the proliferation rate after 23 days. For this, cells were not further treated with 4 µM SFN. SFN-treated HGPS fibroblasts showed the same behavior as control fibroblasts at day 23. While 2 and 3 µM SFN showed no amelioration, 4 µM led to cell death. After 41 days of SFN treatment, both concentrations - 2 and 3 µM - significantly increased the proliferation rates. The proliferation defect of the HGPS mouse fibroblasts was reversed as the SFN-treated HGPS cells reached mock-treated control levels at day 41.

Autophagy levels were investigated after SFN treatment (Fig. 50).

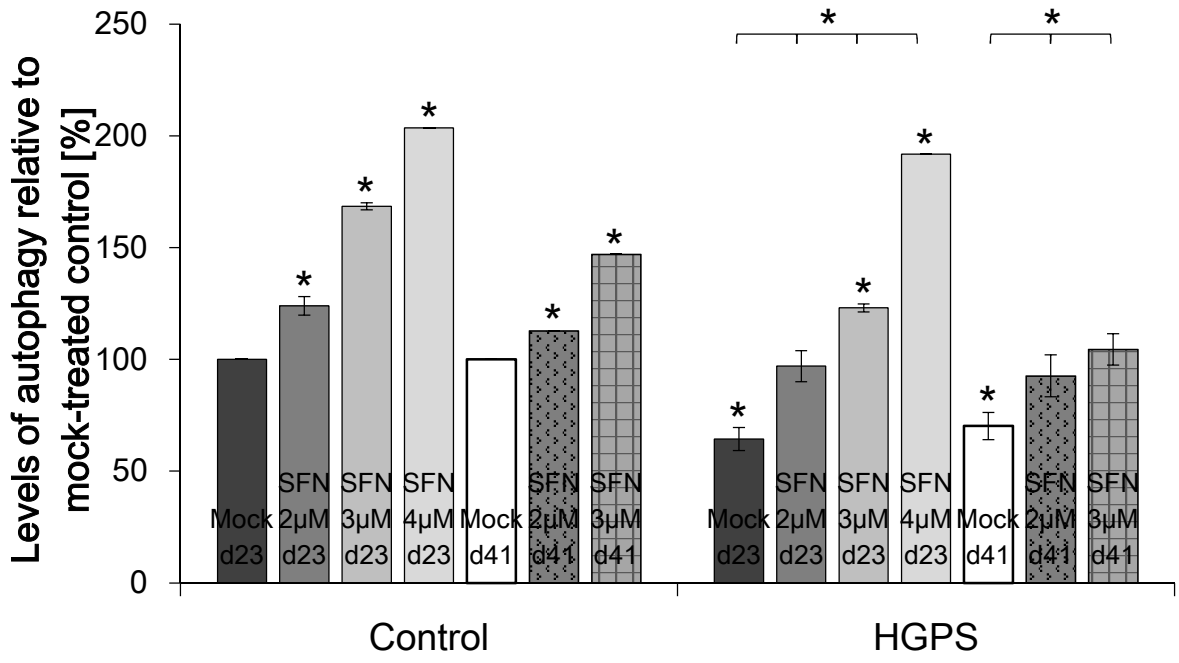

Figure 50: **Autophagy activity of mouse fibroblasts after SFN treatment.** Autophagy activity was measured after the indicated SFN concentrations and time by using monodansylcadaverine (MDC). Data are expressed as the mean ± S.D. relative to mock-treated control (*p ≤ 0.05; n=3).

The autophagic activity was found to be approximately 30 % lower among mock-treated HGPS mouse fibroblasts than mock-treated controls. All SFN concentrations induced a significant increase in autophagy levels of control and HGPS cells at 23 days and 41 days of treatment when compared to their mock-treated counterparts. However, 4 µM SFN induced extraordinary high autophagy levels, which were over the emending limit and led to cell death. After 41 days of SFN treatment in HGPS cells, the concentration of 2 and 3 µM induced the autophagy to the levels of mock-treated controls. Notably, SFN seems less efficient with the time of the treatment as autophagy levels slightly decrease.

Progerin can be cleared through the activation of autophagy.[10] For this, the status of the A-type lamins was investigated (Fig. 51 A, B).

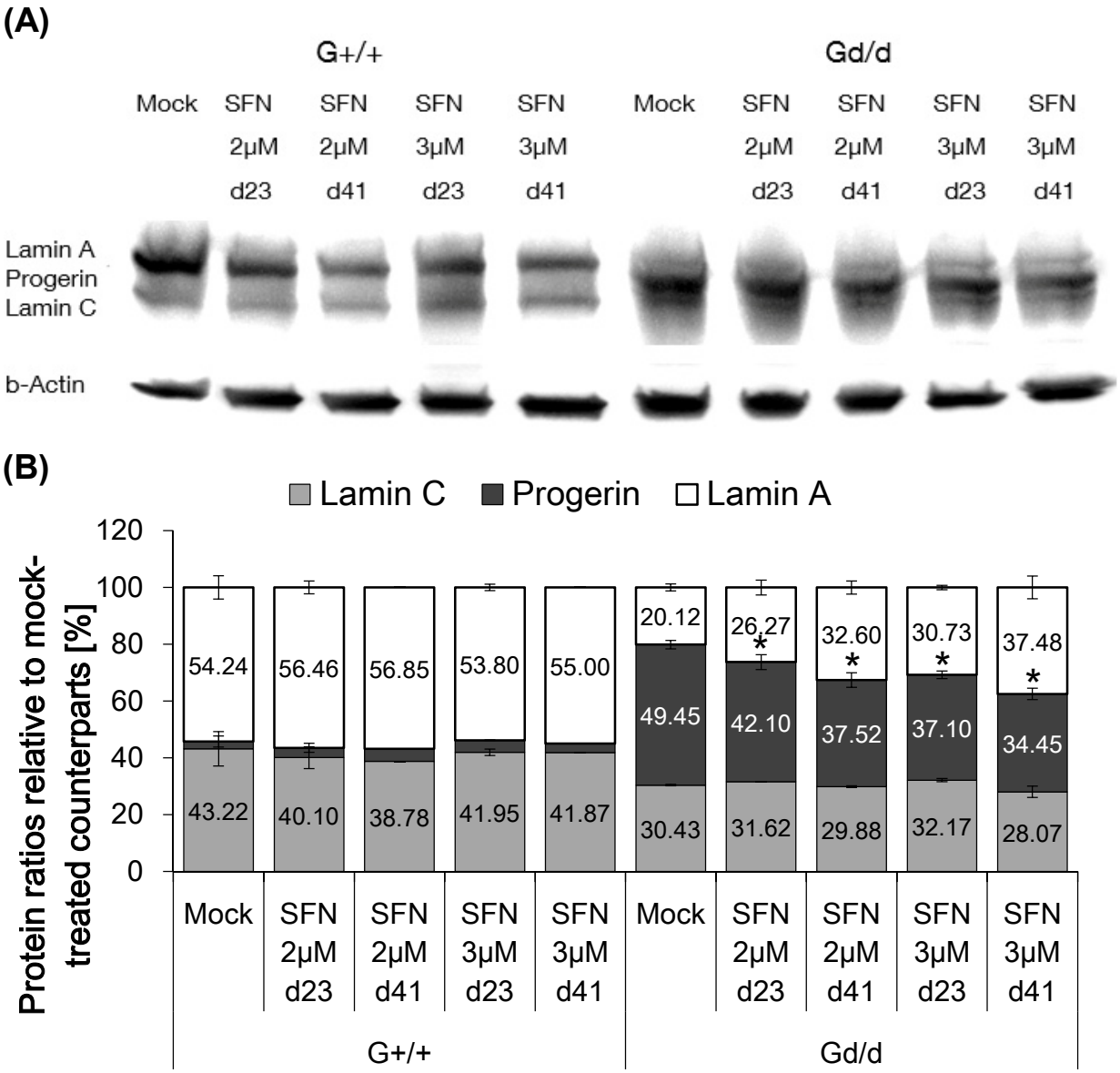

Figure 51: Western blot analyses of mouse fibroblasts after SFN treatment. (A) Western blot evaluation of A-type lamins (lamin A, progerin, Lamin C) in control (G+/+) and HGPS (Gd/d) mouse fibroblasts that were mock-treated or SFN-treated at a concentration of 2 or 3 µM at the indicated times (a representative image is shown; n=3). Blots were probed with lamin A/C, and b-actin antibodies. (B) The proportions of the A-type lamins in each sample were examined by Western blot with an anti-lamin A/C antibody. Data represent the mean ± S.D. with respect to mock-treated control counterparts after values were normalized to b-actin signal (*$p \leq 0.05$; n=3).

Control mouse fibroblasts demonstrated the same ratios of A-type lamins as control human fibroblasts. Treatment with SFN did not significantly alter the ratios of the A-type lamins of control cells. As the G608G mutation was induced in both alleles of the lamin A gene to resemble the human HGPS phenotype, mock-treated HGPS mouse fibroblasts showed massive staining of the progerin protein, while lamin A was barely

detectable. Lamin C remained unaffected. During the 3 µM SFN treatment, progerin staining decreased within the HGPS cells, whereas a distinct band of lamin A was detected. The increase in lamin A and the decrease in progerin was also detected in 2 µM SFN, albeit only after 41 days. The ratios of the A-type lamins of HGPS mouse fibroblasts were ameliorated after SFN treatment in both concentrations after 41 days. Progerin was cleared by 24 % after 41 days of 2 µM SFN and 30 % after 41 days of 3 µM SFN. Compared to 1 µM SFN treatment, 2 µM SFN showed the same progerin clearance but 3 µM SFN induced a higher progerin clearance.

Analysis of the mitochondrial function revealed that 2 and 3 µM SFN were beneficial indicated by measuring the ROS levels and intracellular ATP levels (Fig. 52 A, B).

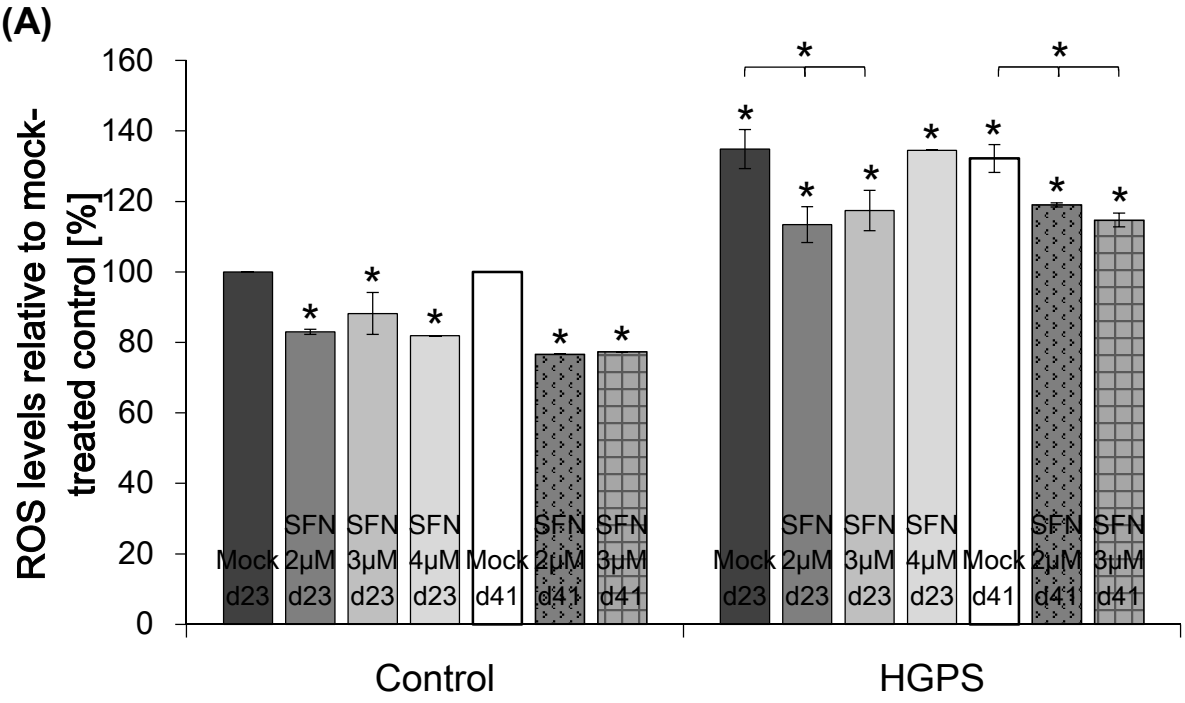

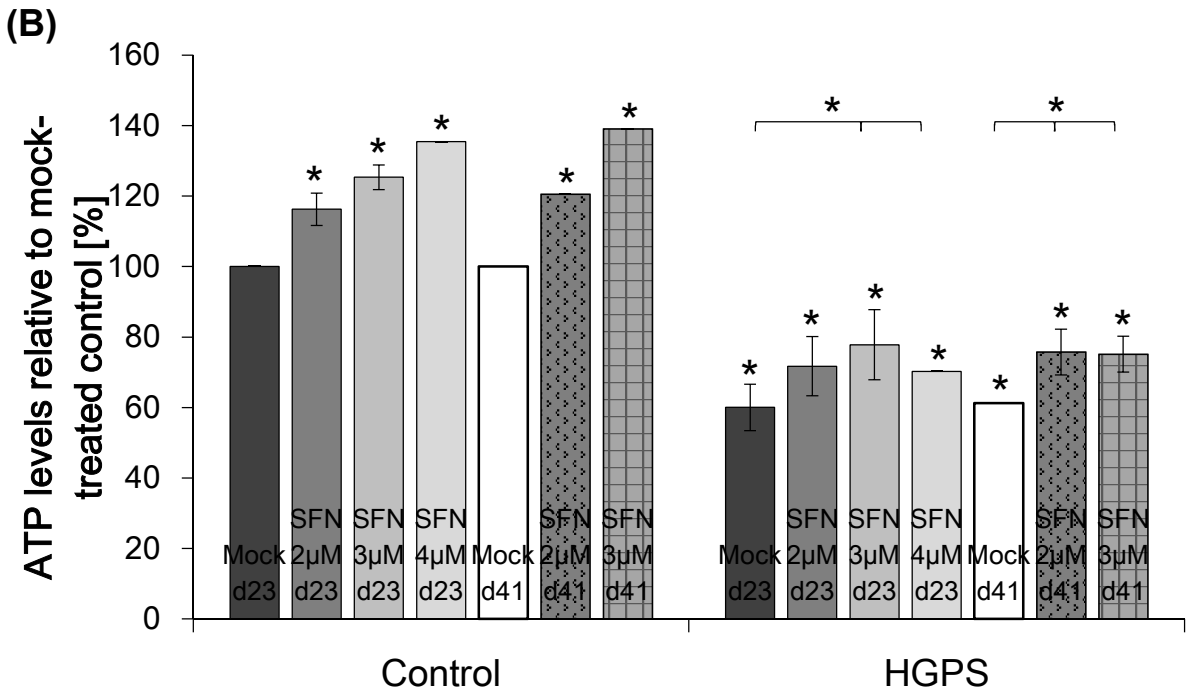

Figure 52: ROS and ATP levels of mouse fibroblasts after SFN treatment. (A) Intracellular ROS levels were determined by measuring oxidized dichlorofluorescin (DCF) levels using a DCFDA cellular ROS detection assay as described in the Methods. Control and HGPS mouse fibroblasts were treated with different SFN concentrations for the indicated time. Data represent the mean ± S.D. (*p ≤ 0.05; n=3) compared to mock-treated control. (C) Intracellular ATP levels were measured using CellTiter Glo luminescence ATP assay as described in the Methods. Same cells as in (A) were used. Data are presented as the mean ± S.D. relative to mock-treated control (*p ≤ 0.05; n=3).

ROS levels were found to be significantly increased in mock-treated HGPS cells compared to mock-treated control by 30 % (Fig. 52 A). SFN treatment at a concentration of 2 and 3 µM induced a significant decrease of ROS levels in control and HGPS cells compared to the mock-treated counterparts. This decrease was maintained during long-term treatment. While control cells showed a significant decrease in ROS levels after 4 µM SFN, HGPS cells showed no amelioration after 23 days. ROS levels did not reach mock-treated control levels in HGPS mouse fibroblasts after all tested SFN concentrations.

By contrast, ATP levels were significantly reduced in mock-treated HGPS cells by 30 % compared to mock-treated control (Fig. 52 B). In control, all SFN concentrations led to a significant increase in ATP levels. The increased levels were maintained during the SFN treatment. In HGPS, 3 and 4 µM SFN induced a significant increase after 23 days of treatment when compared to the mock-treated counterparts. The higher ATP levels were maintained after 41 days of 3 µM SFN treatment. The SFN concentration of 2 µM

only showed a significant increase in ATP after 41 days of treatment compared to the mock-treated counterpart. However, ATP levels of HGPS mouse fibroblasts did not reach the levels of mock-treated control mouse fibroblasts.

Next, immunochemistry analysis was performed to reveal the distribution and expression of nuclear envelope components and the accumulation of DNA damage by γH2A.X (Fig. 53 A-C).

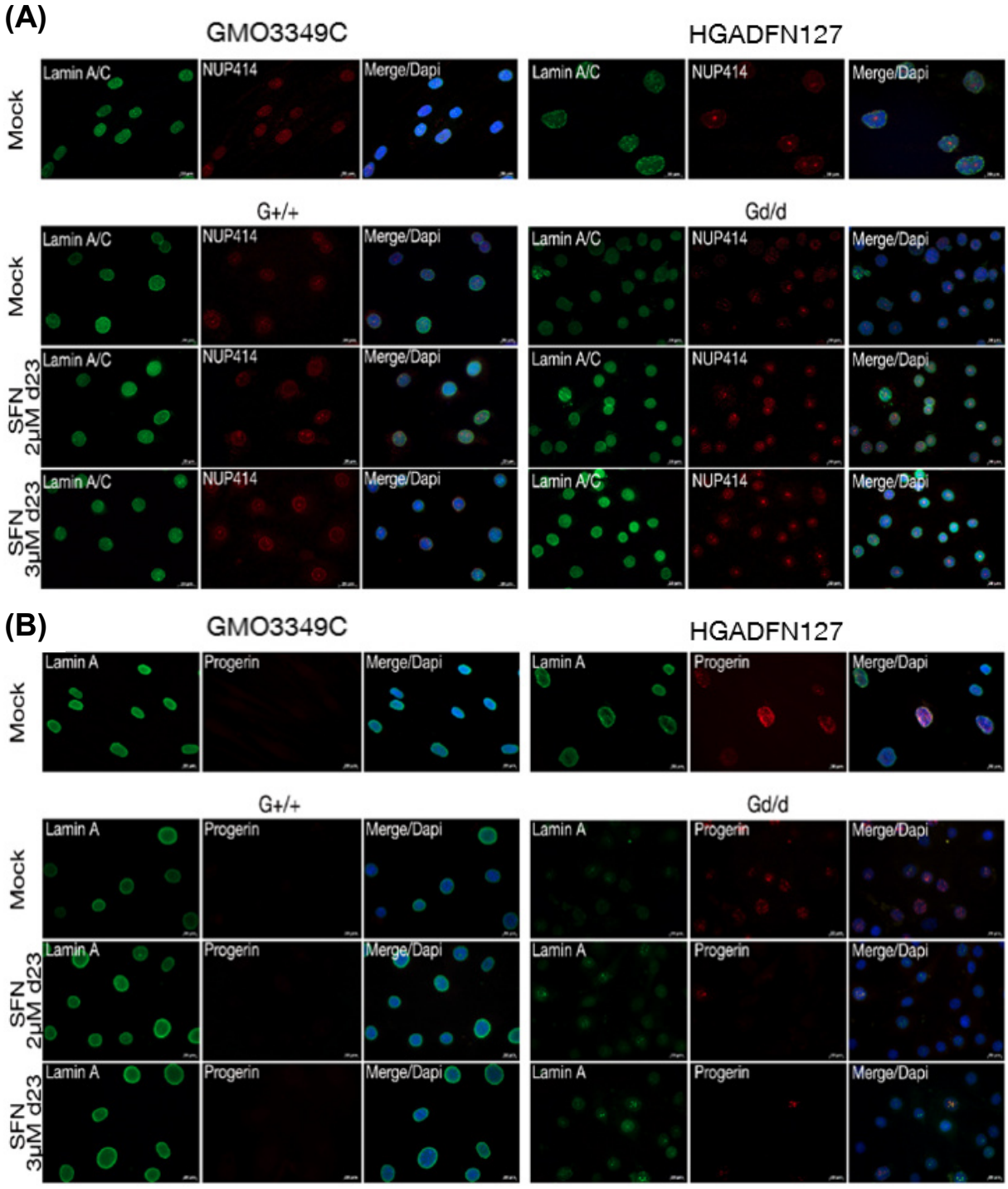

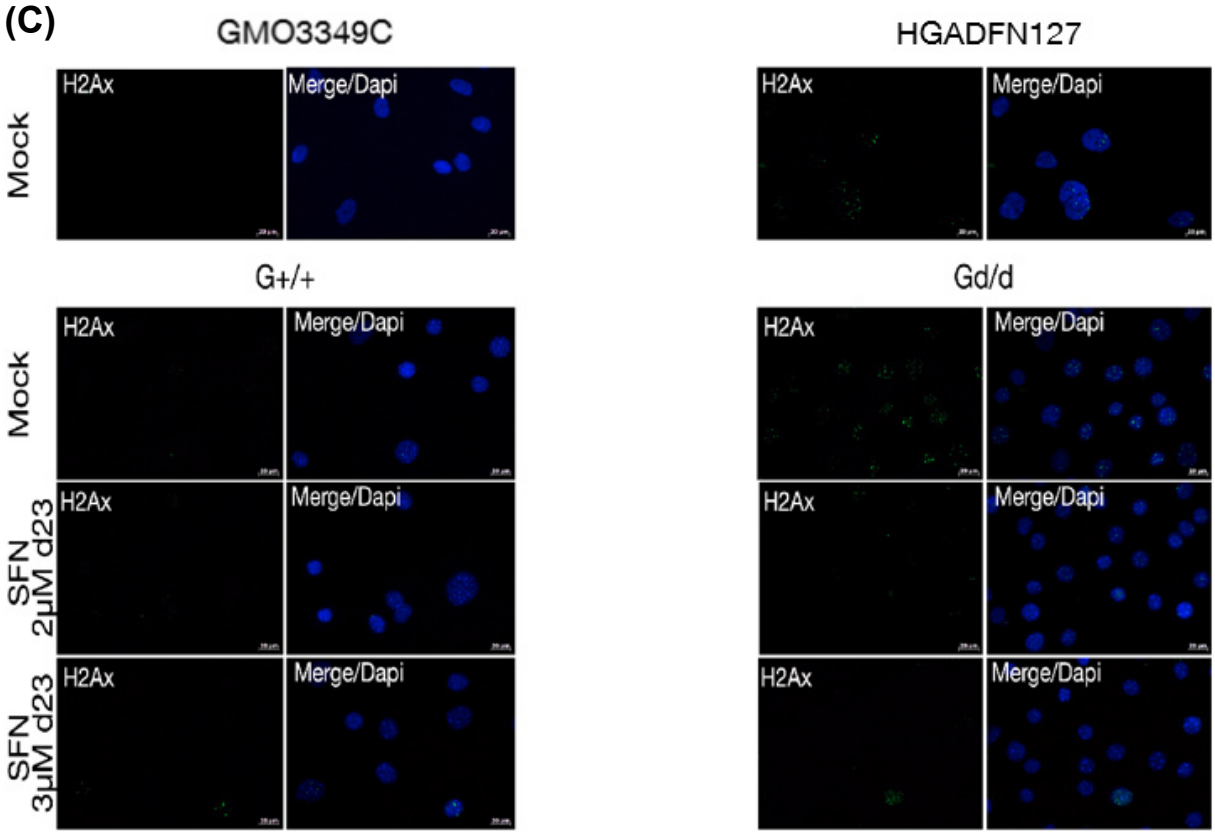

Figure 53: Immunochemistry of mouse fibroblasts after SFN treatment. (A) Immunochemistry using antibodies directed against lamin A/C and nuclear pore protein (Nup414) was performed on control mouse fibroblasts (G+/+) and HGPS mouse fibroblasts (Gd/d) mock-treated or SFN-treated at the indicated concentrations for a period of 23 days (n=3). Human control fibroblasts (GMO3349C) and human HGPS fibroblasts (HGADFN127) were carried along for comparison reasons. (B) Same cells and conditions as in (A) were immunolabeled with anti-lamin A and anti-progerin antibodies (n=3). (C) Same cells as in (A) were used to stain with anti-γH2A.X antibody (n=3). Scale bar: 20 µm.

Human control fibroblasts and mouse control fibroblasts showed the same distribution of lamin A/C and nuclear pores. SFN treatment did not alter the distribution of lamin A/C and the nuclear pores even though the expression of the nuclear pores seemed to be increased in both concentrations of SFN (Fig. 53 A). Human HGPS fibroblasts showed clear nuclear shape abnormalities when stained with anti-lamin A/C compared to human control fibroblasts. Nuclear pores appeared as punctuated dots with some aggregated areas whereas the distribution of the nuclear pores in control cells showed rim-like staining. Mouse HGPS fibroblasts exhibit weaker staining of lamin A/C and nuclear pores compared to human HGPS fibroblasts. Staining with lamin A/C revealed less nuclear shape abnormalities than in the human counterparts and the size of the nuclei were not increased compared to the control counterparts. However, the

distribution of the nuclear pores showed a more accumulated staining compared to human HGPS fibroblasts. After 2 µM and 3 µM SFN treatment, expression of lamin A/C was increased and nuclear shape abnormalities further decreased. The distribution and expression of the nuclear pores were normalized and showed rim-like staining. The expression of lamin A/C and nuclear pores was increased with higher concentrations of SFN.

Staining of lamin A and progerin revealed weaker staining of lamin A in control mouse fibroblasts than in control human fibroblasts (Fig. 53 B). Progerin was not detected in both cell lines. After SFN treatment, lamin A levels increased to the same extent in both concentrations. Human HGPS fibroblasts showed progerin accumulation in the most nuclei and lamin A expression was weaker compared to human control cells. As expected, lamin A was barely detectable in mouse HGPS fibroblasts due to the homozygous mutation. Levels of lamin A were weaker than in the human cell lines and mouse control fibroblasts. Progerin staining showed the same distribution as found in human HGPS fibroblasts. SFN treatment reduced the number of progerin-positive cells and increased the intensity of lamin A. A difference of 2 µM SFN and 3 µM SFN were not observed.

Next, staining with the DNA damage marker γH2A.X revealed that human and mouse HGPS fibroblasts exhibit elevated levels of DNA DSBs compared to their control counterparts (Fig. 53 C). SFN treatment reduced the levels of DNA damage after 23 days of treatment of mouse HGPS fibroblasts. There was no difference observed at 2 and 3 µM of SFN.

In sum, SFN treatment ameliorated the cellular phenotype of HGPS mouse fibroblasts and cleared progerin by 30 % at a concentration of 3 µM. Compared to human HGPS fibroblasts, the same efficiency of progerin clearance was reached, even though the concentration had to be 3 times higher.

4.5 Improving the proteostasis of HGPS fibroblasts with forskolin

Next to Sulforaphane, forskolin has been used to treat HGPS fibroblasts. Forskolin (7ß-acetoxy-1α,6ß,9α-trihydroxy-8,13-epoxy-labd-14-en-11-one, Fors) is a labdane diterpenoid isolated from the Indian *Plectranthus barbatus*. Forskolin has been used to verify whether the activation of different signaling pathways has an impact on reversing the HGPS cellular phenotype. While SFN activates Nrf2-Keap1 pathway, forskolin stimulates AMPK and Sirt1 which in turn can lead to autophagy activation (Fig. 54).[19-24]

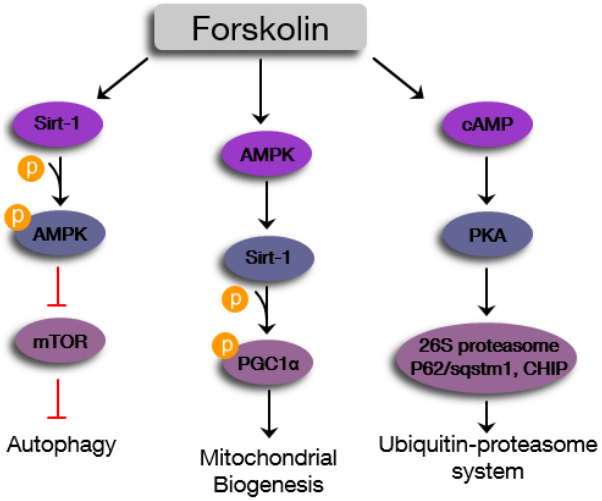

Figure 54: The effect of forskolin on signaling pathways. Forskolin is a known activator of SIRT1, AMPK, and cAMP. The activation of Sirt1 leads in a down-stream cascade to the phosphorylation AMPK. Phosphorylated AMPK blocks mTOR and activates autophagy. In turn, forskolin also activates AMPK which phosphorylates PGC1α via enhancing of Sirt1. This leads to activation of transcription of mitochondrial proteins. Forskolin increases the levels of cAMP which enhances PKA and thereby activating the ubiquitin-proteasome-system.

Increasing the levels of AMPK and Sirt1 not only activate autophagy but also enhance mitochondrial biogenesis.[25-28] Forskolin raises the levels of cyclic AMP by activating the enzyme adenylyl cyclase.[19] cAMP stimulates protein kinase A (PKA) which was found to directly stimulate the chymotrypsin-like and trypsin-like activities of the proteasome.[29] Based on these studies, the possibility that forskolin may have beneficial effects on HGPS cellular homeostasis was tested.

4.5.1 Forskolin improves the level of protein degradation in HGPS fibroblasts

First, the potential toxicity of forskolin was tested by applying different concentrations to fibroblast cultures (Fig. 55 A, B).

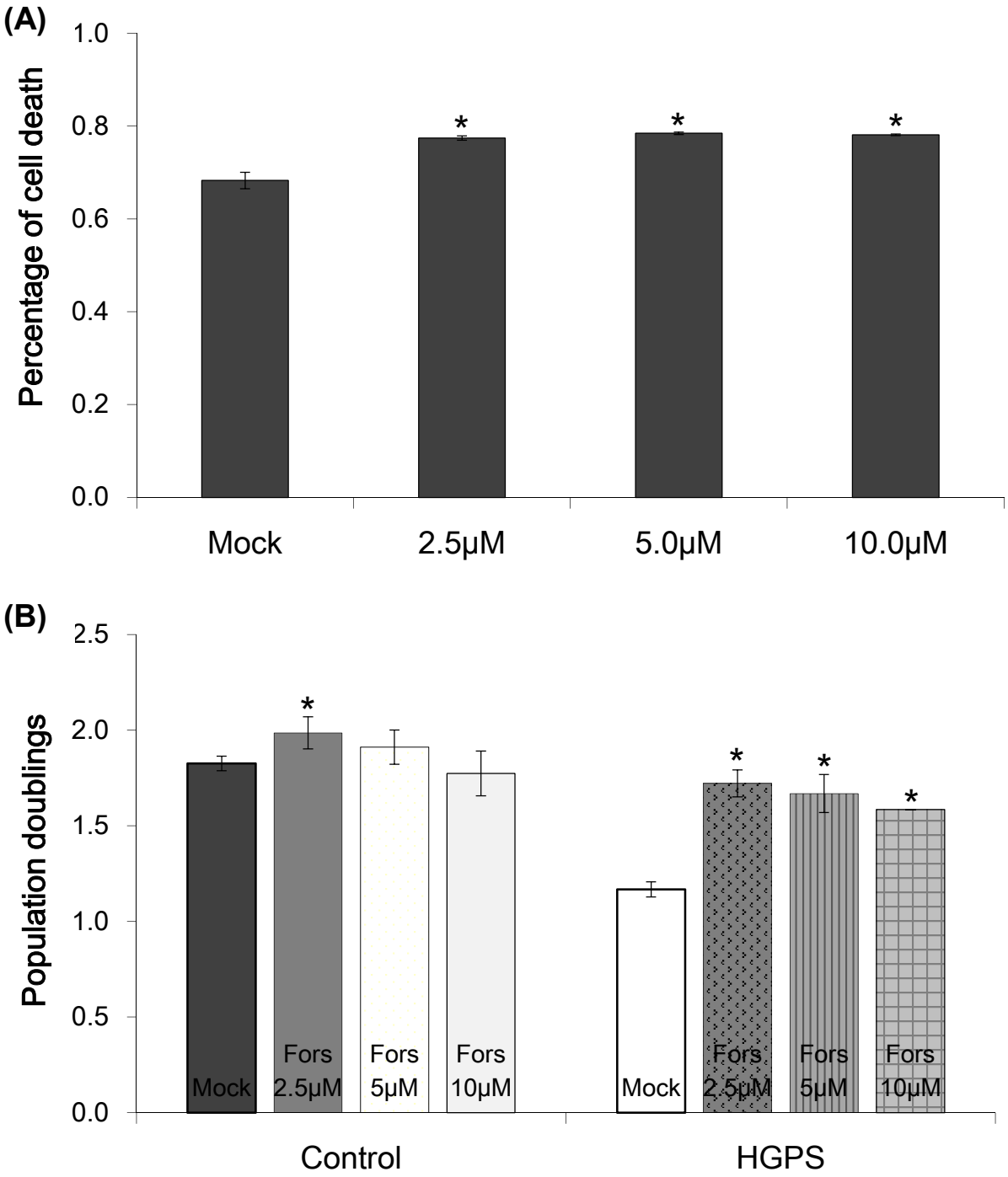

Figure 55: Cytotoxicity of forskolin-treated cells. (A) Control cells were treated daily with forskolin (Fors). Percentage of cell death is shown after 48h at indicated forskolin concentrations. Data are presented as the mean ± S.D. relative to mock-treated counterparts (*p ≤ 0.05; n=3). (B) Population doublings were calculated as stated in Materials and Methods. Control and HGPS cells were mock-treated or treated daily with the indicated forskolin concentrations for 48h.

Forskolin did not lead to greater cell death than 1 % and fibroblasts cells showed increased proliferation rates even at higher concentration. As the highest proliferation rate was detected at 2.5 µM forskolin, further experiments were carried out with this concentration.

During all experiments, control and HGPS cells were fed daily with fresh medium containing the vehicle (DMSO) or 2.5 µM forskolin.

The effect of forskolin on the proliferation rate of control and HGPS cells was investigated (Fig. 56).

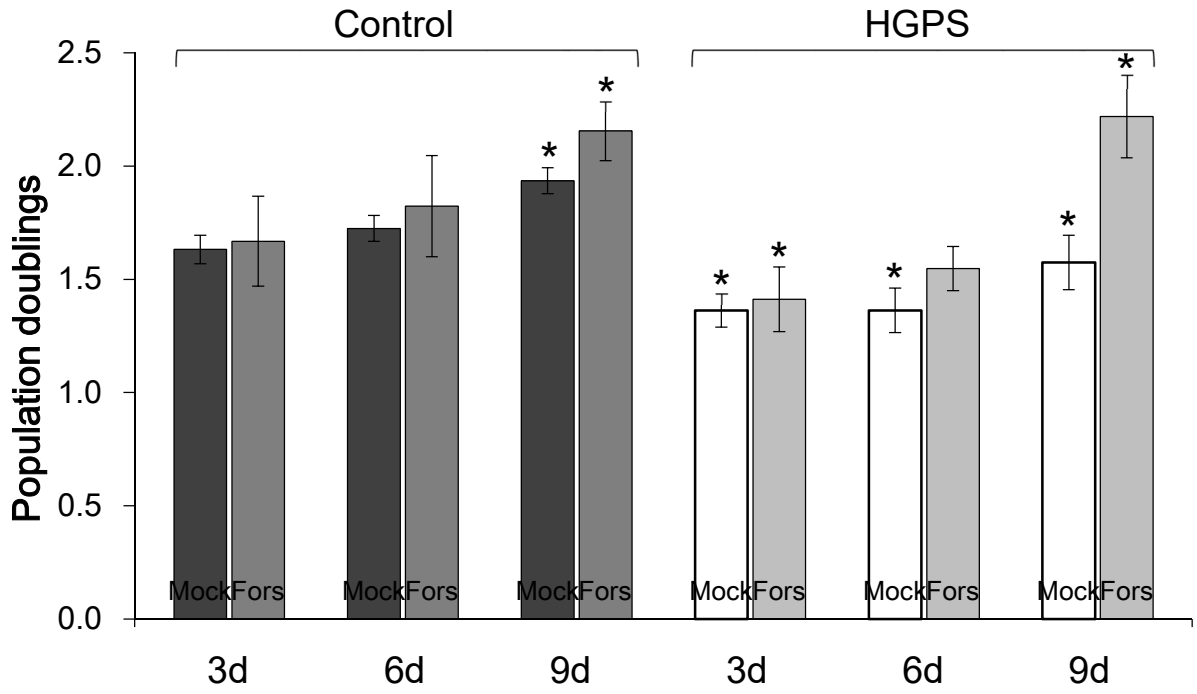

Figure 56: Cell proliferation in mock-treated and Fors-treated fibroblasts. Population doubling levels were calculated as stated in the Materials and Methods relative to mock-treated control. Control and HGPS cells were mock-treated (vehicle DMSO) or treated daily with 2.5 µM forskolin for a period of 3 or 9 days (*p ≤ 0.05; n=4).

HGPS cells treated with 2.5 µM forskolin show a significantly increased growth rate at day 3 and 9 compared to mock-treated counterparts. Control cells show only a significantly increase in growth at day 9 compared to counterparts. Furthermore, the defect in proliferation of HGPS cells was improved after 3 days of forskolin treatment. The proliferation potency of normal and HGPS cells *in vitro* seemed to be ameliorated by forskolin treatment.

Forskolin is known to increase the activity of the ubiquitin-proteasome-system (UPS) over cyclic AMP signaling.[176] For this, the effect of forskolin on the proteasome activity was tested (Fig. 57).

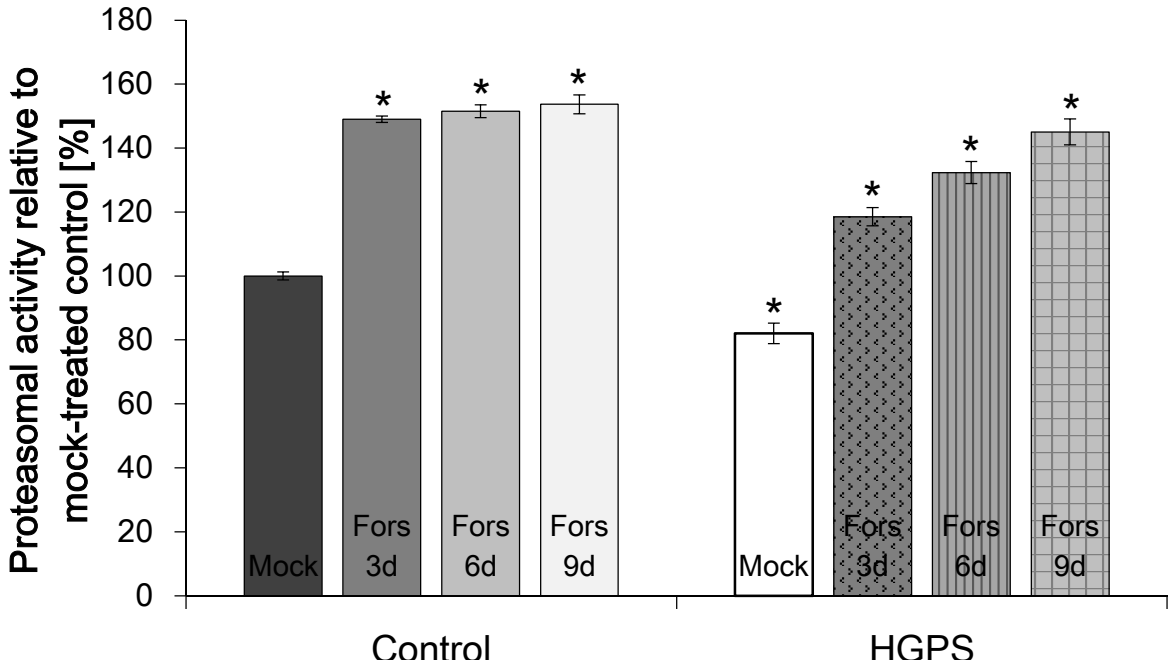

Figure 57: Proteasomal activity after 3 and 9 days of Fors treatment. Proteasome activity was determined by measuring chymotrypsin-like proteasome activity in control and HGPS fibroblasts using Suc-LLVY-AMC as a substrate. Cells were either mock-treated or treated daily with 2.5 µM Fors for a period of 3 or 9 days. The percentage of activity was calculated relative to the mock-treated control. Data are expressed as the mean ± S.D. (*p ≤ 0.05; n=4).

Mock-treated HGPS cells demonstrate a significantly reduced proteasomal activity compared to mock-treated control cells. After only 3 days of forskolin treatment, proteasomal activity of control and HGPS cells were significantly increased. The significantly enhanced proteasome activity was maintained during the forskolin treatment of control and HGPS cells.

As mentioned, cells rely on two major protein degradation systems that are called the ubiquitin-proteasome system and autophagy.[177] Moreover, it was demonstrated that progerin and lamin C are degraded by autophagy while lamin A is degraded via the proteasome.[10] For this, the effect of forskolin on the autophagy activity was determined (Fig. 58).

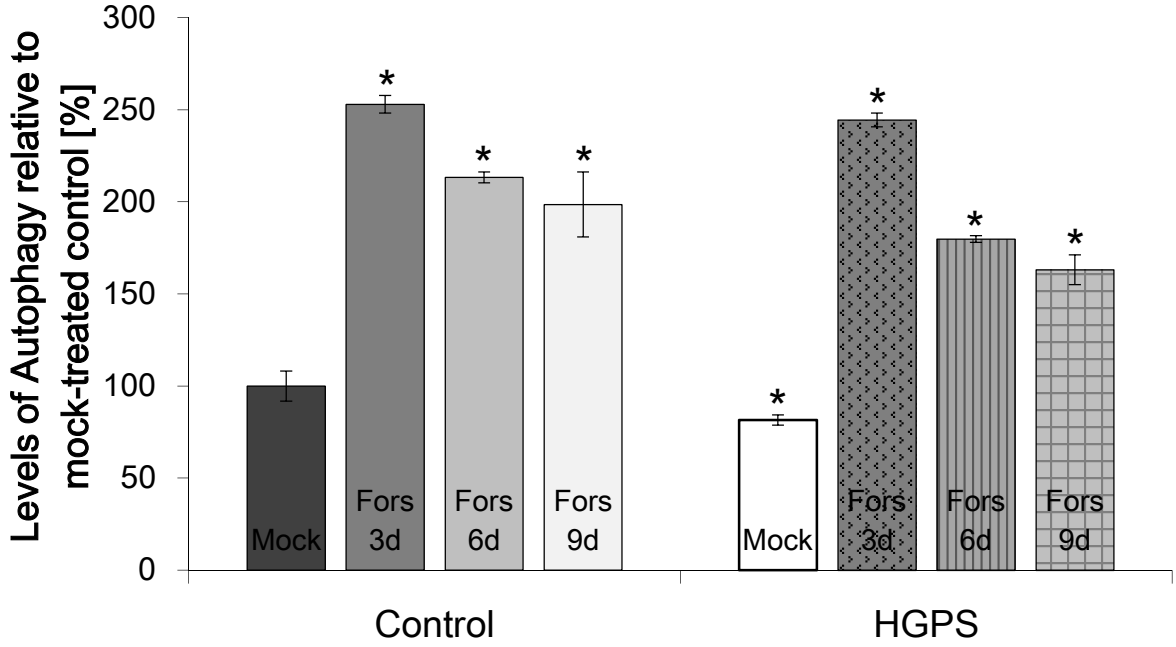

Figure 58: Autophagy levels after 3 and 9 days of Fors treatment. Autophagy was determined in control and HGPS fibroblasts by measuring monodansylcadaverine (MDC) levels with fluorescence photometry. Cells were either mock-treated or treated daily with 2.5 µM Fors for a period of 3 or 9 days. The percentage of activity was calculated relative to the mock-treated control. Data are expressed as the mean ± S.D. (*p ≤ 0.05; n=4).

Mock-treated HGPS cells exhibit a significantly reduced autophagy activity compared to mock-treated control cells. Treatment of 3 days forskolin induced a significant increase in autophagy activity by 2.5-fold in control and HGPS fibroblasts. Thereafter, autophagy activity starts to decrease in control and HGPS fibroblast in the presence of forskolin. However, the activity of autophagy was still found to be significantly increased by 1.8-fold after 9 days of forskolin treatment.

Based on these observations, forskolin appeared to boost the protein degradation systems in HGPS and control cells.

Next, the potentially progerin clearance by forskolin in HGPS cells was examined. Thus, the status of A-type lamins was investigated by performing Western blot analyses of total protein extracts derived from control and HGPS cells mock-treated or forskolin-treated. Lamin A, progerin, and lamin C signals were determined by densitometry from 3 independent Western blots. The signals were normalized to b-actin to correct for any variability in protein sample concentration and/or uneven loading. The Western blot is shown as a representative image in Figure 59.

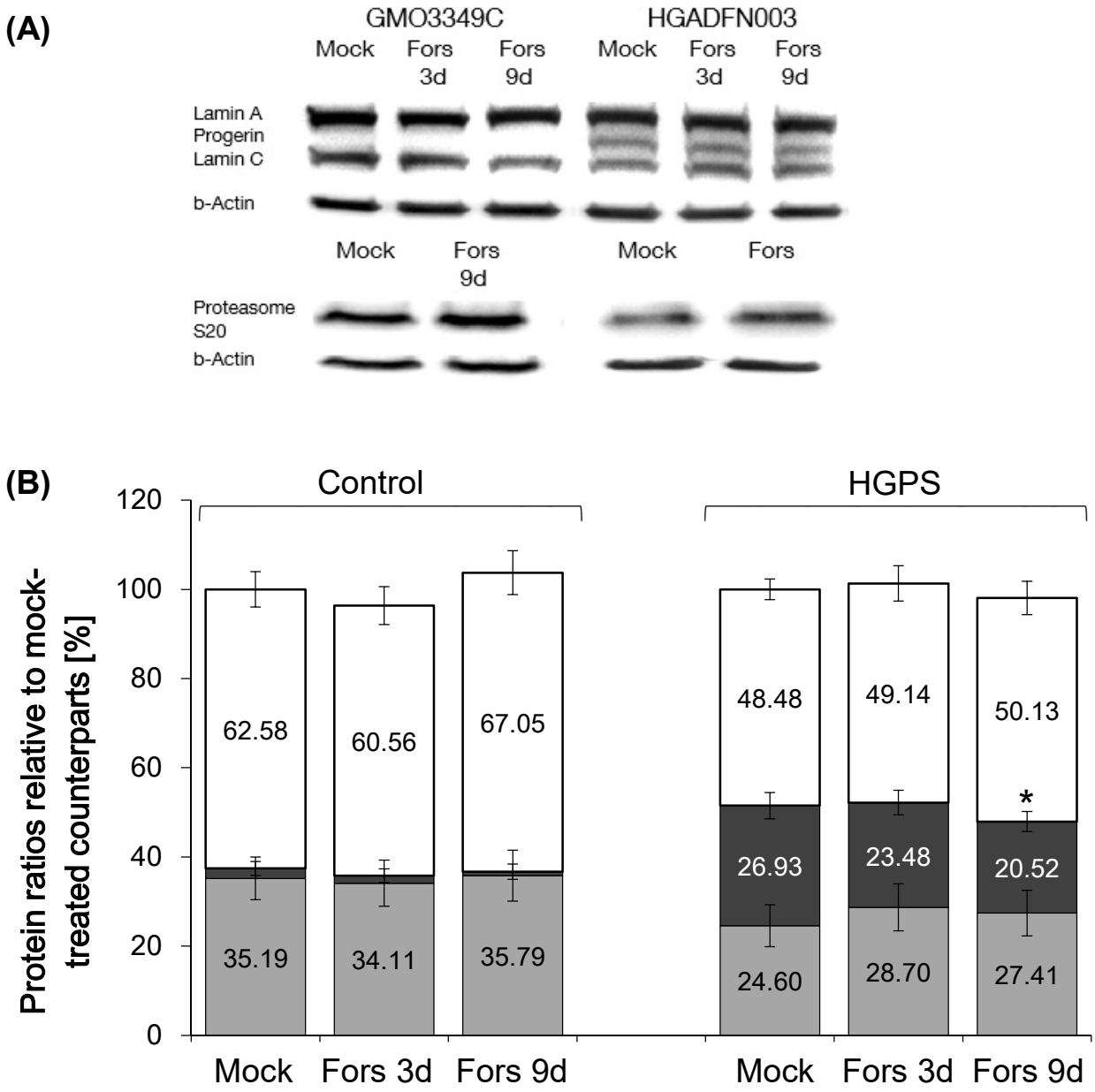

Figure 59: Western blot analyses of cultures treated with Fors. (A) Representative Western blot of lamin A/C, progerin, proteasome subunit S20 C2, Hsp27, and b-actin in control and HGPS total cell extracts either mock-treated or treated with 2.5 µM Fors daily for 3 and 9 days. (B) Quantification of lamin A, lamin C, and progerin levels relative to mock-treated counterparts, and presented as the ratio (*$p \leq 0.05$; n=3).

In control cells, the levels of lamin A, progerin, and lamin C remained unchanged after forskolin treatment. In HGPS cells, the status of A-type lamins is altered. Lamin A levels were slightly lower in HGPS cells compared with control cells. Lamin C levels were not significantly changed in mock-treated HGPS cells compared to mock-treated control cells. Progerin levels were approximately 7-fold higher in HGPS cell extracts compared

to mock-treated control cells. Forskolin treatment induced progerin degradation in HGPS cells, as progerin levels were reduced by 20 % after 9 days of treatment.
These data indicate that forskolin enhances the clearance of progerin in HGPS cells. Levels of the 20S proteasome subunit C2 were significantly increased after 9 days of forskolin treatment in control and HGPS fibroblasts.
To understand the degradation mechanism by which forskolin induces progerin clearance, HGPS cells were exposed to forskolin for 8 days before a proteasome inhibitor (MG132) or an autophagy inhibitor (chloroquine bisphosphate) were added for 12 hours (Fig. 60).

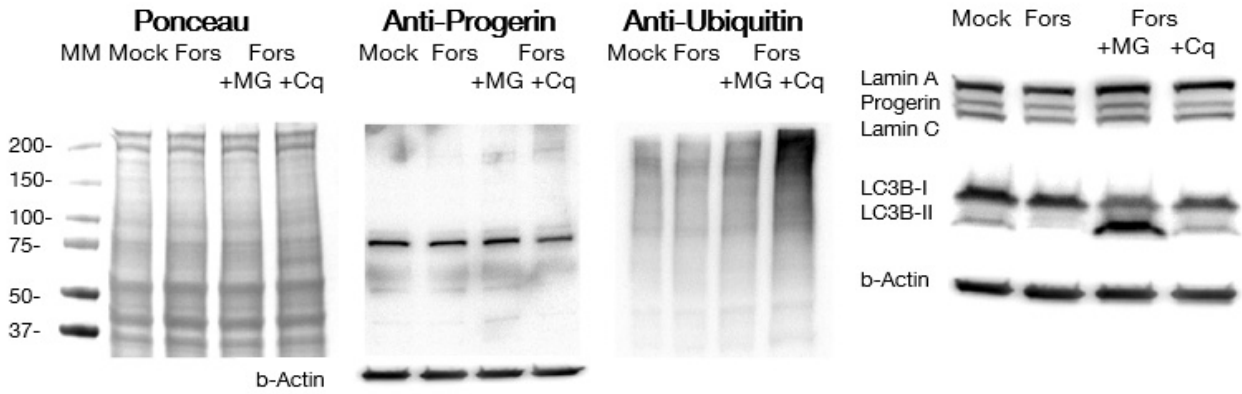

Figure 60: Western blot analyses of proteasome and autophagy proteins after Fors treatment. (A) Representative Western blots of HGPS lysates of mock-treated cells or cells treated with forskolin, forskolin with chloroquine (Cq) or forskolin with MG132. Samples on the left panel were probed with antibodies specific to progerin and ubiquitin (n=3). Right panel corresponds to antibody staining against lamin A/C, LC3B-I and LC3B-II, and b-actin (n=3).

In response to MG132, HGPS fibroblasts show an accumulation of ubiquitinated proteins. Chloroquine treatment induced a significant increase in LC3B-II levels indicating the accumulation of autophagosomes when autophagy is inhibited. Autophagy remained active in forskolin-treated cells, as LC3B-II levels were barely detectable. Progerin levels were significantly reduced by 21 % in forskolin-treated HGPS fibroblasts and by 32 % in forskolin+MG132-treated cells. This result indicates that autophagy is further stimulated by proteasome inhibition.[178] Collectively, forskolin clears progerin via autophagy activation.

HGPS cells are characterized by increased reactive oxygen species (ROS) and reduced ATP levels resulting from defective mitochondria.[148] Forskolin was found to reduce ROS and to increase ATP levels.[179,180] For this, it was tested whether forskolin could ameliorate these cellular alterations in HGPS cells (Fig. 61 A, B).

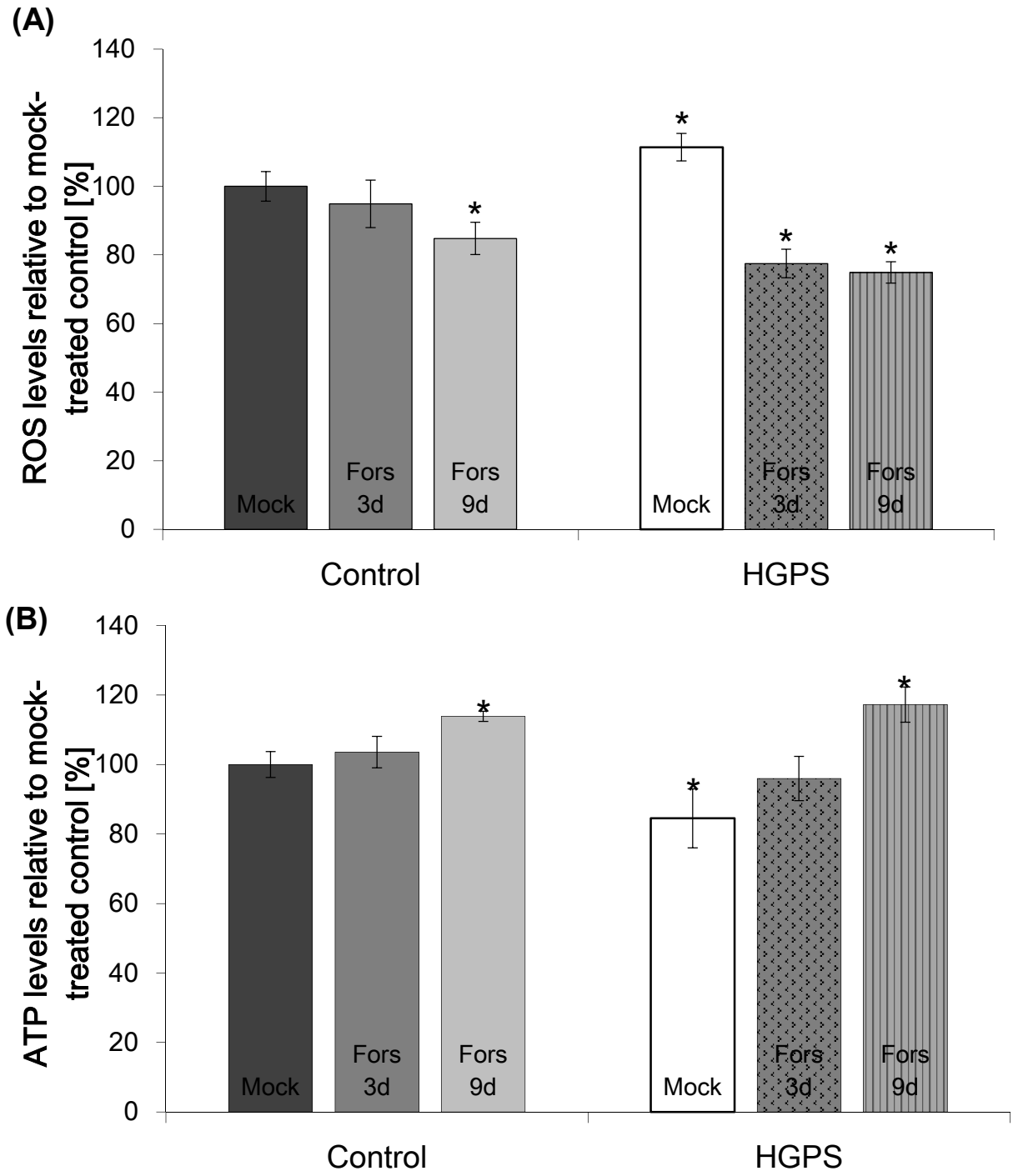

Figure 61: ROS and ATP levels of mock-treated and Fors-treated cells. (A) Intracellular ROS levels were determined by measuring oxidized dichlorofluorescin (DCF) levels as described in the Methods. Cells were treated with the vehicle or 2.5 µM forskolin for the indicated periods. (B) Same cells as in (A) were used to measure cellular ATP levels using CellTiter Glo luminescence ATP assay as described in the Methods. Data represent the mean ± S.D. compared to mock-treated control cells (*$p \leq 0.05$; n=3).

In accordance with earlier studies, ROS levels were found to be increased in mock-treated HGPS cells and appeared to significantly decrease after 3 days of forskolin treatment. The same results were observed in control cells (Fig. 61 A).
ATP levels were significantly reduced in mock-treated HGPS cells compared to control (Fig. 61 B). Forskolin treatment induced a significant increase in intracellular ATP levels in control and HGPS cells after 9 days. These findings indicate that forskolin ameliorate through its antioxidant activity the energy levels in HGPS cells.

4.5.2 Forskolin improves the cell morphology of HGPS fibroblasts

Characteristics of HGPS cells include nuclear envelope alterations such as nuclear blebs, enlargement of the nucleus, and reduced levels of nuclear components.[5] For these experiments, forskolin-treated and mock-treated cells were examined in parallel. Dysmorphic HGPS nuclei exhibited progerin accumulation at the nuclear envelope with aggregated regions when stained with anti-progerin antibody (Fig. 62).

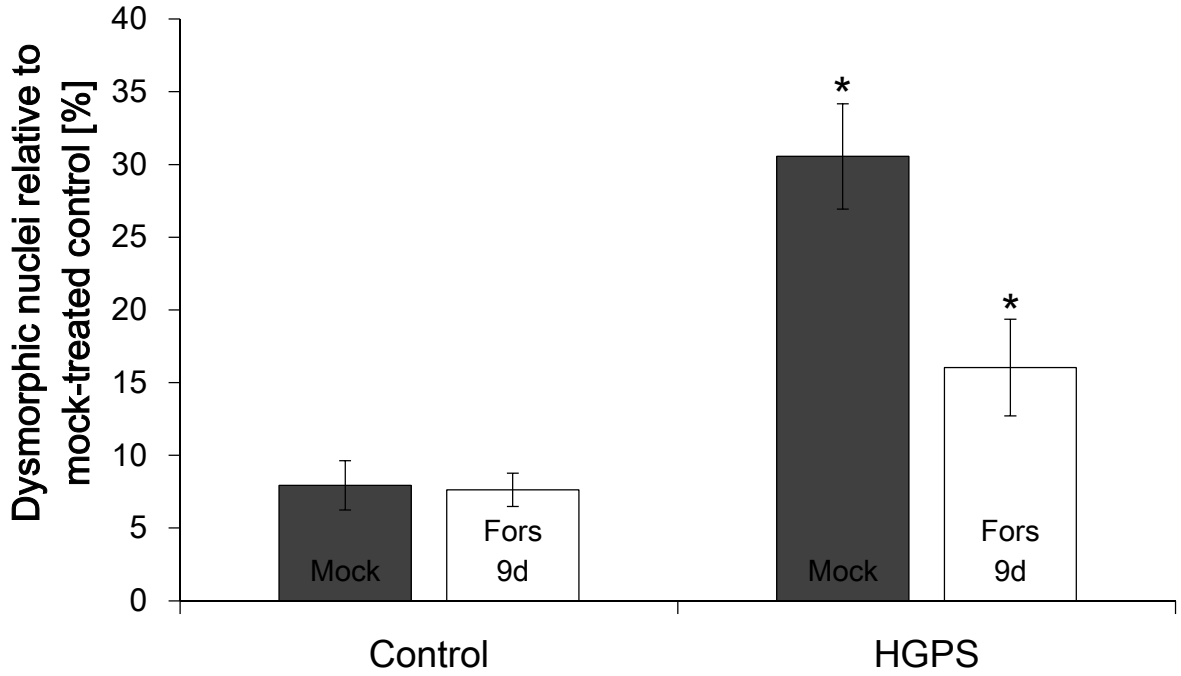

Figure 62: Dysmorphic nuclei after Fors treatment. Frequency of misshapen nuclei (dysmorphic) in control and HGPS fibroblast after 9 days of treatment with either the vehicle or 2.5 µM Fors. An average of 800 nuclei were examined for each control and HGPS cell line and treatment. Data are presented as the mean ± S.D. relative to mock-treated control (*p ≤ 0.05; n=3).

In normal-shaped nuclei of HGPS, progerin staining revealed weak signals with very few dots or foci while other nuclei showed no signal. In forskolin-treated HGPS cells, the number of brightly positive nuclei and the signal intensity of progerin-positive nuclei were reduced compared to mock-treated counterparts. Forskolin treatment significantly reduced the frequency of nuclear blebbing in HGPS cells after 9 days.
Next to the dysmorphic nuclei, HGPS fibroblasts exhibit reduced levels of nuclear components such as lamin B1. For this, the impact of forskolin on the distribution and expression of the nuclear envelope components lamin A/C and lamin B1 were examined. Mock-treated and forskolin-treated control and HGPS cells were studied in parallel by immunofluorescence microscopy (Fig. 63).

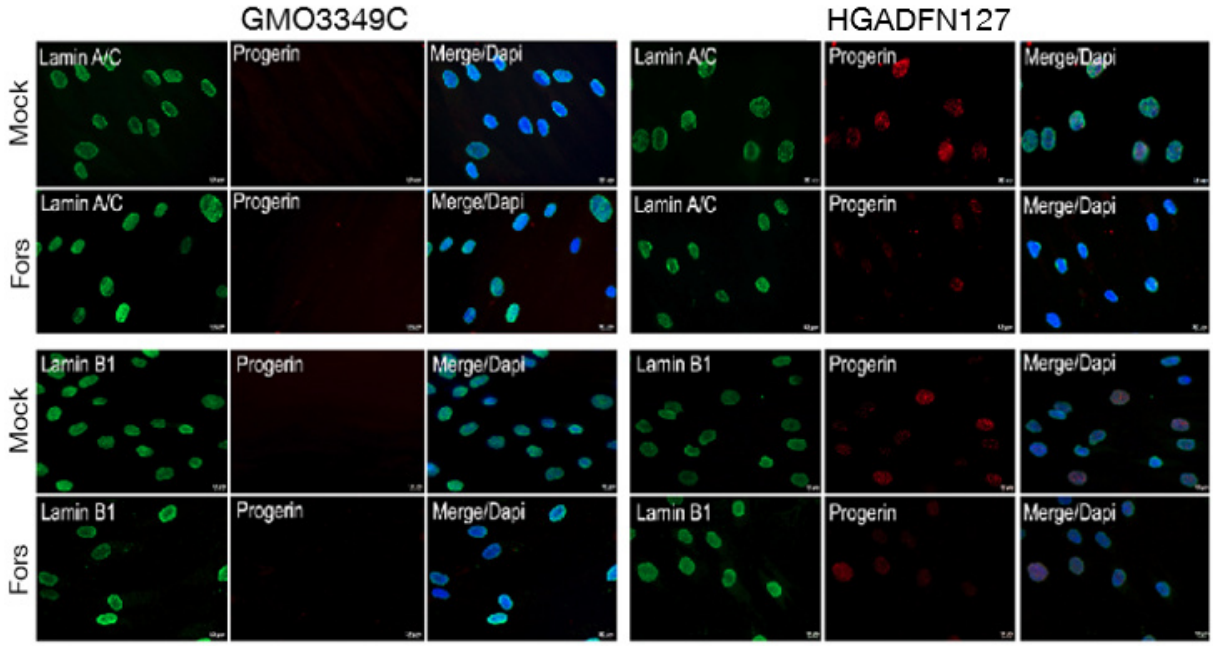

Figure 63: Distribution of nuclear envelope components after Fors treatment. Immunochemistry using antibodies directed against indicated proteins (lamin A/C, progerin, and lamin B1) was performed on control (GMO3349C) and HGPS (HGADFN003) cells mock-treated or Fors-treated for a period of 9 days (n=3). Scale bar: 10 µm.

While no signal of progerin was observed in control nuclei, signals of variable intensity in mock- treated HGPS nuclei were detected as previously reported.[181]
Progerin was found to accumulate in the most dysmorphic HGPS nuclei and localized to the nuclear envelope with aggregated staining in some areas. In nuclei with low progerin levels, progerin appeared as dots or foci within the nuclear compartment.[99]
Lamin A/C was found to be present at the nuclear envelope and throughout the

nucleoplasm in control nuclei and HGPS nuclei. After forskolin treatment, a rim-like staining was observed in control and HGPS nuclei indicating that forskolin did not generally affect the lamin A/C localization. HGPS nuclei exhibit very few dots or foci of progerin staining after forskolin treatment and the number of brightly labeled nuclei were reduced compared to the dysmorphic nuclei of mock-treated HGPS nuclei. The percentage of nuclei that were brightly stained for progerin was reduced from an average of 32 % in mock-treated HGPS cultures to an average of 19 % in forskolin-treated HGPS cultures.

Lamin B1 was reduced in some HGPS nuclei and was linked to the loss of proliferation and senescence.[166,182] In accordance with these findings, very low to barely detectable lamin B1 staining of variable intensity in HGPS nuclei was observed. After forskolin treatment, the overall distribution of lamin B1 in control was not altered. The number of HGPS nuclei exhibiting reduced lamin B1 signals was reduced after forskolin treatment concomitant with a reduced number of bright progerin-positive nuclei.

4.5.3 Long-term forskolin treatment further ameliorates the HGPS cellular phenotype

Forskolin treatment for 9 days induced an improvement in the phenotypic changes of HGPS cells. To analyze the long-term potential of forskolin on control and HGPS cells, cultures were treated every other day with 2.5 µM forskolin or the vehicle, passaged and maintained for several months.

First, the long-term effect of forskolin on the proliferation rate of control and HGPS cells was investigated (Fig. 64 A, B).

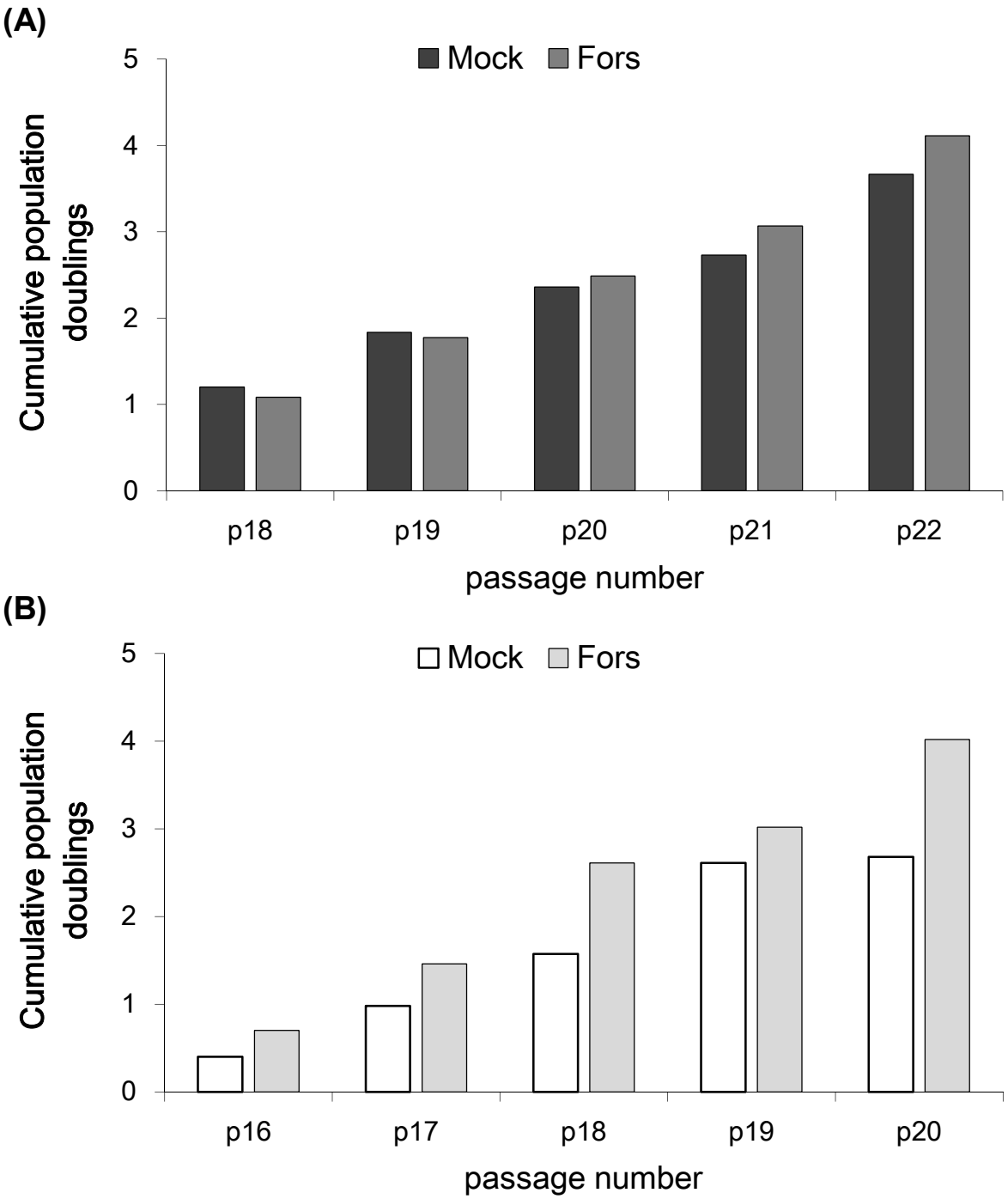

Figure 64: The proliferation rate in long-term Fors cultures. Long-term cultures of control (A) and HGPS (B) cells mock-treated or treated with 2.5 µM Fors. The cumulative population doublings were calculated as described in the Methods.

While mock-treated control cells showed increased proliferation rates, mock-treated HGPS cells reached a growth plateau after several passages. Forskolin treatment induced a sustained increase in the proliferation rates in both control and HGPS cells. During 85 days of forskolin treatment, Western blot analyses were performed on different time points to reveal the status of the A-type lamins (Fig. 65 A, B).

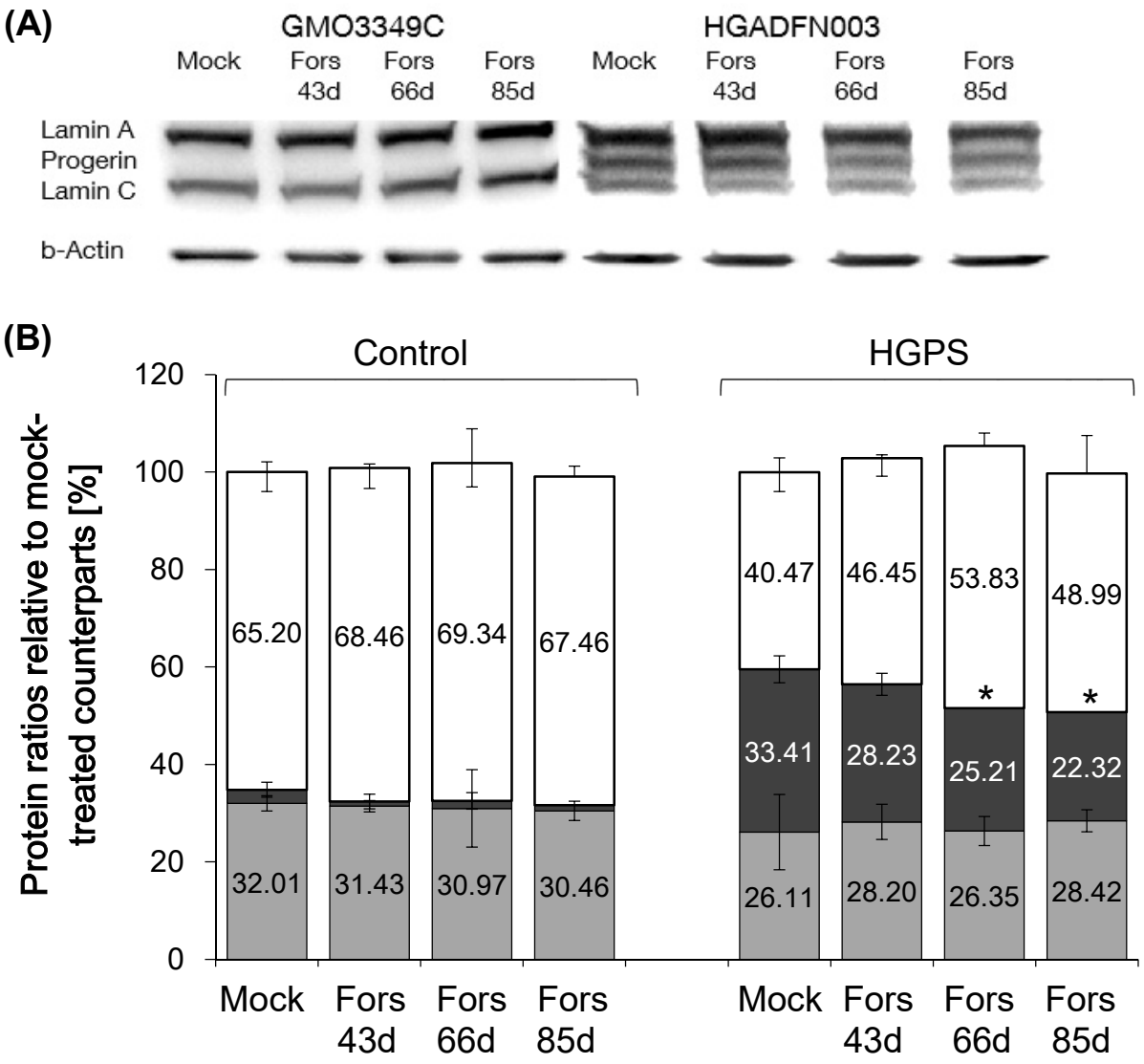

Figure 65: Western blot analyses of long-term Fors cultures. (A) Western blot evaluation of A-type lamins (lamin A, progerin, Lamin C) in control and HGPS cell that were mock-treated or Fors-treated every 2 days for the indicated period. A representative image is shown (n=3). Blots were probed with lamin A/C, progerin, and b-actin antibodies. (B) Densitometric analyses of lamin A, progerin, and lamin C signals obtained from lamin A/C antibody. Data represent the mean ± S.D. with respect to mock-treated counterparts (*$p \leq 0.05$; n=3).

Western blot analyses of control and HGPS cells treated with forskolin for a period of 43 to 85 days indicate that the ratios of lamin A and C remained unchanged compared to mock-treated cells. Progerin levels were reduced by an average of 25 % in forskolin-treated HGPS cells after 43 to 85 days. This result indicates that progerin and lamin C are degraded by autophagy whereas lamin A is degraded by the proteasome system.[183] Consequently, the effect of forskolin on proteasome and autophagy activity during long-term treatment was investigated (Fig. 66 A, B).

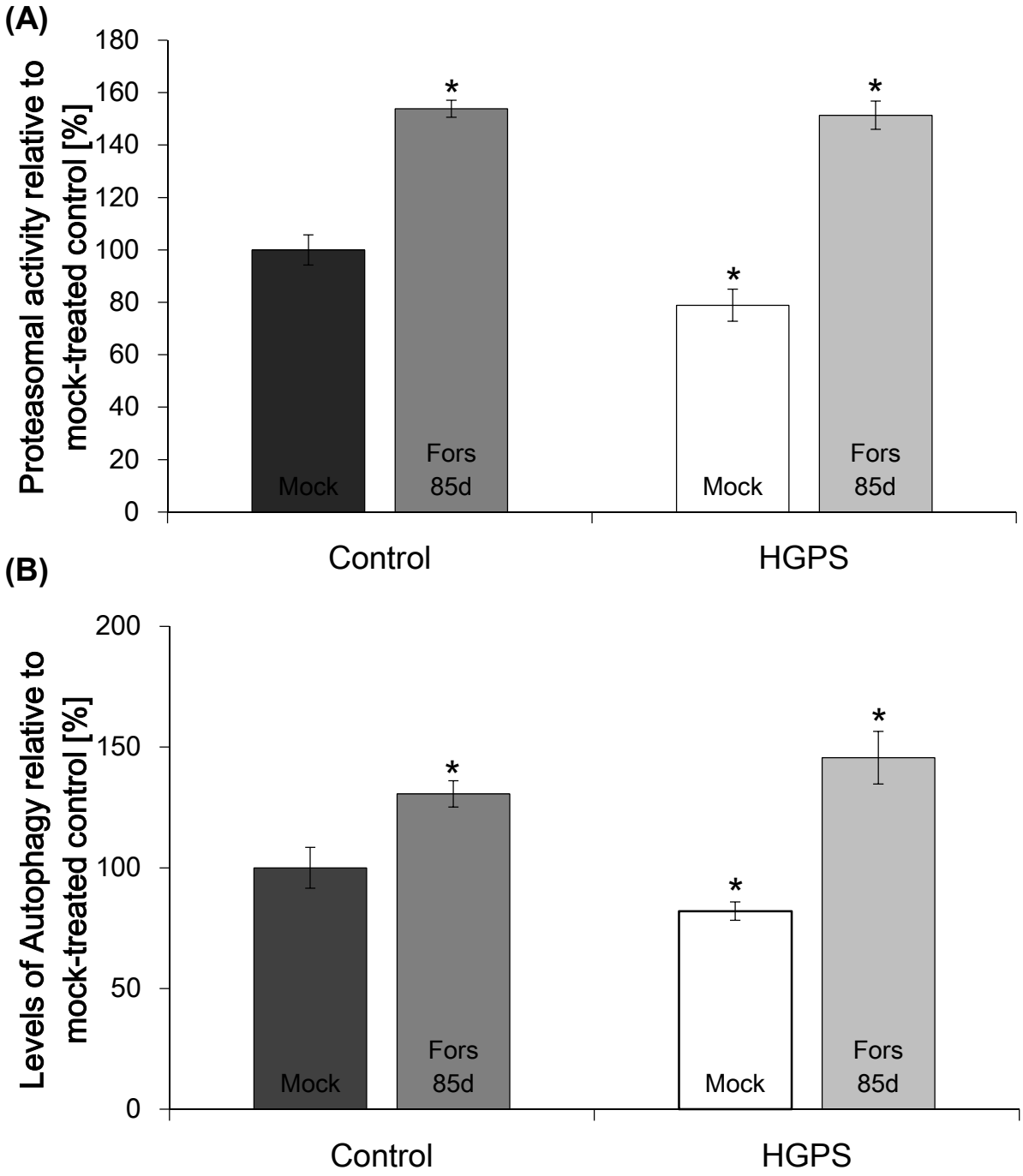

Figure 66: Protein degradation levels of fibroblasts after 85 days of Fors treatment. (A) Proteasome activity was defined by measuring the chymotrypsin-like proteasome activity by Suc-LLVY-AMC in control and HGPS cells. Cells were either mock-treated or treated with 2.5 µM Fors for the indicated period. The percentage of proteasome activity was calculated relative to mock-treated control. Data are presented as mean ± S.D. (*p ≤ 0.05, n=3). (B) The same cells and conditions as in (A) were used to determine autophagy by measuring MDC levels by fluorescence photometry as described in the Methods. Data are expressed as the mean ± S.D. relative to mock-treated control (*p ≤ 0.05; n=3).

While mock-treated HGPS fibroblasts exhibit still significantly reduced levels of proteasome activity and autophagy compared to mock-treated control, forskolin-treated control and HGPS cells demonstrate significantly higher levels of both. Proteasome activity and autophagy levels of forskolin-treated control and HGPS cells showed the same elevated levels of proteasome activity and autophagy as on day 21 of forskolin treatment. The levels of the two protein degradation pathways were maintained during the entire period of 85 days of forskolin treatment.

4.5.4 Forskolin activates Sirt1, AMPK, and their downstream target PGC1α

Samples from HGPS subjects have been associated with alterations in different signaling pathways.[184] Pathways such as MAPK and mTOR were found to be increased in HGPS. Proteins involved in mitochondrial biogenesis, cell metabolism, and activation of transcription factors are altered in HGPS such as AMPK, PGC1α, and Sirt1.[21,88,185-187] The alterations result in reduced autophagy activity and mitochondrial dysfunction. Forskolin has been shown to elevate the levels of these proteins.[21,23,188]
In this study, the ability of forskolin was tested whether it could enhance the activity of AMPK, Sirt1, and PGC1α in HGPS fibroblasts. Control and HGPS fibroblast were treated with the vehicle or 2.5 µM forskolin for 9 days. Cells were analyzed with immunofluorescence and Western blot using phospho-AMPK (pAMPK), PGC1α, and Sirt1 antibodies. Cells were double stained with an anti-progerin or anti-lamin A antibody by immunofluorescence.
AMPK can coordinate cell growth, autophagy, metabolism, and it promotes catabolic pathways to generate ATP.[189] Its activation requires the phosphorylation of Thr172. While pAMPK is distributed throughout the cytoplasm and nucleoplasm in control cells, HGPS cells show barely detectable pAMPK in the nucleoplasm (Fig. 67 A). The expression and distribution of pAMPK were elevated in control cells after forskolin treatment. In HGPS, forskolin increased the expression of pAMPK and the distribution was throughout the cytoplasm and nucleoplasm. Western blot analysis confirmed the increased expression of pAMPK after forskolin treatment in control and HGPS fibroblasts (Fig. 67 B, C).

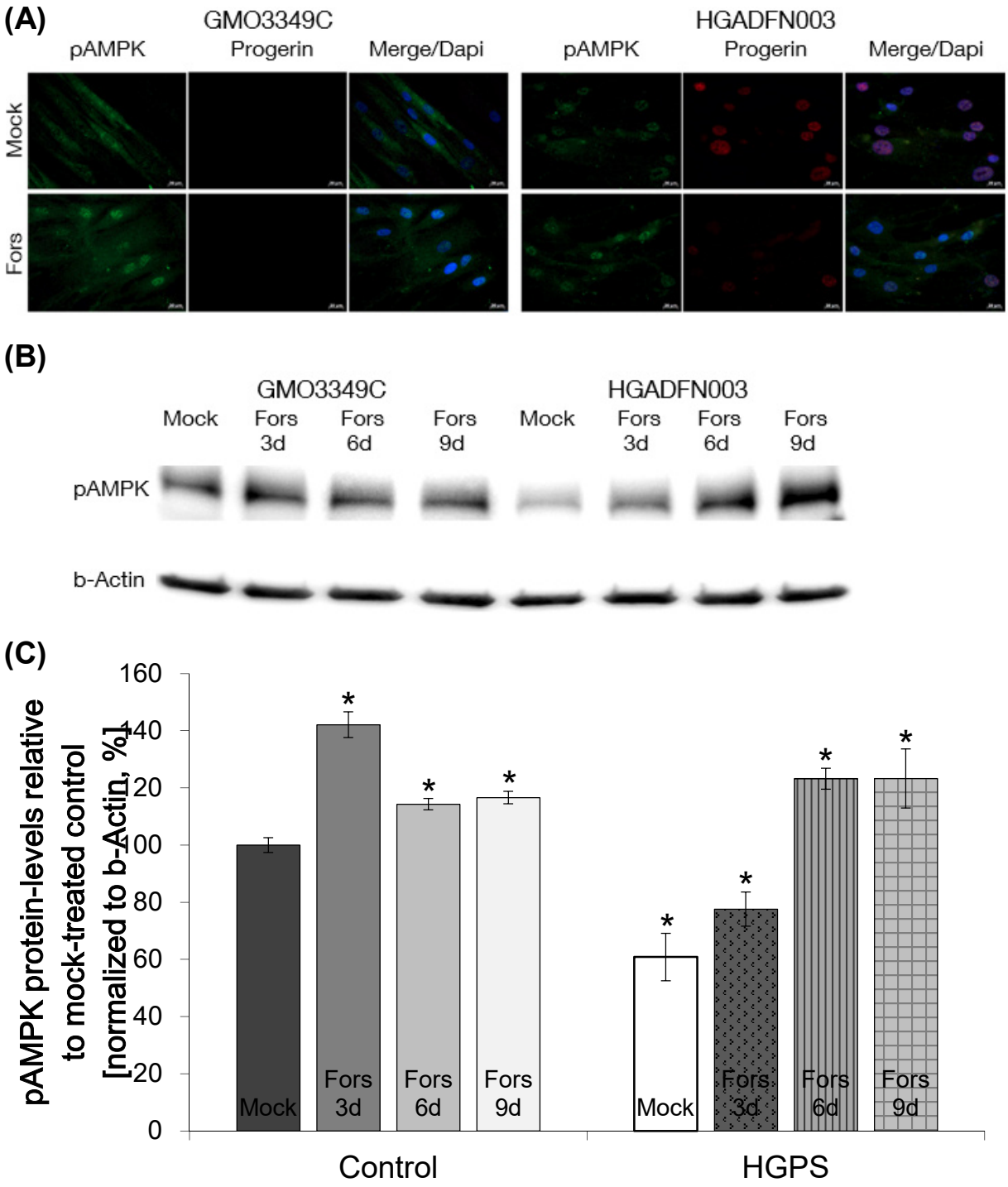

Figure 67: Activation of pAMPK after forskolin treatment. (A) Immunofluorescence of control (GMO3349C) and HGPS (HGADFN003) mock-treated or treated for 9 days with 2.5 µM forskolin. Cells were stained with anti-phospho AMPK (pAMPK) and anti-progerin (n=3). Scale bar: 20 µm. (B) Representative Western blot of pAMPK levels in control (GMO3349C) and HGPS (HGADFN127) fibroblasts mock-treated or forskolin-treated for 3, 6, and 9 days (n=3). (C) Quantification of pAMPK levels normalized to b-actin and presents as the mean ± S.D. relative to control cells (*p ≤ 0.05; n=3).

Sirt1 regulates longevity, apoptosis and DNA repair.[190,191] ROS has been shown to decrease Sirt1 levels, which can lead to dysregulated human vascular smooth muscle cell function.[192] Our experiments show reduced levels of Sirt1 in mock-treated HGPS fibroblasts compared to control cells although the distribution appeared to be similar in the nucleus (Fig. 68 A-C). After forskolin treatment, control and HGPS cells exhibit increased Sirt1 levels.

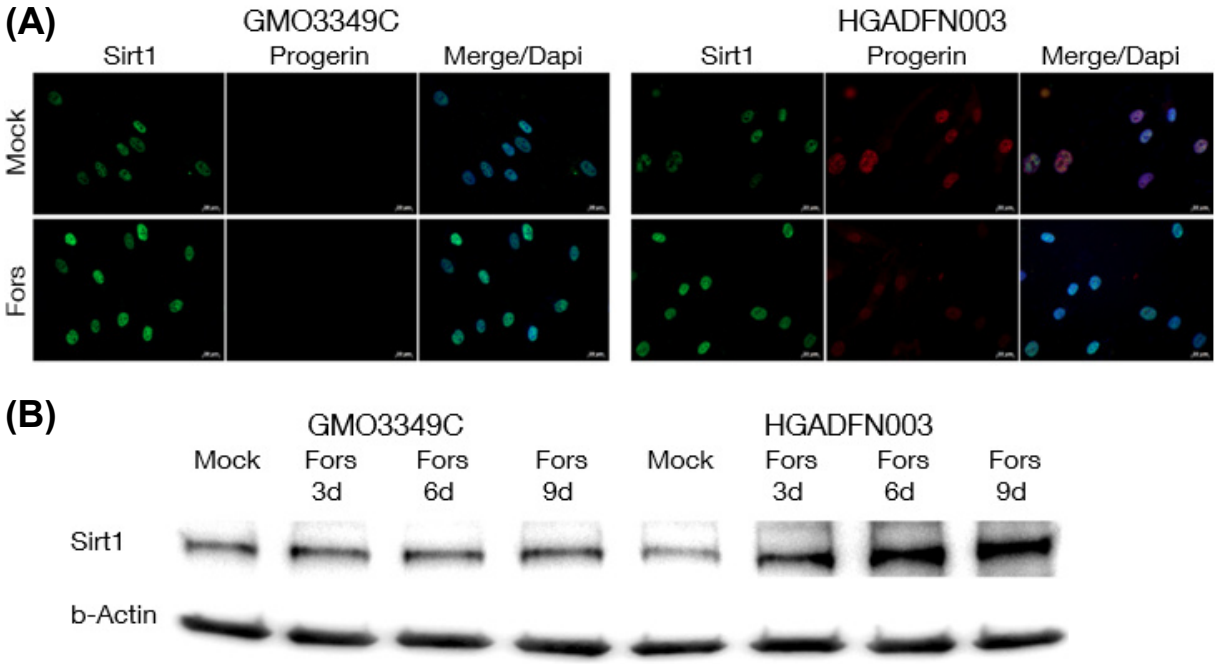

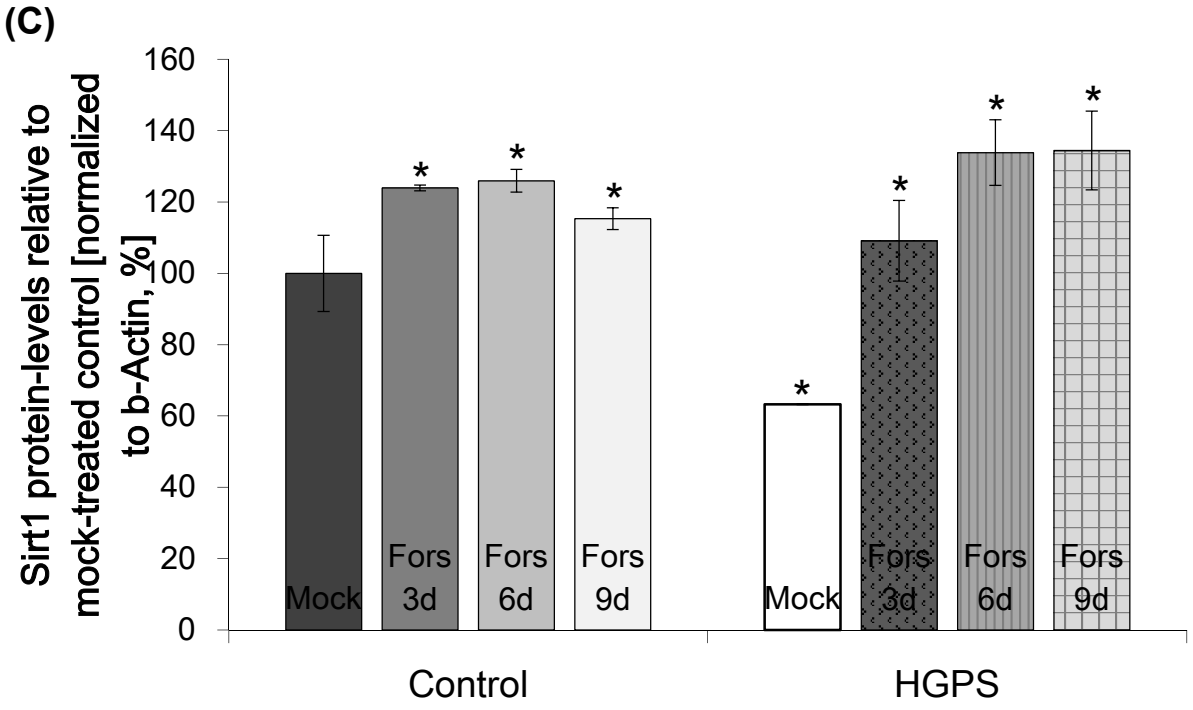

Figure 68: Activation of Sirt1 after forskolin treatment. (A) Immunochemistry using antibodies directed against Sirt1 and progerin as indicated. Control (GMO3349C) and HGPS (HGADFN003) fibroblasts mock-treated or treated with 2.5 µM forskolin for a period of 9 days were used (n=3). Scale bar: 20 µm. (B) Western blot evaluation of Sirt1 in control and HGPS cells treated as described in (A). (C) Quantification of Sirt1 levels normalized to b-actin and presented as the mean ± S.D. relative to control cells (*$p \leq 0.05$; n=3).

PGC1α induces mitochondrial biogenesis through its interaction with several proteins such as mTOR, Nrf 1/2, and Yin Yang1 (YY1).[186] PGC1α is located in the nucleus and cytoplasm and its activity is controlled by pAMPK and Sirt1.[193-195] In our studies, PGC1α was also located in the nucleus and cytoplasm in both control and HGPS fibroblasts (Fig. 69 A-D).

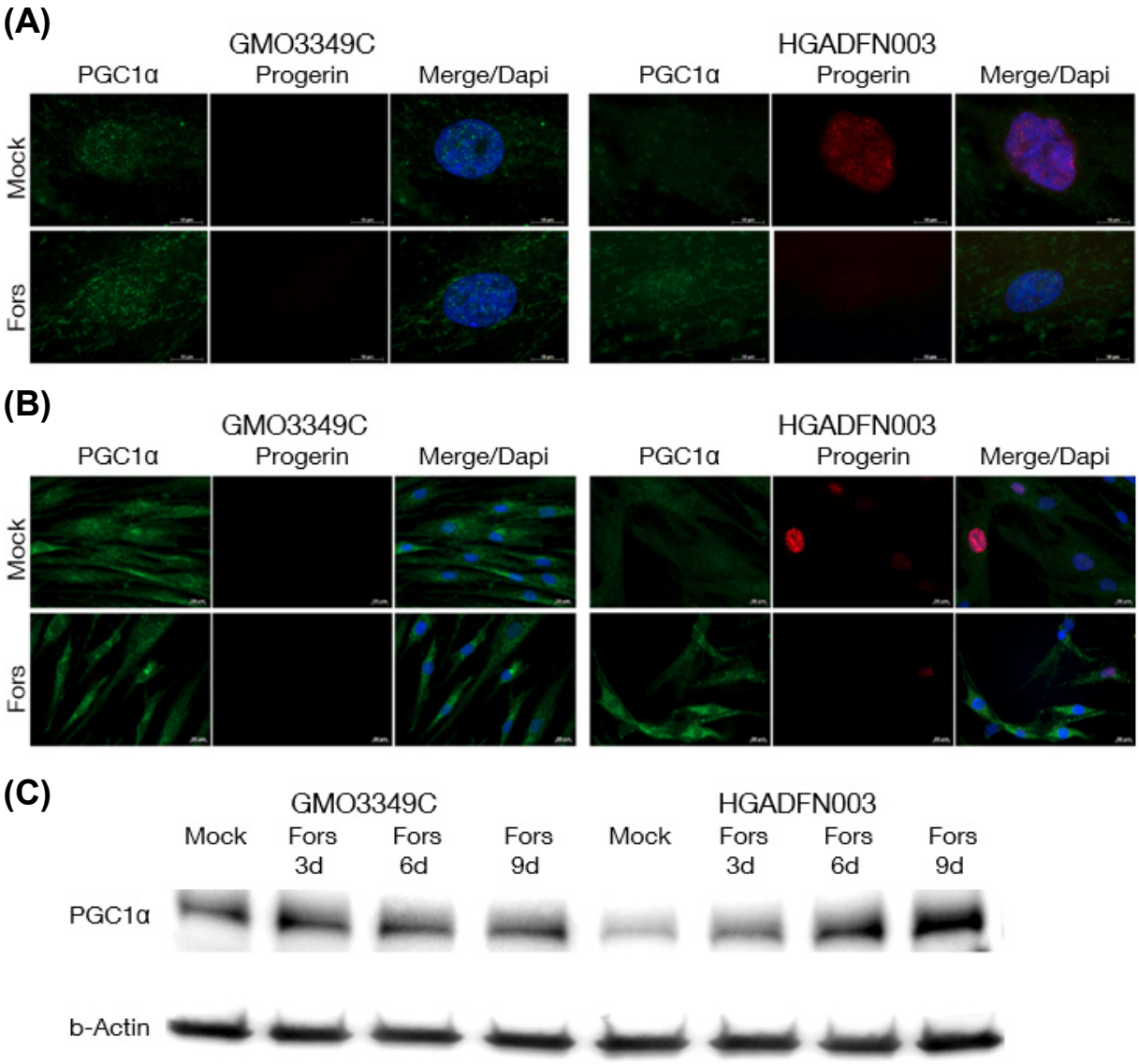
(A)
GMO3349C
HGADFN003
PGC1α
Progerin
Merge/Dapi
Mock
Fors
(B)
(C)
Mock
Fors 3d
Fors 6d
Fors 9d
PGC1α
b-Actin

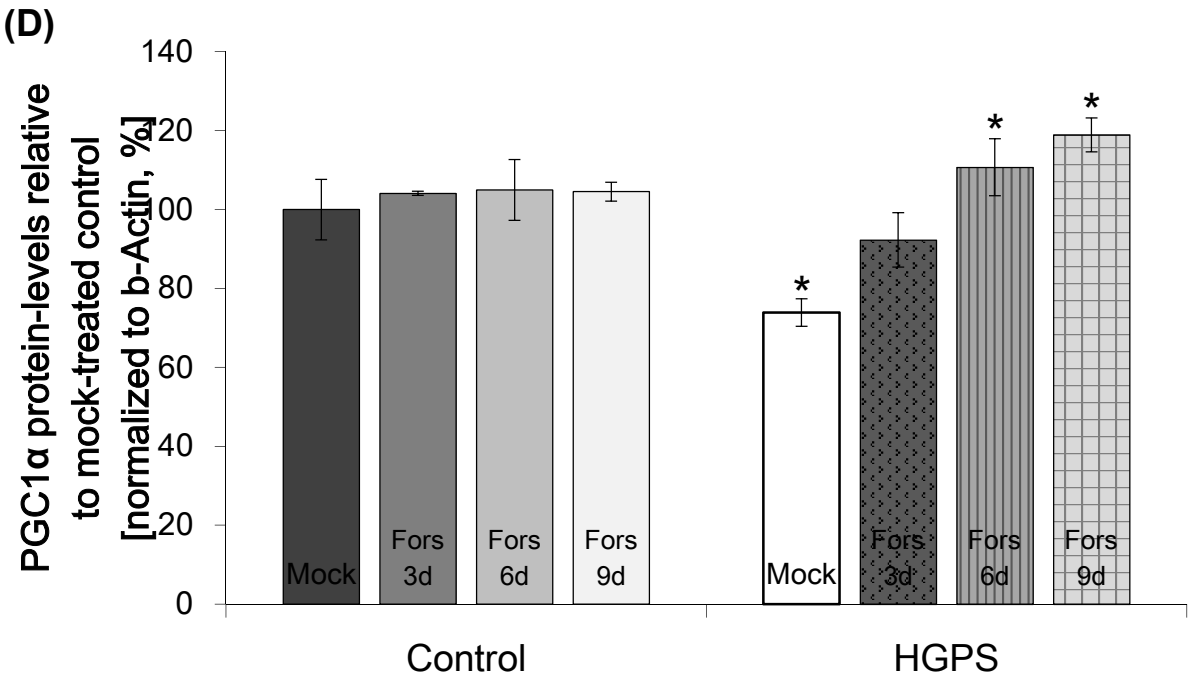

Figure 69: Activation of PGC1α after forskolin treatment. (A) Immunofluorescence of control (GMO3349C) and HGPS (HGADFN003) mock-treated or treated for 9 days with 2.5 µM forskolin. Higher magnification pictures of cells stained with anti-PGC1α and anti-progerin (n=3). Scale bar: 20 µm. (B) Immunofluorescence of control (GMO3349C) and HGPS (HGADFN003) mock-treated or treated for 9 days with 2.5 µM forskolin. Cells were stained with anti-PGC1α and anti-progerin (n=3). Scale bar: 20 µm. (C) Representative Western blot of PGC1α levels in control (GMO3349C) and HGPS (HGPSFN127) fibroblasts mock-treated or forskolin-treated for 3, 6, and 9 days (n=3). (D) Quantification of PGC1α levels normalized to b-actin and presents as the mean ± S.D. relative to control cells (*$p \leq 0.05$; n=3).

In accordance with previous reports, HGPS fibroblasts had lower levels of PGC1α compared to control cells (Fig. 69 A-C).[186] While control cells showed enhanced staining of PGC1α within the nucleus and cytoplasm as a regular aligned network, HGPS cells showed a barely detectable and diffused staining of the cytoplasm and almost no staining of the nucleus (Fig. 69 A, B). Moreover, aggregated staining of PGC1α was observed in certain areas of HGPS cells. Treatment with forskolin maintained the levels in control cells. In HGPS cells, forskolin raised the levels to those of mock-treated controls and PGC1α was expressed throughout the cytoplasm and nucleus (Fig. 69 A, B). These findings were further confirmed by Western blot analysis (Fig. 69 C, D). The impact of forskolin was analyzed on the signaling pathways MAPK and PI3K. Therefore, mock-treated and forskolin-treated cells were stained with antibodies against the phosphorylated forms of Erk1/2 and Akt. Afterwards the staining was measured by flow cytometry. As previously reported, forskolin has been described

to lower the levels of pErk and to maintain the levels of pAkt in control cells.[196,197] Similar levels of pErk1/2 and pAkt were detected after forskolin treatment of control cells. In HGPS, levels of pAkt and pErk were found to be reduced and reached almost mock-treated levels (Fig. 70 A, B).

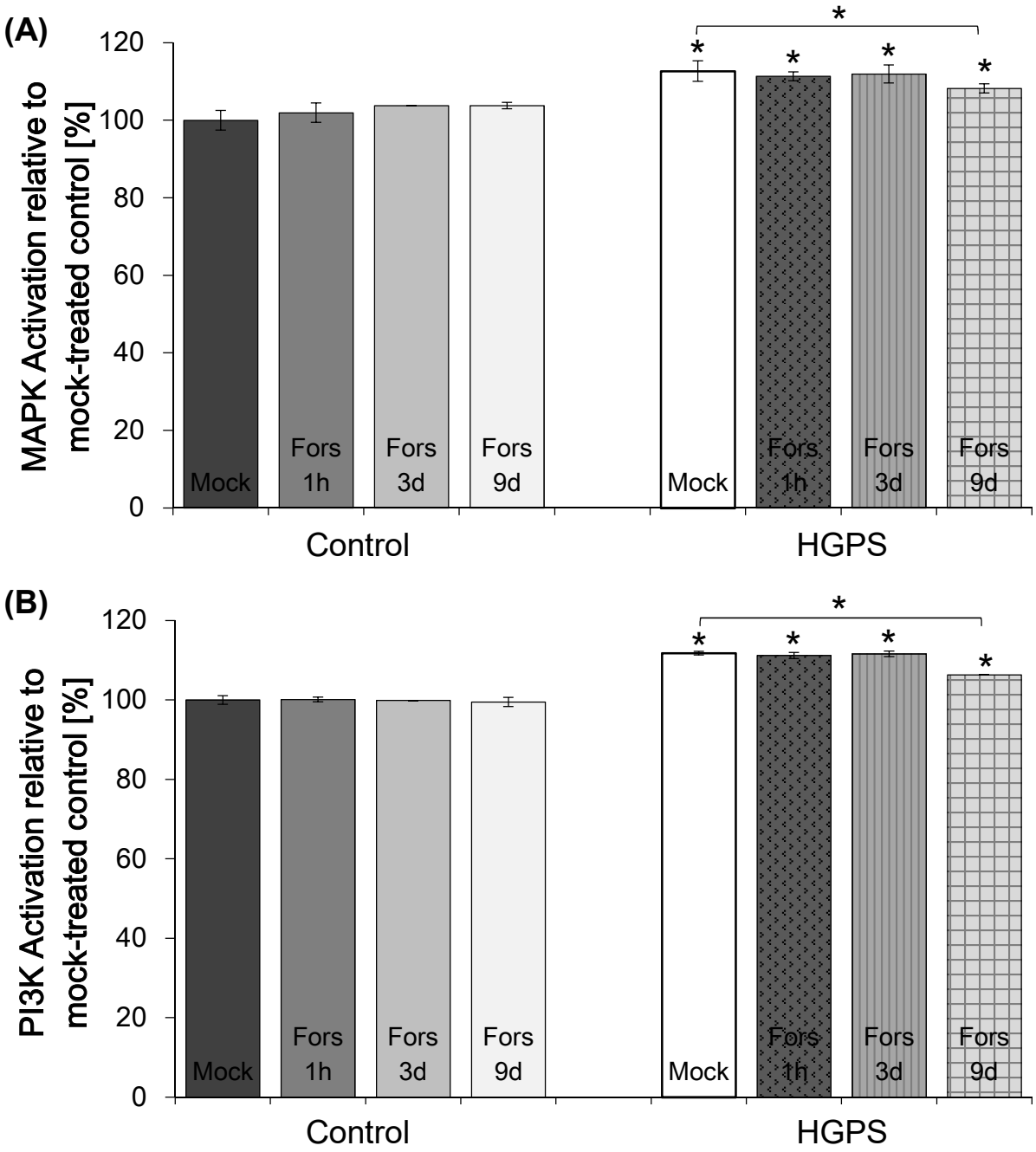

Figure 70: MAPK and PI3K signaling pathway analysis after forskolin treatment. FACS-Analysis of the MAPK signaling pathway (A) and PI3K signaling pathway (B). Control and HGPS cells mock-treated or treated with 2.5 µM forskolin for the indicated time periods were used. Cells were stained as stated in the Methods. Data are presented as the mean ± S.D. (*p ≤ 0.05; n=3).

For a better understanding of the interaction network of these proteins, a signaling pathway map was designed and include the action of forskolin (Fig. 71).
On the right side, it is shown how Sirt1 and pAMPK activate the autophagy pathway by inhibition of mTOR.[198] While pAMPK directly inhibits mTOR, Sirt1 catalyzes the turnover of AMPK to p-AMPK.[199] Inhibition of mTOR has been previously reported to enhance autophagy by blocking the phosphorylation of ULK1.[31] Moreover, pAMPK phosphorylates the ULK1 complex which facilitates autophagy activation.[24] On the left side, the pathways display the impact of pAMPK and Sirt1 on their downstream factor PGC1α. The phosphorylation of AMPK activates phospho-PGC1α by blocking the glycogen synthase kinase 3 beta (GSK3B) thereby enhancing mitochondrial biogenesis.[27,28] Sirt1 catalyzes the deacetylation and phosphorylation of PGC1α directly, which lead to the active form of PGC1α.[25] This step is further required for maintenance of fatty acid oxidation and skeletal muscle function.[26,200] Moreover, Sirt1 activates the transcription of Foxo3.[201] The interaction of Foxo3 with phospho-PGC1α result in mitochondrial biogenesis, autophagy activation, and oxidative stress response.[202,203]

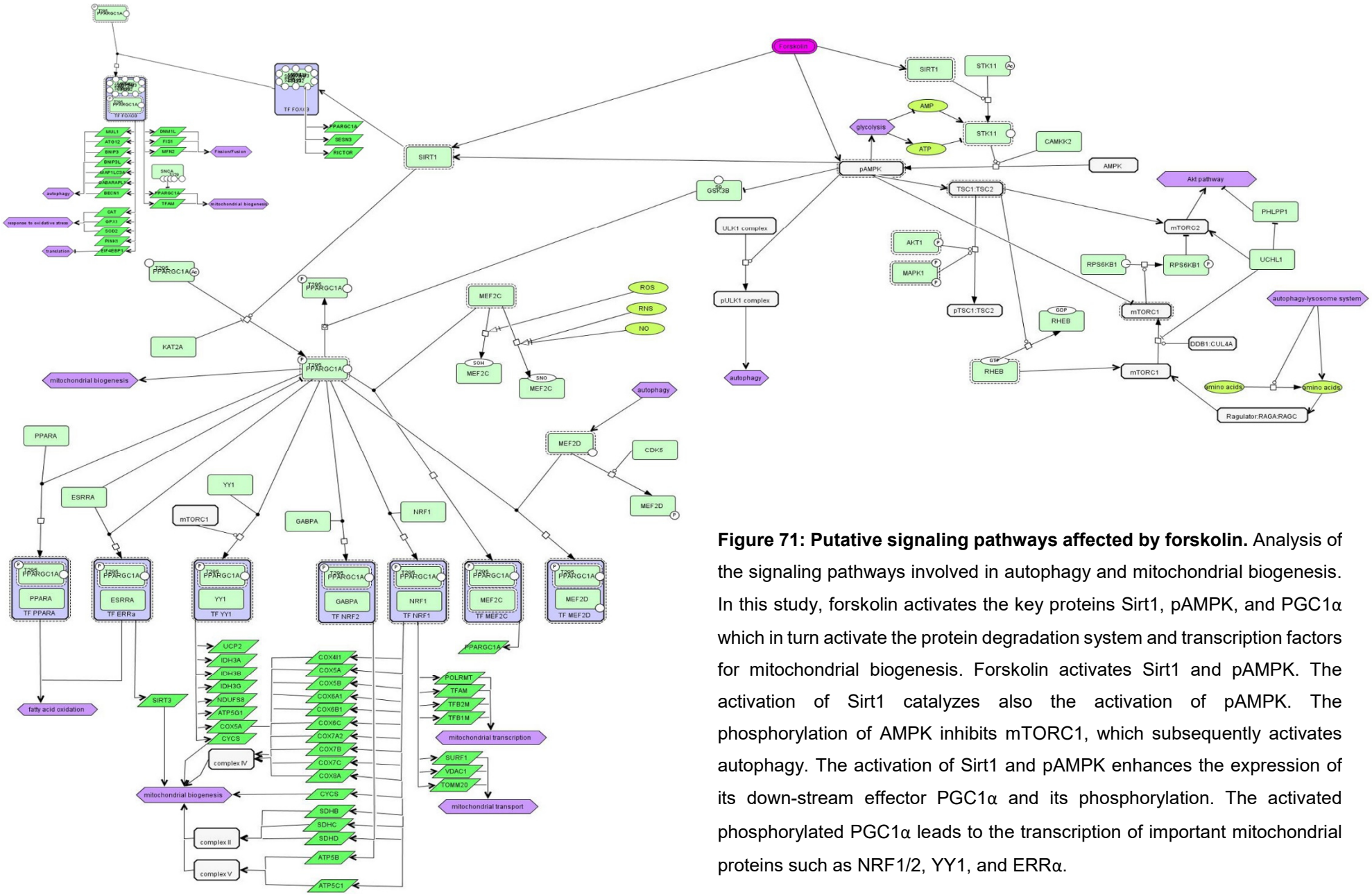

Figure 71: Putative signaling pathways affected by forskolin. Analysis of the signaling pathways involved in autophagy and mitochondrial biogenesis. In this study, forskolin activates the key proteins Sirt1, pAMPK, and PGC1α which in turn activate the protein degradation system and transcription factors for mitochondrial biogenesis. Forskolin activates Sirt1 and pAMPK. The activation of Sirt1 catalyzes also the activation of pAMPK. The phosphorylation of AMPK inhibits mTORC1, which subsequently activates autophagy. The activation of Sirt1 and pAMPK enhances the expression of its down-stream effector PGC1α and its phosphorylation. The activated phosphorylated PGC1α leads to the transcription of important mitochondrial proteins such as NRF1/2, YY1, and ERRα.

Recently, Sirt1 and PGC1α have been shown to interact with lamin A. These interactions are required for the correct functionality of Sirt1 and PGC1α.[185,245]

In this study, reduced expression was observed of both proteins when lamin A was less expressed (Fig. 72, 73).

Sirt1 interacts with lamin A during interphase indicated by the distinct orange aggregates (Fig. 72 A, high magnification Fig. 72 B).

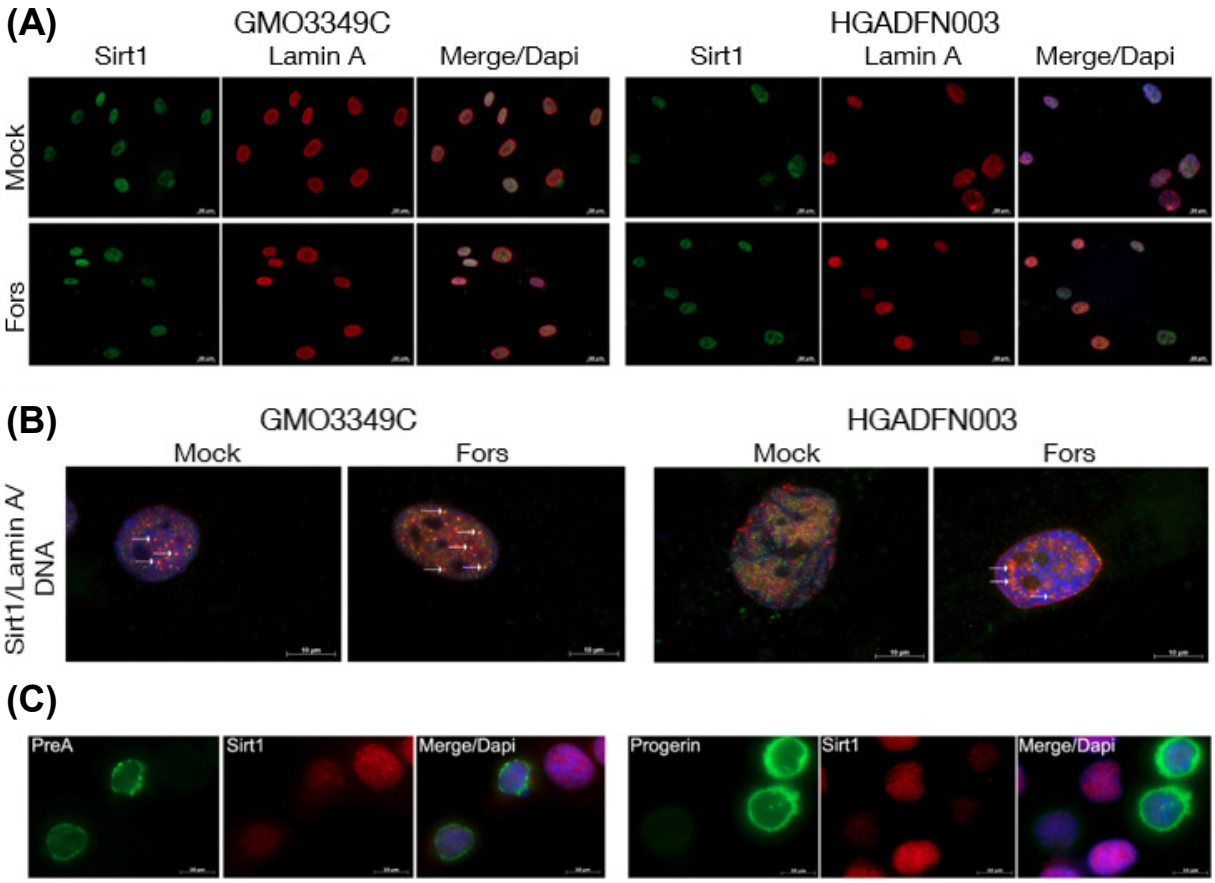

Figure 72: Binding of Sirt1 and lamin A in the presence of forskolin. (A) Immunofluorescence of control (GMO3349C) and HGPS (HGADFN003) mock-treated or treated for 9 days with 2.5 µM forskolin. Cells were stained with anti-Sirt1 and anti-lamin A (n=3). Scale bar: 20 µm. (B) High magnification pictures of the same cells and antibodies as in (A). Arrows indicate Sirt1 and lamin A interaction. Scale bar: 10 µm. (C) Transfection of HeLa cells with prelamin A-GFP and progerin-GFP as indicated. Cells were co-stained with anti-Sirt1 (n=3). Scale bar: 10 µm.

Control cells show more lamin A-Sirt1 binding than HGPS cells. After forskolin treatment, interactions of lamin A with Sirt1 increased in both control and HGPS. Transfection analysis of HeLa cells revealed that neither prelamin A nor progerin can serve as a binding partner for Sirt1 (Fig. 72 C). Prelamin A transfected cells showed

less expressed Sirt1 within the nucleus than non-transfected cells. In progerin-transfected cells, Sirt1 was also less expressed compared to non-transfected cells. PGC1α was less expressed in HGPS cells as lamin A levels are reduced compared to control cells (Fig. 73 A-C).

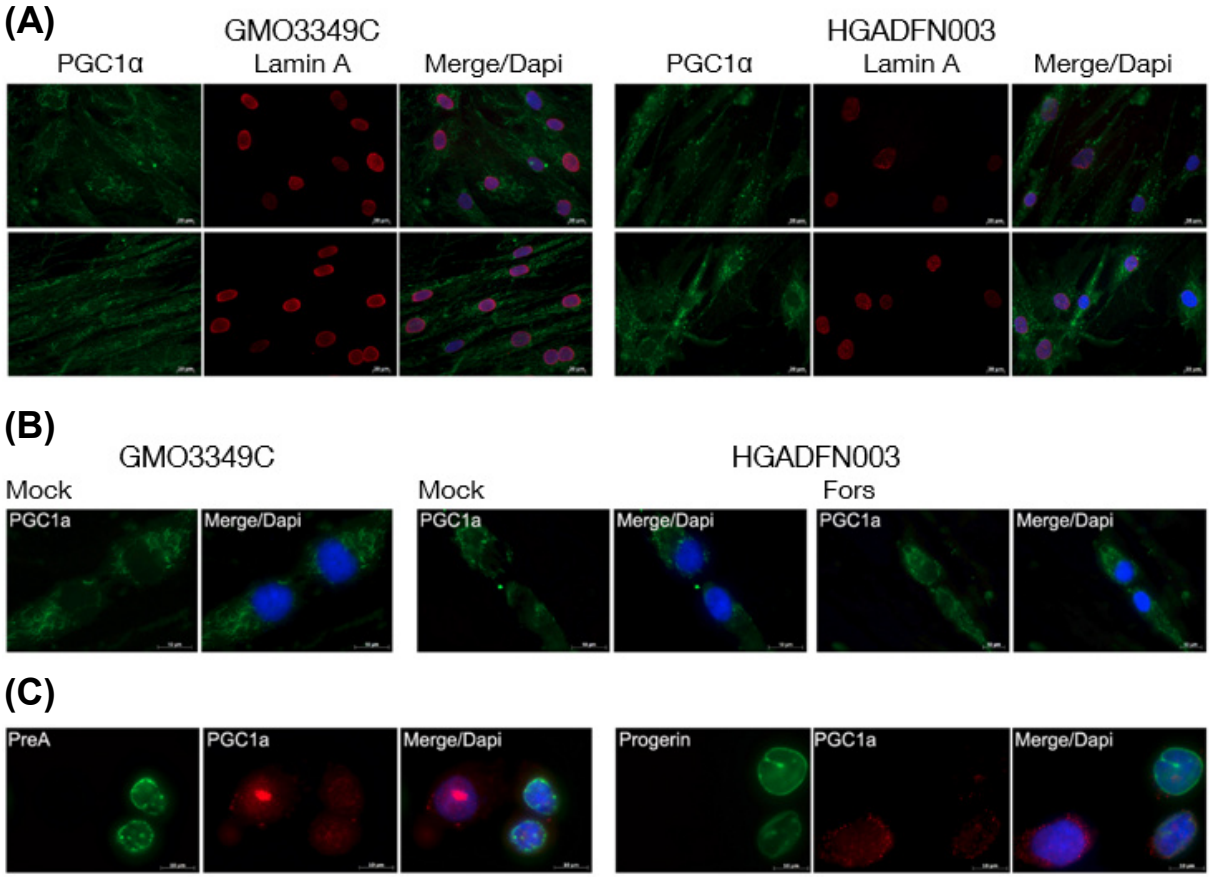

Figure 73: Binding of PGC1α and lamin A in the presence of forskolin. (A) Immunochemistry using antibodies directed against PGC1α and lamin A as indicated. Control (GMO3349C) and HGPS (HGPSFN003) fibroblasts mock-treated or treated with 2.5 µM forskolin for a period of 9 days were used (n=3). Scale bar: 20 µm. (B) Daughter cells of the same cells and antibodies as in (A) are shown. Scale bar: 10 µm. (C) Transfection of HeLa cells with prelamin A-GFP and progerin-GFP as indicated. Cells were co-stained with anti-PGC1α (n=3). Scale bar: 10 µm.

Control cells show a regular aligned network of PGC1α while the network in HGPS is diffused with aggregates in certain areas (Fig. 73 A). Forskolin treatment enhanced the expression of PGC1α in HGPS and the distribution showed control-like pattern. The defective network might occur due to the affected lamin A- PGC1α binding in HGPS. Daughter cells of controls built already a distinct network of PGC1α whereas the network in HGPS is diffused and barely detectable (Fig. 73 B). Moreover, HGPS

daughter cells built aggregates of PGC1α during the separation process. Forskolin ameliorated the defective network of PGC1α in HGPS daughter cells and reduced the aggregated staining. Transfection analysis further provide evidence that lamin A is required for the build-up of PGC1α (Fig. 73 C). Prelamin A-transfected HeLa cells showed reduced expression of PGC1α compared to non-transfected cells. The same findings were seen in progerin-transfected cells.

In summary, the 3 proteins pAMPK, Sirt1, and PGC1α play crucial roles in the mitochondrial biogenesis and metabolism of a cell. The binding of Sirt1 and PGC1α to lamin A seems to be mandatory for their function. Due to progerin in HGPS, the lamin A protein is less expressed which affect those proteins negatively. Forskolin improves the expression and distribution of pAMPK, Sirt1, and PGC1α. This leads to an amelioration of the mitochondrial dysfunction in HGPS.

4.5.5 Forskolin reduces the levels of DNA damage in HGPS

Accumulation of endogenous DNA damage such as DNA double strand breaks (DSBs) was found to be another characteristic of HGPS cells.[167,204] DNA damage is partially resulting from a defective DNA damage repair response. Levels of 53BP1 and Rad51 were found to be altered in HGPS fibroblasts.[14,99,167] For this, the levels of DNA damage were investigated in mock-treated fibroblasts and after 9 days of forskolin treatment. Antibodies against phosphorylated γH2A.X, 53BP1, and Rad51 were used to detect DSBs and DNA damage repair response (Fig. 74 A-C, 75 A-C).

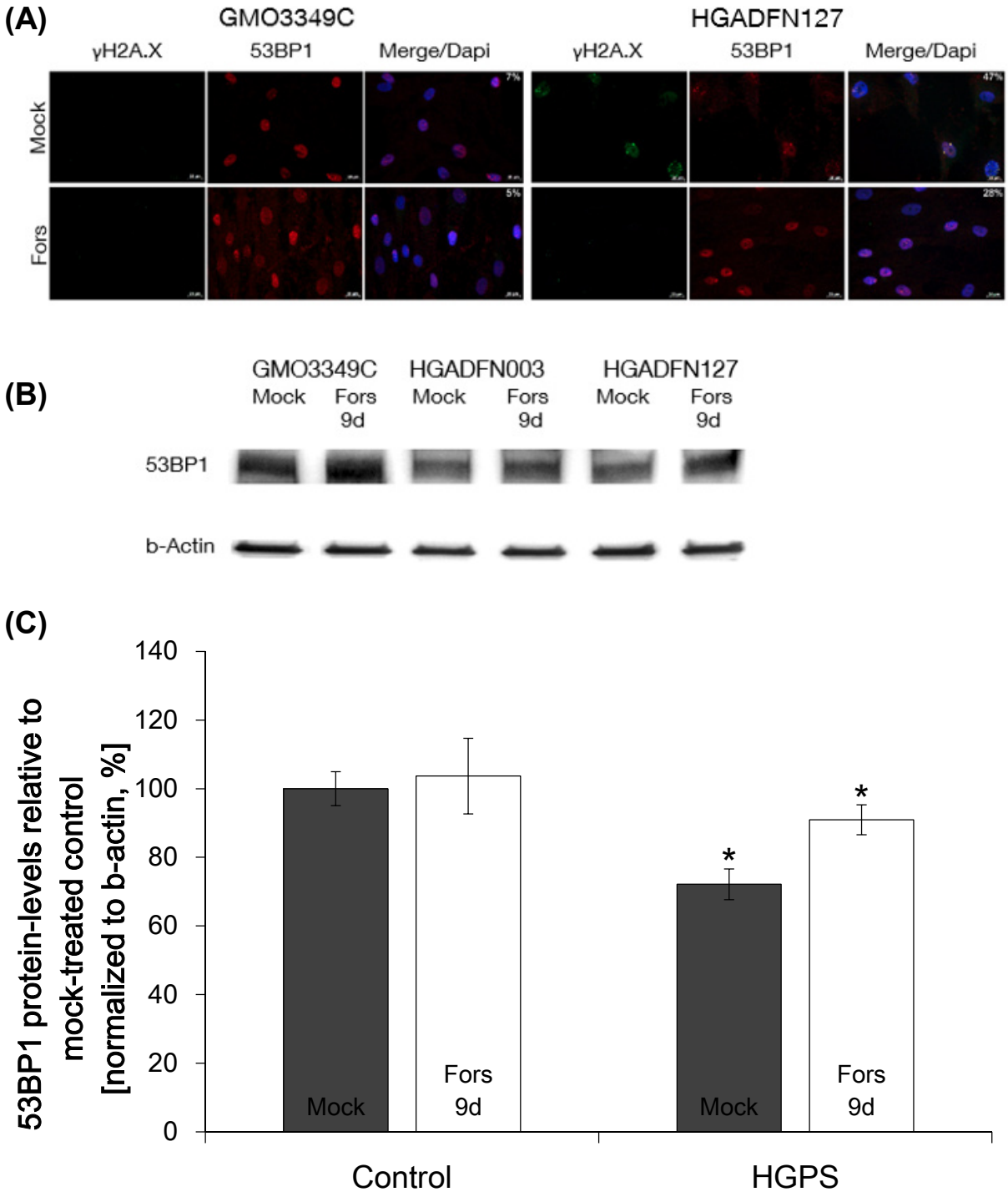

Figure 74: Analysis of the DNA damage repair factor 53BP1 after forskolin treatment. Control (GMO3349C) and HGPS (HGADFN127) cells mock-treated or treated for 9 days with 2.5 µM forskolin were used for immunofluorescence staining against H2A.X and 53BP1. Representative images are shown (n=4). Scale-bar: 20 µm. (B) Western blot analysis of the same cells and conditions as in (A). Antibodies against 53BP1 and b-actin were used. Representative image is shown (n=3). (D) Quantification of 53BP1 levels normalized to b-actin and presented as the mean ± S.D. relative to mock-treated control cells (*p ≤ 0.05; n=3).

The number of detected γH2A.X foci in HGPS cells were on average 47 % which was significantly higher compared to mock-treated control cells that had on average 7 % of γH2A.X foci. Forskolin treatment of HGPS cells reduced the number of nuclei harboring γH2A.X foci to an average of 28 %. These data indicate that forskolin induces efficiently DNA damage repair in HGPS cells. This fact is supported by our findings that forskolin increases the levels of 53BP1 (Fig. 74) and Rad51 (Fig. 75) in HGPS fibroblasts.

(A)

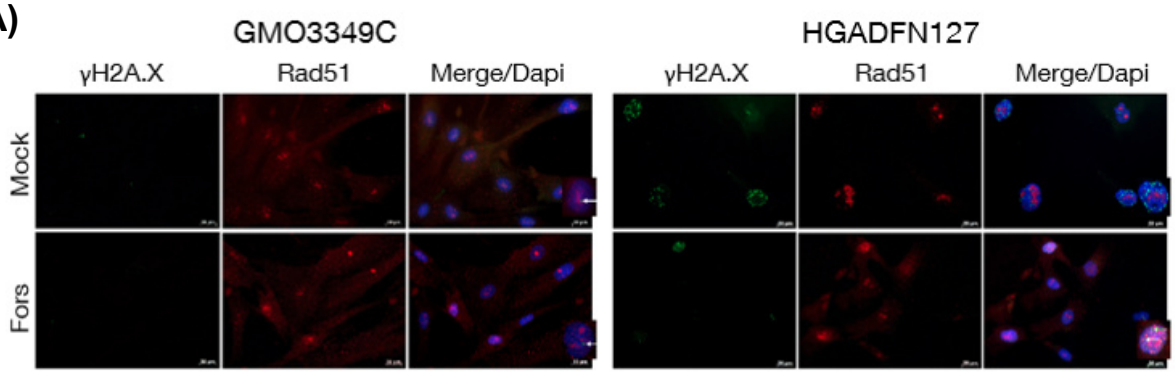

(B)

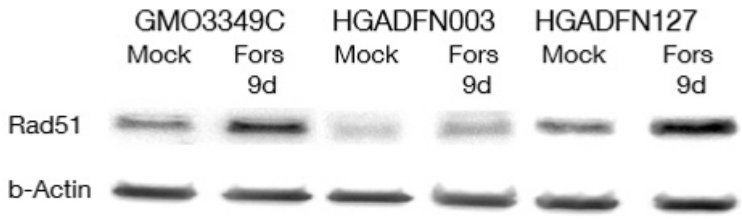

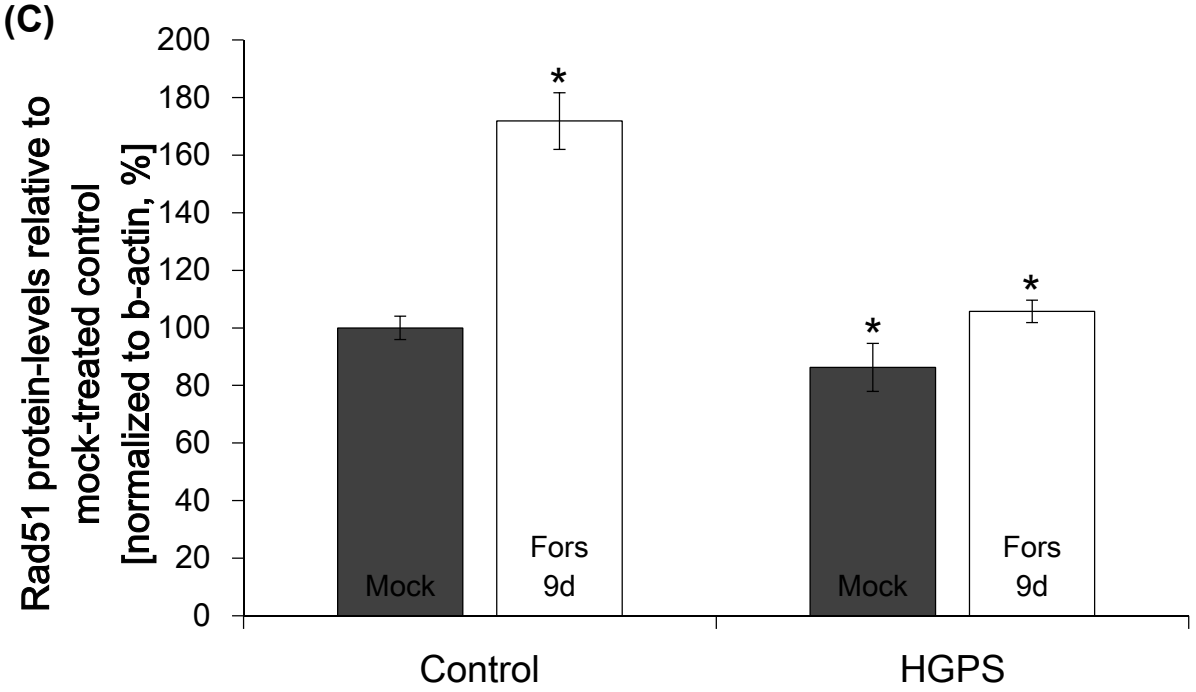

Figure 75: Analysis of the DNA damage repair factor Rad51 after forskolin treatment. Control (GMO3349C) and HGPS (HGADFN127) cells mock-treated or forskolin-treated for 9 days were used for immunochemistry against γH2A.X and Rad51. High magnification pictures are shown attached to the Merge/Dapi channel. Arrows indicate co-localization of γH2A.X and Rad51. Representative images are shown (n=4). Scale-bar: 20 µm. (B) Western blot analysis of the same cells as in (A). Antibodies against Rad51 and b-actin were used. Representative image is shown (n=3). (D) Rad51 levels were quantified, normalized to b-actin, and presented as the mean ± S.D. relative to mock-treated control cells (*p ≤ 0.05; n=3).

These studies provide further evidence that the DNA damage repair proteins 53BP1 and Rad51 are reduced in mock-treated HGPS cells compared to mock-treated control cells. The distribution of 53BP1 was not affected and were found to co-localize with γH2A.X foci in HGPS fibroblasts when compared to mock-treated control. On the contrary, Rad51 showed massive accumulated staining in mock-treated HGPS fibroblasts and no co-localization with γH2A.X foci. After forskolin treatment, HGPS cells exhibited control-like levels of 53BP1 and Rad51 and the nuclear distribution, in particular Rad51, was normalized. The co-localization of Rad51 with γH2A.X was increased (Fig. 75 A, high magnification pictures). In summary, our findings indicate that forskolin improves DNA damage repair in HGPS cells through enhancement of DNA damage repair response.

Next to increased levels of DNA damage, HGPS cells show a loss of heterochromatin and reduced levels of chromatin proteins such as heterochromatin protein 1

(HP1).[5,87,99] In this study, these findings were further supported by finding reduced levels of HP1-γ in mock-treated HGPS fibroblasts compared to control cells (Fig. 76 A-C). However, forskolin treatment of HGPS cells restored the levels of HP1-γ as shown by immunochemistry and Western blot.

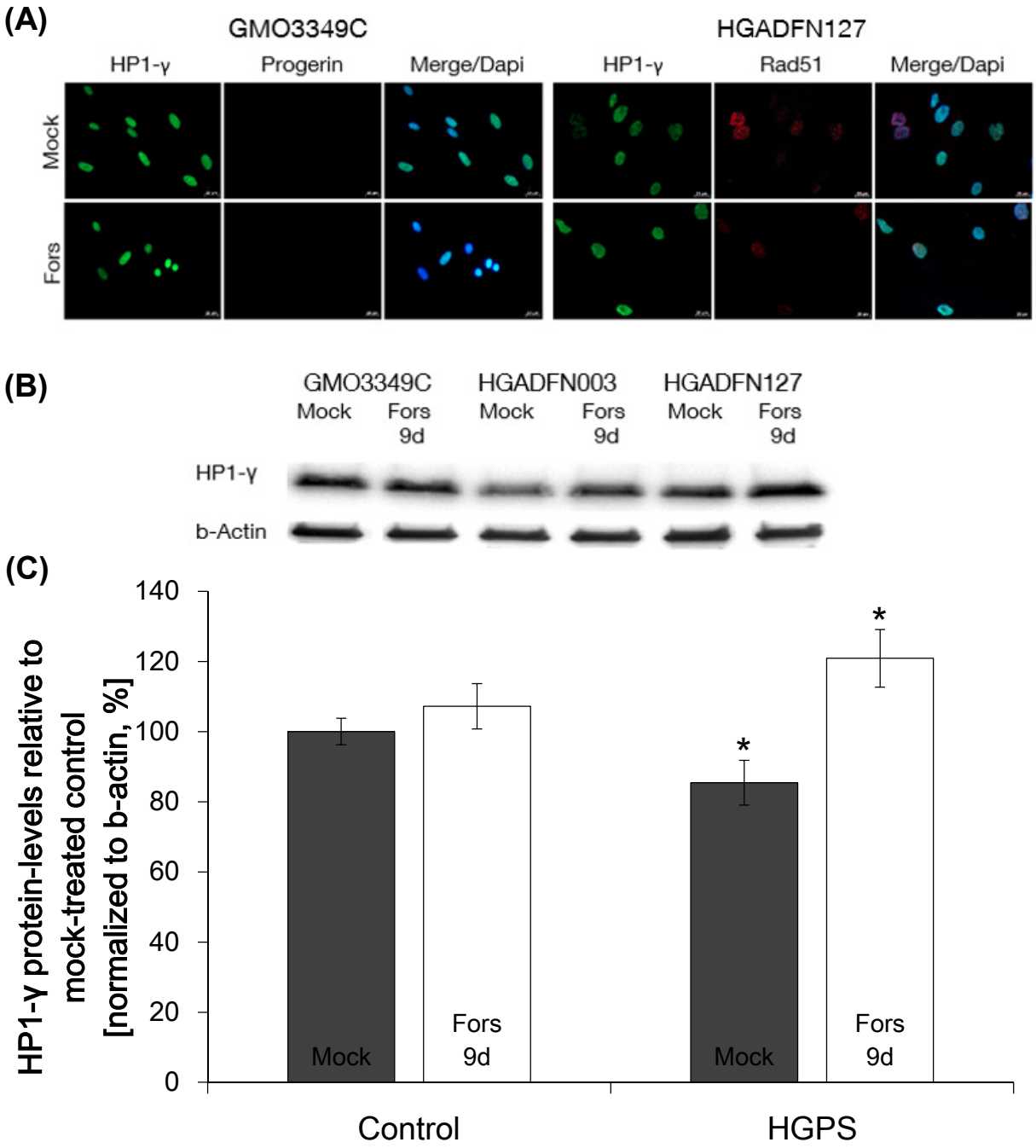

Figure 76: Heterochromatin levels in HGPS after forskolin treatment. (A) Immunocytochemistry using HP1-γ and progerin antibodies on control cells and HGPS cells mock-treated or treated with forskolin for 9 days (n=4). Scale bar: 20 µm. (B) Western blot evaluation of HP1-γ levels of the same cells and condition as in (A). Antibodies directed against HP1-γ and b-actin were used. (C) Quantification of HP1-γ levels normalized to b-actin and compared to mock-treated control cells. Data are presented as the mean ± S.D. (*p ≤ 0.05, n=4).

Collectively, forskolin showed a positive impact on fibroblast homeostasis and progerin clearance. Moreover, forskolin reverse the nuclear phenotypic changes that are characteristic hallmarks of HGPS fibroblasts.

4.6 Temsirolimus (Tem) partially rescues the HGPS cellular phenotype

The macrocyclic antibiotic rapamycin has long been used as an antifungal and immunosuppressive agent and, more recently, it has been shown to improve aging diseases, such as neurodegenerative disorders and arteriosclerosis.[31] Its major cellular target, mammalian target of rapamycin (mTOR), regulates cell growth, hormonal signals, and cell proliferation; when inhibited mTOR activates autophagy (Fig. 77).[205]

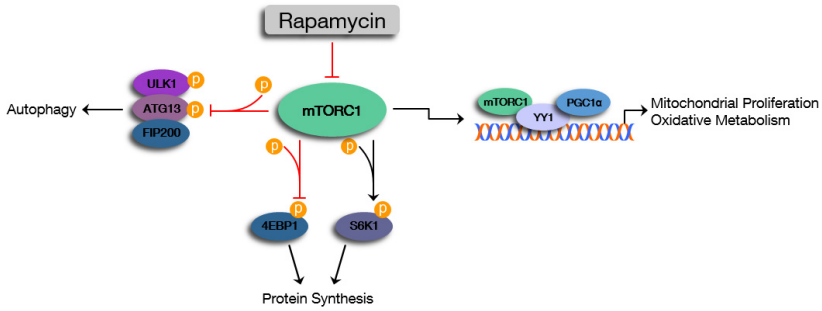

Figure 77: Effect of rapamycin on mTOR signaling. mTOR regulates key signaling pathways such as mitochondrial biogenesis, protein synthesis and autophagy. Rapamycin inhibits mTORC1 thereby blocking the phosphorylation of ULK1 (Unc-51-Like Kinase 1) and ATG13 (autophagy-related gene 13), which in turn leads to activation of autophagy. Inhibition of mTOR leads to accumulation of un-phosphorylated 4EBP1 and S6K1. Both down-stream targets are important activators of protein synthesis. Additionally, rapamycin blocks the interaction of mTOR with Yin Yang 1 (YY1) and PGC1α (Peroxisome proliferator-activated receptor gamma coactivator 1-alpha) which would activate the transcription of proteins for mitochondrial biogenesis.[206]

Although rapamycin was shown to extend lifespan in a number of species, including mice and flies, even when treatment was initiated late in life, only reduced effects on mammalian aging rates have been reported.[31,128,207] In fact, rapamycin might have benefits without a direct effect on aging, as a number of age-related diseases were improved by rapamycin, such as cancer incidence, immune deficiency, myocardial pathology, and arterial degeneration, whereas others were not measurably altered.[128] Critical evaluation of these findings suggest that rapamycin promotes longevity by targeting some, but not all, core molecular processes that drive cellular and systemic aging.[208]

Treating HGPS fibroblasts with rapamycin results in reduced progerin levels, attributed to increased progerin clearance via autophagy activation, which consequently led to amelioration of the HGPS cellular phenotype.[30] The beneficial effect on HGPS fibroblast longevity supports rapamycin treatment as a potential therapeutic avenue for HGPS children. Nevertheless, the side effects of rapamycin, which include gastrointestinal symptoms, delayed wound healing, and interstitial pneumonitis, should be taken into account.[209,210]

Therefore, a soluble ester of rapamycin was tested that displays fewer side effects when administered clinically, the analog temsirolimus (Tem).[211,212] The efficacy of the rapamycin analog temsirolimus has to be proven and more importantly, mitochondrial dysfunction needs to be investigated for rapamycin analogs. To determine its effect on proteostasis, mitochondrial function, DNA damage, proliferation and progerin levels, the effect of short-term and long-term temsirolimus treatments was tested on HGPS primary fibroblast cultures compared to control fibroblasts.

4.6.1 Tem enhances progerin degradation in HGPS via autophagy

First, the potential toxicity of Tem was examined by applying different concentrations to fibroblast cultures for 48 hours. The percentage of cell death was analyzed (Fig. 78).

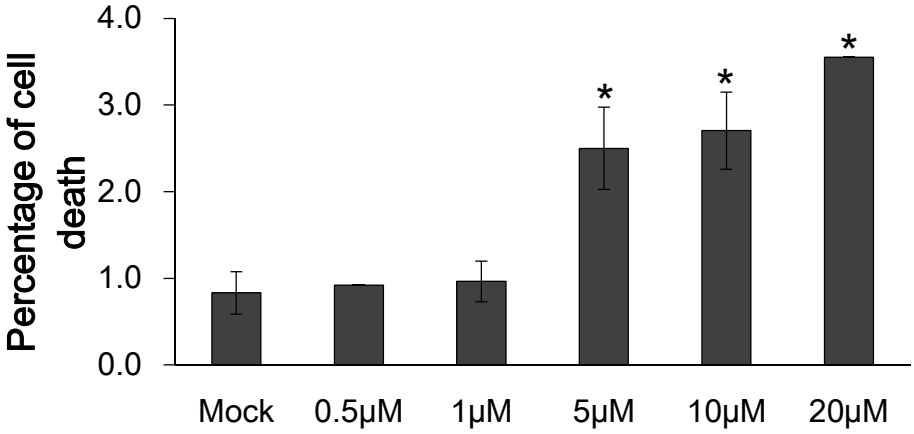

Figure 78: Cytotoxicity of Tem-treated control cells. Cells were treated daily with either the vehicle (DMSO) or with different concentrations Tem up to 48h. Percentage of cell death is shown after 48h at indicated Tem concentrations. Data are presented as the mean ± S.D. relative to mock- treated cells (*p ≤ 0.05; n=3).

Treatment with 5 µM Tem led to greater cell death than 1 % in control cells. A concentration of 1 µM Tem was chosen for all subsequent experiments as the number of cell death was less than 1 %. The proliferation rate of control and HGPS cells treated with the vehicle or 1 µM Tem was examined (Fig. 79).

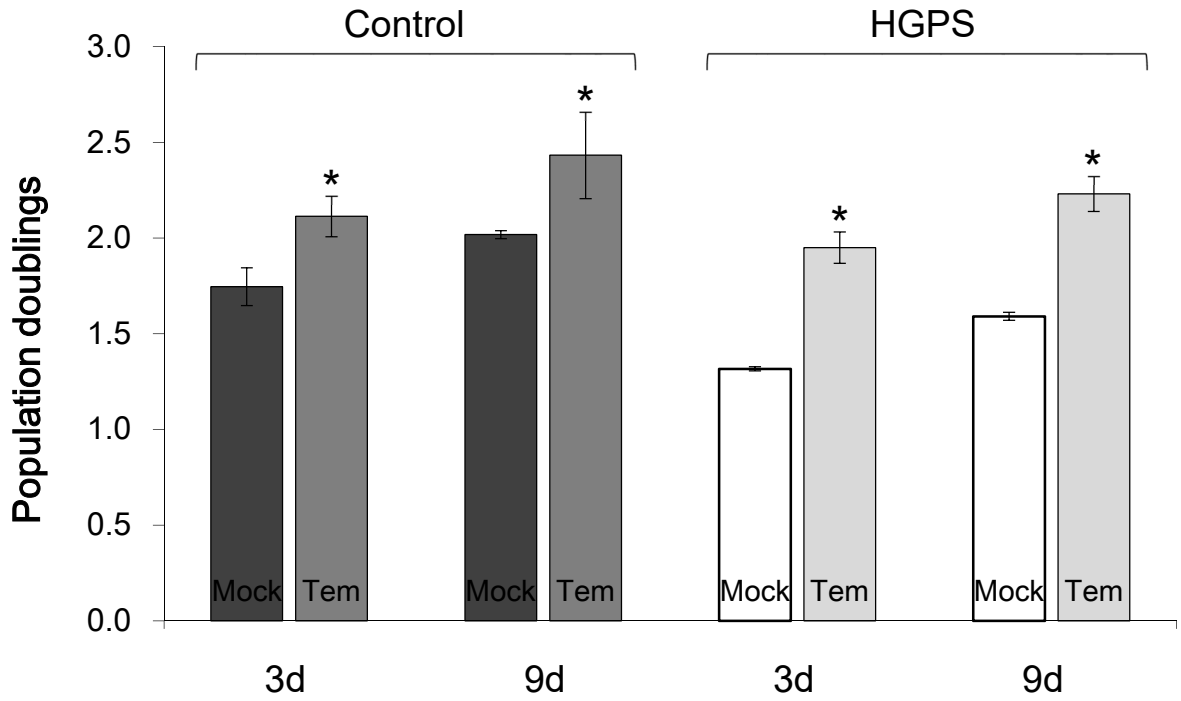

Figure 79: Cell proliferation in mock-treated and Tem-treated fibroblasts. Population doubling levels were calculated as stated in the Materials and Methods relative to mock-treated counterparts. Control and HGPS cells were mock-treated (vehicle DMSO) or treated daily with 1 µM Tem for a period of 3 or 9 days (*p ≤ 0.05; n=4).

Control and HGPS cells treated with 1 µM Tem showed a significantly increased growth rate at day 3 and 9 compared to mock-treated counterparts. Furthermore, the defect in proliferation of HGPS cells was improved after 9 days of Tem treatment.
Next, the effect of Tem on the two major protein degradation pathways was analyzed. Proteasome activity and autophagy activity was measured of mock-treated and Tem-treated control and HGPS cells (Fig. 80, 81).

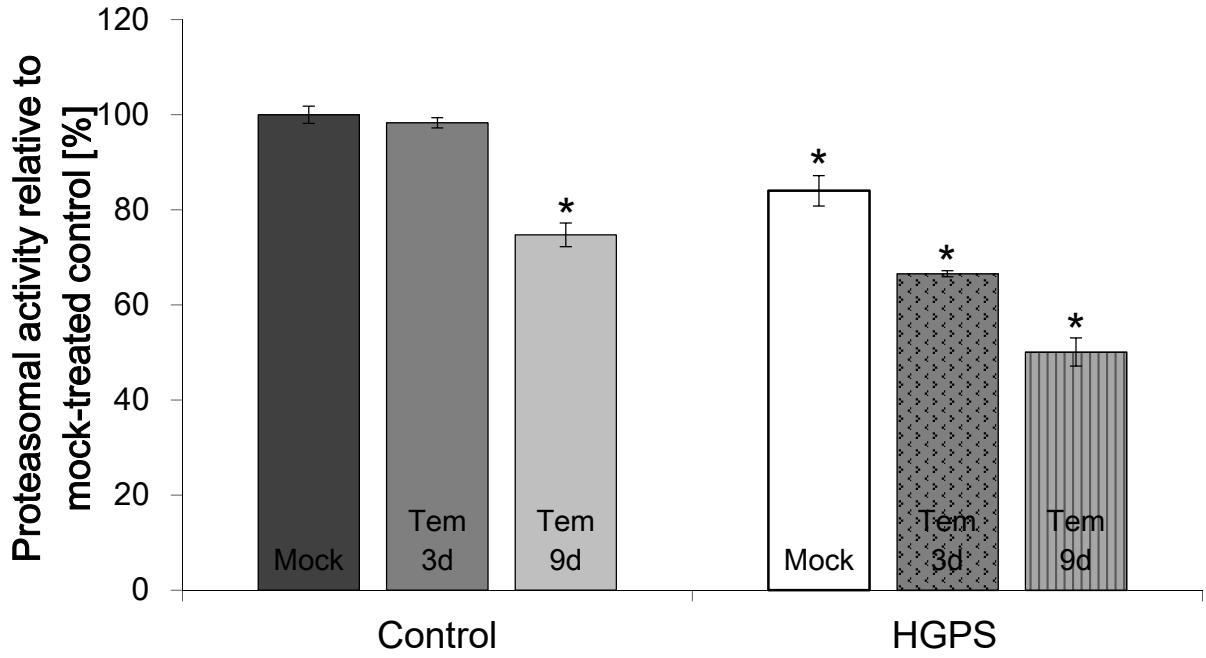

Figure 80: Proteasomal activity Tem treatment. Proteasome activity was determined by measuring chymotrypsin-like proteasome activity in control and HGPS fibroblasts using Suc-LLVY-AMC as a substrate. Cells were either mock-treated or treated daily with 1.0 µM Tem for a period of 3 or 9 days. The percentage of activity was calculated relative to the mock-treated control cells. Data are expressed as the mean ± S.D. (*p ≤ 0.05; n=4).

Initially, mock-treated HGPS fibroblasts showed a significantly reduced proteasome activity compared to control fibroblasts. After Tem treatment, control cells as well as HGPS cells showed a decrease in the proteasome activity after 3 and 9 days compared to mock-treated cells. In accordance with these findings, it was found that rapamycin and its analogs inhibit allosterically the 20S proteasome.[178]

The analysis of the autophagy activity revealed that Tem treatment significantly enhances the autophagy of control and HGPS cells at day 3 and 9 compared to mock-treated control cells (Fig. 81).

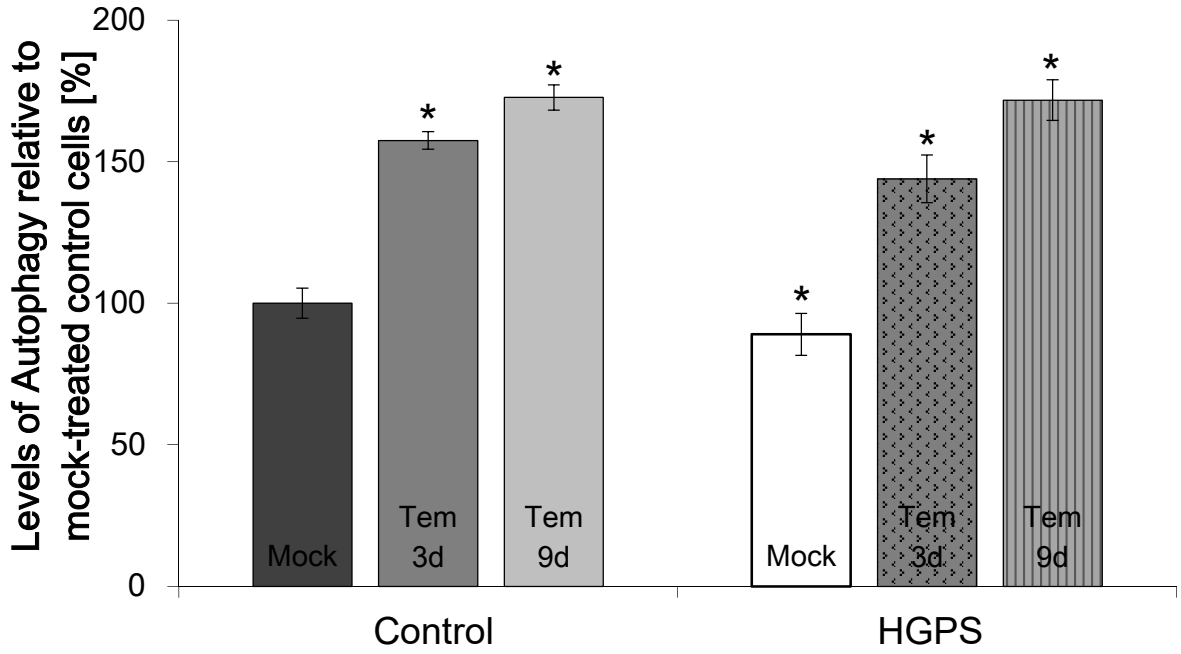

Figure 81: Autophagy levels after Tem treatment. Autophagy was determined in control and HGPS fibroblasts by measuring monodansylcadaverine (MDC) levels with fluorescence photometry. Cells were either mock-treated or treated daily with 1.0 µM Tem for a period of 3 or 9 days. The percentage of activity was calculated relative to the mock-treated cells. Data are expressed as the mean ± S.D. (*p ≤ 0.05; n=4).

The inhibition of the proteasome activity and the activation of autophagy was further supported by Western blot (Fig. 82 A-C). Rapamycin was also found to increase the progerin clearance by up to 50 % in HGPS cells.[30,213] For this, Western blot was stained with lamin A/C antibody and quantified. The status of A-type lamins was investigated of total protein extracts derived from HGPS and control cells mock-treated or Tem-treated for 9 days.

(A)

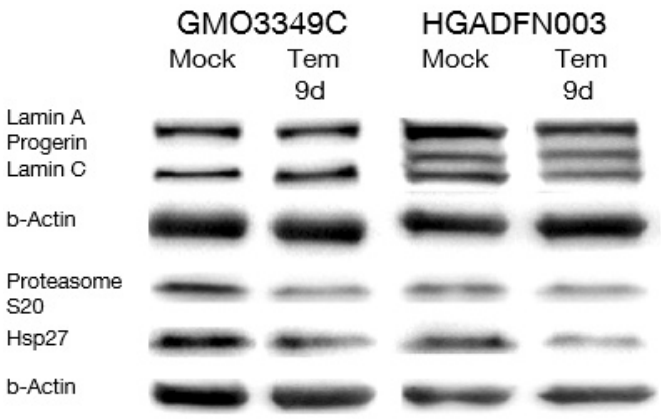

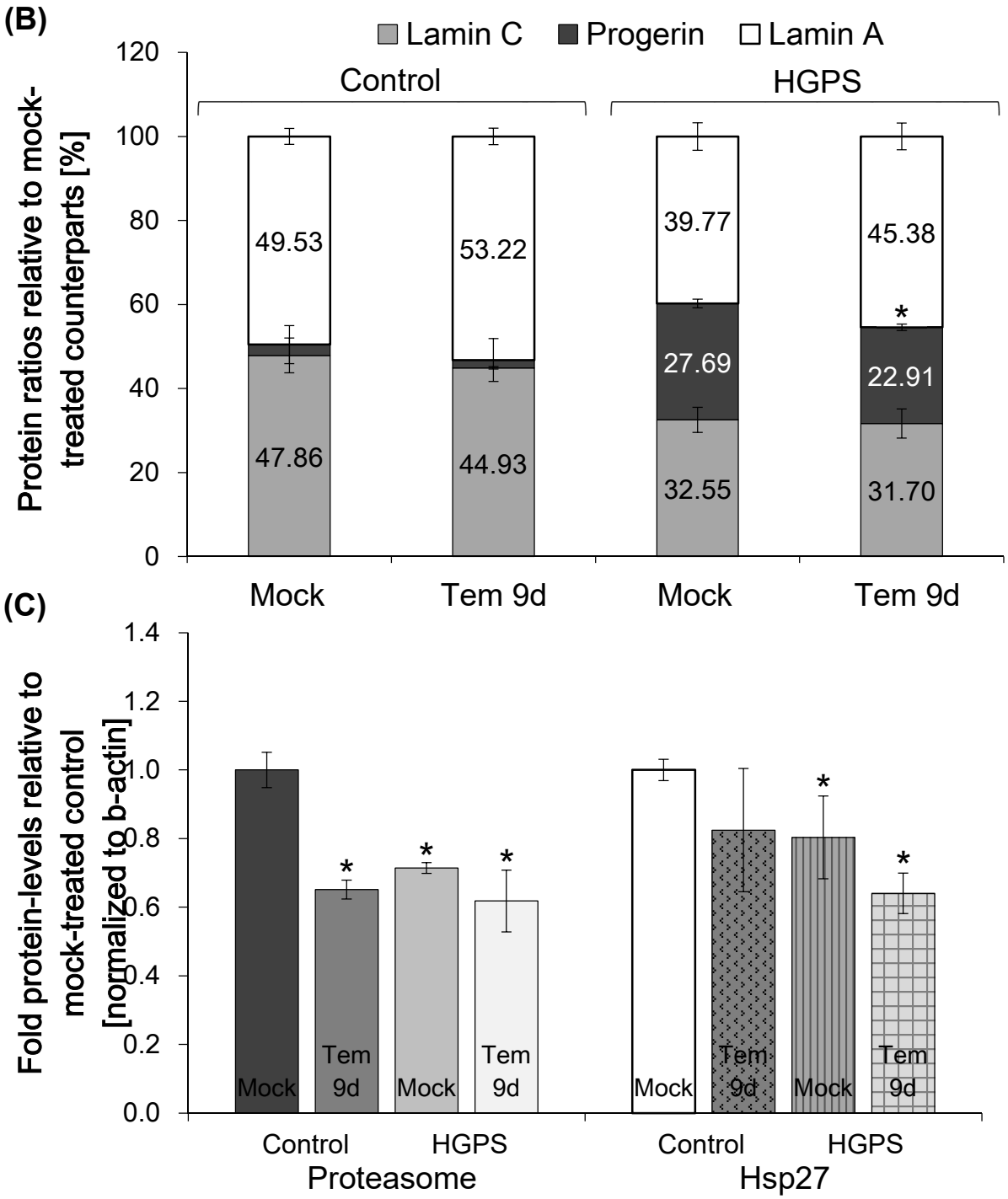

Figure 82: Western blot analyses of mock-treated and Tem-treated fibroblasts. (A) Representative Western blots of lamin A/C, progerin, proteasome subunit S20 C2, Hsp27 and b-actin in control and HGPS total cell extracts either mock-treated or treated with 1.0 µM Tem daily for 9 days. (B and C) Quantification of the ratios of the A-type lamins relative to mock-treated counterparts (lamin A, lamin C, and progerin). Levels of proteasome subunit S20 C2 and Hsp27 were quantified by normalizing to b-actin, and presented as the fold-change ± S.D. relative to mock-treated control cells (*p ≤ 0.05; n=3).

The status of the A-type lamins revealed that progerin levels were increased in HGPS cells by 8-9 fold compared to mock-treated control cells. Temsirolimus treatment

induced a progerin clearance in HGPS cells by 17 %. The levels of lamin A and lamin C remained constant in control and HGPS cells.

The protein expression of the 20S proteasome subunit C2 and Hsp27 were significantly reduced in mock-treated HGPS cells. After temsirolimus treatment, the levels of the 20S proteasome and Hsp27 were not ameliorated in HGPS cells and even reduced in control cells.

To provide evidence that temsirolimus clears progerin via autophagy, HGPS cells were treated with temsirolimus for 8 days and subsequently exposed to temsirolimus with 25 µM chloroquine diphosphate (Cq), an autophagy inhibitor, or 1 µM MG132, a proteasome inhibitor, for 12 hours (Fig. 83).

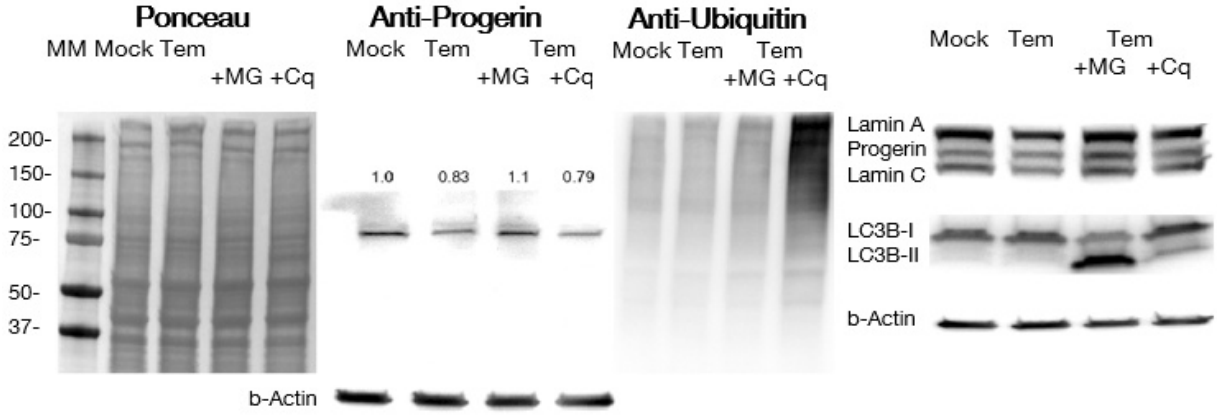

Figure 83: Western blot analyses of proteasome and autophagy proteins after Tem treatment. (A) Representative Western blots of HGPS lysates of mock-treated cells or cells treated with Tem, Tem with chloroquine (Cq) or Tem with MG132. Samples on the left panel were probed with antibodies specific to progerin and ubiquitin (n=3). Right panel corresponds to antibody staining against lamin A/C, LC3B-I and LC3B-II, and b-actin (n=3). Quantification of progerin levels in mock-treated or Tem-treated HGPS cells normalized to b-actin are presented as the fold-change relative to mock-treated cells in the anti-progerin Western blot.

In response to MG132, HGPS fibroblasts showed an accumulation of ubiquitinated proteins. Chloroquine treatment induced a significant increase in LC3B-II levels indicating the accumulation of autophagosomes when autophagy is inhibited. Autophagy remained active in temsirolimus-treated cells as LC3B-II levels were barely detectable. Progerin levels were significantly reduced by 17 % in temsirolimus-treated HGPS fibroblasts and by 21 % in temsirolimus+MG132 treated cells. This result indicates that autophagy is further stimulated by proteasome inhibition.[178] Collectively, temsirolimus clears progerin via autophagy activation and proteasome inhibition.

4.6.2 Tem improves the nuclear shape and clears progerin via inhibition of mTOR

As HGPS nuclei exhibit nuclear envelope alterations and reduced levels of nuclear components the impact of Tem was also examined. Mock-treated and Tem-treated control and HGPS cells were examined in parallel by immunofluorescence microscopy (Fig. 84).

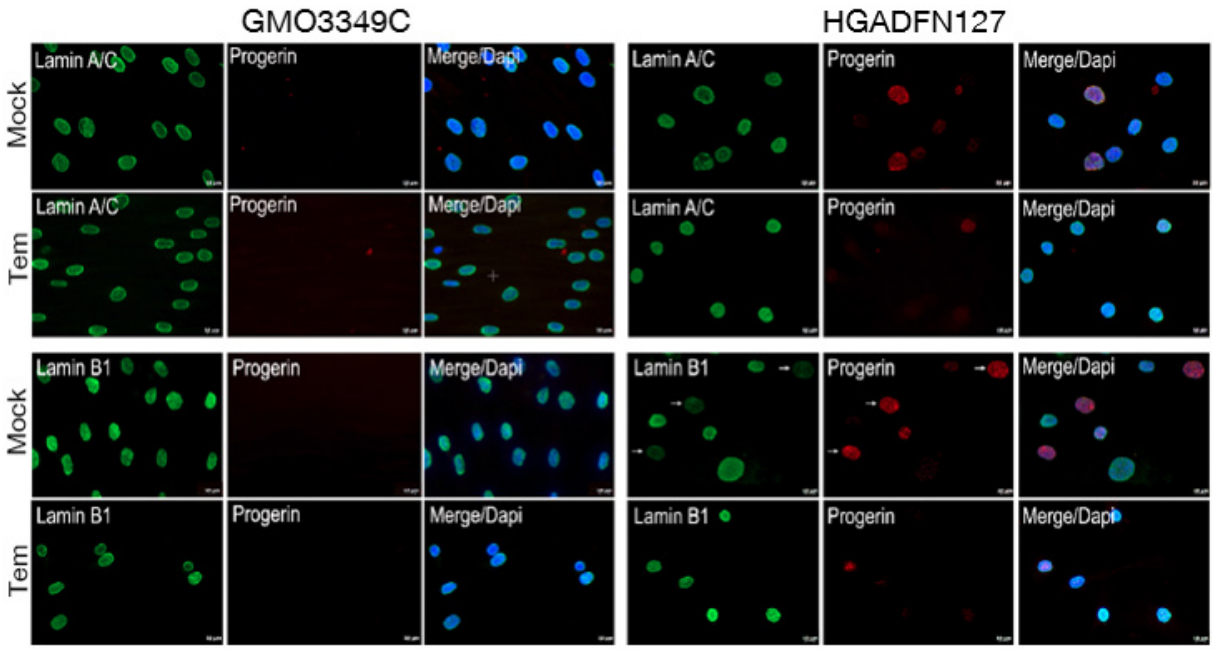

Figure 84: Staining of A-type lamins of temsirolimus-treated cells. Immunochemistry using antibodies directed against lamin A/C, progerin, and lamin B1 was performed on control (GMO3349C) and HGPS (HGADFN127) cells mock-treated or Tem-treated for 9 days (n=3). Scale bar: 10 µm.

While no progerin could be detected in control nuclei, signals of variable intensity in mock-treated HGPS nuclei cells were detected as previously reported.[181] Progerin was found to accumulate in the most dysmorphic HGPS nuclei and localized to the nuclear envelope with aggregated staining in some areas. In nuclei with low progerin levels, progerin appeared as dots or foci within the nuclear compartment. Lamin A/C was found to be present at the nuclear envelope and throughout the nucleoplasm in control nuclei and HGPS nuclei. After Tem treatment, a rim-like staining was observed in control and HGPS nuclei indicating that Tem did not generally affect the lamin A/C localization. Tem-treated HGPS nuclei show weaker signals of progerin staining and a normal-shaped envelope. The number of brightly progerin-labeled nuclei were reduced after 9 days of Tem treatment compared to mock-treated HGPS nuclei.

Lamin B1 was found to be reduced in some HGPS nuclei and was linked to the loss of proliferation and senescence.[166,182] The lamin B1 status was examined in mock-treated and Tem-treated cells by immunofluorescence. In accordance with these findings, very low to barely detectable lamin B1 staining of variable intensity in HGPS nuclei were found concomitant with brightly progerin positive cells. After Tem treatment, HGPS nuclei exhibit higher lamin B1 intensities accompanied with reduced progerin accumulation.

The percentages of dysmorphic nuclei were determined by direct counts (Fig. 85).

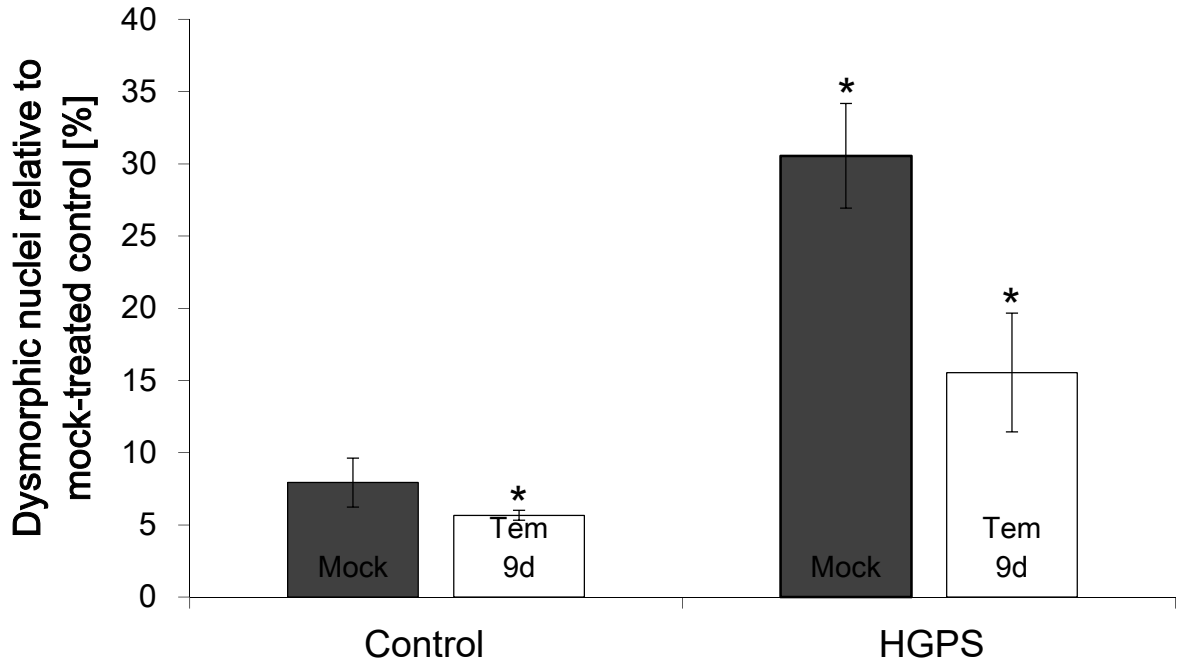

Figure 85: Dysmorphic nuclei after Tem treatment. Frequency of misshapen nuclei (dysmorphic) in 3 control and 3 HGPS fibroblast lines after 9 days of treatment with either the vehicle or 1 µM Tem. The bars indicate the mean frequency of misshapen nuclei. An average of 800 nuclei were examined for each control and HGPS cell lines and treatment. Data are presented as the mean ± S.D. relative to mock-treated control (*p ≤ 0.05; n=3).

Tem treatment significantly reduced the frequency of nuclear blebbing in control cells and HGPS cells after 9 days.

To determine whether Tem treatment inhibits the mTOR pathway, the statuses of two mTOR downstream targets (S6RP and 4EBP1) were determined by their levels of phosphorylation. Both proteins are downstream effectors of mTOR and are reduced when mTOR is inhibited (Fig. 86 A, B).[214]

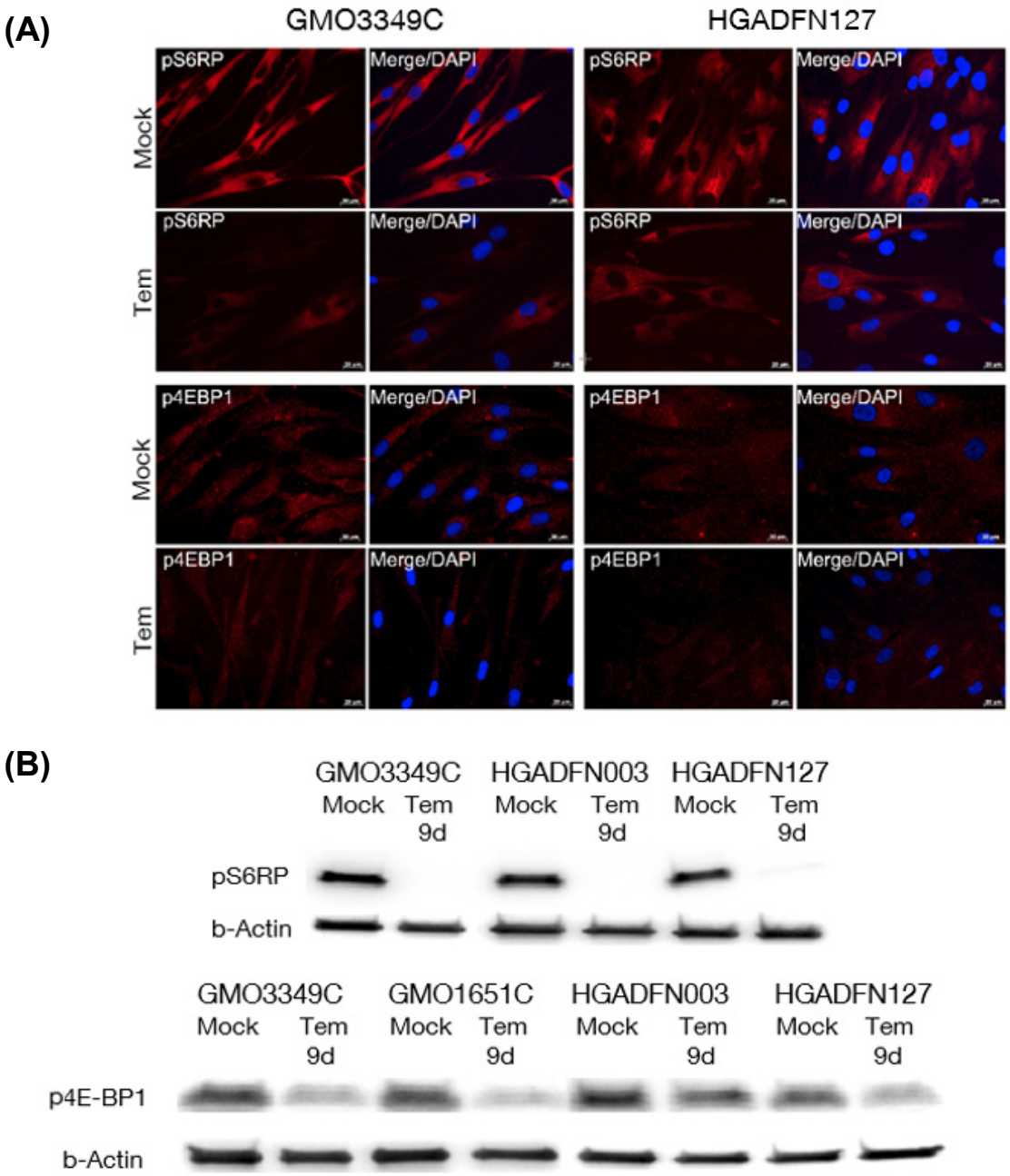

Figure 86: Inhibition of mTOR and its down-stream effectors by Tem. (A) Immunochemistry using antibodies directed against indicated proteins (pS6RP and p4EBP1) was performed on control (GMO3349C) and HGPS (HGADFN127) cells mock-treated or Tem-treated for 9 days (n=3). Scale bar: 20 µm. (B) Same cells as in (A) were used to analyze protein expression of pS6RP and 4EBP1 by Western blot (n=3).

In mock-treated cells, both proteins are adequately expressed while temsirolimus treatment induced a decrease in the signal intensities.

Collectively, temsirolimus ameliorates the nuclear morphology of HGPS nuclei by reducing progerin levels via inhibition of mTOR.

4.6.3 Tem maintains progerin clearance during long-term treatment

To test the efficiency of temsirolimus on long-term HGPS fibroblasts, cultures were treated every other day with 1 µM Tem or the vehicle. Cells were passaged and analyzed at the indicated time points.

First, the effect of temsirolimus on the proliferation rate of control cells and HGPS cells was examined (Fig. 87 A, B).

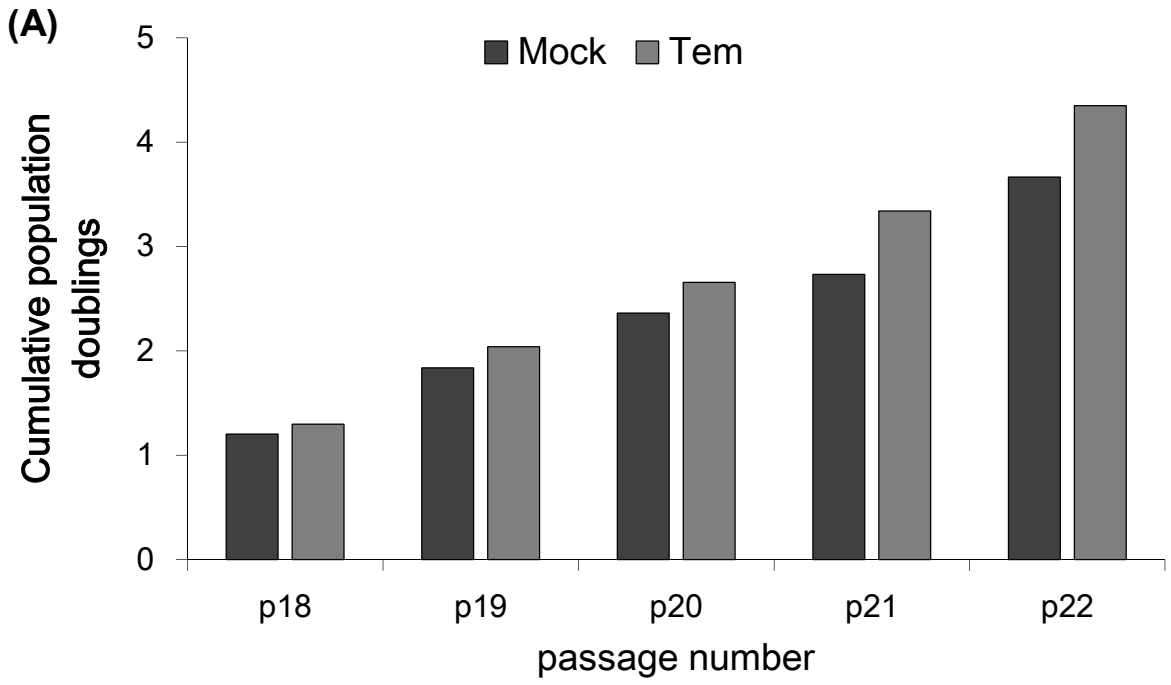

(B)

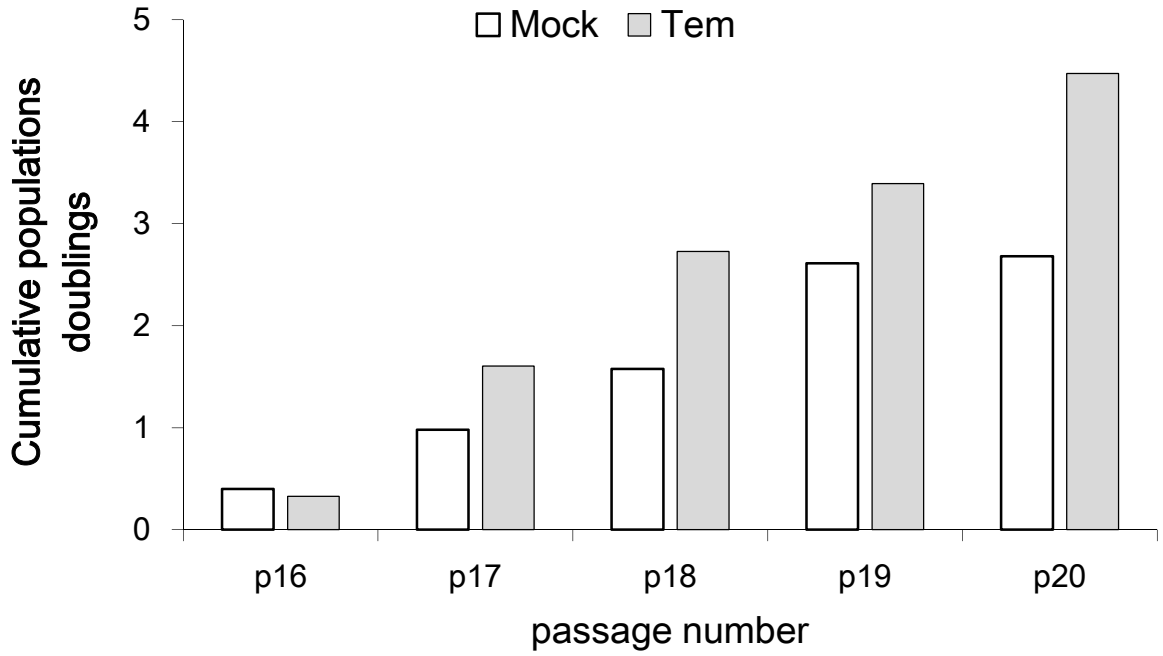

Figure 87: The proliferation rate in long-term temsirolimus cultures. (A) Long-term cultures of control and (B) HGPS cells treated with the vehicle or 1 µM Tem. Cells were fed every second day and analyzed at the indicated passages. The cumulative population doublings were calculated as described in the Methods.

While the mock-treated HGPS fibroblasts reached a growth plateau after several passages, the proliferation rates of temsirolimus-treated control and HGPS cells showed sustained growth.

During 85 days of temsirolimus treatment, Western blot analyses were performed at different time points to reveal the status of the A-type lamins (Fig. 88 A, B).

(A)

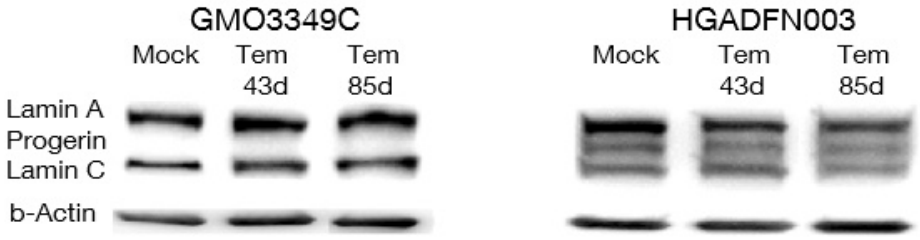

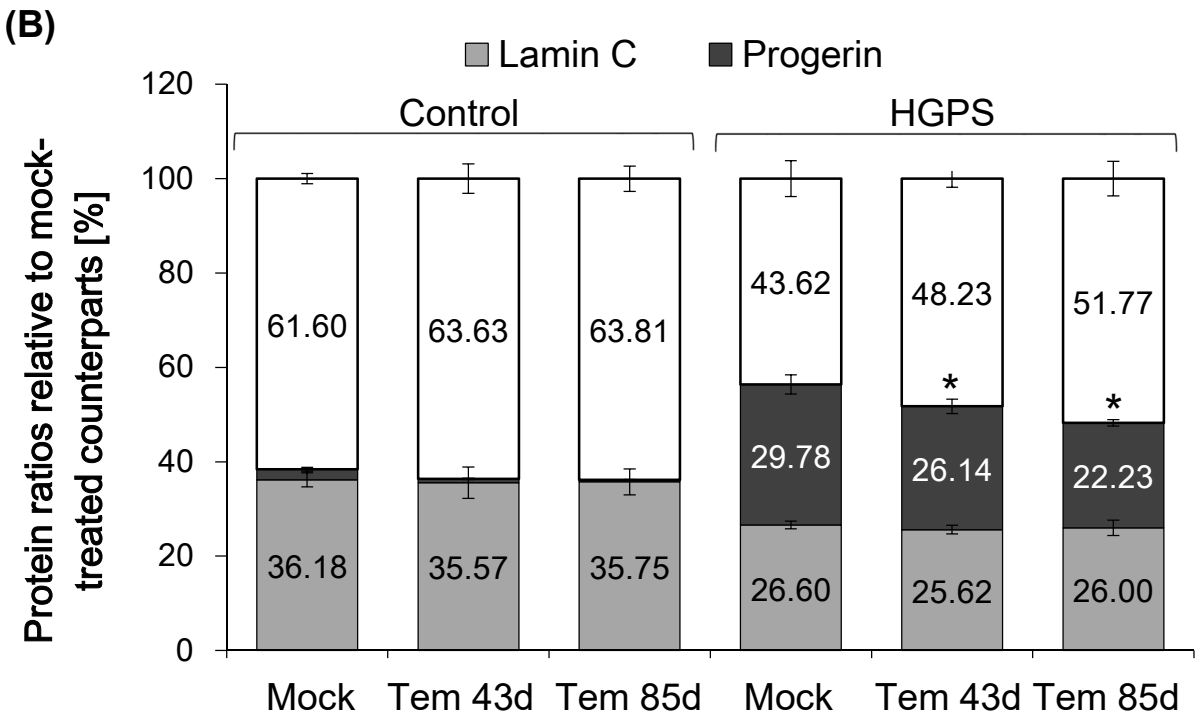

Figure 88: Western blot analyses of long-term Tem cultures. (A) Representative Western blot evaluation of A-type lamins (lamin A, progerin, Lamin C) in control and HGPS cell that were mock-treated or Tem-treated for the indicated period (n=3). Blots were probed with lamin A/C and b-actin antibodies. (B) Densitometric analyses of the ratios of A-type lamin (lamin A, progerin, and lamin C) signals obtained from lamin A/C antibody. Data represent the mean ± S.D. with respect to mock-treated counterparts (*p ≤ 0.05; n=3).

Western blot analyses showed a maintained clearance of progerin of HGPS cells treated with temsirolimus. Analysis of the A-type lamin ratios indicate a decrease in progerin levels by 25 % after 85 days of treatment. The status of the A-type lamins revealed that lamin C levels were maintained while lamin A ratios were increased. This results further supports the fact that progerin and lamin C are degraded by autophagy whereas lamin A is degraded by the proteasome system.[183] Consequently, the effect of temsirolimus on proteasome and autophagy activity during long-term treatment was investigated (Fig. 89 A, B).

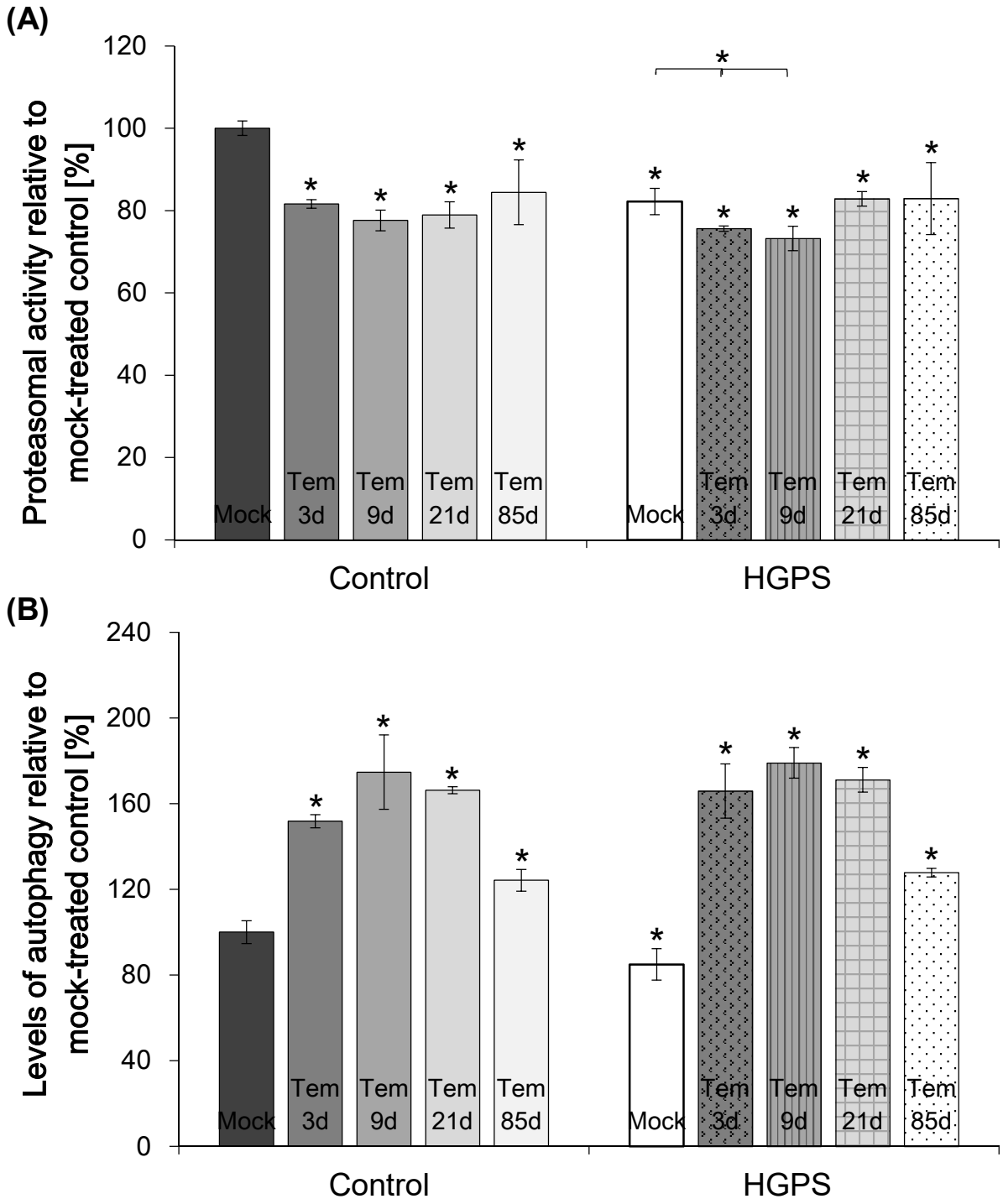

Figure 89: Protein degradation pathways analysis during long-term temsirolimus treatment. (A) Proteasome activity was determined by measuring chymotrypsin-like proteasome activity in control and HGPS fibroblasts using Suc-LLVY-AMC as a substrate. Cells were either mock-treated or treated daily with 1.0 µM Tem for the indicated periods. The percentage of activity was calculated relative to their mock-treated control. Data are expressed as the mean ± S.D. (*p ≤ 0.05; n=4). (B) Same cells as in (A) were used to measure autophagy with a monodansylcadaverine (MDC) assay. The percentage of activity was calculated relative to the mock-treated control. Data are expressed as the mean ± S.D. (*p ≤ 0.05; n=4).

Consistent with the increased lamin A levels, temsirolimus did not enhance the proteasomal activity during the 85 days of long-term treatment (Fig. 89 A). Autophagy levels remained high during long-term treatment of temsirolimus (Fig. 89 B). Profiling autophagy activity at different time points indicated that Tem induced a maximum increase at day 9, with the levels slowly decreasing by day 21 and even further by day 85. Nevertheless, autophagy was significantly higher than in mock-treated counterparts. In parallel, proteasome activity showed an increasing tendency in both normal and HGPS cells. This suggests that activation of an adaptation response mechanism occurred during long-term treatment.

4.6.4 Tem fails to improve mitochondrial dysfunction in HGPS

Mitochondrial dysfunction has been identified as a hallmark of accelerated aging.[215] This earlier study demonstrated that proteins involved in glycolysis were increased whereas proteins involved in oxidative phosphorylation were reduced in HGPS.[215] Therefore the effect of temsirolimus on mitochondrial function was investigated in control and HGPS fibroblasts. To date, this is the first study analyzing the effect of rapalogs on mitochondrial dysfunction.

It was examined whether temsirolimus could ameliorate the activity of NADPH oxidase whose function is to produce reactive oxygen species (ROS) (Fig. 90). Nox4 is 1 isoforms of the NADPH oxidases, enzymes that transport electrons across the plasma membrane and generate superoxide and ROS.[216]

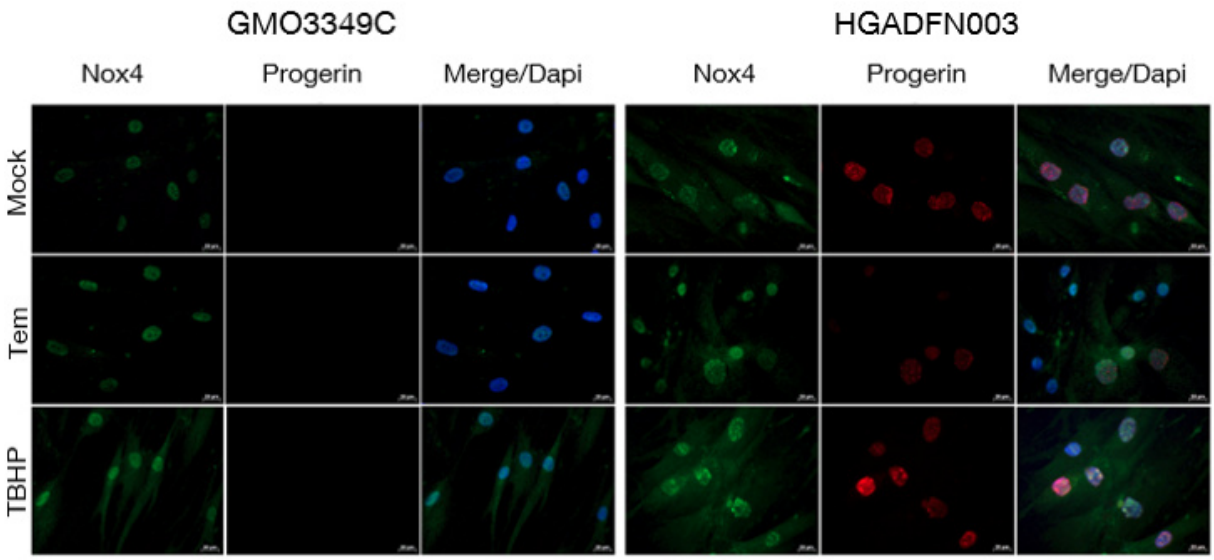

Figure 90: NADPH oxidase (Nox4) staining of temsirolimus-treated cells. Immunochemistry using antibodies directed against NADPH oxidase subunit 4 and progerin was performed on control (GMO3349C) and HGPS (HGADFN003) cells mock-treated or Tem-treated for 9 days (n=3). TBHP was used as a Nox4 inducer. Scale bar: 20 µm.

Mock-treated HGPS fibroblast exhibited increased staining of Nox4 in the nucleus and cytoplasm (Fig. 90). By contrast, mock-treated control cells showed a weak staining throughout the nucleus. Temsirolimus did not affect the levels or the distribution of Nox4 in control and HGPS cells. These data were further confirmed by Western blot analyses (Fig. 91 A, B).

(A)

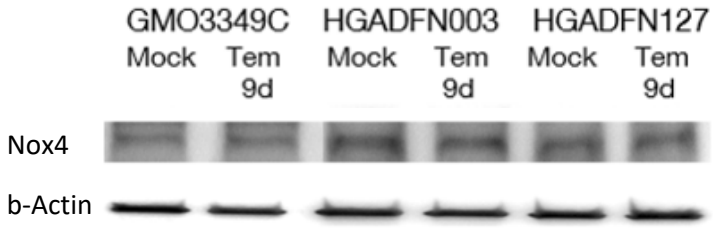

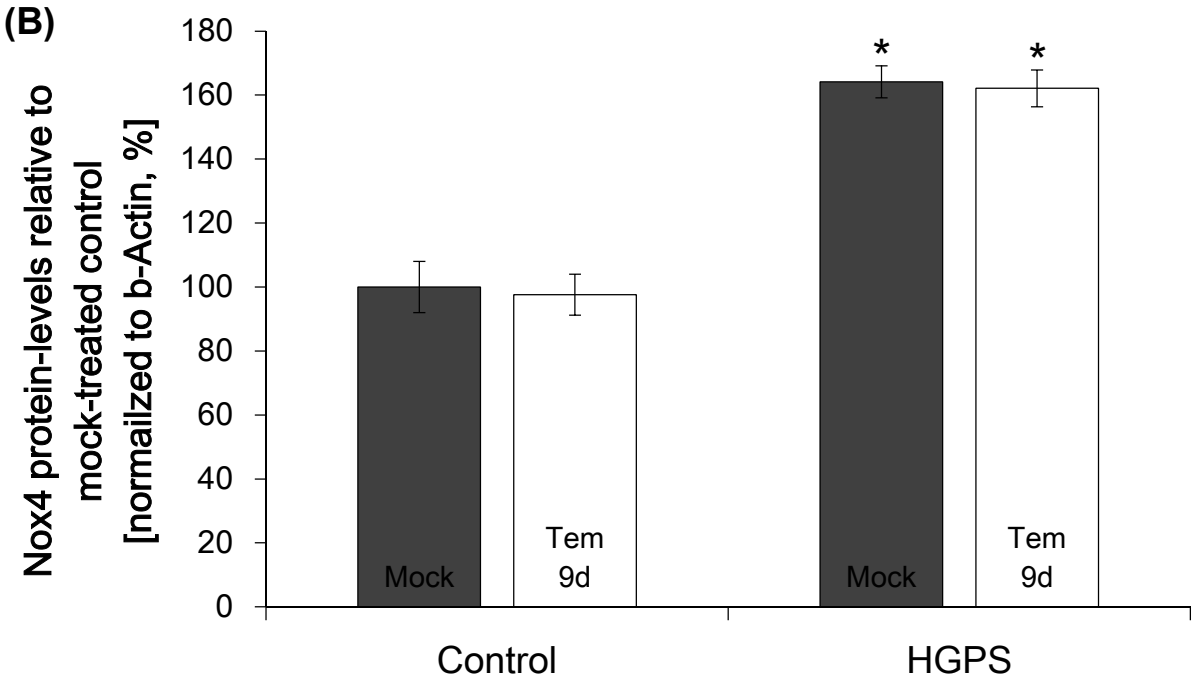

Figure 91: Western blot analyses of NADPH oxidase after Tem treatment. (A) Representative Western blot evaluation of Nox4 in control and HGPS cells that were mock-treated or Tem-treated for the indicated period (n=3). Blots were probed with Nox4, and b-actin antibodies. (B) Densitometric analysis of Nox4 signals. Data represent the mean ± S.D. with respect to mock-treated control cells after values were normalized to b-actin signal (*$p \leq 0.05$; n=3).

The finding that Nox4 was increased in HGPS cells suggested that high levels of superoxide and reactive oxygen species were produced.

Previous studies have shown reduced levels of cytochrome c oxidase subunit II (CoxII) in HGPS cells.[172,217] To further validate this finding, the levels of CoxII were determined, which is an essential component of the mitochondrial respiratory chain responsible for ATP production (Fig. 92). [218,219]

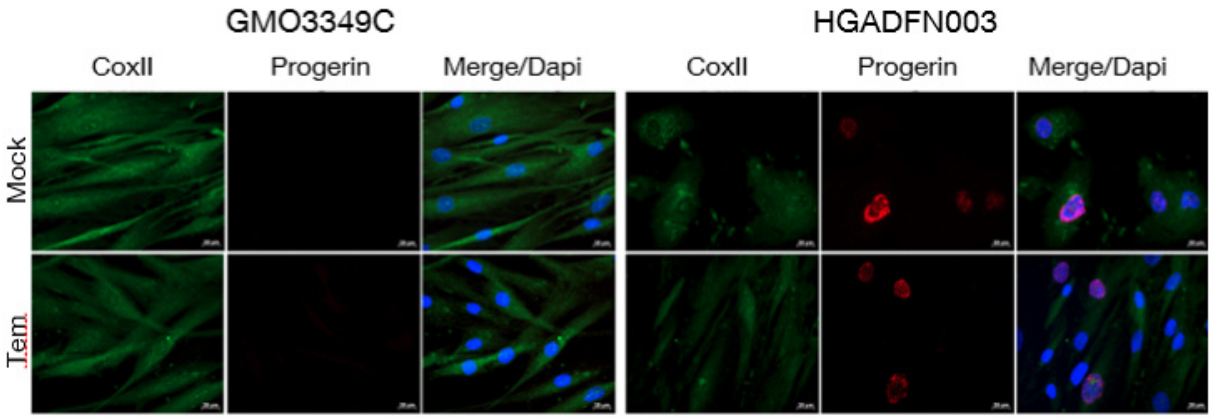

Figure 92: Cytochrome c oxidase staining of temsirolimus-treated cells. Immunochemistry using antibodies directed against cytochrome c oxidase subunit II and progerin was performed on control (GMO3349C) and HGPS (HGADFN003) cells mock-treated or Tem-treated for 9 days (n=3). Scale bar: 20 µm.

In accordance with these studies, CoxII levels were indeed reduced in HGPS cells compared with normal cells. Immunohistochemistry showed that CoxII cytoplasmic aggregates were present in bright progerin-positive HGPS cells; however, the overall CoxII signal was significantly reduced in HGPS cells relative to normal cells. In HGPS cells treated with temsirolimus, the CoxII signal remained weak. These data were further confirmed by Western blot analysis (Fig. 93 A, B).

(A)

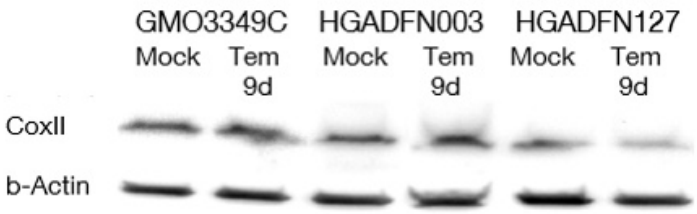

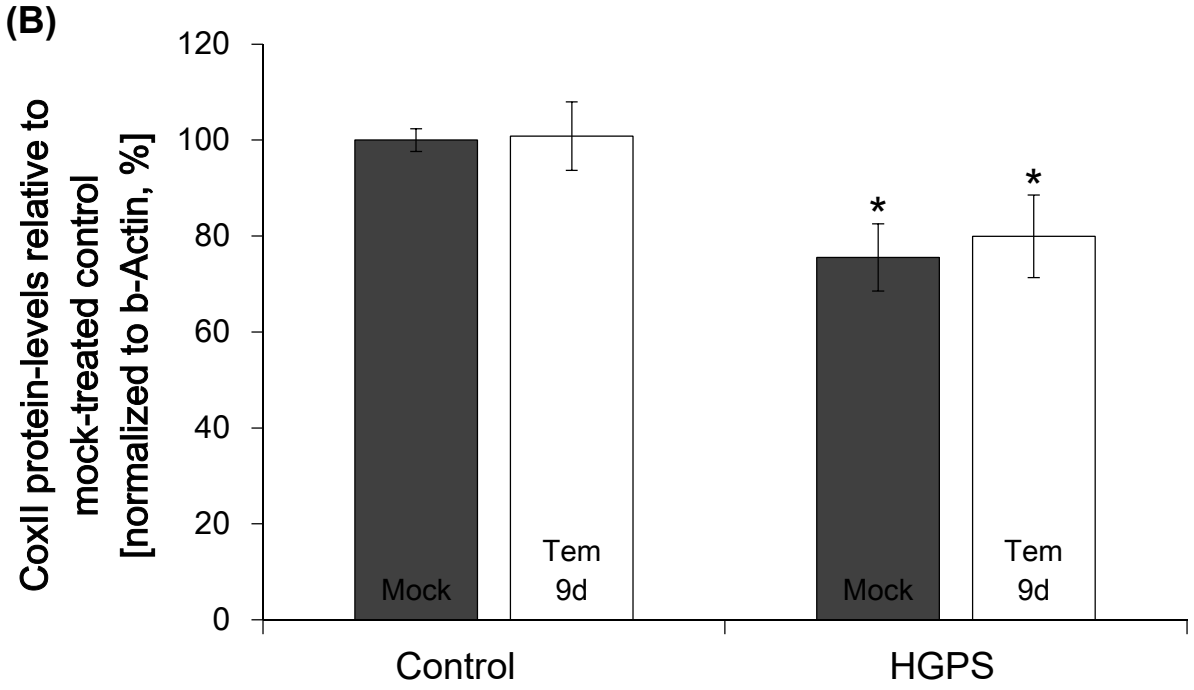

Figure 93: Western blot analyses of cytochrome c oxidase subunit II after Tem treatment. (A) Representative Western blot evaluation of CoxII in control and HGPS cells that were mock-treated or Tem-treated for the indicated period (n=3). Blots were probed with CoxII, and b-actin antibodies. (B) Densitometric analysis of CoxII signals. Data represent the mean ± S.D. with respect to mock-treated control cells after values were normalized to b-actin signal (*$p \leq 0.05$; n=3).

Collectively, these data support the conclusion that temsirolimus treatment of HGPS cells does not improve mitochondria function.

To further validate these findings, the effect of temsirolimus was evaluated by quantifying ROS and ATP levels in HGPS cells. Mock-treated HGPS fibroblasts exhibit a significant increase in basal ROS levels (16.6 %, p=0.003) compared with normal cells (Fig. 94 A).[99] Temsirolimus treatment of normal and HGPS cells resulted in no significant changes in ROS levels. The basal levels of ATP in HGPS fibroblasts were significantly reduced (19.2 %, p=0.032) compared with mock-treated normal cells (Fig. 94 B).[99] Temsirolimus treatment induced no changes in ATP levels in either normal or HGPS fibroblasts.

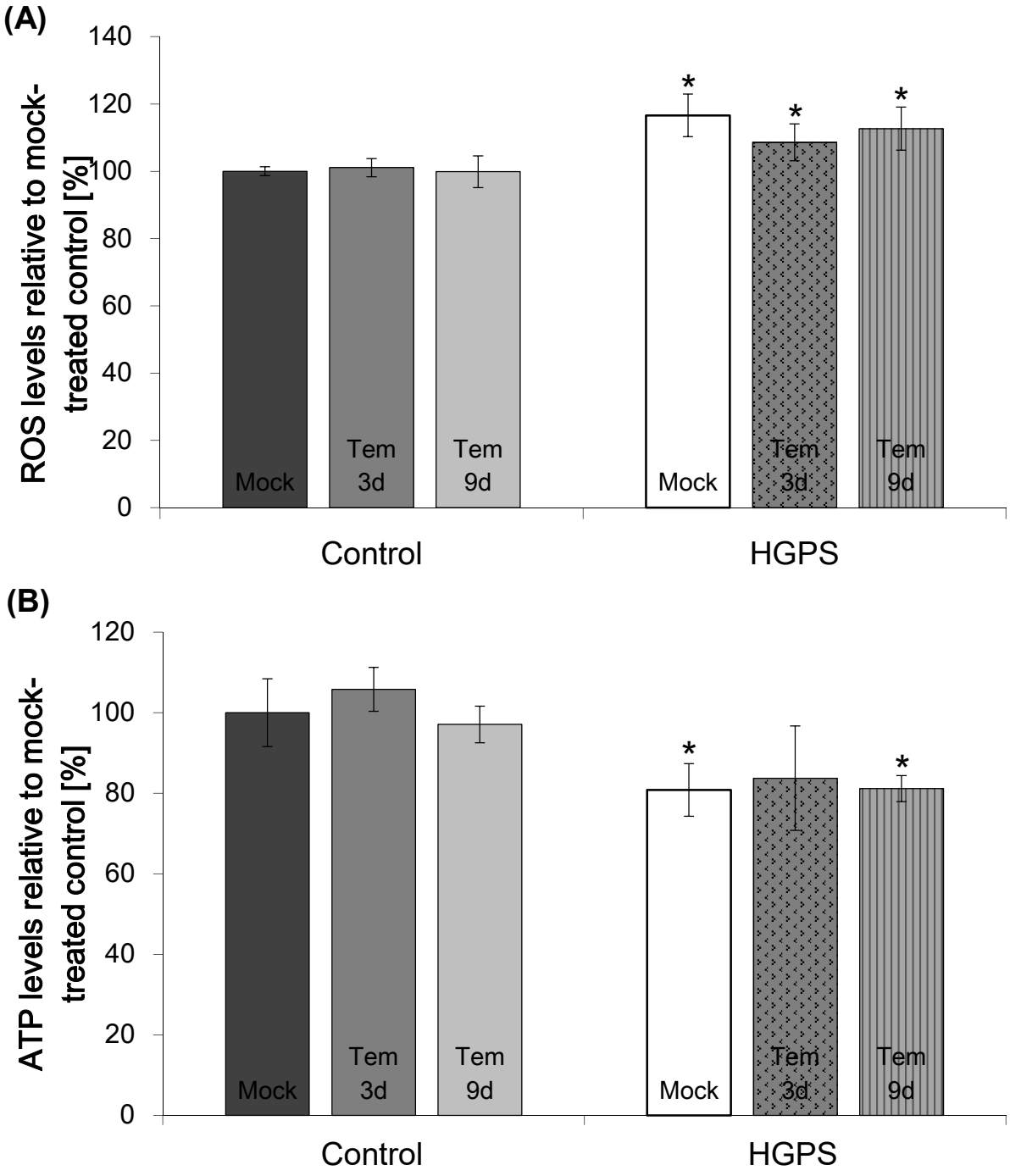

Figure 94: ROS and ATP levels of mock-treated and Tem-treated cells. (A) Intracellular ROS levels were determined by measuring oxidized dichlorofluorescin (DCF) levels as described in the Methods. Cells were treated with the vehicle or 1 µM temsirolimus for the indicated periods. Data are presented as the mean ± S.D. relative to mock-treated control (*$p \leq 0.05$; n=3). (B) Same cells as in (A) were used to measure cellular ATP levels using CellTiter Glo luminescence ATP assay as described in the Methods. Data represent the mean ± S.D. compared to mock-treated control cells (*$p \leq 0.05$; n=3).

Collectively, our findings indicate that the levels of Nox4, CoxII, and ATP were reduced in HGPS cells, whereas ROS levels were increased. In addition, none of these parameters were improved after temsirolimus treatment.

Next, oxygen consumption, which is utilized by mitochondria to produce ATP through oxidative phosphorylation, was measured in HGPS cells; glycolysis was also quantified by measuring the levels of extracellular lactate using a dual assay kit as described in Methods (Fig. 95).

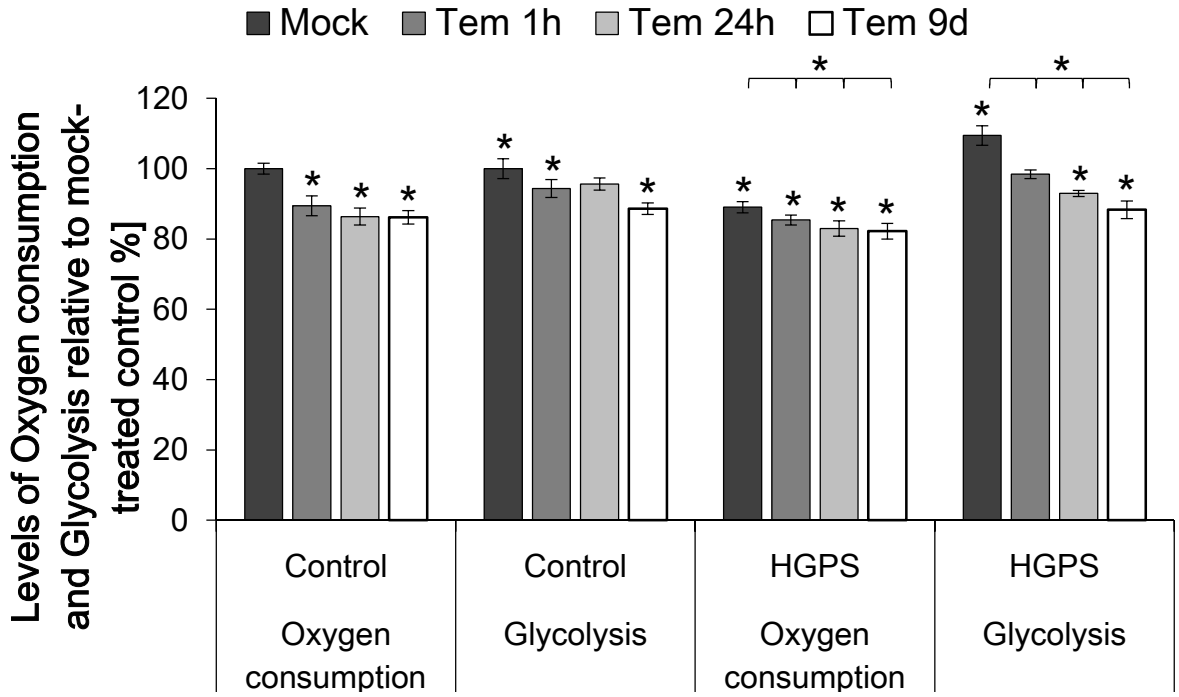

Figure 95: Oxygen consumption and glycolysis after temsirolimus treatment. Oxygen Consumption and glycolysis were measured using a MitoXpress Solution and a tetrazolium substrate, respectively. Cells were mock-treated and Tem-treated in glucose media for the indicated time periods and stained according manufacturer's instructions. Fluorescence was measured in order to detect oxygen consumption and absorbance was measured to detect glycolysis levels. Data are expressed as the mean ± S.D. relative to mock-treated control cells (*$p \leq 0.05$; n=4).

Basal oxygen consumption was reduced in HGPS cells relative to normal cells, the former showed a further reduction in oxygen consumption in the presence of temsirolimus. In addition, the basal rate of glycolysis in HGPS cells was increased relative to normal cells, as reported previously.[172] Temsirolimus treatment reduced glycolysis in both control and HGPS cells as indicated by lower levels of lactate, the end product of glycolysis.

To further evaluate the effect of temsirolimus on mitochondrial functions, cells were grown in either glucose or galactose medium supplemented with vehicle or temsirolimus for up to 72 hours. Cells grown under galactose conditions are forced to rely on mitochondrial oxidative phosphorylation for ATP generation and consequently, are more sensitive to mitochondrial perturbation than cells grown in glucose media.[220,221]

To verify that temsirolimus does not induce mitochondrial toxicity, the impact on membrane integrity was determined in cells grown in glucose or galactose medium supplemented with either the vehicle or temsirolimus for 2 hours or 3 days (Fig. 96).

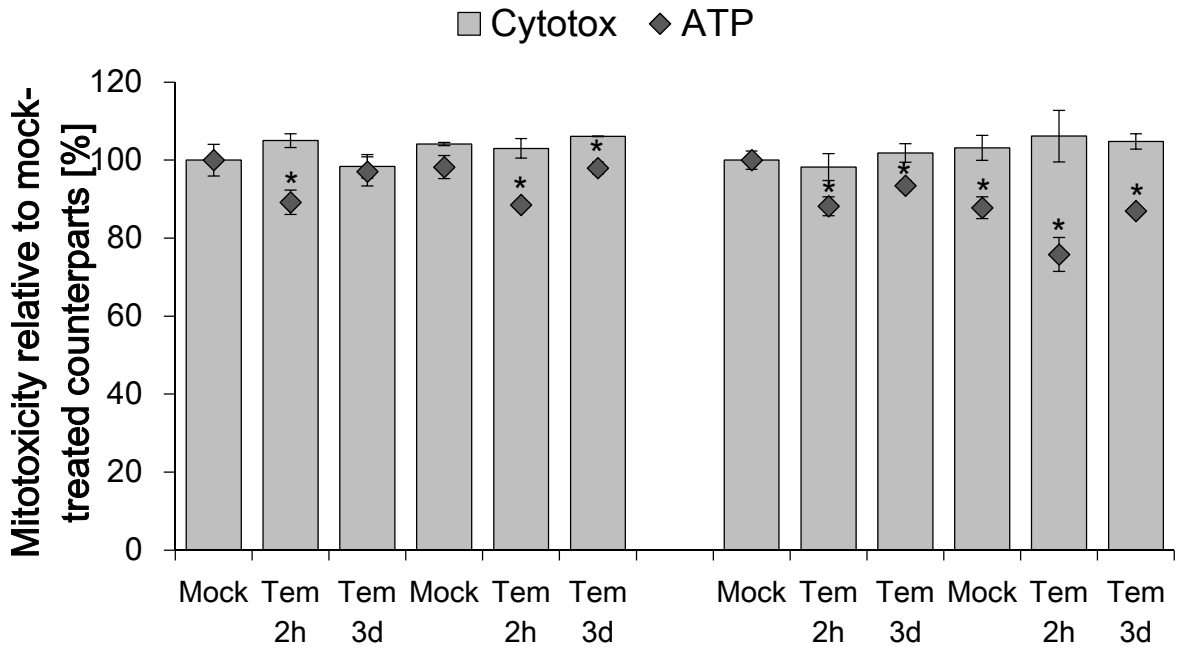

Figure 96: Mitochondrial toxicity after temsirolimus treatment. Cells were cultured in either glucose or galactose medium and treated with the vehicle (DMSO) or temsirolimus for 4 hours. Cytotoxicity and ATP levels were measured as stated in the Methods for mitotoxicity measurement. Data are presented as the mean ± S.D. relative to mock-treated counterparts (*$p \leq 0.05$, n=3).

Temsirolimus treatment induced no change in membrane integrity in either control or HGPS cells. Both cell lines remained viable. The membrane integrity assay allowed the simultaneous measurement of ATP levels in the same samples. This served as an indicator of mitotoxicity. Compared to mock-treated counterparts, ATP levels in both control and HGPS cells were significantly reduced after 2 hours of temsirolimus treatment in glucose medium. After 3 days of treatment, the ATP levels returned to basal levels in both control and HGPS cells. When the measurements were performed

on cells grown in the presence of galactose, the ATP levels were even more reduced in HGPS cells treated with temsirolimus for 2 hours and remained low after 3 days of treatment. These results indicate that temsirolimus exerts some mitochondrial toxicity in HGPS cells within the first hours of treatment. This effect was not observed during longer period of treatment, suggesting cellular adaptation to the presence of temsirolimus.

Cells with mitochondrial deficiency grow slower than normal cells because they are unable to adapt to galactose media.[172]

In this study, the normal cells were able to adapt to galactose media and showed sustained growth after temsirolimus treatment. By contrast, temsirolimus treated-HGPS cells showed reduced growth rates after 24 hours in the presence of galactose media and then increased to the mock-treated levels after 48 hours (Fig. 97).

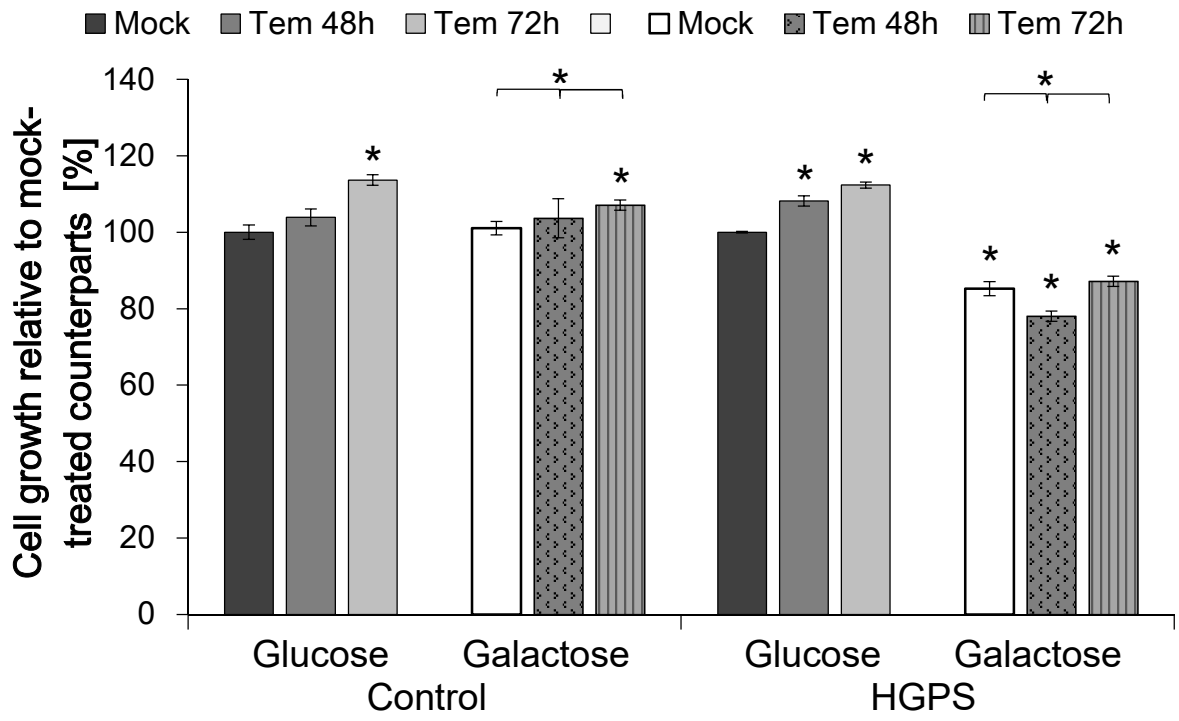

Figure 97: Cell growth of mock-treated and Tem-treated cells in galactose medium. Cells were cultured in either glucose or galactose medium supplemented with either the vehicle (DMSO) or 1 µM temsirolimus for the indicated time. Data represent the mean ± S.D. compared to mock-treated counterparts in glucose (*p ≤ 0.05; n=3).

Control cells grown in galactose medium for a period of 3 days showed no difference in ROS (Fig. 98 A) or ATP levels (Fig. 98 B). HGPS cells grown in galactose medium for 3 days showed increased ROS levels and reduced ATP levels. In the presence of glucose and galactose, temsirolimus treatment induced no changes of ROS and ATP levels in control and HGPS fibroblasts.

(A)

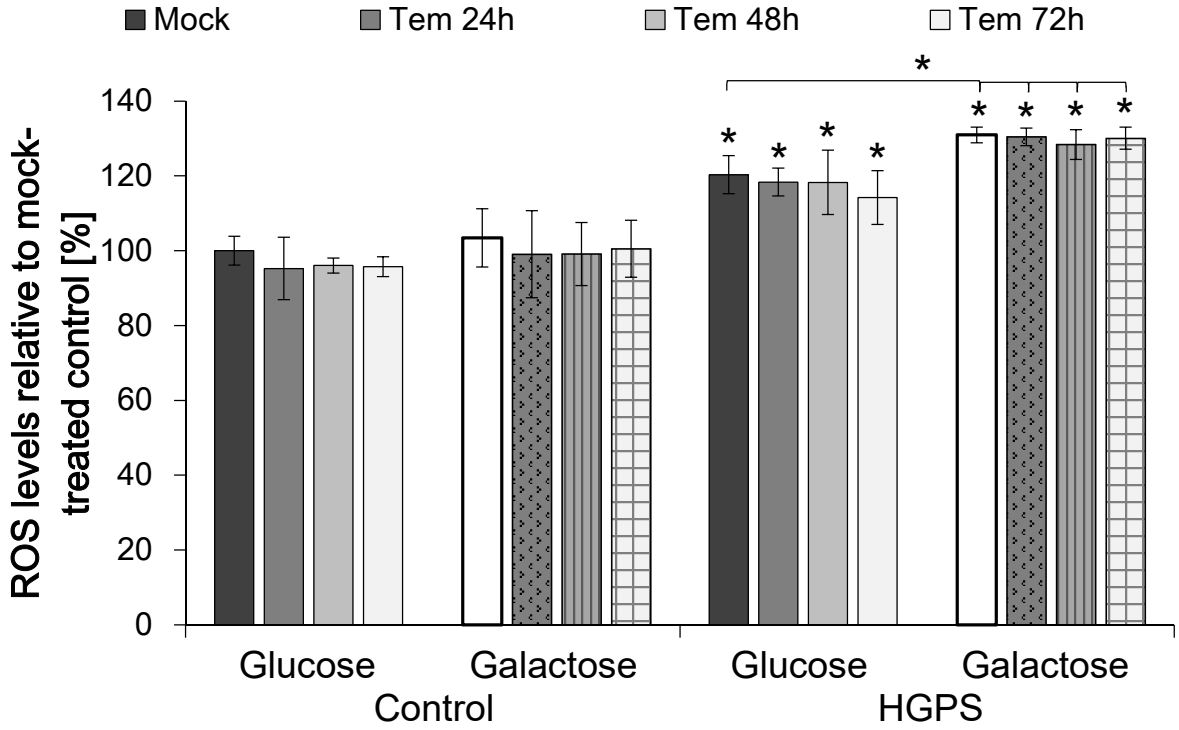

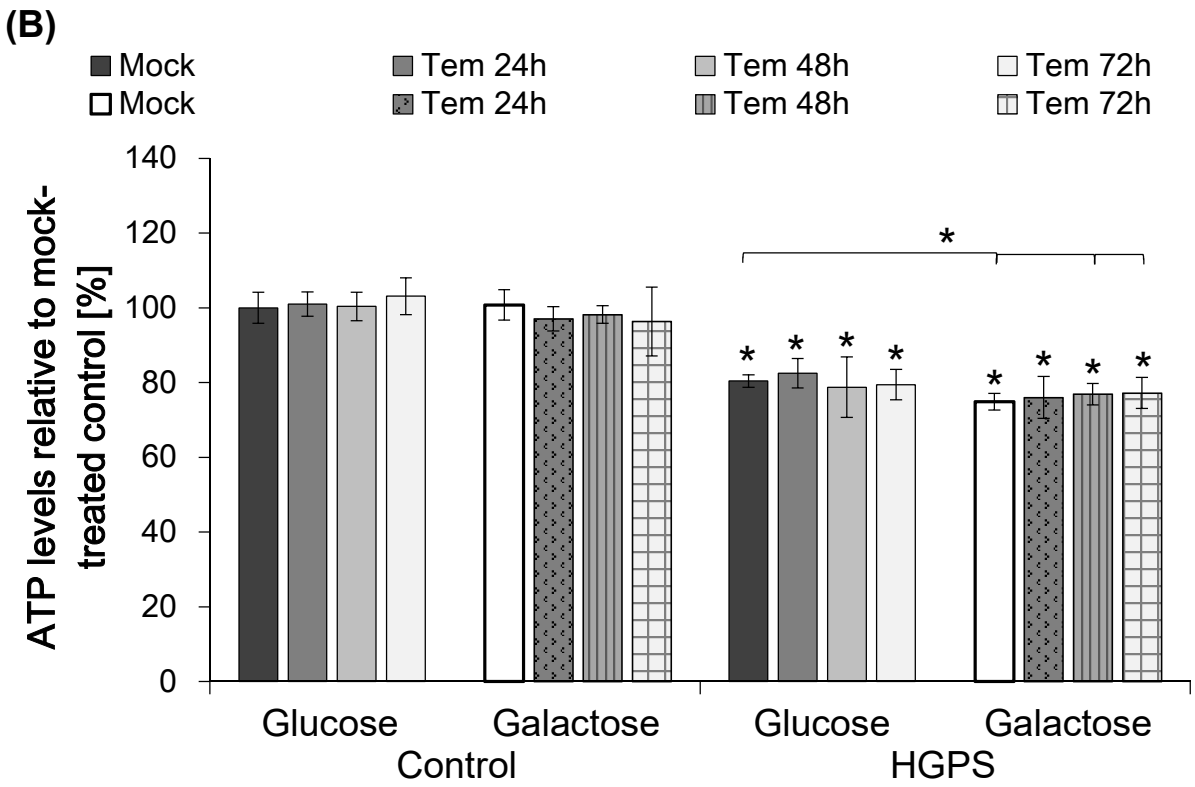

Figure 98: ROS and ATP levels of mock-treated and Tem-treated cells in galactose medium. Cells were cultured in either glucose or galactose medium and treated with either the vehicle (DMSO) or 1 µM temsirolimus for the indicated time. (A) Intracellular ROS levels and (B) cellular ATP levels were measured as described in the Methods. Data represent the mean ± S.D. compared to mock-treated control cells in glucose (*$p \leq 0.05$; n=3).

Together, the different parameters by which mitochondrial oxidative phosphorylation was assessed in HGPS cells indicate functional alterations that are not rescued by treatment with temsirolimus.

4.6.5 Reactive oxygen species and superoxide are not suppressed after Tem treatment

To support the findings that temsirolimus did not improve the levels of the endogenous source of cellular ROS (Nox4), ROS and superoxide levels were determined by performing immunohistochemistry (Fig. 99).

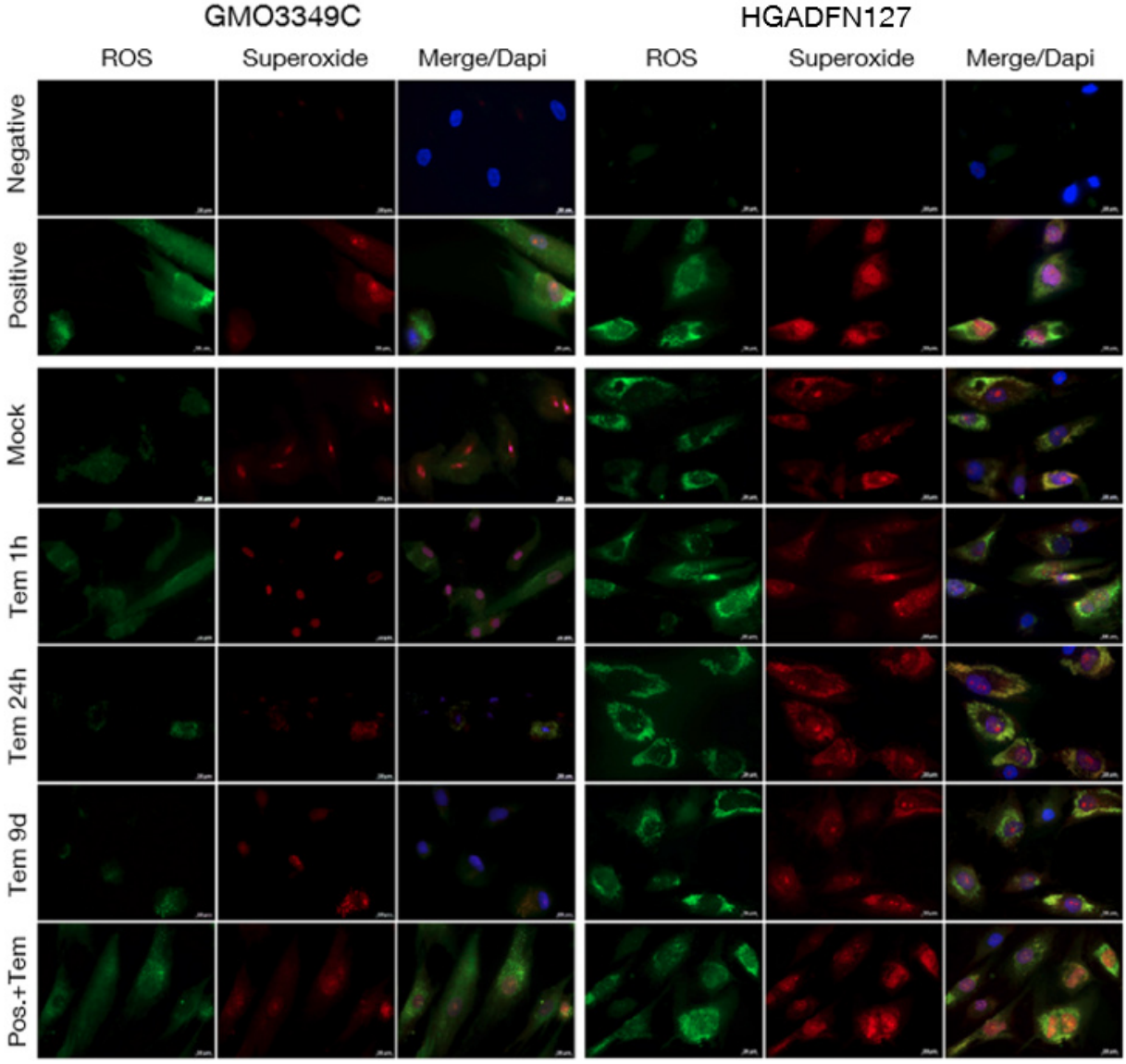

Figure 99: Immunofluorescence of ROS and superoxide after Tem treatment. Immunochemistry was performed of control (GMO3349) and HGPS (HGADFN003) fibroblasts mock-treated and temsirolimus-treated for the indicated periods. Live cells were stained with an oxidative stress detection reagent (ROS) and a superoxide detection reagent. A negative control was treated with N-acetyl-L-cysteine to quench the signal intensity. The positive control was treated with pyocyanin to induce ROS production. Last panel shows cells treated with pyocyanin and temsirolimus (Pos.+Tem). DNA was stained using the fluorescence dye Hoechst33342. Representative images are shown (n=4). Scale-bar: 20 µm.

Strong signals of ROS and superoxide were detected in HGPS cells compared with mock-treated control cells. Control cells exhibited weak staining for ROS in the cytoplasm and for superoxide in the nucleus. HGPS cells were brightly labeled and exhibited clusters of ROS signal close to the outer nuclear membrane as well as clusters of superoxide throughout the cell. These distributions of ROS and superoxide signals remained similar in control and HGPS fibroblasts after treatment with temsirolimus. Furthermore, control and HGPS cells were treated with pyocyanin, which directly oxidizes intracellular pools of NAD(P)H and glutathione (GSH) and produces superoxide and downstream ROS.[222] Temsirolimus treatment did not prevent ROS or superoxide accumulation in the presence of pyocyanin (Fig. 99, last panel).
Temsirolimus treatment for 1 hour induced a significant increase in ROS and superoxide in both control and HGPS fibroblasts as indicated by a 96-well plate format (Fig. 100).

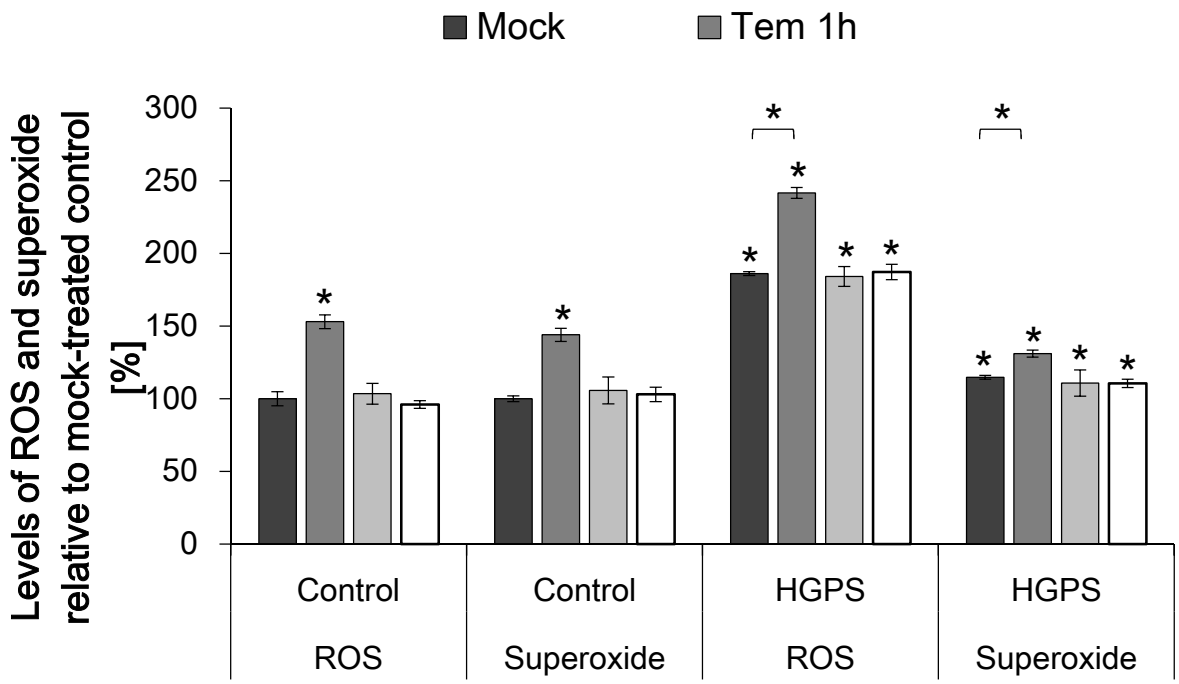

Figure 100: Analysis of reactive oxygen species and superoxide after Tem treatment. 96-well plate assay was performed of control and HGPS fibroblasts mock-treated and temsirolimus-treated for the indicated periods. The percentage of activity was calculated relative to mock-treated control cells. Data are expressed as the mean ± S.D. relative to mock-treated control (*p ≤ 0.05; n=4).

The levels of ROS and superoxide returned to those of mock-treated cells after 24 hours of temsirolimus treatment. The levels remained similar after 9 days of treatment. These results further demonstrate that temsirolimus exerts some degree of

mitochondrial toxicity within the first hours that appears to dissipate under long-term treatment. This is most likely due to cell's adaptive response mechanisms.

4.6.6 Tem does not alter DNA damage levels and heterochromatin loss

Reactive oxygen species (ROS) and oxidizing agents are known to induce DNA damage (Fig. 101 A-D).[223] Consistent with the increased levels of ROS in HGPS cells, the numbers of nuclei exhibiting DNA damage foci (γH2A.X foci) were significantly higher in HGPS (47 %) compared with normal fibroblast cultures (6 %) (Fig. 101). Temsirolimus treatment induced a reduced number in γH2A.X positive HGPS nuclei (36.1 %) signifying a reduction in DNA damage.

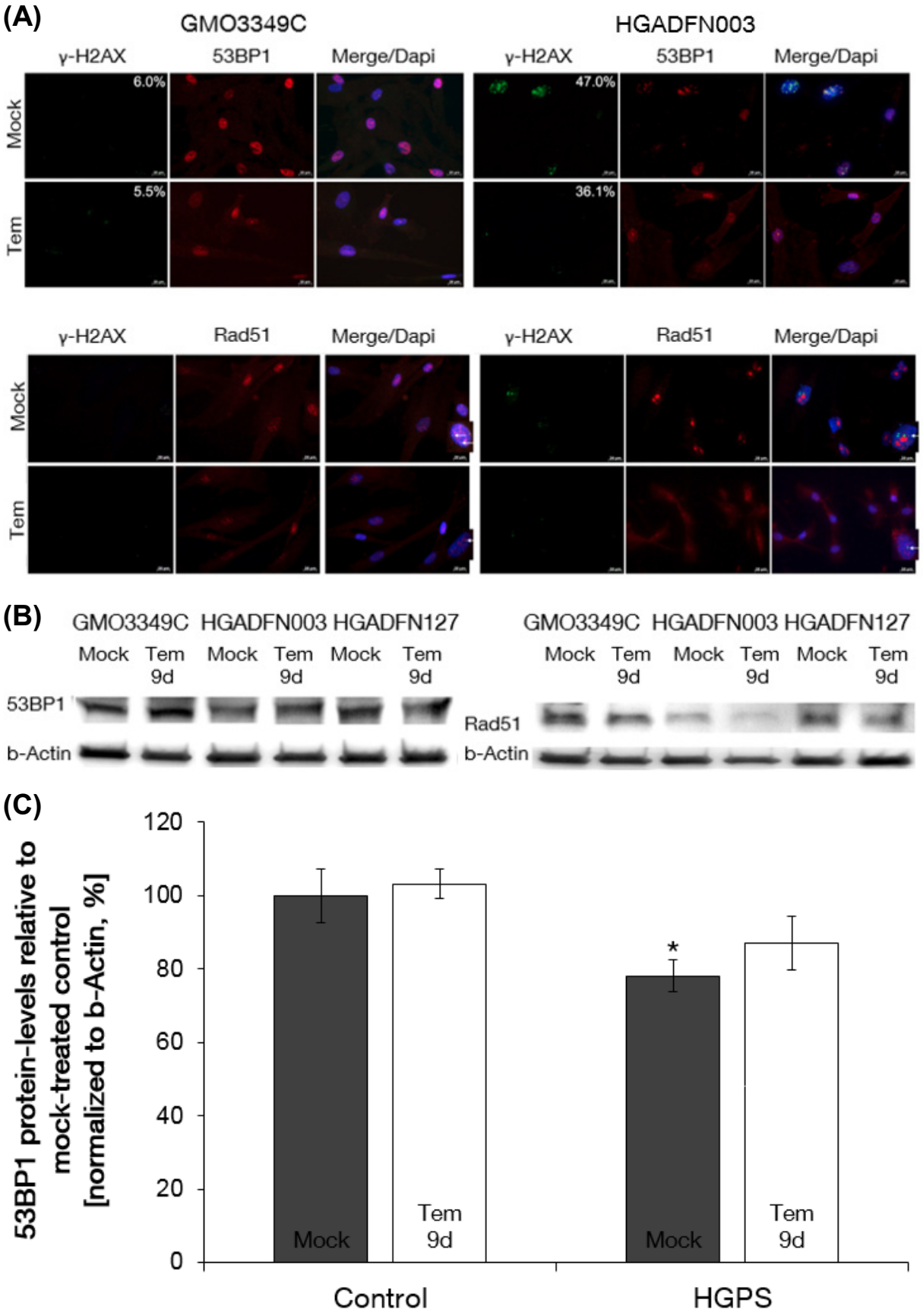
(A)
GMO3349C
HGADFN003
γ-H2AX
53BP1
Merge/Dapi
Mock
Tem
6.0%
5.5%
47.0%
36.1%
γ-H2AX
Rad51
Merge/Dapi
(B)
GMO3349C HGADFN003 HGADFN127
Mock Tem 9d Mock Tem 9d Mock Tem 9d
53BP1
b-Actin
GMO3349C HGADFN003 HGADFN127
Mock Tem 9d Mock Tem 9d Mock Tem 9d
Rad51
b-Actin
(C)
53BP1 protein-levels relative to mock-treated control [normalized to b-Actin, %]
120
100
80
60
40
20
0
*
Mock
Tem 9d
Mock
Tem 9d
Control
HGPS

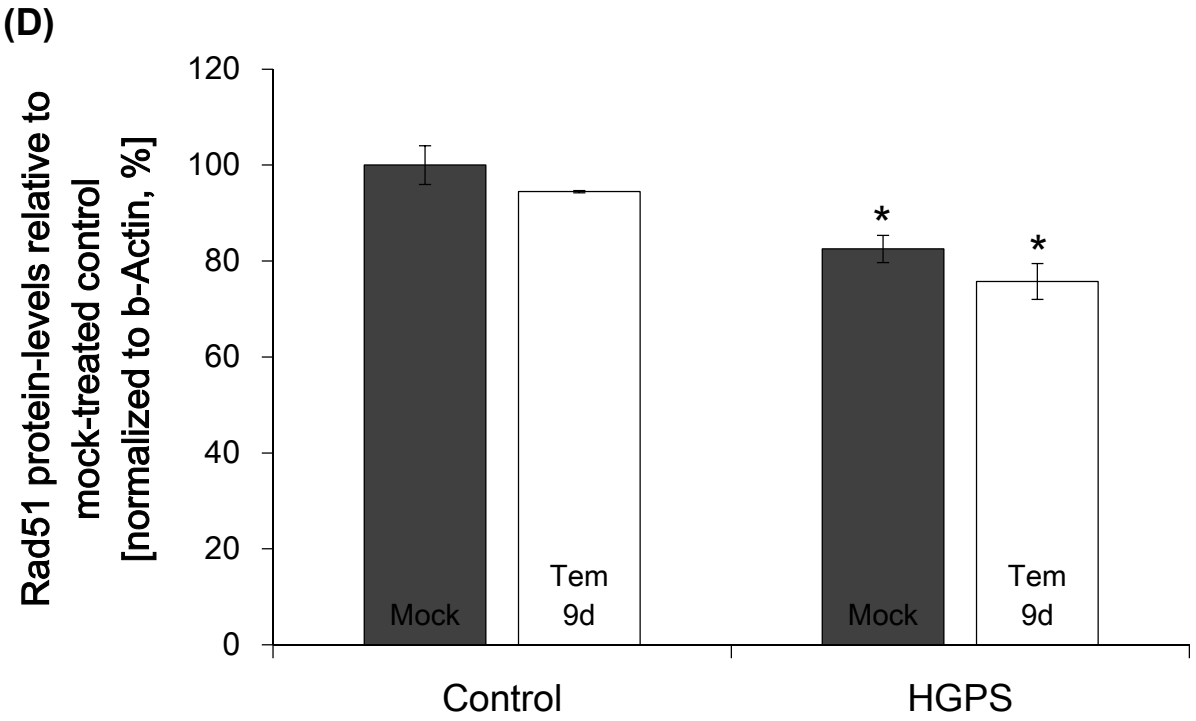

Figure 101: Effects of temsirolimus on DNA damage. (A) Immunohistochemistry of control (GMO3349C) and HGPS (HGADFN003) cells either mock-treated or treated with 1 µM temsirolimus for a period of 9 days. Antibodies against γH2A.X, 53BP1, and Rad 51 were used (n=4). Higher magnification pictures on the right side were added and white arrows indicate localization of γH2A.X and Rad51. Scale bar: 20 µm. (B) Western blot analysis of control (GMO3349C) and HGPS cells (HGADFN003, HGADFN127) treated with 1 µM temsirolimus for 9 days were used. Antibodies against 53BP1, Rad 51, and b-actin were used. Representative image is shown (n=4). (C) Quantification of 53BP1 levels normalized to b-actin and presented as the mean ± S.D. relative to mock-treated control cells (*p ≤ 0.05; n=4). (D) Quantification of Rad51 levels normalized to b-actin and presented as the mean ± S.D. relative to mock-treated control cells (*p ≤ 0.05; n=4).

Repartitioning of two DNA damage repair factors, 53BP1 and Rad 51, were also assessed (Fig. 101).[224,225] While 53BP1 is distributed throughout the nucleoplasm in mock-and temsirolimus-treated control fibroblasts, mock-treated HGPS fibroblasts exhibit accumulated foci of 53BP1 (Fig. 101 A, upper panel). These foci were found to be co-localized with γH2A.X in mock-treated and temsirolimus-treated fibroblasts. Temsirolimus reduced 53BP1 foci in HGPS cells although the protein levels of 53BP1 were increased in both control and HGPS cells (Fig. 101, C). These findings indicate that in the presence of temsirolimus DNA damage repair by 53BP1 is activated.

Co-staining of γH2A.X with Rad51 showed no co-localization of these markers in mock-treated HGPS cells in contrast to mock-treated and temsirolimus-treated control cells (Fig. 101 B, D). While Rad 51 was distributed throughout the nucleoplasm in control cells, mock-treated HGPS fibroblasts exhibit massive aggregated staining of Rad51

(Fig. 101 A, lower panel). Temsirolimus treatment changed the distribution of Rad51 in HGPS to a control-like pattern. However, γH2A.X/Rad51 foci were still not observed in treated HGPS fibroblasts; and protein levels of Rad51 were not changed in both normal and HGPS cells after temsirolimus treatment. This indicates that temsirolimus does not activate DNA damage repair via Rad51.

Altogether, our results indicate that temsirolimus slightly lowers DNA damage in HGPS cells by the activating DNA damage repair via 53BP1.

HGPS nuclei exhibit nuclear morphological changes, including an abnormal shape and the loss of heterochromatin. Such alterations were investigated in cells treated with temsirolimus. The numbers of dysmorphic nuclei in temsirolimus-treated HGPS cells was significantly reduced after 9 days (Fig. 102).

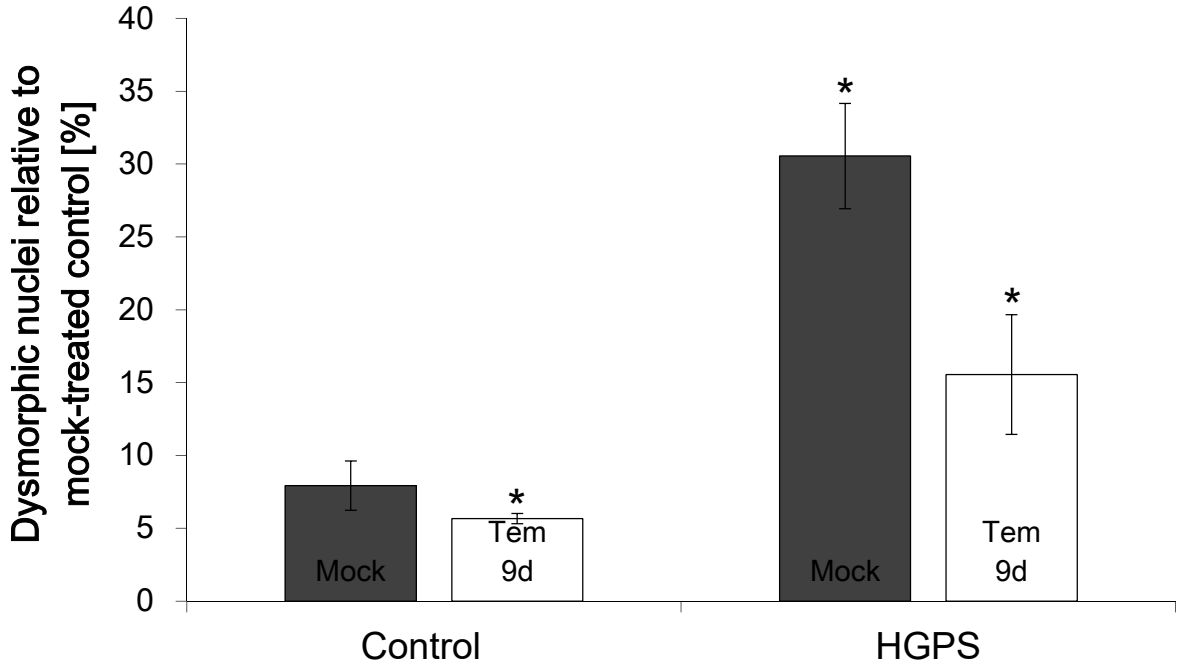

Figure 102: Number of dysmorphic nuclei after temsirolimus treatment. Frequency of misshapen nuclei (dysmorphic) after 9 days of treatment with either the vehicle or 1 µM temsirolimus. An average of 900 nuclei were examined for each condition. Data are presented as the mean ± S.D. relative to mock-treated control (*p ≤ 0.05; n=3).

The levels of heterochromatin protein 1 (HP1) were reduced in HGPS cells as shown by immunofluorescence (Fig. 103). Brightly positive progerin staining in mock-treated HGPS nuclei were found to be accompanied with lower intensities of HP1-γ. Temsirolimus treatment improved the levels of HP1-γ reaching levels similar to those of control cells.

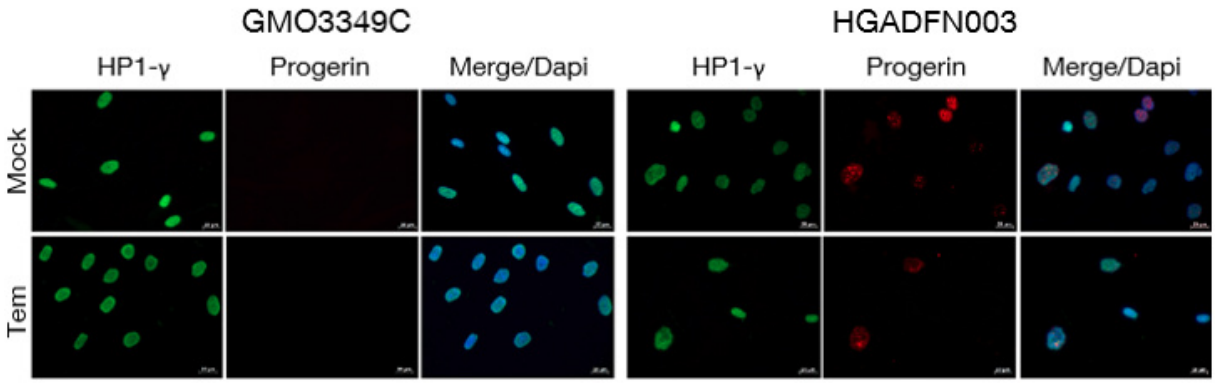

Figure 103: Level of heterochromatin protein after temsirolimus treatment. Immunochemistry using antibodies directed against HP1-γ and progerin as indicated. Control (GMO3349C) and HGPS (HGPSFN003) fibroblasts mock-treated or treated with 1 µM temsirolimus for a period of 9 days were used (n=3). Scale bar: 20 µm.

The preliminary data was further confirmed by Western blot analysis of HP1-γ (Fig. 104 A, B).

(A)

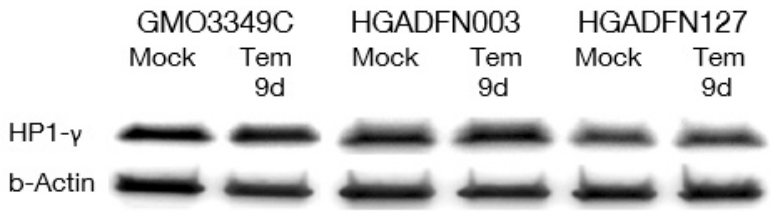

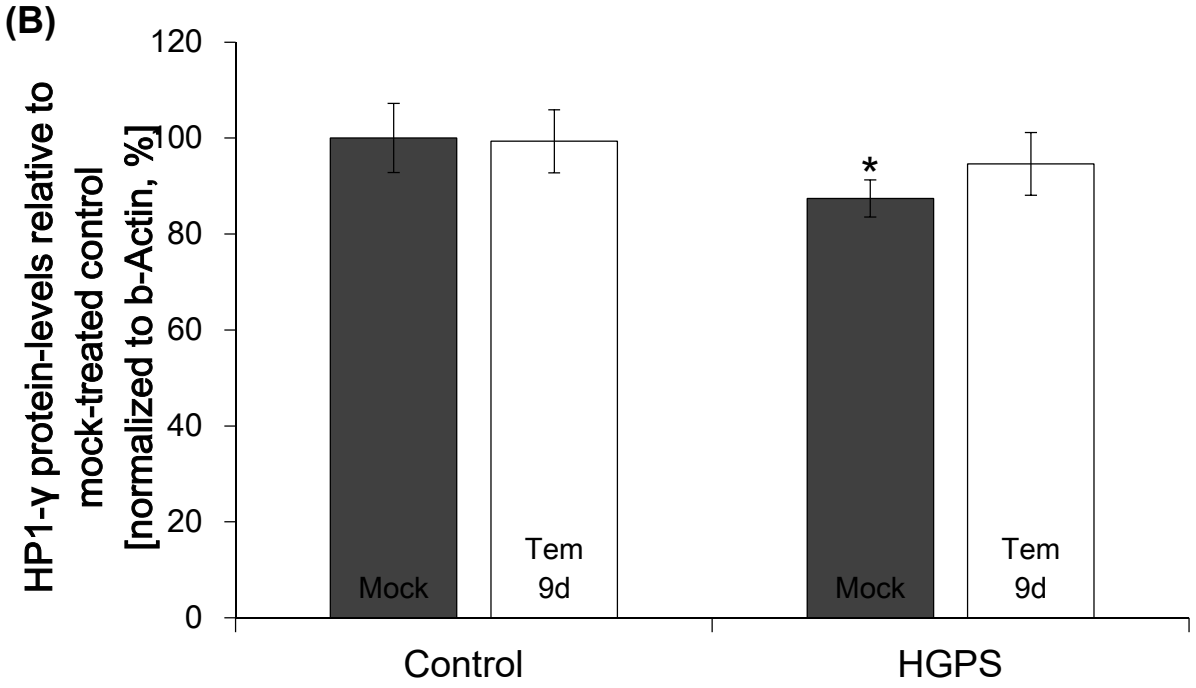

Figure 104: Western blot of heterochromatin protein after temsirolimus treatment. (A) Western blot evaluation of HP1-γ in control and HGPS cells mock-treated or temsirolimus treated for 9 days. (B) Quantification of HP1-γ levels normalized to b-actin and presented as the mean ± S.D. relative to mock-treated control cells (*p ≤ 0.05; n=3).

Those results indicate that temsirolimus ameliorates nuclear morphology and slightly lowers DNA damage in HGPS cells.

5 Discussion

5.1 Protein degradation systems are altered in HGPS

HGPS cells exhibit alterations in the composition of the nucleome due to the accumulation of farnesylated progerin in HGPS nuclei. Alterations are characterized by multiple nuclear defects, which include an abnormal nuclear envelope (blebs, invagination, nuclear pore clustering), altered chromatin organization, altered histone modification patterns, increased DNA damage, and changes in gene expression.[226] Progerin accumulates in HGPS, which may be caused by defective protein degradation pathways.

This study attempts to reveal significant changes in HGPS nuclei protein composition relative to control nuclei using 2D-gelelectrophoreses. Insights from the difference of the HGPS nucleosome might result from the accumulation of progerin. Compared to control nuclei, the expression of progerin in HGPS is up-regulated by up to 20-fold, thus making this lamin A variant the biomarker of HGPS. However, trace amounts of progerin were also detected in control nuclei. Previous studies have shown that the HGPS cryptic splice site is used sporadic in cells of unaffected individuals and that progerin is detected by immunofluorescence in elderly individuals.[41,88] Thus, normal cells might also accumulate progerin over time and manifest similar alterations to those observed in HGPS cells.

Changes of proteins involved in the proteolytic system were observed in the HGPS nucleosome, thus suggesting that HGPS cells lose proteostasis. The heat shock proteins (Hsp27, Hsp70, and Hsp90) were included in these changes. They are linked to the protein degradation via the proteasomal or autophagy pathway. The activity of the heat shock proteins declines with aging and contributes to several age-related diseases such as Alzheimer's disease, Parkinson's disease, and vascular diseases.[227] Several studies have shown a decline in proteasome activity and autophagy not only during physiological aging but also in HGPS fibroblast cells.[101,148,227,228] This suggests that HGPS cells lose their capacity to degrade proteins and thus lose proteostasis. Similar to these studies, a decrease in the proteasome 26S sub-unit C2 and a reduction in the proteasomal activity was observed in HGPS cells compared to control cells.[148] Differential expression patterns of members of the BAG family in HGPS cells were also detected. BAG proteins are co-chaperones and are implicated in protein quality control, regulation of proteasome and autophagy pathways, and aging.[100,229] Furthermore, a

decrease in autophagy levels was also observed in HGPS cells. Previously, autophagy levels were reported to decrease in HGPS cells and appear to exacerbate the cellular phenotype in late cultures.[90]

Collectively, the findings of this study indicated that alterations in proteasomal and autophagy pathways occurred in HGPS cells. Protein expression profiles of proteins involved in proteolysis such as Hsp27, Hsp70, Hsp90, BAG1, BAG2, and BAG3 were found altered. This overall reduction leads to a decrease in the proteasomal activity and autophagy levels. Consequently, these functional defects could explain the accumulation of progerin in HGPS nuclear compartment.

Strategies aimed at reducing progerin levels in HGPS cells using molecular approaches or drug treatments targeting the protein degradation pathways are currently investigated. Previously, the interaction between lamin A and AIMP3 (aminoacyl-tRNA synthetase-interacting multifunctional protein) was shown to promote lamin A degradation via proteasomes, whereas progerin, prelamin A, and lamin C undergo degradation by autophagy because the latter 3 are missing the AIMP3 interaction side.[183] Based upon this current thesis, further evidence of progerin being degraded via autophagy in HGPS cells is provided.

5.2 SFN improves the cellular phenotype of HGPS

Sulforaphane, an isothiocyanate, is derived from cruciferous vegetables such as broccoli or cauliflower. The cellular protection by SFN functions through activating the Nrf2/ARE transcription factor pathway and its direct antioxidant effects.[161,230,231] Recently, data indicate that SFN enhances the proteasome activity by up-regulating the expression of the 26S proteasome sub-unit, PSMB5, and Hsp proteins.[16,17,232]

In this study, SFN treatment of HGPS cells increased the expression of proteasome components as well as Hsps and co-chaperones, thereby increasing proteasome activity and autophagy. Activation of the protein degradation pathways lead to reduced progerin levels, thereby ameliorating the nuclear envelope normalization, proliferation, and proteostasis. The progerin reduction was sustained with SFN and even improved over time. The main protein degradation pathway of which SFN degrades progerin was found to be the autophagy pathway. By using MG132 (proteasome inhibitor) and chloroquine (autophagy inhibitor) in combination with SFN, progerin was shown to be more reduced in MG132+SFN-treated HGPS cells. Collectively, these studies support

the notion that therapies aimed at increasing autophagy could ameliorate the HGPS cellular phenotype.[30,213,233]

Other functional defects of HGPS are also restored after SFN treatment. Mitochondrial dysfunction of HGPS fibroblasts have recently been accompanied with higher reactive oxygen species (ROS) levels, lower ATP levels, and the accumulation of DNA damage.[172] Progerin has been thought to affect the rate of DSB repair.[167] FTI does not reduce DNA damage in HGPS fibroblasts, although it restores certain phenotypic effects of the disease.[6] In the present study, SFN not only reduced the levels of reactive oxygen species but also activated DNA damage repair factors (53BP1 and Rad51), normalized their distribution within the nucleus and induced the co-localization with DNA damage. Furthermore, ATP levels were found to be increased.

In sum, nucleome analysis identified differentially represented proteins that were interconnected and functionally associated with protein degradation pathways, autophagy and proteasome, an important regulator of cellular proteostasis. This indicates that HGPS cells show defects in proteostasis similar to other diseases that accumulate proteins.[227] To restore this defect, the activation of the Nrf2-Keap signaling pathway by SFN has been identified to induce cellular protective mechanisms including proteostasis and mitochondria function.[230] SFN has been identified to restore the defective degradation activity in HGPS and thus clearing progerin, reducing DNA damage and mitochondrial dysfunction.[161,230,231] This approach has proven very efficient in addressing the proteostasis loss of HGPS. The strategy has not only brought knowledge about the mechanism leading to progerin accumulation but also highlighted a direction to counteract it.

5.3 A combination of SFN and FTI further ameliorates the HGPS cellular phenotype

Farnesyltransferase inhibitors belong to a family of anti-cancer agents that add a 15-carbon farnesyl lipid to a diverse group of protein substrates.[173,234] The rationale for FTI treatment of HGPS was to block the farnesylation of the progerin protein, thereby preventing its incorporation into the nuclear envelope.[173] FTI treatment of HGPS fibroblasts led to nuclear shape ameliorations and FTI-treated mice exhibit improved body weight, increased adipose tissue, and prolonged life span.[9] Clinical trials with HGPS children have revealed less stiff arteries, increased body weight, and improved bone mineral density after two years of treatment. However, the effect of FTI treatment during long-term clinical administration are not known and further evidence suggests that FTI has negative side effects *in vitro*. Along with the disruption of the lamin B network, FTIs increase the accumulation of prelamin A, display an inconsistent blocking of non-farnesylated HDJ-2 and do not improve DNA damage by reducing ROS.[6,170] By contrast, the small compound sulforaphane (SFN) has been identified as an antioxidant and an enhancer of the Keap1/Nrf2 pathway.[161] SFN reduced levels of reactive oxygen species, DNA damage, nuclear shape abnormalities, and cleared progerin. The cellular phenotype of HGPS fibroblasts was restored after treatment with SFN.[99]

A phase I clinical trial with rapamycin analog everolimus in combination with FTI was initiated in April 2016. However, the efficacy and potential side effects of the combination *in vitro* are unknown. In this study, the effect of such a treatment regimen was investigated *in vitro* by using FTI in combination with SFN. While FTI inhibits the farnesylation of progerin, SFN activates the Nrf2-Keap1 signaling pathway inducing autophagy and mitochondrial function. Given that cells went into cell cycle arrest when both drugs were administered at the same time, a novel treatment regimen had to be identified. FTI already showed a sufficient prelamin A accumulation at a concentration as low as 0.06 µM but still induced cell proliferation and autophagy. Studies have recently demonstrated that the effect of FTI on the nuclear shape lasts 3 days before it is washed away.[169] SFN showed the most beneficial effects for HGPS at a concentration of 1 µM. Therefore, the idea was to treat the cells for 1 day with FTI followed by 3 days of SFN treatment.

During the experiments, the negative effects of FTI such as prelamin A accumulation, lamin B1 disruption, and donut-shaped nuclei were further aggravated, even when applied at low concentrations. Reactive oxygen species and DNA damage levels were not significantly improved in HGPS fibroblasts. In accordance with a recent study, a significant increase in cellular ATP levels was detected in HGPS fibroblasts but not in control fibroblasts.[172] By comparison, previous SFN findings on HGPS fibroblasts were further confirmed during these experiments. SFN induced progerin clearance and thereby enhanced the proteostasis of HGPS. The mitochondrial dysfunction of HGPS was improved, as indicated by lower reactive oxygen species, increased ATP levels, and reduced DNA damage levels.

With the cycle treatment, the same positive effects were observed as with SFN single treatment of control and HGPS fibroblasts. The proliferation defect of HGPS was reversed, DNA damage levels were reduced and the mitochondrial dysfunction of HGPS was ameliorated, as indicated by lower ROS and higher ATP levels. Importantly, the combination of the two signaling pathways increased progerin clearance in HGPS. Compared to SFN single treatment, progerin clearance was 5 % higher in the cycle-treated cells. With the detachment of progerin from the nuclear envelope by FTI, progerin were more easily degraded by autophagy activation after SFN treatment.

Furthermore, the negative effects of FTI such as prelamin A accumulation and donut-shaped nuclei were significantly reduced during the cycle treatment and reached almost mock-treated levels of control and HGPS fibroblasts. The induction of cell death by FTI in control and HGPS cells were not observed during the cycle treatment. Moreover, the disruption of the lamin B network was observed in FTI-treated cells but not in the cycle-treated ones.

To date, this is the first report showing that a combination of drugs in cycles reverses 1) the negative effects of FTI, and 2) the HGPS cellular phenotype.

In sum, the cycle treatment of FTI and SFN restored the HGPS cellular phenotype. While treatment with both drugs was not synergistic, cycle treatment ameliorated proteostasis, mitochondrial dysfunction, and DNA damage of HGPS fibroblasts. By combining interventions of 2 different signaling pathways, the highest progerin clearance was observed during these studies. Hence, cycle treatment and the combination of therapeutics could display a novel option for treating HGPS children. The application scheme provided and its analysis allows rapid testing of other drug combinations.

5.4 SFN ameliorates the cellular phenotype of Lmna$^{G608G/G608G}$ mouse fibroblasts

As SFN restored the human HGPS cellular phenotype *in vitro*, the effect of SFN on mice fibroblasts harboring the G608G mutation on both alleles of the lamin A gene was tested to establish the scientific basis for further *preclinical* studies. Fibroblasts derived from wild-type and HGPS mouse model were used to test the effect on SFN *in vitro*. First, SFN was tested at a concentration of 1 µM in mouse fibroblasts as it was used in human fibroblasts. Even though 1 µM was sufficient to improve HGPS characteristics of human fibroblasts such as DNA damage, proliferation defect, and mitochondrial dysfunction, the progerin clearance of 23 % in mouse fibroblasts was insufficient to reverse the mouse HGPS cellular phenotype. Therefore, higher concentrations of SFN were tested to have a higher impact on progerin clearance and other traits of HGPS. In this study, 3 µM SFN was the highest concentration that reversed the proliferation defect, DNA damage, and mitochondrial dysfunction of HGPS. Progerin was cleared by 30 %. A higher concentration of SFN led to cell death and showed no improvements in mitochondrial dysfunction.

SFN can be applied at a 3 times higher concentration in mice than tested in human fibroblasts. Moreover, only homozygous mutation in mice displays similar HGPS hallmarks as heterozygous humans, which makes this animal model for drug testing problematic. First of all, mouse fibroblasts show weaker signals of lamin A/C, whereby one could conclude that mouse cells do not have to rely on the functions of lamin A/C as humans. By inducting a homozygous mutation in mice, progerin levels are excessively higher than in human fibroblasts. Drug treatment of mouse fibroblasts could be as effective as with human fibroblasts and reduce progerin to the same extent. However, the effect on the overall appearance in mice *in vivo* is diminishing due to the higher progerin levels. The effect of the treatment of mice *in vivo* is small and could fall into the area of “noise”.

Recent co-expression profiling has revealed that mouse and human genes share fewer similarities than expected. The greatest gene divergence was found within the PI3K, mTOR and Akt2 signaling pathway.[235] Thus, the effect of drugs acting on these signaling pathways might be different in mouse models when compared to human treatments. These alterations of gene expressions in mouse and humans have to be taken into consideration when drugs are tested in mouse models.

5.5 Forskolin reverses the HGPS cellular phenotype

Compared to SFN, forskolin exhibit a different up-stream signaling pathway for protein degradation activation and mitochondrial biogenesis. With this knowledge, the possibility of diverse effects of other signaling pathway activations on HGPS was tested.

Forskolin is a diterpenoid derived from the Indian Coleus plant.[236] It is involved in the enhancement of cellular proliferation and the inhibition of apoptosis and cancer. It was shown that the impact of forskolin on the cAMP level resulted in cellular protective mechanisms, e.g. activation of autophagy and proteasome activity.[29,176,236] The activation of autophagy and mitochondrial biogenesis is induced by enhanced levels of AMPK and Sirt1. [199,237,238]

In this study, forskolin treatment of HGPS induced an increase in proteasomal activity and autophagy. Further experiments revealed that progerin is cleared via the autophagy pathway, as previously described.[10] Nine days of forskolin treatment cleared progerin by 22 % in cells of HGPS. The antioxidant action of forskolin reduced the levels of reactive oxygen species and enhanced ATP levels in HGPS fibroblasts. By clearing progerin, forskolin restored the proliferation defect of HGPS and normalized the nuclear shape of HGPS fibroblasts. The positive effects were maintained during long-term treatment and further increased. After 85 days of forskolin treatment, autophagy and proteasome levels were still significantly enhanced, progerin was cleared by 33 % and control and HGPS cells showed sustained cell growth.

The underlying mechanism of forskolin's positive impact is believed to occur through the activation of PKA, pAMPK, and Sirt1.[28,239,240] These proteins lead to the inhibition of mTOR, thereby enhancing autophagy. At the same time, Sirt1 and pAMPK activation catalyzes the phosphorylation and deacetylation of PGC1α*,* which in turn is necessary for mitochondrial biogenesis.[26,240-242] Another Sirtuin is activated by higher Sirt1 levels, called Sirt3.[240] The activation of Sirt3 reduces reactive oxygen species and prolongs lifespan.[240]

During our studies, enhanced levels of pAMPK, Sirt1 and PGC1α were found after forskolin treatment of HGPS cells. The design of a signaling cascade allowed verification of the positive impact of forskolin on autophagy and mitochondrial biogenesis. Other pathways such as MAPK and PI3K were found to be increased in HGPS.[184] These results were confirmed by this study. The permanent activation of

MAPK and PI3K has been associated with cardiac hypertrophy and proinflammatory response.[243,244] Forskolin treatment lowered the levels of MAPK and PI3K to those of control cells.

Lamin A has been shown to interact with Sirt1 via its C-terminal domain, while prelamin A and progerin abolish the interaction with Sirt1.[245] This leads to a compromised localization of Sirt1 to the nuclear matrix. Mislocalization of Sirt1 resulted in reduced activity of its deacetylase activity of e.g. Foxo3 and PGC1α.[245] During our studies, the loss of lamin A in HGPS fibroblasts leads to reduced Sirt1 activity and less lamin A-Sirt1 interaction. Forskolin enhances the expression and binding of Sirt1 to lamin A and it was further confirmed that neither prelamin A nor progerin could serve as a binding partner for Sirt1.

The expression of PGC1α is altered when lamin A is replaced by progerin.[186] It was further confirmed that lamin A serves as a binding partner for PGC1α. Reduced lamin A expression resulted in the loss of PGC1α activity. Transfections with prelamin A and progerin validate the notion that only lamin A interacts with PGC1α correctly. Daughter cells of HGPS show that the assembly of PGC1α is already affected shortly after mitosis. This suggest that lamin A - PGC1α binding occurs during mitosis for the accurate function of mitochondria. Further experiments have to proof that the binding of lamin A and PGC1α is mandatory for mitochondrial biogenesis.

Increased levels of cAMP through forskolin have been accompanied with enhanced DNA damage repair.[246] In HGPS, DNA damage repair response by 53BP1 and Rad51 was elevated after forskolin treatment and thus DNA damage was reduced. The distribution of 53BP1 and Rad51 was normalized and co-localized with DNA damage. By clearing progerin, forskolin restored the proliferation defect of HGPS and normalized the nuclear shape of HGPS fibroblasts. Moreover, forskolin activated a cascade of downstream effectors, which reduced reactive oxygen species, enhanced ATP levels and reduced DNA damage. The positive effects of forskolin were maintained and appeared to be improved during long-term treatment.

In sum, with its antioxidant properties forskolin ameliorated all tested hallmarks of HGPS such as nuclear shape, DNA damage, mitochondrial dysfunction, and progerin accumulation. To our knowledge, this is the first report showing that forskolin reverse the HGPS cellular phenotype. Regardless, the different up-stream signaling of SFN and forskolin showed no significant difference in ameliorating the HGPS cellular phenotype, suggesting that the amelioration is independent of specific signaling

pathways. For this, drugs should target the protein degradation pathways as well as mitochondrial signaling.

5.6 Tem improves progerin accumulation but not mitochondrial dysfunction of HGPS

In this study, the rapamycin analog temsirolimus was used to test its ability to reverse some of the hallmarks of HGPS cellular phenotype.[247] Temsirolimus is a dihydroxymethyl propionic acid ester of rapamycin, which exhibits improved solubility and specifically inhibits mTOR signaling with an effectiveness comparable to that of rapamycin.[248] It has been approved by the Food and Drug Administration (FDA). The safety, tolerability, and efficacy of temsirolimus have been evaluated in phase I, II, and III clinical trials (https://clinicaltrials.gov), indicating that temsirolimus is less immune-suppressive and displays improved pharmacological characteristics compared to rapamycin.[249]

In recent years, rapamycin has emerged as a potential candidate drug for future clinical trial for children with HGPS disease.[30,90,213,233] The efficiency of the rapamycin analog temsirolimus was further investigated in terms of whether it corrects the HGPS cellular defects. This study supports previous studies indicating that the inhibition of the mTORC1 signaling pathway by rapamycin leads to autophagy activation in HGPS cells.[30,228] Additional evidence was provided that progerin is degraded via the autophagy pathway.[30,213,233,250] Temsirolimus treatment reduces the progerin nuclear build-up, and improves the HGPS cell growth rate and lifespan *in vitro*, as previously reported for rapamycin.[30] Reduction in progerin levels ameliorates the HGPS nuclear morphology as observed by the decrease in nuclear envelope abnormalities including blebs and invaginations.[250] Additionally, this study found restoration of normal levels of lamin B1 after temsirolimus treatment. All of these studies indicate that rapamycin or temsirolimus can partially rescue the aforementioned HGPS phenotypic changes. To further assess the efficacy of temsirolimus, the impact on proteostasis, mitochondrial function, and DNA damage levels was investigates in HGPS fibroblasts.

The autophagy and the ubiquitin-proteasome pathway constitute the 2 major protein degradation pathways to maintain proteostasis.[100] In this study, it was found that HGPS cells display alterations in the protein degradation system with reduced autophagy and

proteasome activity, as previously reported.[99] HGPS cells display a strong activation of autophagy after temsirolimus treatment, leading to reduced progerin levels. This stimulation occurs through the inhibitory action of temsirolimus on the mTOR pathway, as evidenced by reduced levels of the phosphorylated form of its two downstream effectors S6 ribosomal protein and E4BP1. These findings are in accordance with previous studies reporting that rapamycin inhibited mTOR pathway and stimulated autophagy in HGPS fibroblasts.[30,213,233,250] The effect of temsirolimus was similar to rapamycin and originates from mTOR inhibition. However, autophagy stimulation by temsirolimus was higher during short-term treatment, with a maximum induction observed on day 9. Long-term temsirolimus treatment resulted in higher levels of autophagy compared to the basal levels in mock-treated cells, although a declining tendency by day 21 was observed and further reduced at day 85 of treatment. This indicated that temsirolimus efficiently stimulated autophagy in both control and HGPS cells, although the amplitude of activation decreased during long-term treatment.

Proteasome activity was reduced during short-term temsirolimus treatment in both normal and HGPS cells. Rapamycin was previously shown to allosterically inhibit the activity of the 20S proteasome [251]. Rapamycin induces a conformational shift of the 20S proteasome, which results in compromised gating of substrates. Rapalogs might directly compete with canonical ligands for the same binding grooves, which manifests in weak-to-moderate inhibition of the chymotrypsin-like activity.[178] Proteasome activity in HGPS cells slightly increased during long-term temsirolimus treatment, which was concomitant with a reduction in autophagy stimulation. The inverse correlation between the activities of these two protein degradation pathways suggests that treatment with temsirolimus for a prolonged period (weeks) might lead to activation of a cellular adaptation response to prevent a further decrease in proteasome activity. Alternatively, cells might become less sensitive to the drug during long-term treatment. Further studies are needed to determine how cells maintain a balance between autophagy and proteasome activity during long-term treatment and thus evaluating the effects of intermittent treatments with rapamycin or temsirolimus on proteostasis is warranted.

Previous studies have demonstrated increased levels of reactive oxygen species (ROS) and reduced levels of ATP in HGPS cells.[148] A SILAC study provided important insights into the mitochondrial dysfunction of HGPS cells.[172] The down-regulation of several components of the mitochondrial ATPase complex and up-regulation of glycolytic enzymes have been identified as feature of progeria. Alterations of the

mitochondrial complex such as cytochrome c oxidase activity and glycolytic enzymes developed in a time- and dose-dependent manner in HGPS. Thus, energy production in HGPS appears to be switched from oxidative phosphorylation to glycolysis.[172]
Experiments revealed reduced ATP levels and increased superoxide and ROS levels in HGPS, as well as higher levels of NADPH oxidase sub-unit 4 and lower expression levels of cytochrome c oxidase sub-unit II in comparison to control cells. The oxygen consumption rate was lowered in HGPS fibroblasts, whereas the glycolytic activity was enhanced.
Temsirolimus treatment did not significantly affect mitochondrial function in HGPS cells. Levels of ROS, ATP, superoxide, NADPH oxidase sub-unit 4 and cytochrome c oxidase sub-unit II were not ameliorated. Temsirolimus worsened the status of the mitochondrial function within the first hours of treatment in control and HGPS cells, although continued treatment returned the levels of these parameters to those of the mock-treated counterparts.
By changing the energy source from glucose to galactose, cells are forced to rely on mitochondrial oxidative phosphorylation to generate energy. In these studies, HGPS cells were more sensitive to mitochondrial stress as indicated by further reduced ATP levels and enhanced ROS levels. Temsirolimus did not improve these changes but rather increased mitochondrial toxicity under galactose growth conditions. Further studies are needed to elucidate the limitations of the effect of rapamycin on mitochondrial function, as recently suggested in skeletal muscles from mice treated with rapamycin.[252]
HGPS cells accumulate DNA DSBs and progerin is thought to affect the rate of DSB repair.[167] Despite restoring certain phenotypic effects of the disease, treatment of HGPS fibroblasts with FTIs does not reduce DNA damage.[6] Rapamycin treatment was found to recover DNA damage repair in HGPS fibroblasts, as indicated by higher 53BP1 levels.[213] The expression and organization of the heterochromatin marker trimethyl-H3K9 was improved by rapamycin in HGPS fibroblasts.[213] However, other studies detected a reduced proliferation in HGPS fibroblasts after rapamycin treatment and no change of DNA damage in mice.[10,128] In this cell-based study, temsirolimus ameliorated the DNA damage repair, as indicated by reduced DNA damage foci within a cell. However, the number of cells exhibiting DNA damage was only slightly reduced after temsirolimus treatment. This limited impact of temsirolimus might be the result of its limited ability to reduce ROS levels in HGPS cells.

Recent studies have provided evidence that antioxidant compounds such as the ROS scavenger N-acetylcysteine (NAC) and sulforaphane appear to restore the mitochondrial function in HGPS, leading to reduced ROS levels.[99,253] Accordingly, DNA damage was further reduced in HGPS fibroblasts.

In summary, HGPS fibroblasts used in this research phenotypically appear as highly altered cells with extensive A-type lamins alteration accompanied by nuclear dysmorphy. The purpose of this research was to test the extent to which temsirolimus could restore HGPS cellular phenotypic changes and identify the cellular functions that remained to be improved. In accordance with previous findings for rapamycin, this study indicates that temsirolimus restores a normal morphological phenotype in HGPS fibroblasts and improves their growth potency. While temsirolimus activated autophagy and enhances progerin clearance, it seems to reduce proteasome activity in HGPS cells. Temsirolimus might only partially ameliorate HGPS proteostasis. During long-term cultures, temsirolimus treatment appears to elicit cellular adaptation response, leading to a reduction in its potency to stimulate autophagy and concomitantly inducing increased proteasome activity. These findings suggest that discontinuous temsirolimus treatment might need to be considered and further investigated. Because temsirolimus showed only partial benefits regarding DNA damage and mitochondrial function, these findings suggest that antioxidant compounds might be required to reverse these defects in HGPS cells.

Co-expression networks analysis has recently revealed that the divergence of human and mouse is caused by the most crucial genes of the PI3K signaling pathway, mTOR and Akt2.[235] While humans exhibit 809 mTOR homologs and mouse 782, only 11 genes were found to be co-expressed.[235] For this, the inhibition of mTOR by rapamycin and its analogs in mouse models could lead to false positive results. It is also questionable whether the potential benefit of rapamycin and its analogs outweigh the severe side effects and the minor positive effect on HGPS fibroblasts.

With the emerging and increasing number of candidate compounds for treatment of HGPS disease, further therapeutic avenues will require finding the appropriate drug combination and treatment regimens to target the numerous phenotypic hallmarks that characterize HGPS cells.[254]

5.7 The combination of SFN with forskolin or Tem induces cell death of HGPS fibroblasts

As the combination of SFN with FTI had such a positive outcome, the possibility of other combinations with SFN was tested. For this, SFN was combined with temsirolimus and forskolin (Appendix 8.4). Thus far, all tested combinations led to either cell death or meager progerin clearance. These treatments did not induce synergistic effects on HGPS homeostasis. Under the experimental conditions, sulforaphane, forskolin, and temsirolimus treatment alone appeared to be more efficient in correcting the phenotypic changes of HGPS. These experiments further confirm that novel drug combinations and treatment regimens have to be identified.

6 Conclusion and Outlook

This study was commissioned to examine the molecular mechanisms triggered by progerin accumulation in order to target defective signaling pathways with specific drugs.

The research draws attention to various defective signaling pathways in HGPS, including protein degradation pathways, Nrf2, AMPK, and mTOR. Identifying defective signaling pathways has improved the understanding of some molecular mechanisms underlying the HGPS cellular phenotype, providing specific targets for drug interventions. The report clearly shows that the most important target is preventing progerin accumulation by autophagy as this causes defects in the lamina composition and thereby defects in nuclear function. These findings prompt a variety of opportunities, starting with research applications that benefit from the approach of 2D-gelelectrophoresis. This allows the identification of over-accumulated and differentially expressed proteins in age-related disorders characterized by abnormal protein accumulations. Subsequently, these proteins could be linked to specific functions that identify putative defective signaling pathways, offering the opportunity to significantly simplify the development of new drug targets.

The following novel drugs activated autophagy by targeting the above-mentioned signaling pathways:

1) Nrf2 signaling by sulforaphane (SFN)
2) AMPK signaling by forskolin (Fors)
3) mTOR signaling by temsirolimus (Tem)

Each drug appears to remedy some aspects of the HGPS cellular phenotype, including loss of proteostasis, mitochondrial dysfunction, and DNA damage response. As these drugs target different signaling pathways, this study shows the extent to which modulation of each signaling can remedy the HGPS cellular phenotype. While SFN and forskolin ameliorated all tested hallmarks of HGPS, temsirolimus failed to improve the mitochondrial dysfunction of HGPS. This knowledge offers a treatment effect mechanism that should be strongly considered in any future clinical trials using these drugs. In this context, the knowledge of signaling pathways influencing the disease state is gaining importance. This study emphasizes the analysis of signaling pathways before using drugs e.g. diseases with a mitochondrial deficiency must avoid the use of rapalogs or combine them with anti-oxidants to restore mitochondrial function. Further investigations reveal a potential future therapy for HGPS involving the drug combination of SFN and FTI, which induced the highest progerin clearance in HGPS.

These results are the first to show that a combination of two signaling pathways constitutes a valuable option for treatment of HGPS. This evaluation not only offers an application sequence of the drugs but also a fast evaluation by screening autophagy levels, which allows rapid testing of further drug combinations. The new regimen reflects the importance of signaling pathway analysis given that the additive effect of two drugs could be cytotoxic.

Several age-related diseases, such as Alzheimer's disease and Parkinson's disease, share mechanistic links with HGPS in that they lose proteostasis. Consequently, patients with these diseases could benefit from increased proteostasis levels. With this study, four therapeutic options to enhance proteostasis have been identified and several biological parameters established for screening a drugs' efficacy *in vitro*. Moreover, drug combination represents a novel approach to age-related diseases showing a multimorbid cellular phenotype caused by different defective signaling pathways.

Nowadays, the trend in clinical projects is towards the use of natural compounds with low side-effect profiles. While rapalogs and farnesyltransferase inhibitors are connected to risks such as acute respiratory failure and hypertension, SFN and forskolin could be used as low-risk therapeutics with a better reversibility of the HGPS cellular phenotype. In these cases it would be beneficial to analyze whether the benefits of a drug outweigh its side effects.

This report evaluates defective signaling pathways in HGPS and concludes that enhanced proteostasis of HGPS can be achieved by activating the protein degradation pathways by Nrf2, AMPK, and mTOR signaling. All candidate drugs used in this study have the potential for the use in future clinical trials of HGPS and other age-related disorders by providing detailed treatment effects.

However, there remain questions concerning how progerin induces these functional defects. A direct link between progerin and the different functional changes in HGPS is still missing. Accordingly, future work on identifying possible progerin direct targets and the link to signaling pathways warrants further investigation.

7 References

1 Gordon, L. B., Rothman, F. G., Lopez-Otin, C. & Misteli, T. Progeria: a paradigm for translational medicine. *Cell* **156**, 400-407, doi:10.1016/j.cell.2013.12.028 (2014).

2 Eriksson, M. *et al.* Recurrent de novo point mutations in lamin A cause Hutchinson-Gilford progeria syndrome. *Nature* **423**, 293-298 (2003).

3 Sinensky, M. *et al.* The processing pathway of prelamin A. *J Cell Sci* **107 (Pt 1)**, 61-67 (1994).

4 Young, S. G., Meta, M., Yang, S. H. & Fong, L. G. Prelamin A farnesylation and progeroid syndromes. *J Biol Chem* **281**, 39741-39745 (2006).

5 Goldman, R. D. *et al.* Accumulation of mutant lamin A causes progressive changes in nuclear architecture in Hutchinson-Gilford progeria syndrome. *Proc Natl Acad Sci U S A* **101**, 8963-8968, doi:10.1073/pnas.0402943101 (2004).

6 Liu, Y., Rusinol, A., Sinensky, M., Wang, Y. & Zou, Y. DNA damage responses in progeroid syndromes arise from defective maturation of prelamin A. *J Cell Sci* **119**, 4644-4649 (2006).

7 Fong, L. G. *et al.* A protein farnesyltransferase inhibitor ameliorates disease in a mouse model of progeria. *Science* **311**, 1621-1623, doi:10.1126/science.1124875 (2006).

8 Capell, B. C. *et al.* A farnesyltransferase inhibitor prevents both the onset and late progression of cardiovascular disease in a progeria mouse model. *Proc Natl Acad Sci U S A* **105**, 15902-15907 (2008).

9 Yang, S. H., Qiao, X., Fong, L. G. & Young, S. G. Treatment with a farnesyltransferase inhibitor improves survival in mice with a Hutchinson-Gilford progeria syndrome mutation. *Biochim Biophys Acta* **1781**, 36-39 (2008).

10 Ibrahim, M. X. *et al.* Targeting isoprenylcysteine methylation ameliorates disease in a mouse model of progeria. *Science* **340**, 1330-1333, doi:10.1126/science.1238880 (2013).

11 Gordon, L. B. *et al.* Clinical trial of a farnesyltransferase inhibitor in children with Hutchinson-Gilford progeria syndrome. *Proc Natl Acad Sci U S A* **109**, 16666-16671 (2012).

12 Verstraeten, V. L. *et al.* Protein farnesylation inhibitors cause donut-shaped cell nuclei attributable to a centrosome separation defect. *Proc Natl Acad Sci U S A* **108**, 4997-5002 (2011).

13 Adam, S. A., Butin-Israeli, V., Cleland, M. M., Shimi, T. & Goldman, R. D. Disruption of lamin B1 and lamin B2 processing and localization by farnesyltransferase inhibitors. *Nucleus* **4**, 142-150, doi:10.4161/nucl.24089 (2013).

14 Liu, B. & Zhou, Z. Lamin A/C, laminopathies and premature ageing. *Histol Histopathol* **23**, 747-763 (2008).

15 Verkerk, R. *et al.* Glucosinolates in Brassica vegetables: the influence of the food supply chain on intake, bioavailability and human health. *Mol Nutr Food Res* **53 Suppl 2**, S219, doi:10.1002/mnfr.200800065 (2009).

16 Kwak, M. K., Cho, J. M., Huang, B., Shin, S. & Kensler, T. W. Role of increased expression of the proteasome in the protective effects of sulforaphane against hydrogen peroxide-mediated cytotoxicity in murine neuroblastoma cells. *Free Radic Biol Med* **43**, 809-817, doi:10.1016/j.freeradbiomed.2007.05.029 (2007).

17 Gan, N. *et al.* Sulforaphane activates heat shock response and enhances proteasome activity through up-regulation of Hsp27. *J Biol Chem* **285**, 35528-35536, doi:10.1074/jbc.M110.152686 (2010).

18 Baird, L., Swift, S., Lleres, D. & Dinkova-Kostova, A. T. Monitoring Keap1-Nrf2 interactions in single live cells. *Biotechnol Adv* **32**, 1133-1144, doi:10.1016/j.biotechadv.2014.03.004 (2014).

19 Alasbahi, R. H. & Melzig, M. F. Forskolin and derivatives as tools for studying the role of cAMP. *Die Pharmazie* **67**, 5-13 (2012).

20 White, A. T. & Schenk, S. NAD(+)/NADH and skeletal muscle mitochondrial adaptations to exercise. *American journal of physiology. Endocrinology and metabolism* **303**, E308-321, doi:10.1152/ajpendo.00054.2012 (2012).

21 Fusco, S. *et al.* A role for neuronal cAMP responsive-element binding (CREB)-1 in brain responses to calorie restriction. *Proc Natl Acad Sci U S A* **109**, 621-626, doi:10.1073/pnas.1109237109 (2012).

22 Ugland, H., Naderi, S., Brech, A., Collas, P. & Blomhoff, H. K. cAMP induces autophagy via a novel pathway involving ERK, cyclin E and Beclin 1. *Autophagy* **7**, 1199-1211, doi:10.4161/auto.7.10.16649 (2011).

23 Egawa, M. *et al.* Long-term forskolin stimulation induces AMPK activation and thereby enhances tight junction formation in human placental trophoblast BeWo cells. *Placenta* **29**, 1003-1008, doi:10.1016/j.placenta.2008.09.008 (2008).

24 Kim, J., Kundu, M., Viollet, B. & Guan, K. L. AMPK and mTOR regulate autophagy through direct phosphorylation of Ulk1. *Nat Cell Biol* **13**, 132-141, doi:10.1038/ncb2152 (2011).

25 Nemoto, S., Fergusson, M. M. & Finkel, T. SIRT1 functionally interacts with the metabolic regulator and transcriptional coactivator PGC-1{alpha}. *J Biol Chem* **280**, 16456-16460, doi:10.1074/jbc.M501485200 (2005).

26 Gurd, B. J. Deacetylation of PGC-1alpha by SIRT1: importance for skeletal muscle function and exercise-induced mitochondrial biogenesis. *Applied physiology, nutrition, and metabolism = Physiologie appliquee, nutrition et metabolisme* **36**, 589-597, doi:10.1139/h11-070 (2011).

27 Canto, C. & Auwerx, J. PGC-1alpha, SIRT1 and AMPK, an energy sensing network that controls energy expenditure. *Curr Opin Lipidol* **20**, 98-105, doi:10.1097/MOL.0b013e328328d0a4 (2009).

28 Canto, C. *et al.* AMPK regulates energy expenditure by modulating NAD+ metabolism and SIRT1 activity. *Nature* **458**, 1056-1060, doi:10.1038/nature07813 (2009).

29 Zhang, F. *et al.* Proteasome function is regulated by cyclic AMP-dependent protein kinase through phosphorylation of Rpt6. *J Biol Chem* **282**, 22460-22471, doi:10.1074/jbc.M702439200 (2007).

30 Cao, K. *et al.* Rapamycin reverses cellular phenotypes and enhances mutant protein clearance in Hutchinson-Gilford progeria syndrome cells. *Sci Transl Med* **3**, 89ra58, doi:10.1126/scitranslmed.3002346 (2011).

31 Graziotto, J. J., Cao, K., Collins, F. S. & Krainc, D. Rapamycin activates autophagy in Hutchinson-Gilford progeria syndrome: implications for normal aging and age-dependent neurodegenerative disorders. *Autophagy* **8**, 147-151, doi:10.4161/auto.8.1.18331 (2012).

32 Morita, M. *et al.* mTORC1 controls mitochondrial activity and biogenesis through 4E-BP-dependent translational regulation. *Cell Metab* **18**, 698-711, doi:10.1016/j.cmet.2013.10.001 (2013).

33 Fontana, L., Partridge, L. & Longo, V. D. Extending healthy life span--from yeast to humans. *Science* **328**, 321-326, doi:10.1126/science.1172539 (2010).

34 Fund, U. N. P. Ageing in the Twenty-First Century: A Celebration and a Challenge. (2012).

35 Jin, K. Modern Biological Theories of Aging. *Aging Dis* **1**, 72-74 (2010).

36 Schulz-Aellen, M.-F. Aging and Longevity. *Springer Science+Business Media*, 284 (1997).

37 Martin, G. M. Syndromes of accelerated aging. *Natl Cancer Inst Monogr* **60**, 241-247 (1982).

38 Hennekam, R. C. Hutchinson-Gilford progeria syndrome: review of the phenotype. *Am J Med Genet A* **140**, 2603-2624 (2006).

39 Gordon, L. B. *et al.* Disease progression in Hutchinson-Gilford progeria syndrome: impact on growth and development. *Pediatrics* **120**, 824-833 (2007).

40 Shumaker, D. K. *et al.* The highly conserved nuclear lamin Ig-fold binds to PCNA: its role in DNA replication. *J Cell Biol* **181**, 269-280 (2008).

41 Olive, M. *et al.* Cardiovascular pathology in Hutchinson-Gilford progeria: correlation with the vascular pathology of aging. *Arterioscler Thromb Vasc Biol* **30**, 2301-2309 (2010).

42 Gordon, L. B., Brown, W. T. & Collins, F. S. Hutchinson-Gilford Progeria Syndrome. (1993).

43 Russo-Menna, I. & Arancibias, C. The Hutchinson-Gilford Progeria Syndrome: a case report. *Minerva Anestesiol* **76**, 151-154 (2010).

44 Pereira, S. *et al.* HGPS and related premature aging disorders: from genomic identification to the first therapeutic approaches. *Mech Ageing Dev* **129**, 449-459 (2008).

45 Paradisi, M. *et al.* Dermal fibroblasts in Hutchinson-Gilford progeria syndrome with the lamin A G608G mutation have dysmorphic nuclei and are hypersensitive to heat stress. *BMC Cell Biol* **6**, 27, doi:10.1186/1471-2121-6-27 (2005).

46 Columbaro, M. *et al.* Rescue of heterochromatin organization in Hutchinson-Gilford progeria by drug treatment. *Cell Mol Life Sci* **62**, 2669-2678 (2005).

47 Csoka, A. B. *et al.* Genome-scale expression profiling of Hutchinson-Gilford progeria syndrome reveals widespread transcriptional misregulation leading to mesodermal/mesenchymal defects and accelerated atherosclerosis. *Aging Cell* **3**, 235-243 (2004).

48 Scaffidi, P. & Misteli, T. Reversal of the cellular phenotype in the premature aging disease Hutchinson-Gilford progeria syndrome. *Nat Med* **11**, 440-445 (2005).

49 Ly, D. H., Lockhart, D. J., Lerner, R. A. & Schultz, P. G. Mitotic misregulation and human aging. *Science* **287**, 2486-2492 (2000).

50 Constantinescu, D., Csoka, A. B., Navara, C. S. & Schatten, G. P. Defective DSB repair correlates with abnormal nuclear morphology and is improved with FTI treatment in Hutchinson-Gilford progeria syndrome fibroblasts. *Exp Cell Res* **316**, 2747-2759 (2010).

51 Cao, K., Capell, B. C., Erdos, M. R., Djabali, K. & Collins, F. S. A lamin A protein isoform overexpressed in Hutchinson-Gilford progeria syndrome interferes with mitosis in progeria and normal cells. *Proc Natl Acad Sci U S A* **104**, 4949-4954 (2007).

52 Benson, E. K., Lee, S. W. & Aaronson, S. A. Role of progerin-induced telomere dysfunction in HGPS premature cellular senescence. *J Cell Sci* **123**, 2605-2612 (2010).

53 De Sandre-Giovannoli, A. *et al.* Lamin a truncation in Hutchinson-Gilford progeria. *Science* **300**, 2055 (2003).

54 Goldman, R. D., Gruenbaum, Y., Moir, R. D., Shumaker, D. K. & Spann, T. P. Nuclear lamins: building blocks of nuclear architecture. *Genes Dev* **16**, 533-547 (2002).

55 Lenz-Bohme, B. *et al.* Insertional mutation of the Drosophila nuclear lamin Dm0 gene results in defective nuclear envelopes, clustering of nuclear pore complexes, and accumulation of annulate lamellae. *J Cell Biol* **137**, 1001-1016 (1997).

56 Broers, J. L., Ramaekers, F. C., Bonne, G., Yaou, R. B. & Hutchison, C. J. Nuclear lamins: laminopathies and their role in premature ageing. *Physiol Rev* **86**, 967-1008 (2006).

57 Stuurman, N., Heins, S. & Aebi, U. Nuclear lamins: their structure, assembly, and interactions. *J Struct Biol* **122**, 42-66 (1998).

58 Capell, B. C. & Collins, F. S. Human laminopathies: nuclei gone genetically awry. *Nat Rev Genet* **7**, 940-952, doi:10.1038/nrg1906 (2006).

59 Verstraeten, V. L. *et al.* Compound heterozygosity for mutations in LMNA causes a progeria syndrome without prelamin A accumulation. *Hum Mol Genet* **15**, 2509-2522 (2006).

60 Riemer, D., Wang, J., Zimek, A., Swalla, B. J. & Weber, K. Tunicates have unusual nuclear lamins with a large deletion in the carboxyterminal tail domain. *Gene* **255**, 317-325 (2000).

61 Cohen, M., Lee, K. K., Wilson, K. L. & Gruenbaum, Y. Transcriptional repression, apoptosis, human disease and the functional evolution of the nuclear lamina. *Trends Biochem Sci* **26**, 41-47 (2001).

62 Wydner, K. L., McNeil, J. A., Lin, F., Worman, H. J. & Lawrence, J. B. Chromosomal assignment of human nuclear envelope protein genes LMNA, LMNB1, and LBR by fluorescence in situ hybridization. *Genomics* **32**, 474-478 (1996).

63 Moir, R. D., Donaldson, A. D. & Stewart, M. Expression in Escherichia coli of human lamins A and C: influence of head and tail domains on assembly properties and paracrystal formation. *J Cell Sci* **99 (Pt 2)**, 363-372 (1991).

64 Vergnes, L., Peterfy, M., Bergo, M. O., Young, S. G. & Reue, K. Lamin B1 is required for mouse development and nuclear integrity. *Proc Natl Acad Sci U S A* **101**, 10428-10433, doi:10.1073/pnas.0401424101 (2004).

65 Rober, R. A., Weber, K. & Osborn, M. Differential timing of nuclear lamin A/C expression in the various organs of the mouse embryo and the young animal: a developmental study. *Development* **105**, 365-378 (1989).
66 Izumi, M., Vaughan, O. A., Hutchison, C. J. & Gilbert, D. M. Head and/or CaaX domain deletions of lamin proteins disrupt preformed lamin A and C but not lamin B structure in mammalian cells. *Mol Biol Cell* **11**, 4323-4337 (2000).
67 Worman, H. J., Fong, L. G., Muchir, A. & Young, S. G. Laminopathies and the long strange trip from basic cell biology to therapy. *J Clin Invest* **119**, 1825-1836 (2009).
68 Loewinger, L. & McKeon, F. Mutations in the nuclear lamin proteins resulting in their aberrant assembly in the cytoplasm. *Embo J* **7**, 2301-2309 (1988).
69 Moir, R. D., Spann, T. P. & Goldman, R. D. The dynamic properties and possible functions of nuclear lamins. *Int Rev Cytol* **162B**, 141-182 (1995).
70 Stewart, C. L., Roux, K. J. & Burke, B. Blurring the boundary: the nuclear envelope extends its reach. *Science* **318**, 1408-1412, doi:10.1126/science.1142034 (2007).
71 Grossman, E., Medalia, O. & Zwerger, M. Functional architecture of the nuclear pore complex. *Annu Rev Biophys* **41**, 557-584, doi:10.1146/annurev-biophys-050511-102328 (2012).
72 Mattout-Drubezki, A. & Gruenbaum, Y. Dynamic interactions of nuclear lamina proteins with chromatin and transcriptional machinery. *Cell Mol Life Sci* **60**, 2053-2063 (2003).
73 Dechat, T., Adam, S. A., Taimen, P., Shimi, T. & Goldman, R. D. Nuclear lamins. *Cold Spring Harb Perspect Biol* **2**, a000547 (2010).
74 Harborth, J., Elbashir, S. M., Bechert, K., Tuschl, T. & Weber, K. Identification of essential genes in cultured mammalian cells using small interfering RNAs. *J Cell Sci* **114**, 4557-4565 (2001).
75 Broers, J. L. *et al.* Decreased mechanical stiffness in LMNA-/- cells is caused by defective nucleo-cytoskeletal integrity: implications for the development of laminopathies. *Hum Mol Genet* **13**, 2567-2580 (2004).
76 Vaughan, A. *et al.* Both emerin and lamin C depend on lamin A for localization at the nuclear envelope. *J Cell Sci* **114**, 2577-2590 (2001).
77 Puente, X. S. *et al.* Exome sequencing and functional analysis identifies BANF1 mutation as the cause of a hereditary progeroid syndrome. *Am J Hum Genet* **88**, 650-656, doi:10.1016/j.ajhg.2011.04.010 (2011).
78 Solovei, I. *et al.* LBR and lamin A/C sequentially tether peripheral heterochromatin and inversely regulate differentiation. *Cell* **152**, 584-598, doi:10.1016/j.cell.2013.01.009 (2013).
79 Kumaran, R. I., Muralikrishna, B. & Parnaik, V. K. Lamin A/C speckles mediate spatial organization of splicing factor compartments and RNA polymerase II transcription. *J Cell Biol* **159**, 783-793 (2002).
80 Moir, R. D. *et al.* Review: the dynamics of the nuclear lamins during the cell cycle--relationship between structure and function. *J Struct Biol* **129**, 324-334 (2000).
81 Kennedy, B. K., Barbie, D. A., Classon, M., Dyson, N. & Harlow, E. Nuclear organization of DNA replication in primary mammalian cells. *Genes Dev* **14**, 2855-2868 (2000).
82 Steen, R. L., Martins, S. B., Tasken, K. & Collas, P. Recruitment of protein phosphatase 1 to the nuclear envelope by A-kinase anchoring protein AKAP149 is a prerequisite for nuclear lamina assembly. *J Cell Biol* **150**, 1251-1262 (2000).
83 Rao, L., Perez, D. & White, E. Lamin proteolysis facilitates nuclear events during apoptosis. *J Cell Biol* **135**, 1441-1455 (1996).
84 Pendas, A. M. *et al.* Defective prelamin A processing and muscular and adipocyte alterations in Zmpste24 metalloproteinase-deficient mice. *Nat Genet* **31**, 94-99 (2002).
85 Beck, L. A., Hosick, T. J. & Sinensky, M. Isoprenylation is required for the processing of the lamin A precursor. *J Cell Biol* **110**, 1489-1499 (1990).
86 Corrigan, D. P. & East Tennessee State, U. *Role of Zmpste24 in prelamin A maturation*. (East Tennessee State University, 2005).

87 Scaffidi, P. & Misteli, T. Lamin A-dependent nuclear defects in human aging. *Science* **312**, 1059-1063 (2006).

88 McClintock, D. *et al.* The mutant form of lamin A that causes Hutchinson-Gilford progeria is a biomarker of cellular aging in human skin. *PLoS One* **2**, e1269 (2007).

89 Wenzel, V. *et al.* Naive adult stem cells from patients with Hutchinson-Gilford progeria syndrome express low levels of progerin in vivo. *Biol Open* **1**, 516-526, doi:10.1242/bio.20121149 (2012).

90 Cao, K. *et al.* Progerin and telomere dysfunction collaborate to trigger cellular senescence in normal human fibroblasts. *J Clin Invest* (2011).

91 Gordon, L. B. Farnesyltransferase Inhibitors (FTIs) as potential Drug Therapy for Children with Progeria. *http://www.progeriaresearch.org/assets/files/pdf/FTIQ&AAugust2006Final.pdf* (2006).

92 Toth, J. I. *et al.* Blocking protein farnesyltransferase improves nuclear shape in fibroblasts from humans with progeroid syndromes. *Proc Natl Acad Sci U S A* **102**, 12873-12878 (2005).

93 Capell, B. C. *et al.* Inhibiting farnesylation of progerin prevents the characteristic nuclear blebbing of Hutchinson-Gilford progeria syndrome. *Proc Natl Acad Sci U S A* **102**, 12879-12884 (2005).

94 Glynn, M. W. & Glover, T. W. Incomplete processing of mutant lamin A in Hutchinson-Gilford progeria leads to nuclear abnormalities, which are reversed by farnesyltransferase inhibition. *Hum Mol Genet* **14**, 2959-2969 (2005).

95 Marji, J. *et al.* Defective lamin A-Rb signaling in Hutchinson-Gilford Progeria Syndrome and reversal by farnesyltransferase inhibition. *PLoS One* **5**, e11132 (2010).

96 Yang, S. H., Andres, D. A., Spielmann, H. P., Young, S. G. & Fong, L. G. Progerin elicits disease phenotypes of progeria in mice whether or not it is farnesylated. *J Clin Invest* **118**, 3291-3300 (2008).

97 Varela, I. *et al.* Combined treatment with statins and aminobisphosphonates extends longevity in a mouse model of human premature aging. *Nat Med* **14**, 767-772 (2008).

98 Fong, L. G. *et al.* Heterozygosity for Lmna deficiency eliminates the progeria-like phenotypes in Zmpste24-deficient mice. *Proc Natl Acad Sci U S A* **101**, 18111-18116 (2004).

99 Gabriel, D., Roedl, D., Gordon, L. B. & Djabali, K. Sulforaphane enhances progerin clearance in Hutchinson-Gilford progeria fibroblasts. *Aging Cell* **14**, 78-91, doi:10.1111/acel.12300 (2015).

100 Gamerdinger, M. *et al.* Protein quality control during aging involves recruitment of the macroautophagy pathway by BAG3. *EMBO J* **28**, 889-901, doi:10.1038/emboj.2009.29 (2009).

101 Rubinsztein, D. C., Marino, G. & Kroemer, G. Autophagy and aging. *Cell* **146**, 682-695, doi:10.1016/j.cell.2011.07.030 (2011).

102 Lok, C. N., Sy, L. K., Liu, F. & Che, C. M. Activation of autophagy of aggregation-prone ubiquitinated proteins by timosaponin A-III. *J Biol Chem* **286**, 31684-31696 (2011).

103 Xie, Z. & Klionsky, D. J. Autophagosome formation: core machinery and adaptations. *Nat Cell Biol* **9**, 1102-1109 (2007).

104 Tooze, S. A. & Yoshimori, T. The origin of the autophagosomal membrane. *Nat Cell Biol* **12**, 831-835 (2010).

105 Burman, C. & Ktistakis, N. T. Regulation of autophagy by phosphatidylinositol 3-phosphate. *FEBS Lett* **584**, 1302-1312 (2010).

106 Ravikumar, B. *et al.* Regulation of mammalian autophagy in physiology and pathophysiology. *Physiol Rev* **90**, 1383-1435 (2010).

107 Sancak, Y. *et al.* Ragulator-Rag complex targets mTORC1 to the lysosomal surface and is necessary for its activation by amino acids. *Cell* **141**, 290-303 (2010).

108 Korolchuk, V. I. *et al.* Lysosomal positioning coordinates cellular nutrient responses. *Nat Cell Biol* **13**, 453-460 (2011).

109 Tasdemir, E. *et al.* Regulation of autophagy by cytoplasmic p53. *Nat Cell Biol* **10**, 676-687 (2008).

110 Fleming, A., Noda, T., Yoshimori, T. & Rubinsztein, D. C. Chemical modulators of autophagy as biological probes and potential therapeutics. *Nat Chem Biol* **7**, 9-17 (2011).

111 Egan, D. F. *et al.* Phosphorylation of ULK1 (hATG1) by AMP-activated protein kinase connects energy sensing to mitophagy. *Science* **331**, 456-461 (2011).

112 Fougeray, S. & Pallet, N. Mechanisms and biological functions of autophagy in diseased and ageing kidneys. *Nat Rev Nephrol* **11**, 34-45, doi:10.1038/nrneph.2014.201 (2015).

113 Aronson, L. I. & Davies, F. E. DangER: protein ovERload. Targeting protein degradation to treat myeloma. *Haematologica* **97**, 1119-1130, doi:10.3324/haematol.2012.064923 (2012).

114 Rubinsztein, D. C., Gestwicki, J. E., Murphy, L. O. & Klionsky, D. J. Potential therapeutic applications of autophagy. *Nat Rev Drug Discov* **6**, 304-312 (2007).

115 Kroemer, G. & Levine, B. Autophagic cell death: the story of a misnomer. *Nat Rev Mol Cell Biol* **9**, 1004-1010 (2008).

116 Zhang, C. & Cuervo, A. M. Restoration of chaperone-mediated autophagy in aging liver improves cellular maintenance and hepatic function. *Nat Med* **14**, 959-965 (2008).

117 Gottlieb, R. A. & Mentzer, R. M. Autophagy during cardiac stress: joys and frustrations of autophagy. *Annu Rev Physiol* **72**, 45-59 (2010).

118 Jiang, M., Liu, K., Luo, J. & Dong, Z. Autophagy is a renoprotective mechanism during in vitro hypoxia and in vivo ischemia-reperfusion injury. *Am J Pathol* **176**, 1181-1192 (2010).

119 Madeo, F., Tavernarakis, N. & Kroemer, G. Can autophagy promote longevity? *Nat Cell Biol* **12**, 842-846 (2010).

120 Zhang, L. *et al.* Small molecule regulators of autophagy identified by an image-based high-throughput screen. *Proc Natl Acad Sci U S A* **104**, 19023-19028 (2007).

121 Sarkar, S. *et al.* Small molecules enhance autophagy and reduce toxicity in Huntington's disease models. *Nat Chem Biol* **3**, 331-338 (2007).

122 Sarkar, S., Davies, J. E., Huang, Z., Tunnacliffe, A. & Rubinsztein, D. C. Trehalose, a novel mTOR-independent autophagy enhancer, accelerates the clearance of mutant huntingtin and alpha-synuclein. *J Biol Chem* **282**, 5641-5652 (2007).

123 Blagosklonny, M. V. Progeria, rapamycin and normal aging: recent breakthrough. *Aging (Albany NY)* **3**, 685-691 (2011).

124 Demidenko, Z. N. & Blagosklonny, M. V. Growth stimulation leads to cellular senescence when the cell cycle is blocked. *Cell Cycle* **7**, 3355-3361 (2008).

125 Demidenko, Z. N. *et al.* Rapamycin decelerates cellular senescence. *Cell Cycle* **8**, 1888-1895 (2009).

126 Zhao, L. *et al.* Low-dose oral sirolimus reduces atherogenesis, vascular inflammation and modulates plaque composition in mice lacking the LDL receptor. *Br J Pharmacol* **156**, 774-785 (2009).

127 Mueller, M. A., Beutner, F., Teupser, D., Ceglarek, U. & Thiery, J. Prevention of atherosclerosis by the mTOR inhibitor everolimus in LDLR-/- mice despite severe hypercholesterolemia. *Atherosclerosis* **198**, 39-48 (2008).

128 Neff, F. *et al.* Rapamycin extends murine lifespan but has limited effects on aging. *J Clin Invest* **123**, 3272-3291, doi:10.1172/JCI67674 (2013).

129 Kloetzel, P. M. The proteasome and MHC class I antigen processing. *Biochim Biophys Acta* **1695**, 225-233 (2004).

130 Tomaru, U. *et al.* Decreased proteasomal activity causes age-related phenotypes and promotes the development of metabolic abnormalities. *Am J Pathol* **180**, 963-972 (2012).

131 Baumeister, W., Walz, J., Zuhl, F. & Seemuller, E. The proteasome: paradigm of a self-compartmentalizing protease. *Cell* **92**, 367-380 (1998).

132 Ebrahimi-Fakhari, D., Wahlster, L. & McLean, P. J. Protein degradation pathways in Parkinson's disease: curse or blessing. *Acta Neuropathol* **124**, 153-172 (2012).

133 Adams, J. The proteasome: structure, function, and role in the cell. *Cancer Treat Rev* **29 Suppl 1**, 3-9 (2003).

134 Wilkinson, K. D. Ubiquitin-dependent signaling: the role of ubiquitination in the response of cells to their environment. *J Nutr* **129**, 1933-1936 (1999).

135 Pickart, C. M. Mechanisms underlying ubiquitination. *Annu Rev Biochem* **70**, 503-533 (2001).

136 Ludwig, H., Khayat, D., Giaccone, G. & Facon, T. Proteasome inhibition and its clinical prospects in the treatment of hematologic and solid malignancies. *Cancer* **104**, 1794-1807 (2005).
137 Li, Y. F. & Wang, X. The role of the proteasome in heart disease. *Biochim Biophys Acta* **1809**, 141-149 (2011).
138 Oddo, S. The ubiquitin-proteasome system in Alzheimer's disease. *J Cell Mol Med* **12**, 363-373 (2008).
139 Almeida, C. G., Takahashi, R. H. & Gouras, G. K. Beta-amyloid accumulation impairs multivesicular body sorting by inhibiting the ubiquitin-proteasome system. *J Neurosci* **26**, 4277-4288 (2006).
140 McNaught, K. S., Belizaire, R., Isacson, O., Jenner, P. & Olanow, C. W. Altered proteasomal function in sporadic Parkinson's disease. *Exp Neurol* **179**, 38-46 (2003).
141 Lim, K. L. & Tan, J. M. Role of the ubiquitin proteasome system in Parkinson's disease. *BMC Biochem* **8 Suppl 1**, S13 (2007).
142 Tofaris, G. K., Razzaq, A., Ghetti, B., Lilley, K. S. & Spillantini, M. G. Ubiquitination of alpha-synuclein in Lewy bodies is a pathological event not associated with impairment of proteasome function. *J Biol Chem* **278**, 44405-44411 (2003).
143 Tonoki, A. *et al.* Genetic evidence linking age-dependent attenuation of the 26S proteasome with the aging process. *Mol Cell Biol* **29**, 1095-1106 (2009).
144 Chondrogianni, N. & Gonos, E. S. Proteasome dysfunction in mammalian aging: steps and factors involved. *Exp Gerontol* **40**, 931-938 (2005).
145 Dahlmann, B. Role of proteasomes in disease. *BMC Biochem* **8 Suppl 1**, S3 (2007).
146 Sasaki, K. *et al.* PAC1 gene knockout reveals an essential role of chaperone-mediated 20S proteasome biogenesis and latent 20S proteasomes in cellular homeostasis. *Mol Cell Biol* **30**, 3864-3874 (2010).
147 Hwang, J. S., Hwang, J. S., Chang, I. & Kim, S. Age-associated decrease in proteasome content and activities in human dermal fibroblasts: restoration of normal level of proteasome subunits reduces aging markers in fibroblasts from elderly persons. *J Gerontol A Biol Sci Med Sci* **62**, 490-499 (2007).
148 Viteri, G., Chung, Y. W. & Stadtman, E. R. Effect of progerin on the accumulation of oxidized proteins in fibroblasts from Hutchinson Gilford progeria patients. *Mech Ageing Dev* **131**, 2-8, doi:10.1016/j.mad.2009.11.006 (2010).
149 Patterson, C. & Hohfeld, J. Molecular Chaperones and the Ubiquitin-Proteasome System. *Protein Degradation, Wiley-VCH Verlag GmbH* **2** (2006).
150 Patel, S. B. *et al.* Everolimus Versus Temsirolimus in Metastatic Renal Cell Carcinoma After Progression With Previous Systemic Therapies. *Clin Genitourin Cancer* **14**, 153-159, doi:10.1016/j.clgc.2015.12.011 (2016).
151 Chaudhary, N. & Courvalin, J. C. Stepwise reassembly of the nuclear envelope at the end of mitosis. *J Cell Biol* **122**, 295-306 (1993).
152 Davies, B. S., Fong, L. G., Yang, S. H., Coffinier, C. & Young, S. G. The posttranslational processing of prelamin A and disease. *Annu Rev Genomics Hum Genet* **10**, 153-174, doi:10.1146/annurev-genom-082908-150150 (2009).
153 Corrigan, D. P. *et al.* Prelamin A endoproteolytic processing in vitro by recombinant Zmpste24. *Biochem J* **387**, 129-138, doi:10.1042/BJ20041359 (2005).
154 Peter, M., Nakagawa, J., Doree, M., Labbe, J. C. & Nigg, E. A. In vitro disassembly of the nuclear lamina and M phase-specific phosphorylation of lamins by cdc2 kinase. *Cell* **61**, 591-602 (1990).
155 Mounkes, L. C. & Stewart, C. L. Aging and nuclear organization: lamins and progeria. *Curr Opin Cell Biol* **16**, 322-327, doi:10.1016/j.ceb.2004.03.009 (2004).
156 Bartlett, J. M. & Stirling, D. A short history of the polymerase chain reaction. *Methods in molecular biology* **226**, 3-6, doi:10.1385/1-59259-384-4:3 (2003).
157 VanGuilder, H. D., Vrana, K. E. & Freeman, W. M. Twenty-five years of quantitative PCR for gene expression analysis. *Biotechniques* **44**, 619-626 (2008).

158 Udvardi, M. K., Czechowski, T. & Scheible, W. R. Eleven golden rules of quantitative RT-PCR. *Plant Cell* **20**, 1736-1737 (2008).
159 Livak, K. J. & Schmittgen, T. D. Analysis of relative gene expression data using real-time quantitative PCR and the 2(-Delta Delta C(T)) Method. *Methods* **25**, 402-408, doi:10.1006/meth.2001.1262 (2001).
160 Arndt, V., Daniel, C., Nastainczyk, W., Alberti, S. & Hohfeld, J. BAG-2 acts as an inhibitor of the chaperone-associated ubiquitin ligase CHIP. *Mol Biol Cell* **16**, 5891-5900 (2005).
161 Darvekar, S. R., Elvenes, J., Brenne, H. B., Johansen, T. & Sjottem, E. SPBP is a sulforaphane induced transcriptional coactivator of NRF2 regulating expression of the autophagy receptor p62/SQSTM1. *PLoS One* **9**, e85262, doi:10.1371/journal.pone.0085262 (2014).
162 Zhu, J. *et al.* Targeting the NF-E2-related factor 2 pathway: a novel strategy for glioblastoma (review). *Oncol Rep* **32**, 443-450, doi:10.3892/or.2014.3259 (2014).
163 Lee, Y. J. & Lee, S. H. Sulforaphane induces antioxidative and antiproliferative responses by generating reactive oxygen species in human bronchial epithelial BEAS-2B cells. *J Korean Med Sci* **26**, 1474-1482 (2011).
164 Ciechanover, A. Proteolysis: from the lysosome to ubiquitin and the proteasome. *Nat Rev Mol Cell Biol* **6**, 79-87, doi:10.1038/nrm1552 (2005).
165 Milani, M. *et al.* The role of ATF4 stabilization and autophagy in resistance of breast cancer cells treated with Bortezomib. *Cancer Res* **69**, 4415-4423, doi:10.1158/0008-5472.CAN-08-2839 (2009).
166 Shimi, T. *et al.* The role of nuclear lamin B1 in cell proliferation and senescence. *Genes Dev* **25**, 2579-2593, doi:10.1101/gad.179515.111 (2011).
167 Liu, B. *et al.* Genomic instability in laminopathy-based premature aging. *Nat Med* **11**, 780-785, doi:10.1038/nm1266 (2005).
168 Liu, Y. *et al.* Involvement of xeroderma pigmentosum group A (XPA) in progeria arising from defective maturation of prelamin A. *Faseb J* **22**, 603-611 (2008).
169 Liu, Q. *et al.* Dynamics of lamin-A processing following precursor accumulation. *PLoS One* **5**, e10874 (2010).
170 Pan, J., She, M., Xu, Z. X., Sun, L. & Yeung, S. C. Farnesyltransferase inhibitors induce DNA damage via reactive oxygen species in human cancer cells. *Cancer Res* **65**, 3671-3681, doi:10.1158/0008-5472.CAN-04-2744 (2005).
171 Chu, U. B., Duellman, T., Weaver, S. J., Tao, Y. & Yang, J. Endothelial protective genes induced by statin are mimicked by ERK5 activation as triggered by a drug combination of FTI-277 and GGTI-298. *Biochim Biophys Acta* **1850**, 1415-1425, doi:10.1016/j.bbagen.2015.03.011 (2015).
172 Rivera-Torres, J. *et al.* Identification of mitochondrial dysfunction in Hutchinson-Gilford progeria syndrome through use of stable isotope labeling with amino acids in cell culture. *J Proteomics* **91**, 466-477, doi:10.1016/j.jprot.2013.08.008 (2013).
173 Young, S. G., Yang, S. H., Davies, B. S., Jung, H. J. & Fong, L. G. Targeting protein prenylation in progeria. *Sci Transl Med* **5**, 171ps173, doi:10.1126/scitranslmed.3005229 (2013).
174 Musich, P. R. & Zou, Y. Genomic instability and DNA damage responses in progeria arising from defective maturation of prelamin A. *Aging (Albany NY)* **1**, 28-37 (2009).
175 Osorio, F. G. *et al.* Splicing-directed therapy in a new mouse model of human accelerated aging. *Sci Transl Med* **3**, 106ra107, doi:10.1126/scitranslmed.3002847 (2011).
176 Shao, W., Yu, Z., Fantus, I. G. & Jin, T. Cyclic AMP signaling stimulates proteasome degradation of thioredoxin interacting protein (TxNIP) in pancreatic beta-cells. *Cellular signalling* **22**, 1240-1246, doi:10.1016/j.cellsig.2010.04.001 (2010).
177 Kraft, C., Peter, M. & Hofmann, K. Selective autophagy: ubiquitin-mediated recognition and beyond. *Nat Cell Biol* **12**, 836-841, doi:10.1038/ncb0910-836 (2010).
178 Osmulski, P. A. & Gaczynska, M. Rapamycin allosterically inhibits the proteasome. *Molecular pharmacology* **84**, 104-113, doi:10.1124/mol.112.083873 (2013).
179 Ouedraogo, R. *et al.* Adiponectin suppression of high-glucose-induced reactive oxygen species in vascular endothelial cells: evidence for involvement of a cAMP signaling pathway. *Diabetes* **55**, 1840-1846, doi:10.2337/db05-1174 (2006).

180 Wang, S. M. & Yang, W. L. Circulating hormone adrenomedullin and its binding protein protect neural cells from hypoxia-induced apoptosis. *Biochim Biophys Acta* **1790**, 361-367, doi:10.1016/j.bbagen.2009.03.012 (2009).
181 McClintock, D., Gordon, L. B. & Djabali, K. Hutchinson-Gilford progeria mutant lamin A primarily targets human vascular cells as detected by an anti-Lamin A G608G antibody. *Proc Natl Acad Sci U S A* **103**, 2154-2159, doi:10.1073/pnas.0511133103 (2006).
182 Freund, A., Laberge, R. M., Demaria, M. & Campisi, J. Lamin B1 loss is a senescence-associated biomarker. *Mol Biol Cell* **23**, 2066-2075, doi:10.1091/mbc.E11-10-0884 (2012).
183 Oh, Y. S. *et al.* Downregulation of lamin A by tumor suppressor AIMP3/p18 leads to a progeroid phenotype in mice. *Aging Cell* **9**, 810-822, doi:10.1111/j.1474-9726.2010.00614.x (2010).
184 Aliper, A. M. *et al.* Signaling pathway activation drift during aging: Hutchinson-Gilford Progeria Syndrome fibroblasts are comparable to normal middle-age and old-age cells. *Aging (Albany NY)* **7**, 26-37 (2015).
185 Liu, B. & Zhou, Z. Activation of SIRT1 by resveratrol requires lamin A. *Aging (Albany NY)* **5**, 94-95 (2013).
186 Xiong, Z. M. *et al.* Methylene blue alleviates nuclear and mitochondrial abnormalities in progeria. *Aging Cell*, doi:10.1111/acel.12434 (2015).
187 Salminen, A. & Kaarniranta, K. AMP-activated protein kinase (AMPK) controls the aging process via an integrated signaling network. *Ageing Res Rev* **11**, 230-241, doi:10.1016/j.arr.2011.12.005 (2012).
188 Cowell, R. M., Blake, K. R., Inoue, T. & Russell, J. W. Regulation of PGC-1alpha and PGC-1alpha-responsive genes with forskolin-induced Schwann cell differentiation. *Neurosci Lett* **439**, 269-274, doi:10.1016/j.neulet.2008.04.104 (2008).
189 Mihaylova, M. M. & Shaw, R. J. The AMPK signalling pathway coordinates cell growth, autophagy and metabolism. *Nat Cell Biol* **13**, 1016-1023, doi:10.1038/ncb2329 (2011).
190 Sinclair, D. A. Toward a unified theory of caloric restriction and longevity regulation. *Mech Ageing Dev* **126**, 987-1002, doi:10.1016/j.mad.2005.03.019 (2005).
191 Blander, G. & Guarente, L. The Sir2 family of protein deacetylases. *Annu Rev Biochem* **73**, 417-435, doi:10.1146/annurev.biochem.73.011303.073651 (2004).
192 Thompson, A. M., Wagner, R. & Rzucidlo, E. M. Age-related loss of SirT1 expression results in dysregulated human vascular smooth muscle cell function. *Am J Physiol Heart Circ Physiol* **307**, H533-541, doi:10.1152/ajpheart.00871.2013 (2014).
193 Ciron, C. *et al.* PGC-1alpha activity in nigral dopamine neurons determines vulnerability to alpha-synuclein. *Acta Neuropathol Commun* **3**, 16, doi:10.1186/s40478-015-0200-8 (2015).
194 Zhang, Y. *et al.* Multiple signaling pathways regulate contractile activity-mediated PGC-1alpha gene expression and activity in skeletal muscle cells. *Physiol Rep* **2**, doi:10.14814/phy2.12008 (2014).
195 LeBleu, V. S. *et al.* PGC-1alpha mediates mitochondrial biogenesis and oxidative phosphorylation in cancer cells to promote metastasis. *Nat Cell Biol* **16**, 992-1003, 1001-1015, doi:10.1038/ncb3039 (2014).
196 Walther, S. *et al.* Urocortin 2 stimulates nitric oxide production in ventricular myocytes via Akt- and PKA-mediated phosphorylation of eNOS at serine 1177. *Am J Physiol Heart Circ Physiol* **307**, H689-700, doi:10.1152/ajpheart.00694.2013 (2014).
197 Soltoff, S. P. & Hedden, L. Isoproterenol and cAMP block ERK phosphorylation and enhance [Ca2+]i increases and oxygen consumption by muscarinic receptor stimulation in rat parotid and submandibular acinar cells. *J Biol Chem* **285**, 13337-13348, doi:10.1074/jbc.M110.112094 (2010).
198 Jewell, J. L., Russell, R. C. & Guan, K. L. Amino acid signalling upstream of mTOR. *Nat Rev Mol Cell Biol* **14**, 133-139, doi:10.1038/nrm3522 (2013).
199 Lan, F., Cacicedo, J. M., Ruderman, N. & Ido, Y. SIRT1 modulation of the acetylation status, cytosolic localization, and activity of LKB1. Possible role in AMP-activated protein kinase activation. *J Biol Chem* **283**, 27628-27635, doi:10.1074/jbc.M805711200 (2008).

200 Gerhart-Hines, Z. *et al.* Metabolic control of muscle mitochondrial function and fatty acid oxidation through SIRT1/PGC-1alpha. *EMBO J* **26**, 1913-1923, doi:10.1038/sj.emboj.7601633 (2007).
201 Wang, F., Nguyen, M., Qin, F. X. & Tong, Q. SIRT2 deacetylates FOXO3a in response to oxidative stress and caloric restriction. *Aging Cell* **6**, 505-514, doi:10.1111/j.1474-9726.2007.00304.x (2007).
202 Olmos, Y. *et al.* SirT1 regulation of antioxidant genes is dependent on the formation of a FoxO3a/PGC-1alpha complex. *Antioxid Redox Signal* **19**, 1507-1521, doi:10.1089/ars.2012.4713 (2013).
203 Olmos, Y. *et al.* Mutual dependence of Foxo3a and PGC-1alpha in the induction of oxidative stress genes. *J Biol Chem* **284**, 14476-14484, doi:10.1074/jbc.M807397200 (2009).
204 Misteli, T. & Scaffidi, P. Genome instability in progeria: when repair gets old. *Nat Med* **11**, 718-719 (2005).
205 Balgi, A. D. *et al.* Screen for chemical modulators of autophagy reveals novel therapeutic inhibitors of mTORC1 signaling. *PLoS One* **4**, e7124, doi:10.1371/journal.pone.0007124 (2009).
206 Laplante, M. & Sabatini, D. M. mTOR signaling at a glance. *J Cell Sci* **122**, 3589-3594, doi:10.1242/jcs.051011 (2009).
207 Miller, R. A. *et al.* Rapamycin-mediated lifespan increase in mice is dose and sex dependent and metabolically distinct from dietary restriction. *Aging Cell* **13**, 468-477, doi:10.1111/acel.12194 (2014).
208 Johnson, S. C., Rabinovitch, P. S. & Kaeberlein, M. mTOR is a key modulator of ageing and age-related disease. *Nature* **493**, 338-345, doi:10.1038/nature11861 (2013).
209 Ekberg, H. *et al.* Cyclosporine, tacrolimus and sirolimus retain their distinct toxicity profiles despite low doses in the Symphony study. *Nephrol Dial Transplant* **25**, 2004-2010, doi:10.1093/ndt/gfp778 (2010).
210 Baur, B., Oroszlan, M., Hess, O., Carrel, T. & Mohacsi, P. Efficacy and safety of sirolimus and everolimus in heart transplant patients: a retrospective analysis. *Transplant Proc* **43**, 1853-1861, doi:10.1016/j.transproceed.2011.01.174 (2011).
211 Rini, B. I. Temsirolimus, an inhibitor of mammalian target of rapamycin. *Clin Cancer Res* **14**, 1286-1290, doi:10.1158/1078-0432.CCR-07-4719 (2008).
212 Hidalgo, M. *et al.* A phase I and pharmacokinetic study of temsirolimus (CCI-779) administered intravenously daily for 5 days every 2 weeks to patients with advanced cancer. *Clin Cancer Res* **12**, 5755-5763, doi:10.1158/1078-0432.CCR-06-0118 (2006).
213 Cenni, V. *et al.* Autophagic degradation of farnesylated prelamin A as a therapeutic approach to lamin-linked progeria. *European journal of histochemistry : EJH* **55**, e36, doi:10.4081/ejh.2011.e36 (2011).
214 Theodoropoulou, S. *et al.* Aminoimidazole carboxamide ribonucleotide (AICAR) inhibits the growth of retinoblastoma in vivo by decreasing angiogenesis and inducing apoptosis. *PLoS One* **8**, e52852, doi:10.1371/journal.pone.0052852 (2013).
215 Rodriguez, S., Coppede, F., Sagelius, H. & Eriksson, M. Increased expression of the Hutchinson-Gilford progeria syndrome truncated lamin A transcript during cell aging. *Eur J Hum Genet* **17**, 928-937 (2009).
216 Bedard, K. & Krause, K. H. The NOX family of ROS-generating NADPH oxidases: physiology and pathophysiology. *Physiol Rev* **87**, 245-313, doi:10.1152/physrev.00044.2005 (2007).
217 Villa-Bellosta, R. *et al.* Defective extracellular pyrophosphate metabolism promotes vascular calcification in a mouse model of Hutchinson-Gilford progeria syndrome that is ameliorated on pyrophosphate treatment. *Circulation* **127**, 2442-2451, doi:10.1161/CIRCULATIONAHA.112.000571 (2013).
218 Adkins, R. M., Honeycutt, R. L. & Disotell, T. R. Evolution of eutherian cytochrome c oxidase subunit II: heterogeneous rates of protein evolution and altered interaction with cytochrome c. *Mol Biol Evol* **13**, 1393-1404 (1996).

219 Li, Y., Park, J. S., Deng, J. H. & Bai, Y. Cytochrome c oxidase subunit IV is essential for assembly and respiratory function of the enzyme complex. *J Bioenerg Biomembr* **38**, 283-291, doi:10.1007/s10863-006-9052-z (2006).

220 Gohil, V. M. *et al.* Nutrient-sensitized screening for drugs that shift energy metabolism from mitochondrial respiration to glycolysis. *Nat Biotechnol* **28**, 249-255, doi:10.1038/nbt.1606 (2010).

221 Dott, W., Mistry, P., Wright, J., Cain, K. & Herbert, K. E. Modulation of mitochondrial bioenergetics in a skeletal muscle cell line model of mitochondrial toxicity. *Redox Biol* **2**, 224-233, doi:10.1016/j.redox.2013.12.028 (2014).

222 Lau, G. W., Hassett, D. J., Ran, H. & Kong, F. The role of pyocyanin in Pseudomonas aeruginosa infection. *Trends Mol Med* **10**, 599-606, doi:10.1016/j.molmed.2004.10.002 (2004).

223 Cadet, J. & Wagner, J. R. DNA base damage by reactive oxygen species, oxidizing agents, and UV radiation. *Cold Spring Harb Perspect Biol* **5**, doi:10.1101/cshperspect.a012559 (2013).

224 Zimmermann, M. & de Lange, T. 53BP1: pro choice in DNA repair. *Trends Cell Biol* **24**, 108-117, doi:10.1016/j.tcb.2013.09.003 (2014).

225 Krejci, L., Altmannova, V., Spirek, M. & Zhao, X. Homologous recombination and its regulation. *Nucleic Acids Res* **40**, 5795-5818, doi:10.1093/nar/gks270 (2012).

226 Prokocimer, M., Barkan, R. & Gruenbaum, Y. Hutchinson-Gilford progeria syndrome through the lens of transcription. *Aging Cell* **12**, 533-543, doi:10.1111/acel.12070 (2013).

227 Koga, H., Kaushik, S. & Cuervo, A. M. Protein homeostasis and aging: The importance of exquisite quality control. *Ageing Res Rev* **10**, 205-215, doi:10.1016/j.arr.2010.02.001 (2011).

228 Choi, J. C. *et al.* Temsirolimus activates autophagy and ameliorates cardiomyopathy caused by lamin A/C gene mutation. *Sci Transl Med* **4**, 144ra102, doi:10.1126/scitranslmed.3003875 (2012).

229 Behl, C. BAG3 and friends: co-chaperones in selective autophagy during aging and disease. *Autophagy* **7**, 795-798 (2011).

230 Baird, L. & Dinkova-Kostova, A. T. The cytoprotective role of the Keap1-Nrf2 pathway. *Archives of toxicology* **85**, 241-272, doi:10.1007/s00204-011-0674-5 (2011).

231 Liu, Y. *et al.* Sulforaphane enhances proteasomal and autophagic activities in mice and is a potential therapeutic reagent for Huntington's disease. *J Neurochem* **129**, 539-547, doi:10.1111/jnc.12647 (2014).

232 Vallanat, B. *et al.* Analysis of the heat shock response in mouse liver reveals transcriptional dependence on the nuclear receptor peroxisome proliferator-activated receptor alpha (PPARalpha). *BMC genomics* **11**, 16, doi:10.1186/1471-2164-11-16 (2010).

233 Blondel, S. *et al.* Induced pluripotent stem cells reveal functional differences between drugs currently investigated in patients with hutchinson-gilford progeria syndrome. *Stem cells translational medicine* **3**, 510-519, doi:10.5966/sctm.2013-0168 (2014).

234 Schafer-Hales, K. *et al.* Farnesyl transferase inhibitors impair chromosomal maintenance in cell lines and human tumors by compromising CENP-E and CENP-F function. *Mol Cancer Ther* **6**, 1317-1328, doi:10.1158/1535-7163.MCT-06-0703 (2007).

235 Monaco, G., van Dam, S., Casal Novo Ribeiro, J. L., Larbi, A. & de Magalhaes, J. P. A comparison of human and mouse gene co-expression networks reveals conservation and divergence at the tissue, pathway and disease levels. *BMC Evol Biol* **15**, 259, doi:10.1186/s12862-015-0534-7 (2015).

236 Wagh, V. D., Patil, P. N., Surana, S. J. & Wagh, K. V. Forskolin: upcoming antiglaucoma molecule. *Journal of postgraduate medicine* **58**, 199-202, doi:10.4103/0022-3859.101396 (2012).

237 Ferretta, A. *et al.* Effect of resveratrol on mitochondrial function: implications in parkin-associated familiar Parkinson's disease. *Biochim Biophys Acta* **1842**, 902-915, doi:10.1016/j.bbadis.2014.02.010 (2014).

238 Chung, J. H., Manganiello, V. & Dyck, J. R. Resveratrol as a calorie restriction mimetic: therapeutic implications. *Trends Cell Biol* **22**, 546-554, doi:10.1016/j.tcb.2012.07.004 (2012).

239 Gomes, L. C., Di Benedetto, G. & Scorrano, L. During autophagy mitochondria elongate, are spared from degradation and sustain cell viability. *Nat Cell Biol* **13**, 589-598, doi:10.1038/ncb2220 (2011).
240 Bell, E. L. & Guarente, L. The SirT3 divining rod points to oxidative stress. *Molecular cell* **42**, 561-568, doi:10.1016/j.molcel.2011.05.008 (2011).
241 Cunningham, J. T. *et al.* mTOR controls mitochondrial oxidative function through a YY1-PGC-1alpha transcriptional complex. *Nature* **450**, 736-740, doi:10.1038/nature06322 (2007).
242 Mick, D. U., Fox, T. D. & Rehling, P. Inventory control: cytochrome c oxidase assembly regulates mitochondrial translation. *Nat Rev Mol Cell Biol* **12**, 14-20, doi:10.1038/nrm3029 (2011).
243 Castello, L. *et al.* Alternate-day fasting reverses the age-associated hypertrophy phenotype in rat heart by influencing the ERK and PI3K signaling pathways. *Mech Ageing Dev* **132**, 305-314, doi:10.1016/j.mad.2011.06.006 (2011).
244 Li, Z. *et al.* Age-induced augmentation of p38 MAPK phosphorylation in mouse lung. *Exp Gerontol* **46**, 694-702, doi:10.1016/j.exger.2011.04.005 (2011).
245 Ghosh, S., Liu, B. & Zhou, Z. Resveratrol activates SIRT1 in a Lamin A-dependent manner. *Cell Cycle* **12**, 872-876, doi:10.4161/cc.24061 (2013).
246 Passeron, T., Namiki, T., Passeron, H. J., Le Pape, E. & Hearing, V. J. Forskolin protects keratinocytes from UVB-induced apoptosis and increases DNA repair independent of its effects on melanogenesis. *J Invest Dermatol* **129**, 162-166, doi:10.1038/jid.2008.182 (2009).
247 Gordon, L. B. *et al.* Impact of Farnesylation Inhibitors on Survival in Hutchinson-Gilford Progeria Syndrome. *Circulation*, doi:10.1161/CIRCULATIONAHA.113.008285 (2014).
248 Dudkin, L. *et al.* Biochemical correlates of mTOR inhibition by the rapamycin ester CCI-779 and tumor growth inhibition. *Clin Cancer Res* **7**, 1758-1764 (2001).
249 Arriola Apelo, S. I. *et al.* Alternative rapamycin treatment regimens mitigate the impact of rapamycin on glucose homeostasis and the immune system. *Aging Cell*, doi:10.1111/acel.12405 (2015).
250 Pellegrini, C. *et al.* All-trans retinoic acid and rapamycin normalize Hutchinson Gilford progeria fibroblast phenotype. *Oncotarget* **6**, 29914-29928, doi:10.18632/oncotarget.4939 (2015).
251 Osmulski, P. A. & Gaczynska, M. Rapamycin allosterically inhibits the proteasome. *Mol. Pharmacol.* **84**, 104-113 (2013).
252 Ye, L. *et al.* Rapamycin doses sufficient to extend lifespan do not compromise muscle mitochondrial content or endurance. *Aging (Albany NY)* **5**, 539-550 (2013).
253 Richards, S. A., Muter, J., Ritchie, P., Lattanzi, G. & Hutchison, C. J. The accumulation of un-repairable DNA damage in laminopathy progeria fibroblasts is caused by ROS generation and is prevented by treatment with N-acetyl cysteine. *Hum Mol Genet* **20**, 3997-4004, doi:10.1093/hmg/ddr327 (2011).
254 Ullrich, N. J. & Gordon, L. B. Hutchinson-Gilford progeria syndrome. *Handb Clin Neurol* **132**, 249-264, doi:10.1016/B978-0-444-62702-5.00018-4 (2015).
255 Wang, Y. *et al.* Blocking farnesylation of the prelamin A variant in Hutchinson-Gilford progeria syndrome alters the distribution of A-type lamins. *Nucleus* **3**, 452-462, doi:10.4161/nucl.21675 (2012).

8 Appendix

8.1 Tested concentrations of the combination SFN and FTI

SFN and FTI were used to establish a potential future therapy and to investigate the effect of such a drug combination. For this, it was investigated whether the simultaneous application of SFN (1 µM) and lonafarnib (FTI, 1.5 µM) could exert a synergistic effect on HGPS cells.

As shown in a representative Western blot, FTI treatment induced the accumulation of prelamin A in both control and HGPS cells treated for 4 days (Fig. 105 A, B).

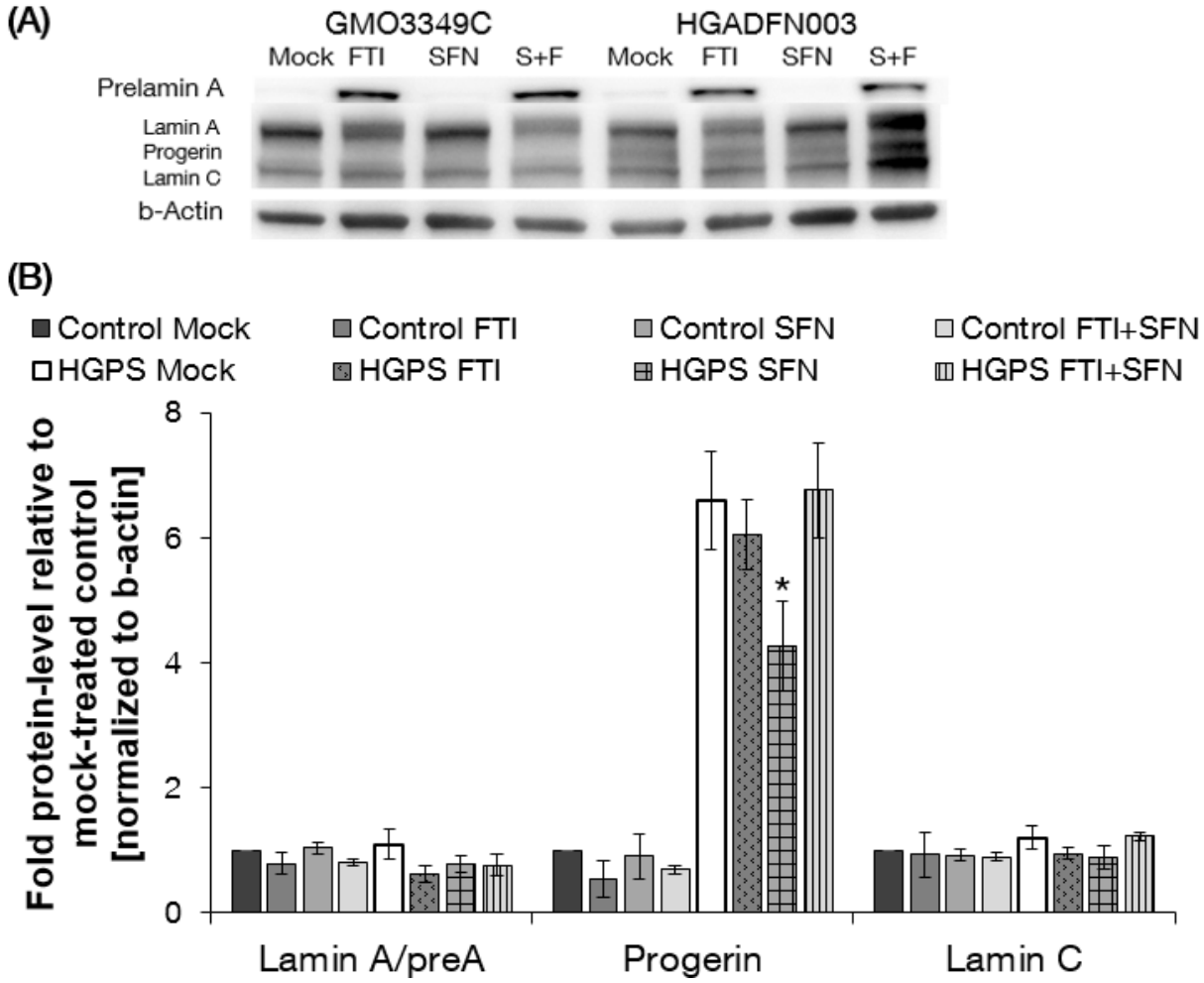

Figure 105: Western blot analyses of cells treated with vehicle, FTI, SFN or SFN+FTI. Control cells (left) and HGPS cells (right) were treated daily with the indicated drugs for 4 days (a representative image is shown, n=4). Blots were probed with prelamin A, lamin A/C, and b-actin antibodies. (B) Densitometric analyses of lamin A/prelamin A, progerin, and lamin C. Data represent the mean ± S.D. with respect to mock-treated control cells after values were normalized to b-actin (*p ≤ 0.05; n=4).

Prelamin A was barely detectable in either mock-treated or SFN-treated cells. The total lamin A and lamin C level was not changed significantly after SFN or FTI treatment in control or HGPS cells. Progerin levels were significantly reduced in HGPS cells treated with SFN for a period of 4 days. FTI treatment in combination with SFN did not lead to a reduction in progerin levels.

To further assess the effect of FTI ± SFN on the nuclear morphology, immunohistochemical analyses were performed with anti-prelamin A and anti-progerin antibodies (Fig. 106 A, B).

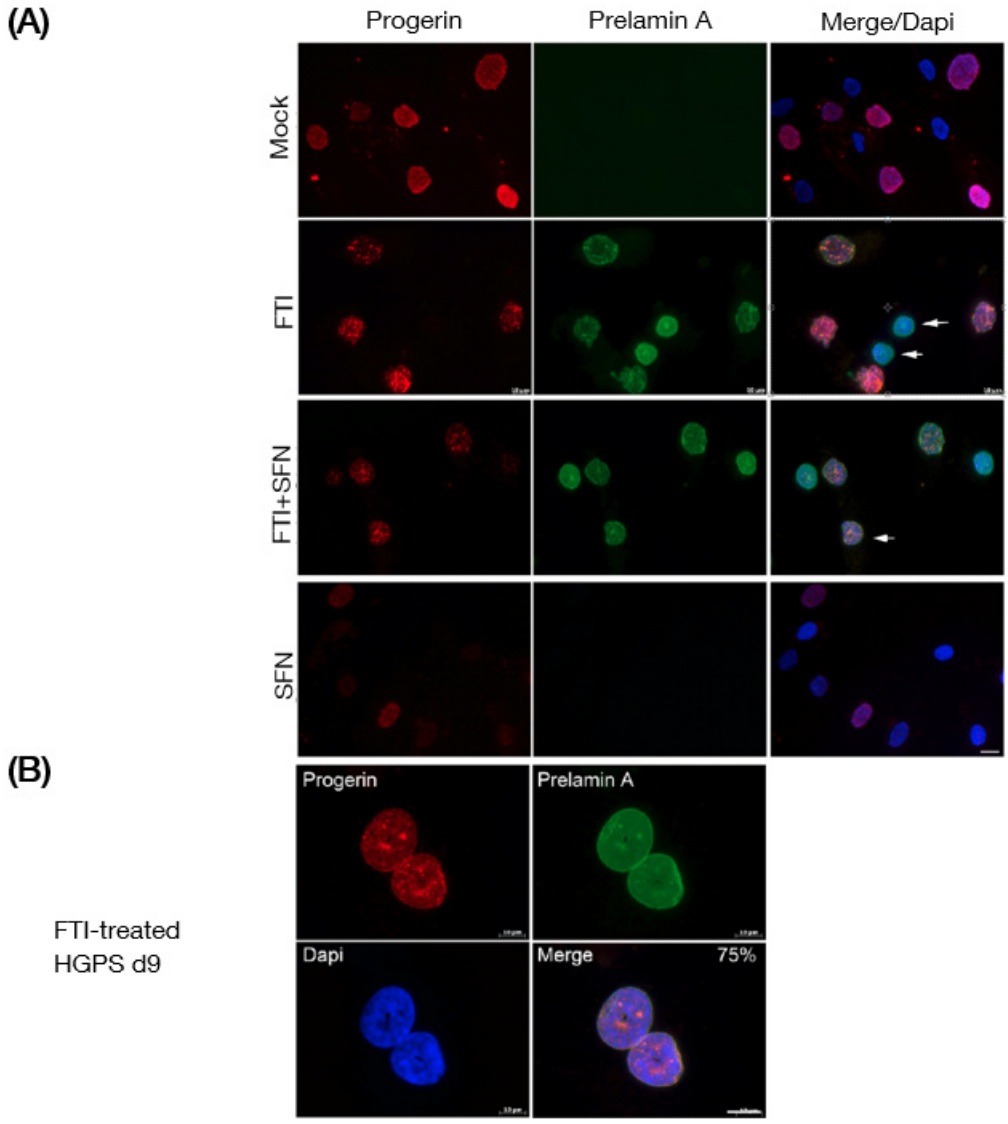

Figure 106: The localization of progerin and prelamin A in HGPS cells. (A) HGPS cells were mock-treated, treated with 1.5 µM FTI, 1 µM SFN or treated with a combination of 1.5 µM FTI and 1 µM SFN daily for 4 days. The merged images correspond to progerin, prelamin A and Dapi signals. The arrows indicate donut-shaped nuclei. Scale bar: 10 µM. (B) High magnification images of donut-shaped nuclei in HGPS cells treated with 1.5 µM FTI for 9 days. The cells were stained as indicated (n=3). Scale bar: 10 µm.

After 4 days of treatment, prelamin A was detected in FTI-treated cells only (Fig. 106 A). Progerin was detected in FTI- or FTI+SFN-treated cells as large aggregates within the nucleoplasm. The frequency of progerin-positive nuclei in these cells were similar to those observed in mock-treated HGPS cells. In the presence of FTI or FTI+SFN, HGPS nuclei exhibit a more ovoid nuclear shape. However, a significant number of cells harbored donut-shaped nuclei after 4 days of FTI treatment, as reported previously.[12,255] The average frequency of donut-shaped nuclei was 7% on day 4 of FTI treatment and had increased to approximately 35% by day 9. Moreover, after 9 days of FTI or FTI+SFN treatment, the frequencies of donut-shaped nuclei were similar and 75% of these nuclei were binucleated (Fig. 106 B). These nuclear alterations were not observed in mock- or SFN-treated cells. Suspecting that these nuclear alterations would affect the cellular growth, the proliferative properties of cells after treatment with both drugs was investigated (Fig. 107).

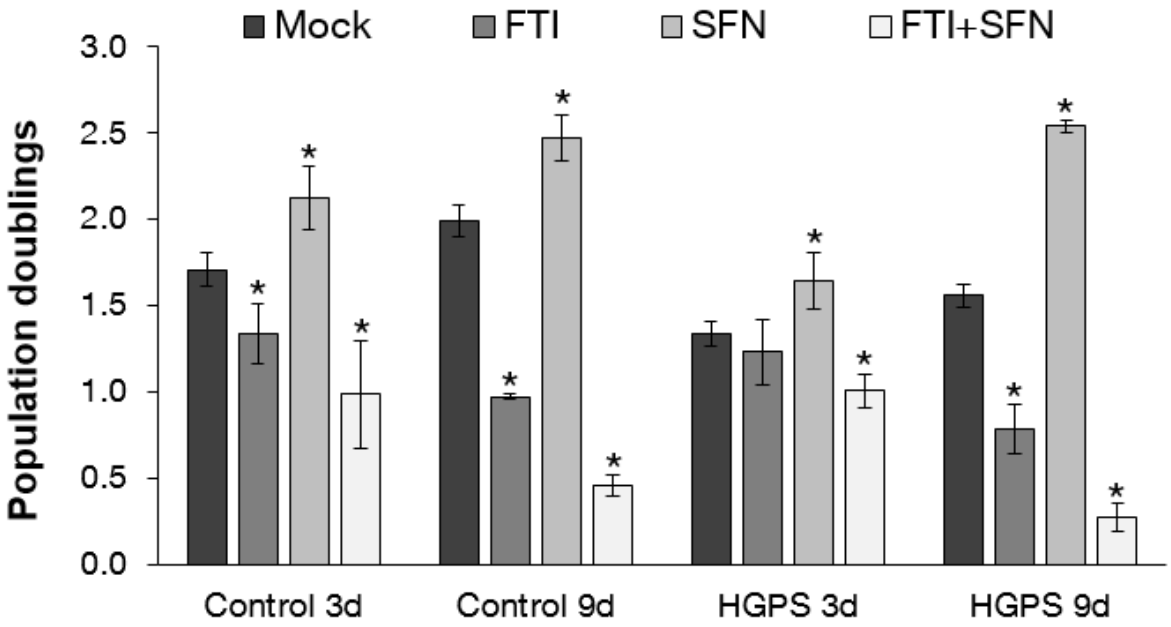

Figure 107: Cell proliferation of fibroblasts treated with the vehicle, FTI, SFN and FTI+SFN. Population doubling levels were calculated as stated in the Materials and Methods relative to mock-treated counterparts. Control and HGPS cells were mock-treated (vehicle DMSO) or treated daily with 1.5 µM FTI, 1 µM SFN, and 1.5 µM FTI+ 1 µM SFN for a period of 3 or 9 days (*$p \leq 0.05$; n=4).

While SFN treatment increased the growth potential of control and HGPS cells, FTI treatment with or without SFN reduced the growth rate of both cells.

To further validate the non-synergistic effect of SFN in combination with FTI, the levels of autophagy and proteasome activity were investigated (Fig. 108 A, B).

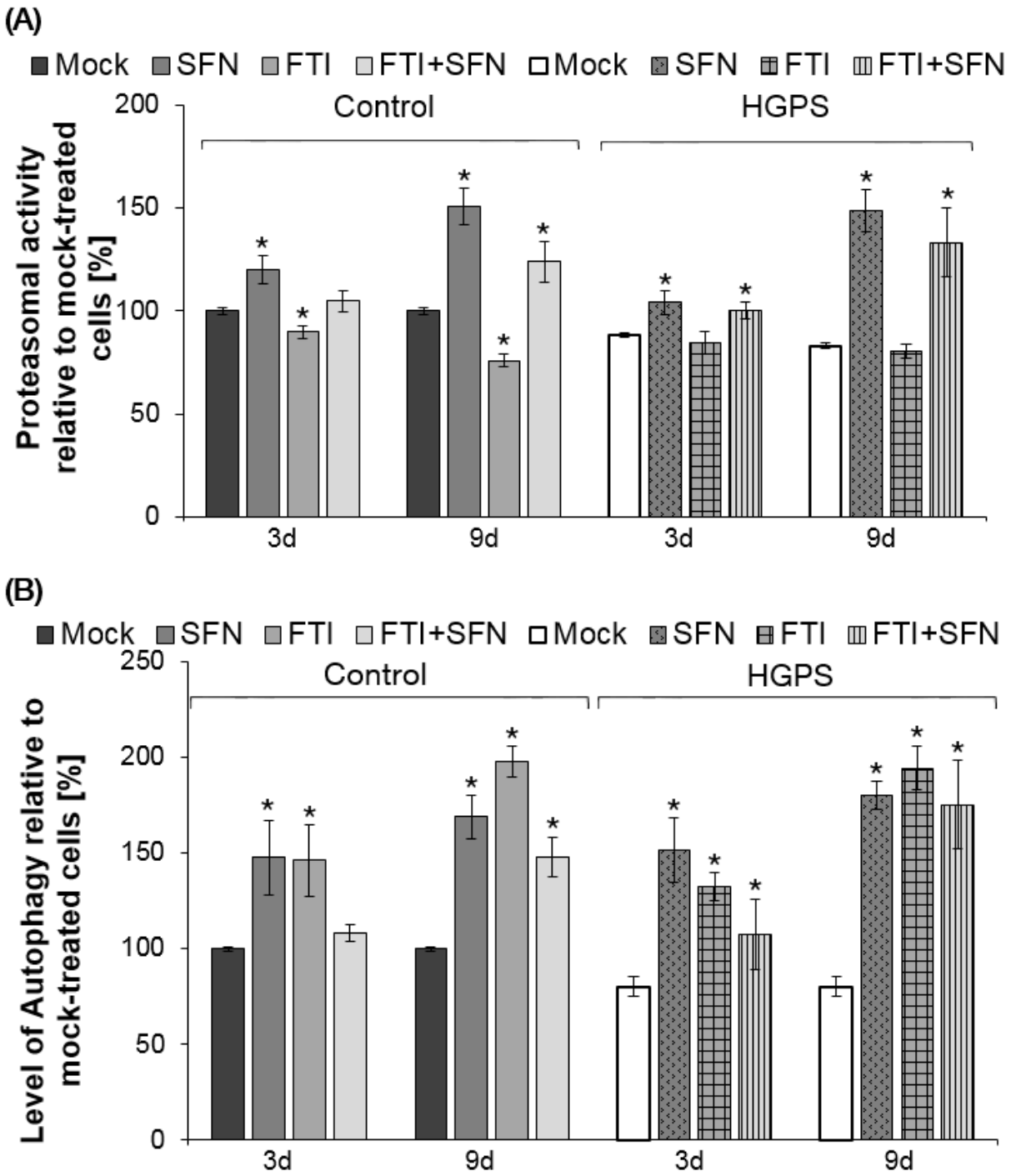

Figure 108: Alterations of the protein degradation after treatment with SFN, FTI or SFN+FTI. (A) Proteasome activity was determined by measuring chymotrypsin-like proteasome activity in 4 control and 4 HGPS cells using Suc-LLVY-AMC as a substrate. The percentage of activity was calculated relative to mock-treated cells. Data are presented as the mean ± S.D. (*p ≤ 0.05; n=4). (B) The same cells and culture condition as in (A) were used to determine autophagy activity by measuring monodansylcadaverine (MDC) levels with fluorescence photometry, as indicated in the Methods. Data are expressed as the mean ± S.D. relative to mock-treated control cells (*p ≤ 0.05; n=4).

As observed, SFN alone increased the proteasome activity of control and HGPS cells (Fig. 108 A) as well as the autophagy levels after 3 days and even more after 9 days

of treatment (Fig. 108 B). FTI was observed to decrease the proteasomal activity but enhances the autophagy levels after the indicated period of time. SFN in combination with FTI exhibit no synergistic effect. The proteasomal activity and autophagy activity were not as high as with SFN alone.
Collectively, these findings indicate that FTI induced cell cycle arrest and early cell death.[12]

FTI in combination with SFN exhibit no synergistic effect when applied at a concentration of 1.5 µM and 1.0 µM, respectively. For this, different concentration of FTI (0.5 µM, 1.0 µM) in combination with SFN (1.0 µM) were tested to investigate a positive effect.
First, the cellular growth of control and HGPS cells mock-treated or treated with the indicated drugs was investigated (Fig. 109 A, B).

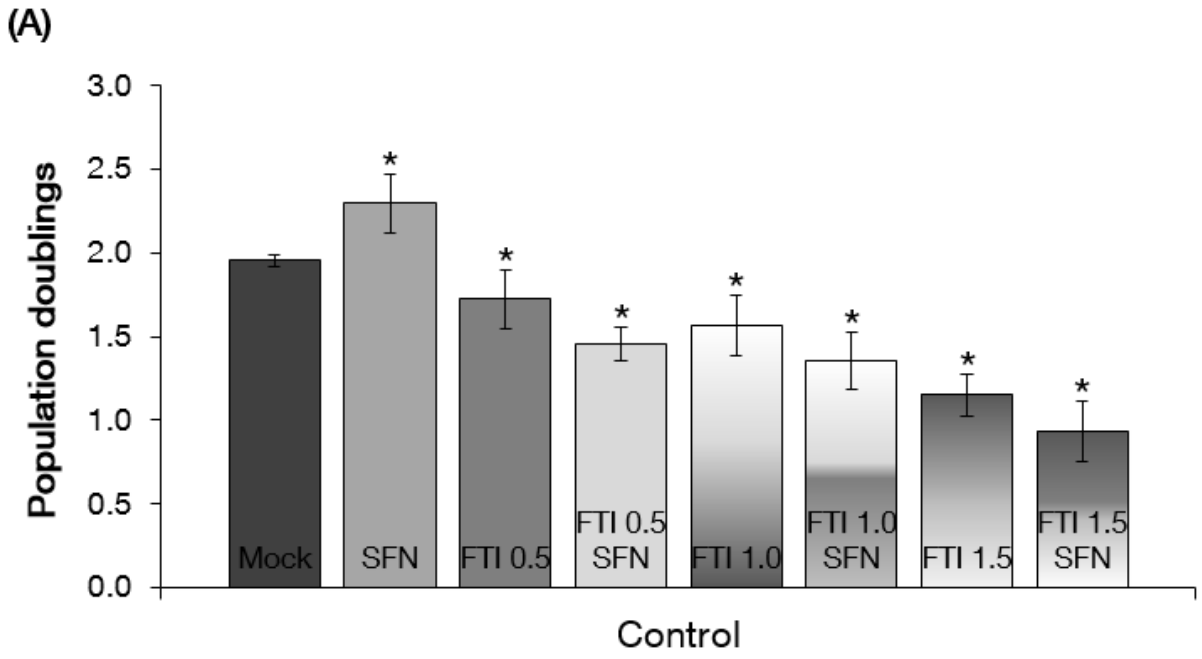

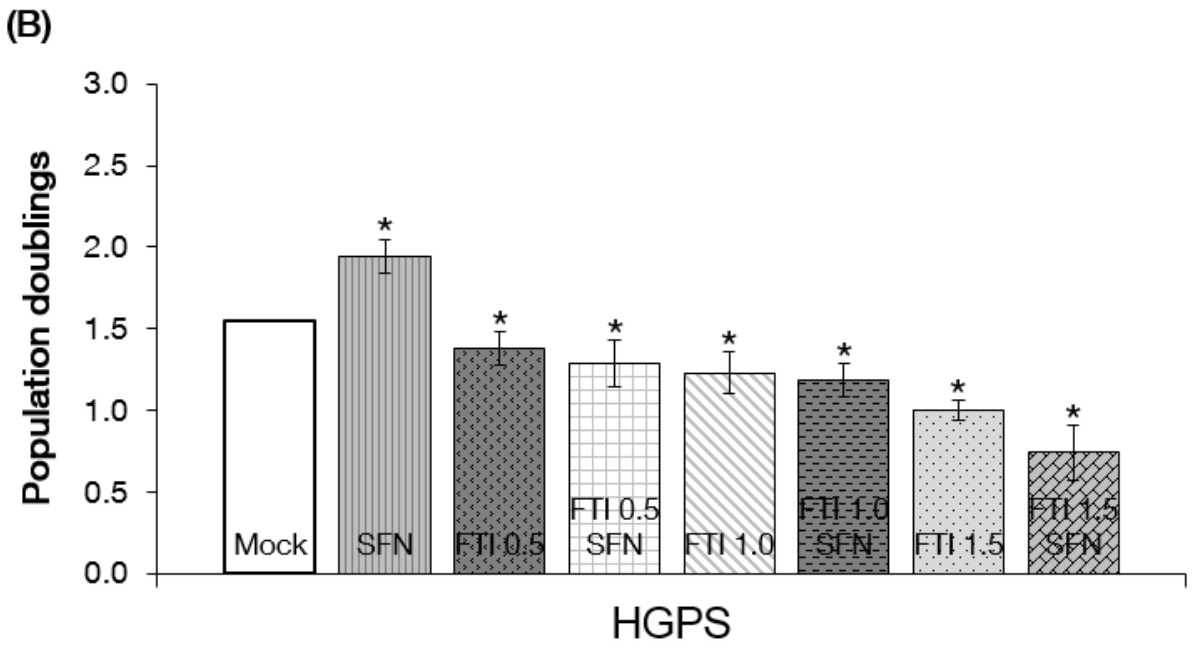

Figure 109: Cell proliferation of fibroblasts treated with the vehicle, SFN, FTI and FTI+SFN. Population doubling levels were calculated as stated in the Materials and Methods for control (A) and HGPS (B) cells that were mock-treated (vehicle DMSO) or treated daily with 1 µM SFN, 0.5 µM FTI, 1.0 µM FTI, 1.5 µM FTI, 1.0 µM SFN+0.5 µM FTI, 1.0 µM SFN+1.0 µM FTI, and 1.0 µM SFN+ 1.5 µM FTI for a period of 4 days. Data are expressed as the mean ± S.D. (*p ≤ 0.05; n=4).

While SFN-treated control and HGPS cells exhibit higher proliferation rates than mock-treated cells, FTI-treated cells show lower proliferation rates even at 0.5 µM. The proliferation rate was further reduced after treatment with the combinations of SFN and FTI.

Same samples as used for proliferation analysis were used for Western blot. A representative image is shown (Fig. 110).

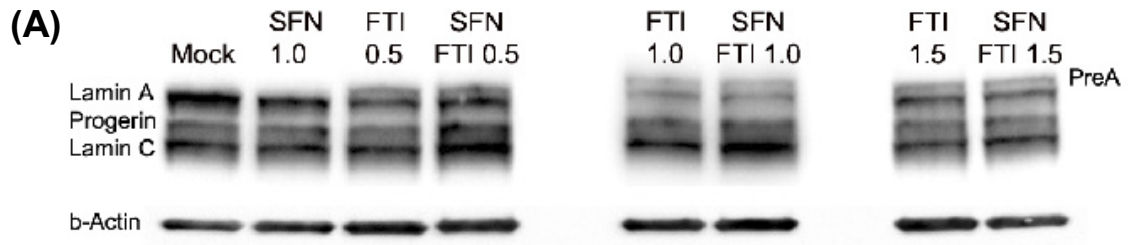

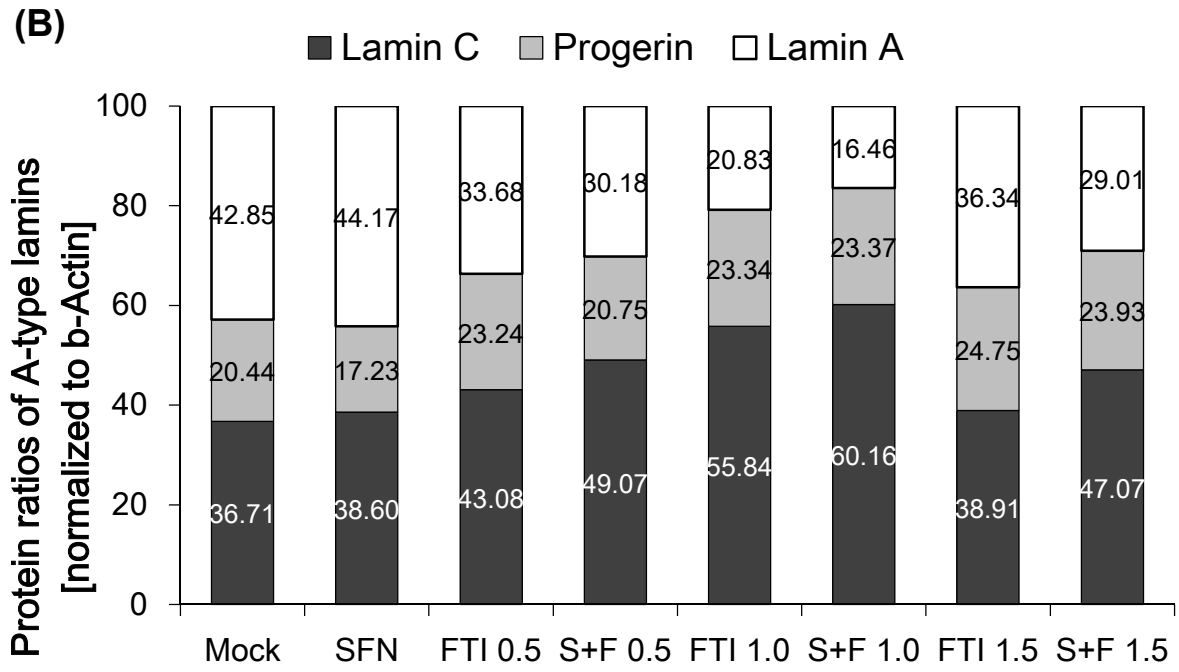

Figure 110: Western blot of HGPS cells treated with vehicle, SFN (S), FTI (F) or SFN+FTI. Cells were treated daily with the indicated drugs for 4 days (a representative image is shown). Blots were probed with lamin A/C and b-actin antibodies. (B) The ratios of lamin A, progerin, and lamin C were determined of HGPS cells within each sample analyzed by Western blot with anti-lamin A/C antibody in panel (A). Levels are presented as the ratios.

FTI treatment induced the accumulation of prelamin A in HGPS cells after treatment of 4 days. Even the lowest concentration of 0.5 µM FTI induced prelamin A expression. Prelamin A was barely detectable in either mock-treated or SFN-treated cells. The total lamin A and lamin C level was not changed significantly after SFN or FTI treatment in control or HGPS cells. Progerin levels were significantly reduced in HGPS cells treated with SFN for a period of 4 days. FTI treatment and FTI in combination with SFN did not lead to a reduction in progerin levels.

As all combinations of FTI and SFN resulted in cell death and no progerin clearance, the concentration of both drugs were lowered to have a less cytotoxic effect. FTI and SFN were applied at a concentration of 0.25 µM as single treatment or in combination for 9 days. The effect of the treatment was investigated by Western blot (Fig. 111 A, B) and by analysis of the proliferation rate (Fig. 112).

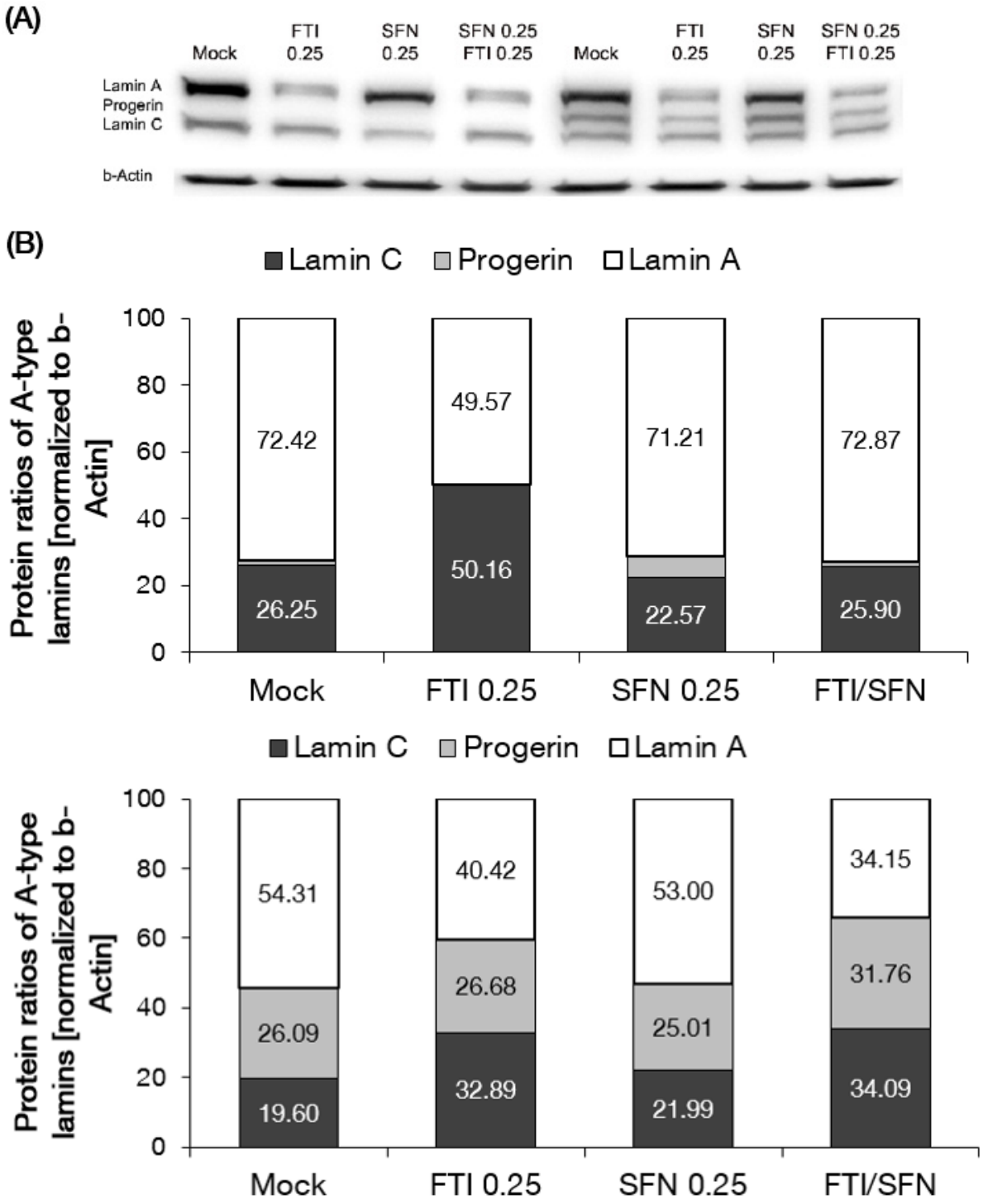

Figure 111: Western blot analyses of FTI and SFN at lower concentrations. Control and HGPS cells mock-treated or treated with 0.25 µM SFN, 0.25 µM FTI, and their combination for a period of 9 days were used for probing with antibodies against lamin A/C and b-Actin. Representative image is shown. (B) The ratios of lamin A, progerin, and lamin C were determined of control cells (upper panel) and HGPS cells (lower panel) within each sample analyzed by Western blot with anti-lamin A/C antibody in panel (A). Levels are presented as the ratios relative to mock-treated control cells.

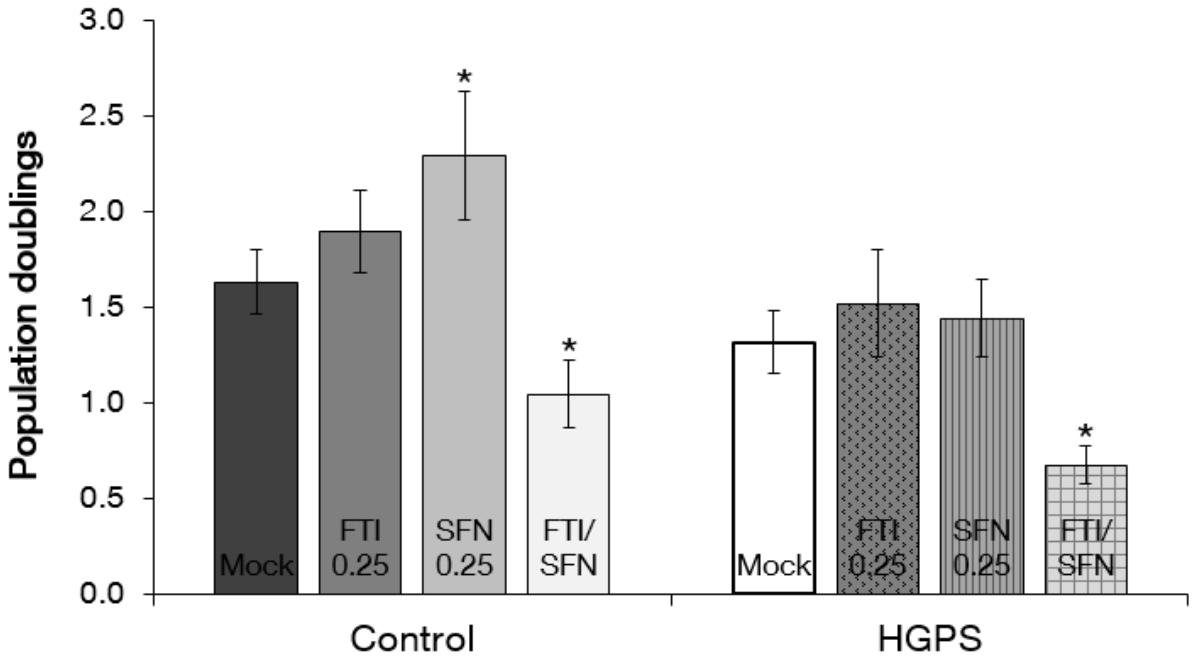

Figure 112: Population doublings of SFN/FTI in combination at low concentrations. Control and HGPS fibroblasts mock-treated or treated with 0.25 µM SFN, 0.25 µM FTI, and their combination for a period of 9 days were used to calculate the population doublings as stated in Material and Methods relative to mock-treated counterparts (*p ≤ 0.05, n=3).

Even at these low concentrations only the SFN single treatment showed beneficial effects in proliferation and progerin clearance of HGPS fibroblasts. This strategy of combining FTI and SFN and apply them at the same time for drug treatment failed.

8.2 Cycle treatment of 1 day 0.06 µM FTI and 2 days 1.0 µM SFN

In the following, data are only presented (Fig. 113-121) as the results were discussed in the main text (Chapter 4.3) according to the experiments.

8.2.1 Analysis of the effect of cycle treatment on HGPS proteostasis

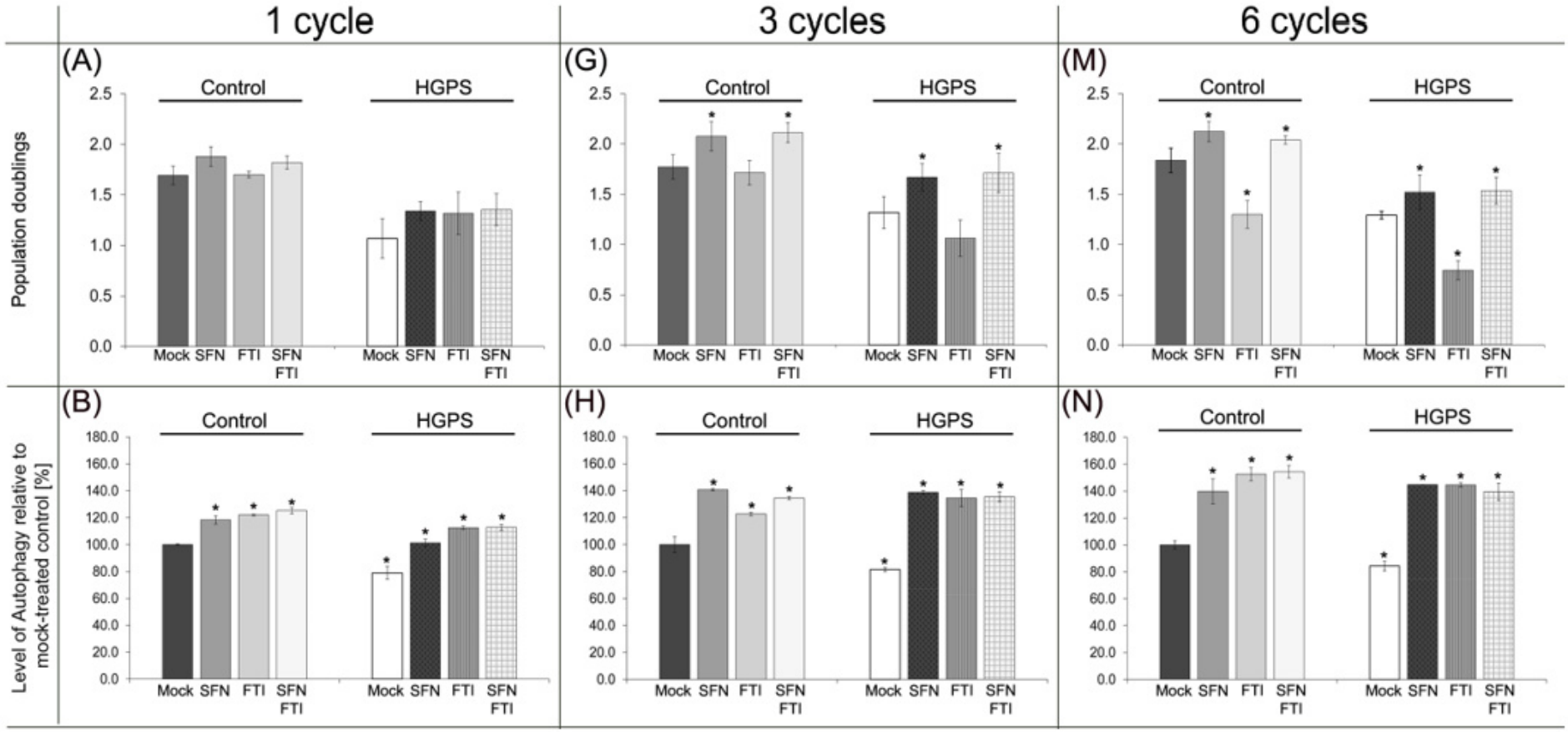

Figure 113: Different cycle length of SFN/FTI are not as effective as single SFN treatment.

(A, G, and M) Population doublings were calculated as stated in Materials and Methods for control and HGPS fibroblasts after the indicated cycles. Cells were mock-treated (vehicle DMSO) or treated with 1d 0.06 µM FTI/2d 1 µM SFN treatment (corresponds to 1 cycle). Single treatment of 0.06 µM FTI and 1 µM SFN for the corresponding time duration (3 days, 9 days, and 18 days) was carried along for comparison reasons (n=5). (B, H, and N) Same cells and culture conditions as above were used to measure the autophagy activity. Data are expressed as the mean ± S.D. relative to mock-treated control (*p ≤ 0.05; n=5).

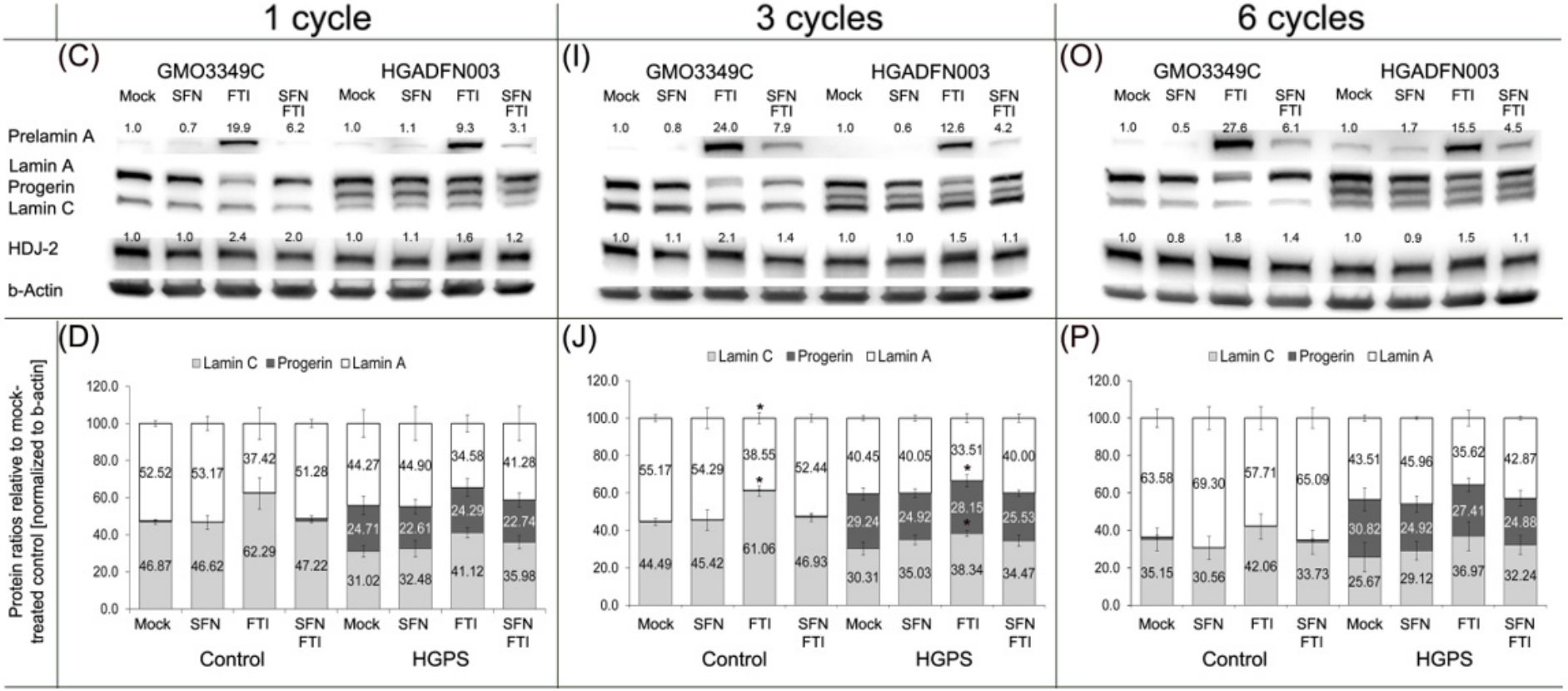

Figure 114: Different cycle length of SFN/FTI are not as effective as single SFN treatment (part 2).

(C, I, and O) Representative Western blots of A-type lamins in control and HGPS fibroblasts. Cells were treated in cycles where 1 cycle represents 1 day 0.06 µM FTI treatment followed by 2 days of 1 µM SFN. Blots were probed with prelamin A, lamin a/c, HDJ-2, and b-actin antibodies (n=4). Numbers above prelamin A and HDJ-2 bands indicate the fold-change of these proteins relative to their mock-treated counterparts. (D, J, and P) The ratios of A-type lamins were determined within each sample (*p ≤ 0.05; n=4) analyzed by Western blot with lamin A/C antibody in panel (C, I, and O).

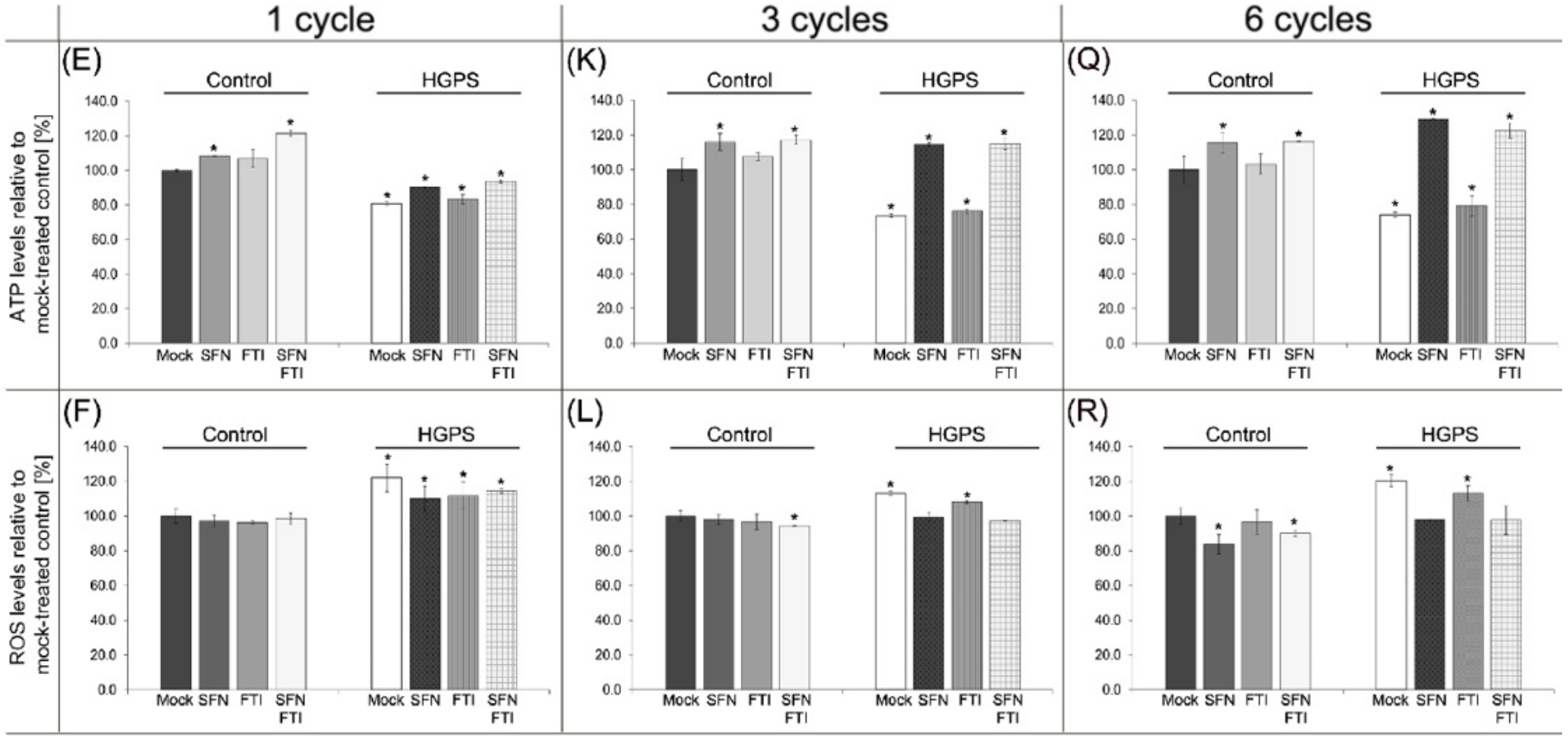

Figure 115: Different cycle length of SFN/FTI are not as effective as single SFN treatment (part 3).

(E, K, and Q) Cellular ATP levels of control and HGPS cells mock-treated or treated as described in (A) were measured using a CellTiter Glo assay as described in the Methods. Data represents the mean percentage ± S.D. relative to mock-treated control cells (*p ≤ 0.05; n=5). (F, L, and R) Intracellular ROS levels of mock-treated and FTI-, SFN-, and 1d FTI/2d SFN-treated control and HGPS cells were determined by measuring oxidized dichlorofluorescein (DCF) levels as described in the Methods. Data represents the mean percentage ± S.D. relative to mock-treated control (*p ≤ 0.05; n=5).

8.2.2 Analysis of the effect of cycle treatment on HGPS nuclear shape and prelamin A

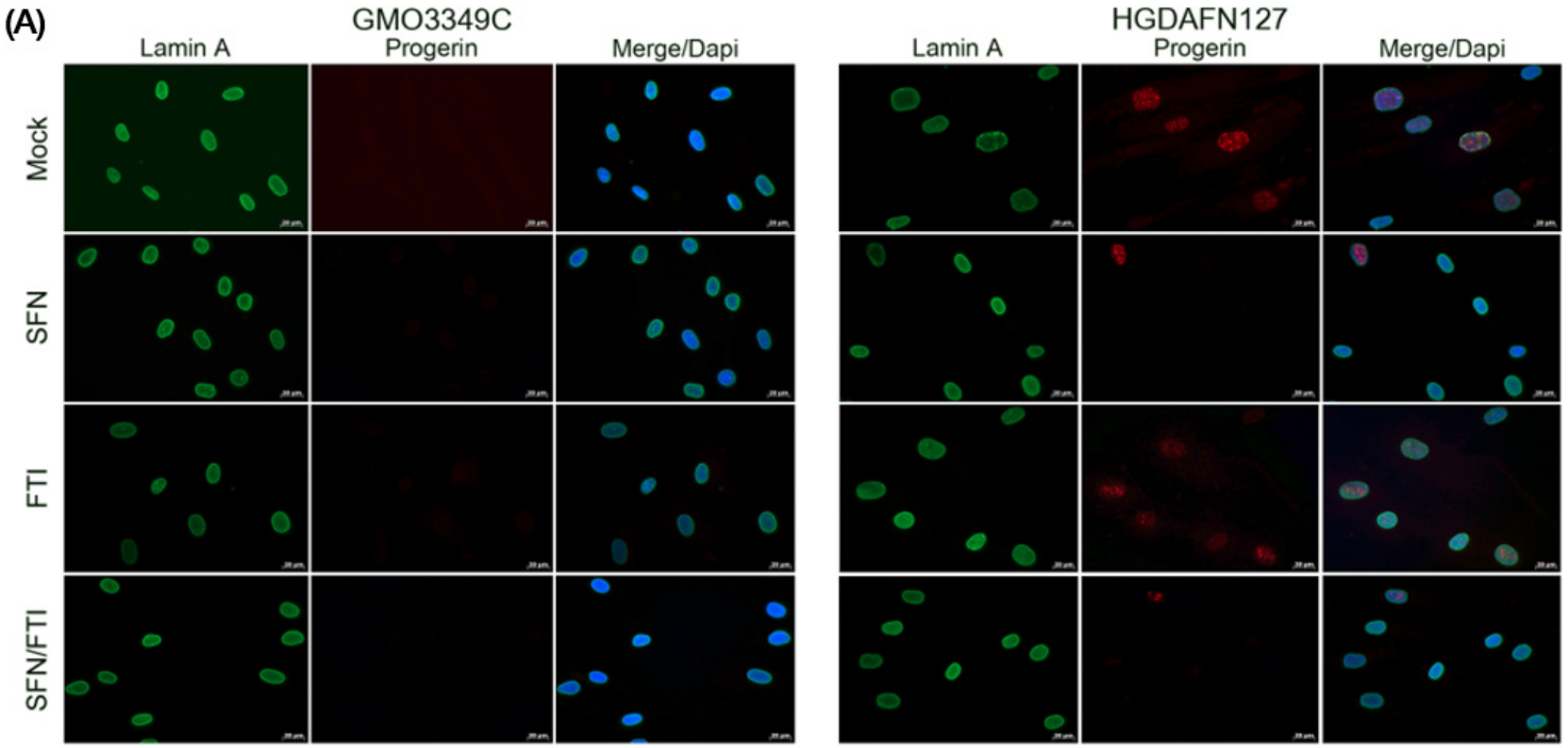

Figure 116: **A different cycle length of SFN/FTI reverses the nuclear shape alterations but shows prelamin A accumulation.**

(A) Immunochemistry was performed of control (GMO3349C) and HGPS (HGADFN127) fibroblast after 3 cycles of 1 day 0.06 µM FTI and 2 days 1 µM SFN treatment using antibodies directed against indicated proteins (lamin A and progerin). Single treatment of 0.06 µM FTI and 1 µM SFN for 9 days was carried along for comparison reasons. Cells were treated daily with fresh medium. Representative images are shown (n=4). Scale-bar: 20 µm.

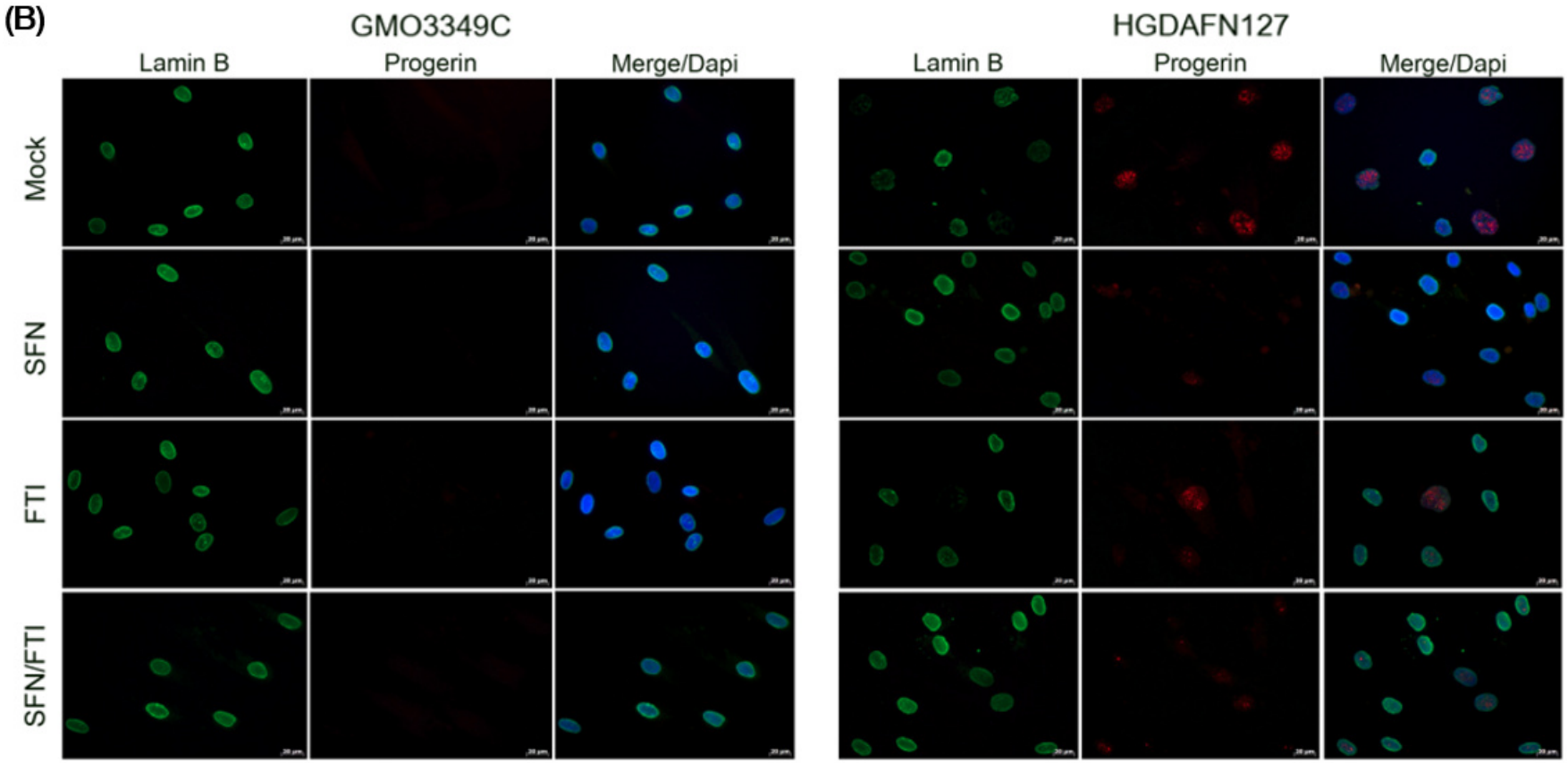

Figure 117: **A different cycle length of SFN/FTI reverses the nuclear shape alterations but shows prelamin A accumulation (part 2).**

(B) Immunochemistry was performed of the same cells as in (A). Antibodies directed against indicated proteins were used (lamin B1 and progerin). Representative images are shown (n=4) Scale bar: 20 µm.

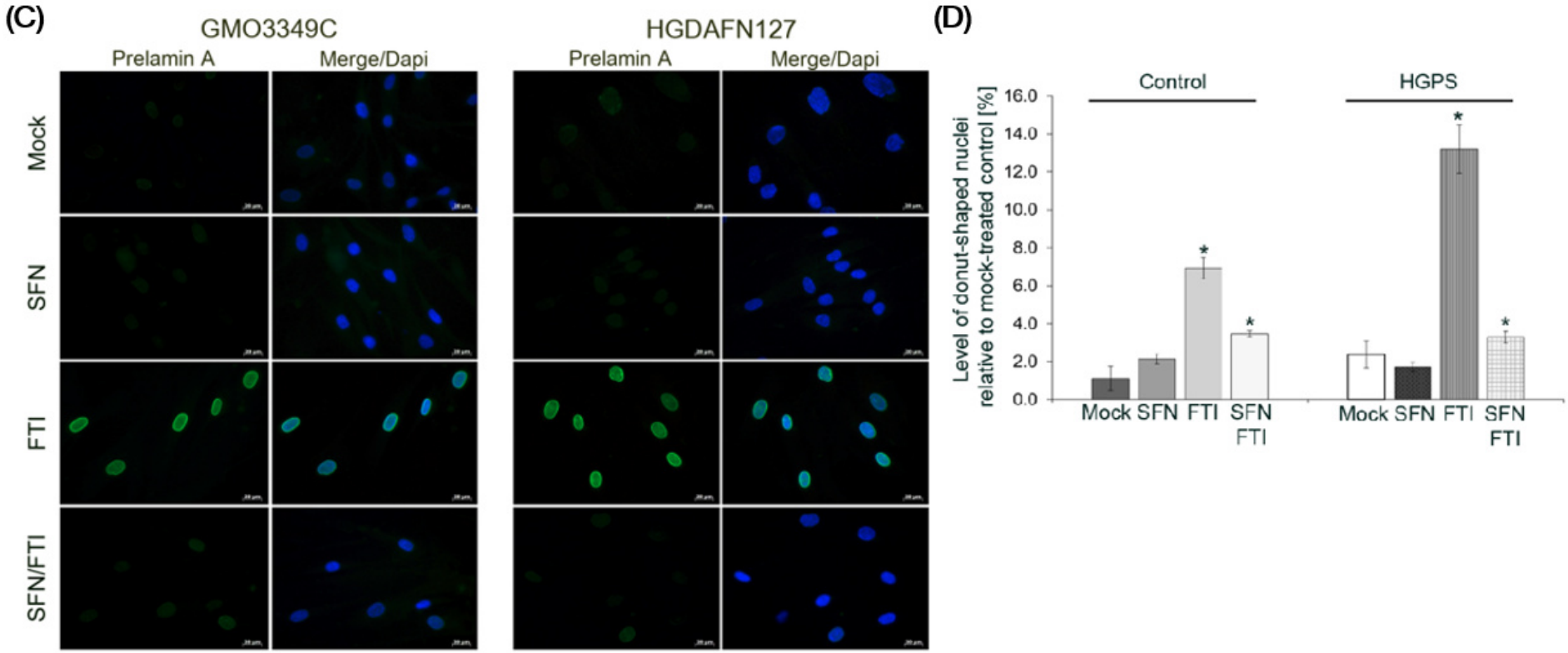

Figure 118: **A different cycle length of SFN/FTI reverses the nuclear shape alterations but shows prelamin A accumulation (part 3).**

(C) Immunochemistry was performed of the same cells as in (A). Antibody directed against prelamin A was used. Representative images are shown (n=4). Scale bar: 20 µm. (D) Same cells and conditions as in (A) were used to analyze donut-shaped nuclei by direct counts of lamin A-stained nuclei. An average of 1000 nuclei were counted. Upper panel shows donut-shaped nuclei. Lower panel shows the quantification of donut-shaped nuclei relative to mock-treated control. Data are presented as the mean ± S.D. (*$p \leq 0.05$; n=3).

8.2.3 Analysis of the effect of cycle treatment on HGPS DNA damage and repair

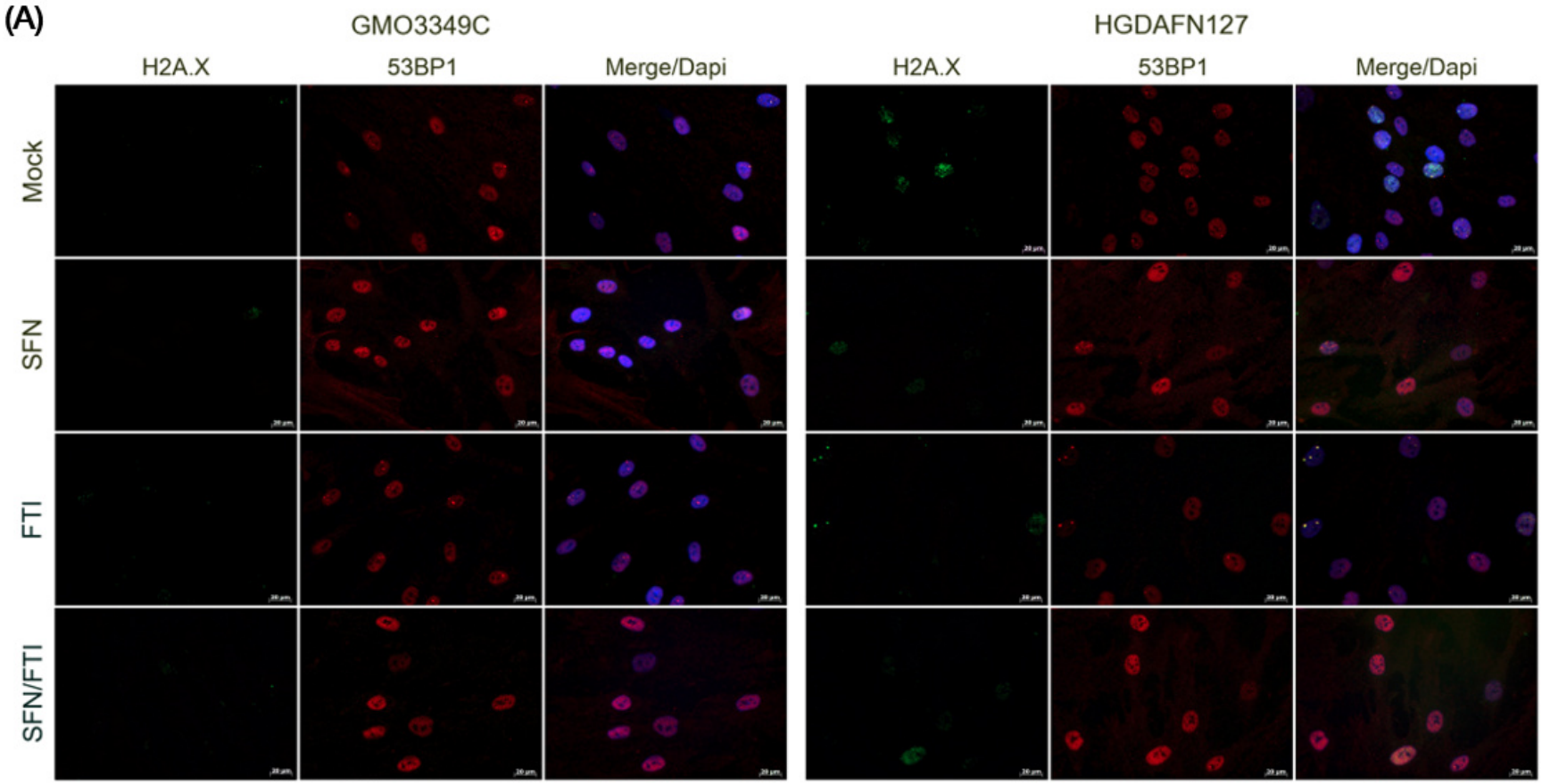

Figure 119: **DNA damage reduction is not as effective SFN single treatment when applying a different cycle length of SFN/FTI.**

(A) Immunochemistry was performed of control (GMO3349C) and HGPS (HGADFN003) fibroblast mock-treated or treated for 2 cycles with 1 day 0.06 µM FTI followed by 2 days 1 µM SFN. Single treatment of 0.06 µM FTI and 1 µM SFN for 9 days was carried along for comparison reasons. Cells were treated daily with fresh medium. Antibodies directed against H2A.X and 53BP1 were used. Representative images are shown (n=4). Scale-bar: 20 µm.

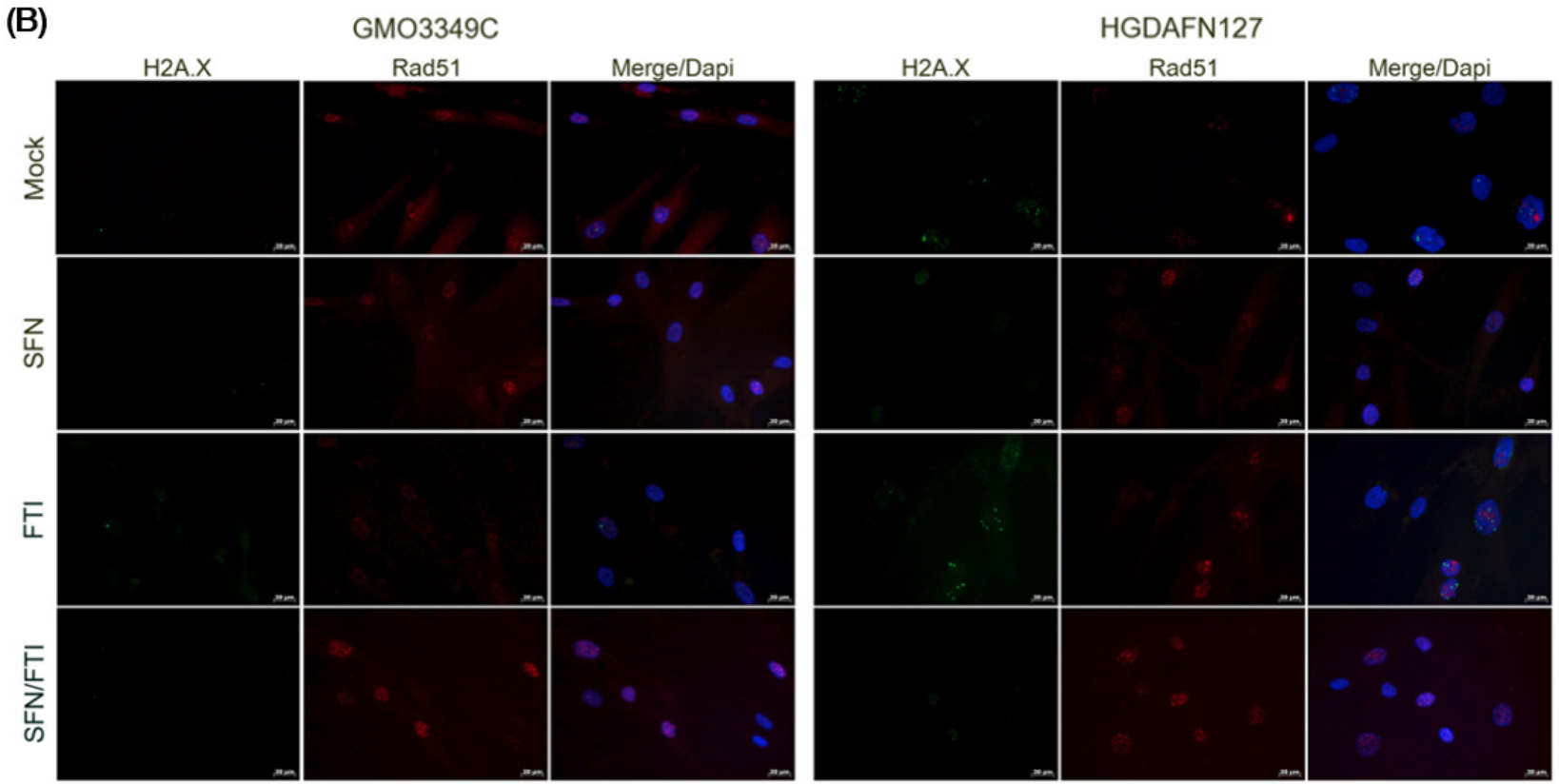

Figure 120: **DNA damage reduction is not as effective SFN single treatment when applying a different cycle length of SFN/FTI (part 2).**

(B) Same cells and conditions as in (A) were used to perform immunochemistry using antibodies directed against H2A.X and Rad51. Representative images are shown (n=4). Scale-bar: 20 µm.

(C)

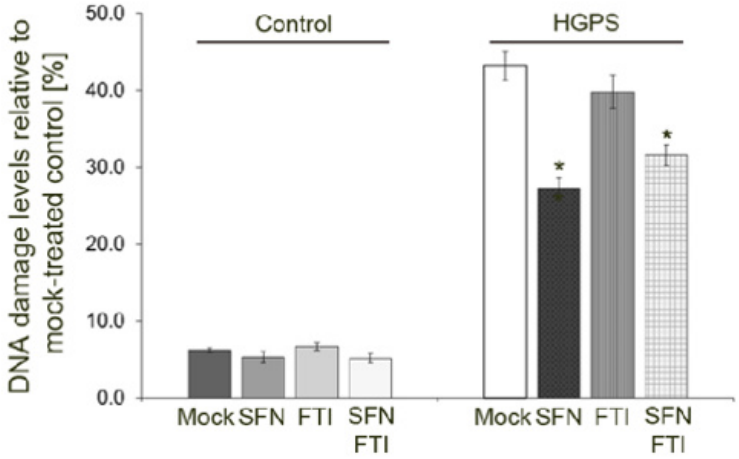

Figure 121: DNA damage reduction is not as effective SFN single treatment when applying a different cycle length of SFN/FTI (part 3).

(C) Same cells and conditions as in (A) were used to analyze DNA damage by direct counts of H2A.X-stained nuclei. An average of 1000 nuclei were counted. Quantification of DNA damage levels are relative to mock-treated control. Data are presented as the mean ± S.D. (*$p \leq 0.05$; n=3).

8.3 The effect of 1 µM SFN on mouse fibroblasts with Lmna$^{G609G/G609G}$ mutation

First, SFN was applied at a concentration of 1 µM to mouse fibroblasts harboring a homozygous mutation (G609G, Gd/d) and to control mouse fibroblasts (G+/+). Proliferation rates (Fig. 122 A, B) as well as protein degradation activation, progerin clearance, and mitochondrial function were investigated after the indicated time points.

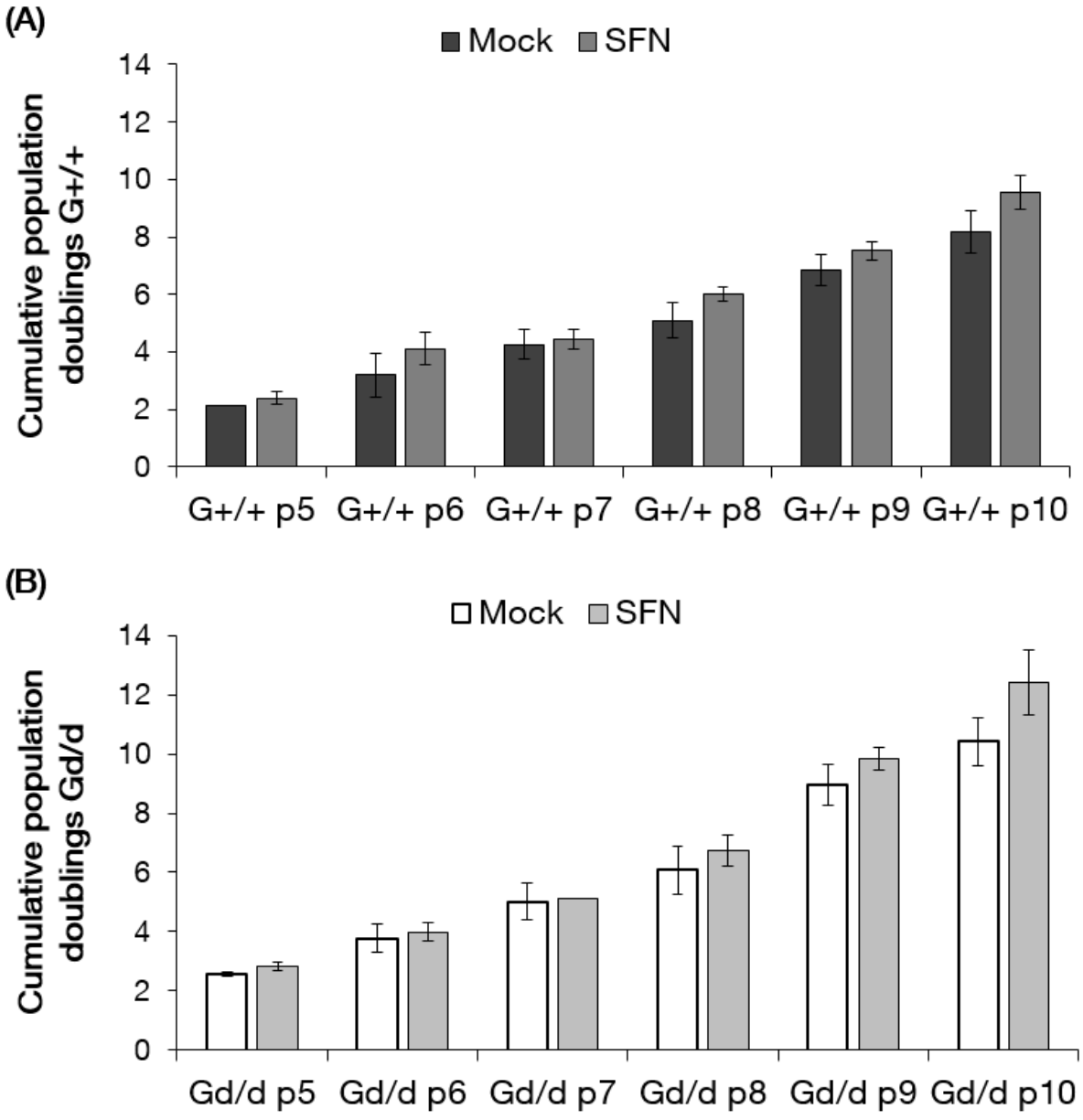

Figure 122: CPD of mouse fibroblasts mock-treated or treated with 1 µM SFN. Cumulative population doublings were calculated as stated in Materials and Methods for control (G+/+, A) and HGPS (Gd/d, B) mouse fibroblasts after the passage numbers. Cells were either mock-treated (vehicle DMSO) or treated with 1 µM SFN.

SFN induced a sustained growth of both control and HGPS mouse fibroblasts compared to mock-treated cells. However, the increased proliferation rate of SFN-treated cells was not significant.

The analysis of the two protein degradation pathways, proteasome and autophagy, revealed a significant increase after 9 days of SFN treatment of HGPS mouse fibroblasts compared to mock-treated counterpart (Fig. 123 A, B). In control mouse fibroblasts, proteasome was significantly increased after 50 days of SFN treatment and autophagy levels were significantly increased after 41 days of SFN.

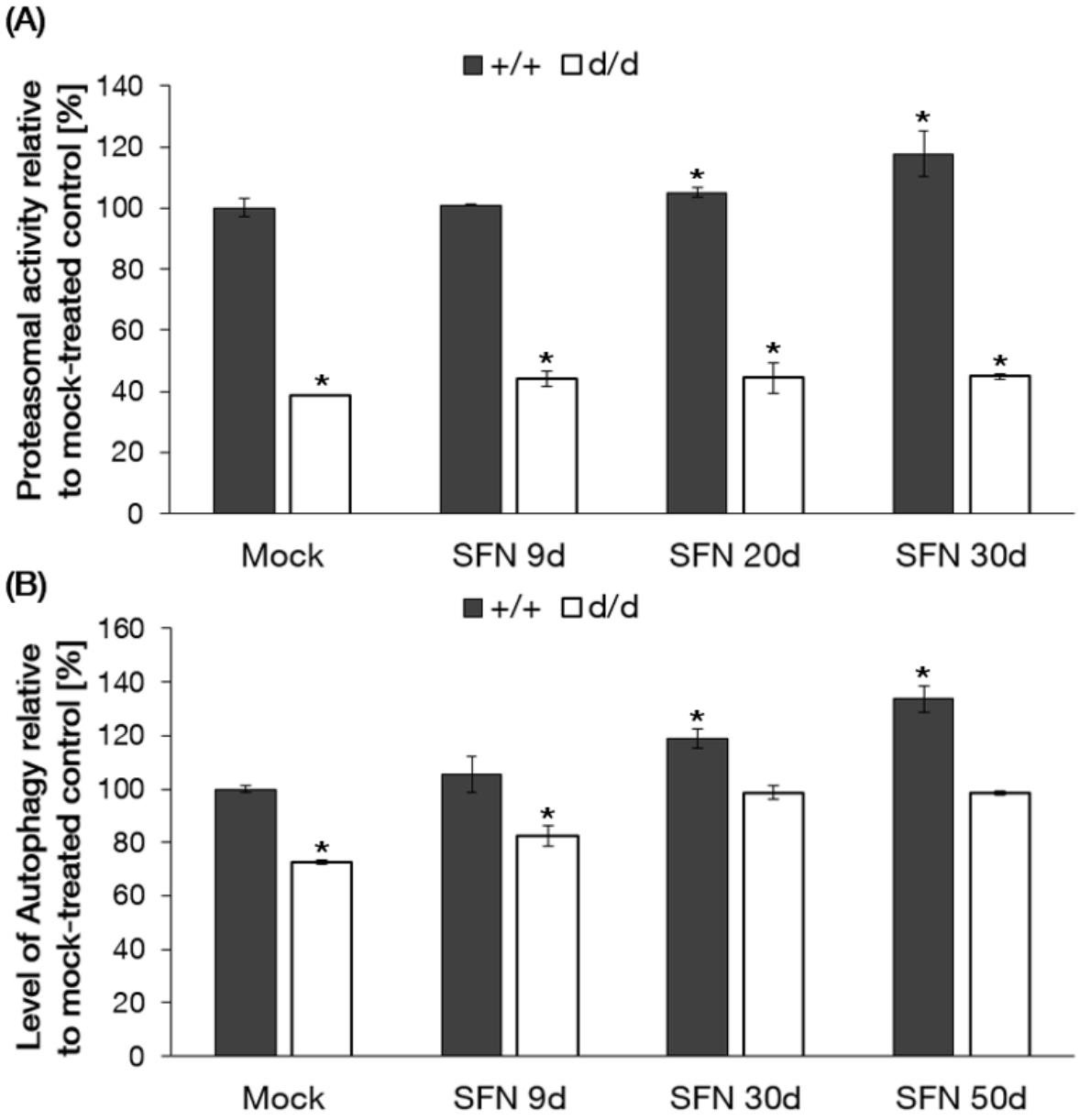

Figure 123: Activation of protein degradation pathways of mouse fibroblasts mock-treated or treated with 1 µM SFN. (A) Proteasomal activity and (B) Autophagy activity of control (G+/+) and HGPS (Gd/d) mock-treated or SFN-treated was measured as stated in Material and Methods. Data are presented as the mean ± S.D. relative to mock-treated control cells (*p ≤ 0.05; n=3).

The higher levels of the protein degradation pathways led to a decrease of progerin by 24 % (Fig. 124 A, B). While lamin A levels were increased, lamin C levels were maintained after treatment with SFN.

(A)

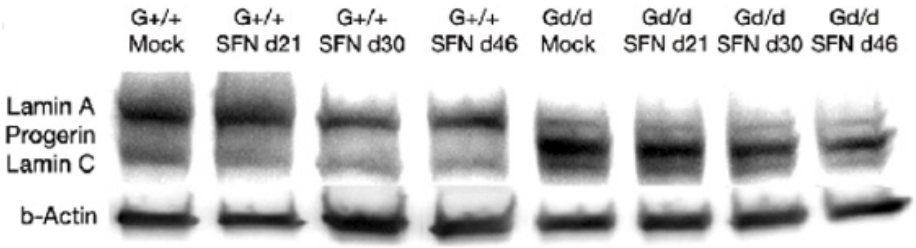

(B)

Ratio	G+/+	G+/+ SFN d21	G+/+ SFN d41	G+/+ SFN d66
Lamin A	54.35 ± 1.64	62.16 ± 3.08	64.62 ± 2.29	65.40 ± 1.57
Progerin	2.60 ± 0.23	2.23 ± 0.56	2.49 ± 0.54	2.79 ± 1.12
Lamin C	43.05 ± 1.71	35.61 ± 2.06	32.89 ± 1.95	31.81 ± 1.14

Ratio	Gd/d	Gd/d SFN d21	Gd/d SFN d41	Gd/d SFN d66
Lamin A	16.15 ± 4.81	20.75 ±4.40	25.42 ± 4.66	26.99 ± 3.98
Progerin	48.61 ± 4.11	41.64 ± 3.23	37.84 ± 3.45	36.93 ± 1.06
Lamin C	35.24 ± 5.60	37.61 ± 3.24	36.74 ± 2.18	36.08 ± 2.28

Figure 124: Western blot of mouse fibroblasts mock-treated or treated with 1 µM SFN. (A) Representative Western blot of control (G+/+) and HGPS (Gd/d) mock-treated or treated with 1 µM SFN at the indicated time. Antibodies against lamin A/C and b-Actin were used (n=2). (B) Quantification of the ratios of A-type lamins. Data are presented as the mean ± S.D. (n=2).

Reactive oxygen species levels and intracellular ATP levels were also found to be improved by 1 µM SFN (Fig. 125 A, B). Control and HGPS mouse fibroblasts showed significantly reduced ROS levels after 9 days of SFN treatment. ATP levels were significantly increased after 41 days of SFN treatment. The improvements of ROS and ATP levels were sustained during the long-term treatment of SFN.

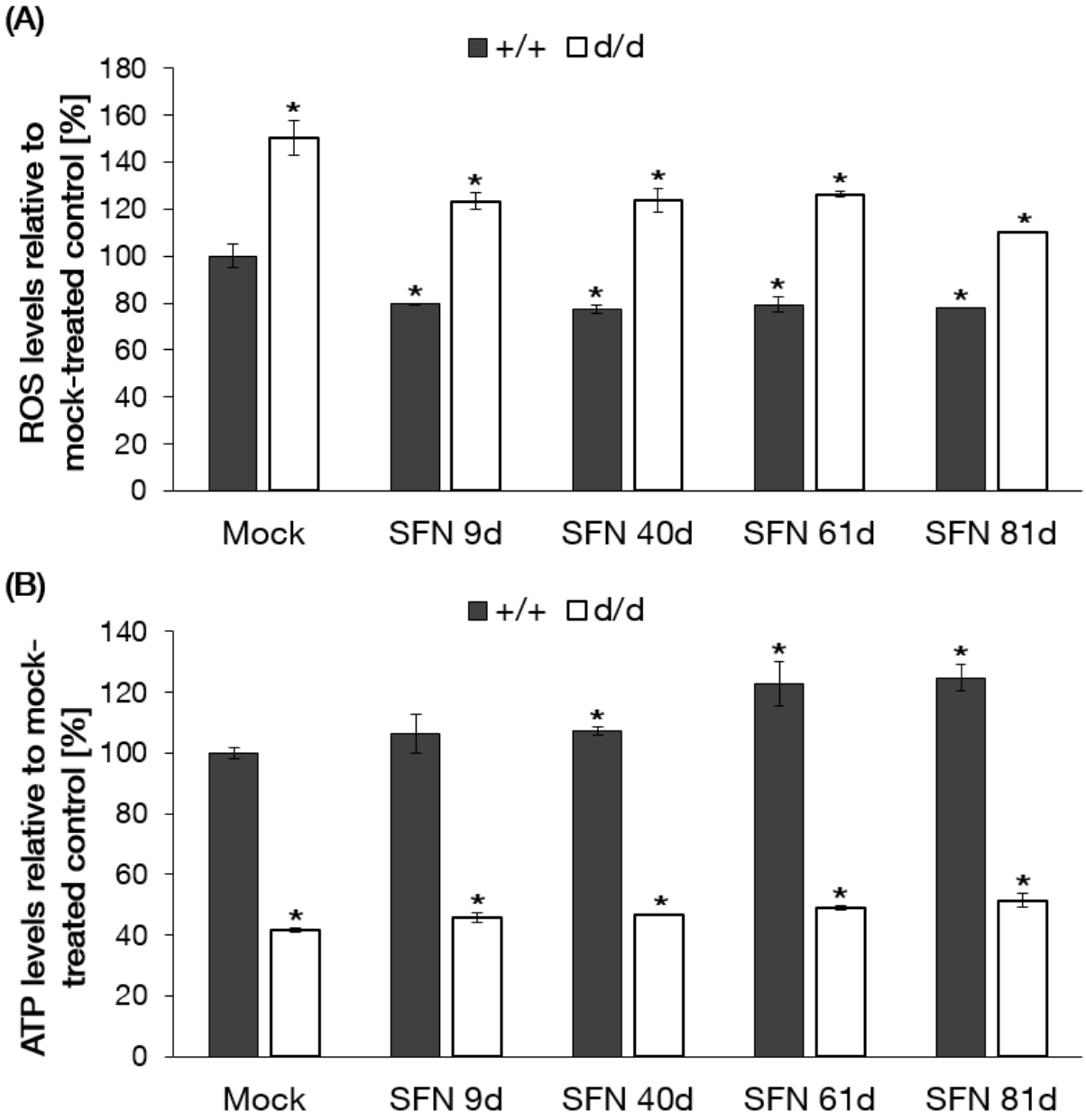

Figure 125: Mitochondrial function of mouse fibroblasts treated with 1 µM SFN. (A) Reactive oxygen species (ROS) levels of control (G+/+) and HGPS (Gd/d) mock-treated or treated with 1 µM SFN at the indicated time were measured as stated in Material and Methods. Data are presents as the mean percentage ± S.D. (*p ≤ 0.05; n=2). (B) Intracellular ATP levels were determined of the same cells as in (A). Data are presents as the mean ± S.D. (*p ≤ 0.05; n=2).

Immunofluorescence analysis were performed to investigate the distribution and expression of nuclear envelope proteins and the DNA damage marker γH2A.X (Fig. 126 A-D).

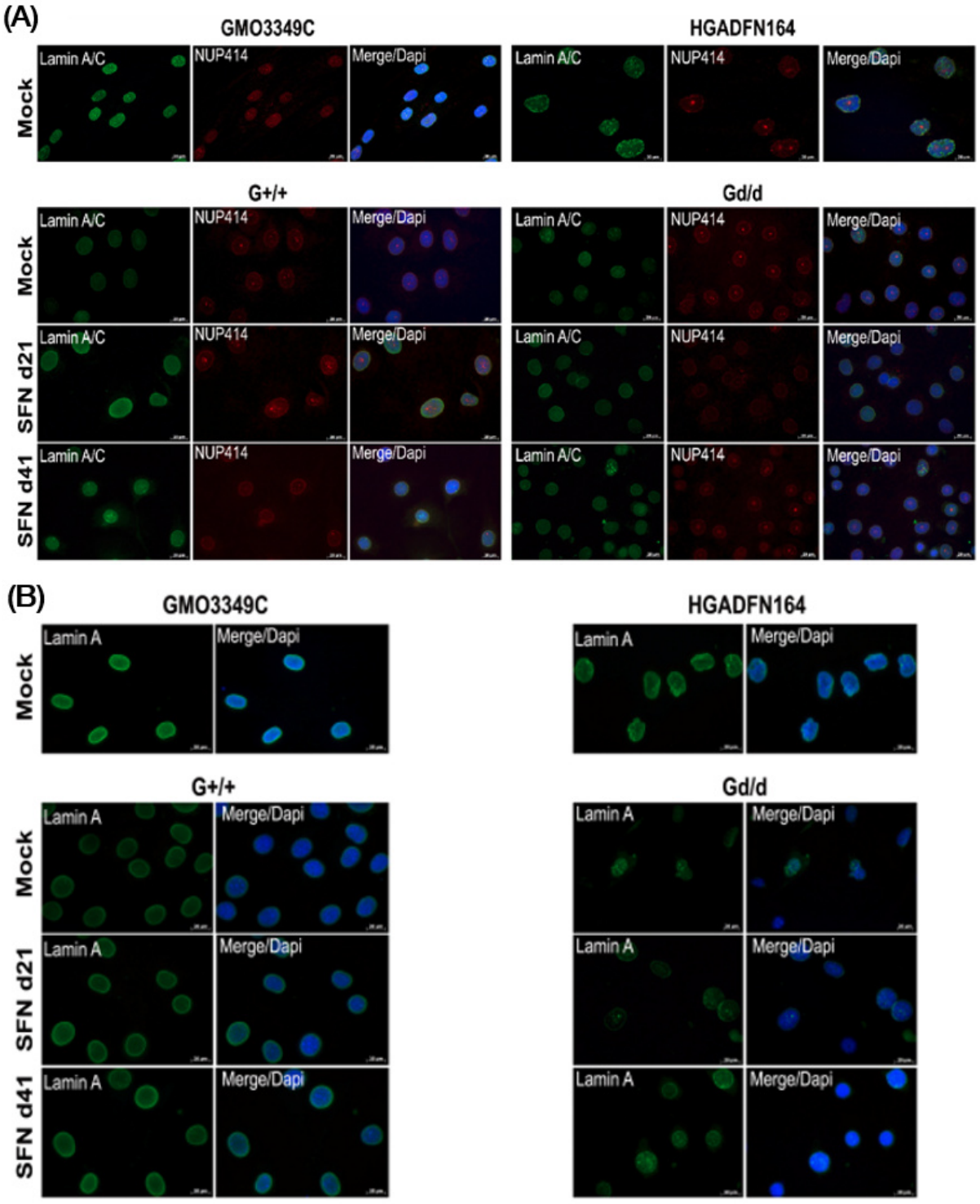
(A)
GMO3349C
HGADFN164
G+/+
Gd/d
Mock
SFN d21
SFN d41
Lamin A/C
NUP414
Merge/Dapi
(B)
GMO3349C
HGADFN164
G+/+
Gd/d
Mock
SFN d21
SFN d41
Lamin A
Merge/Dapi

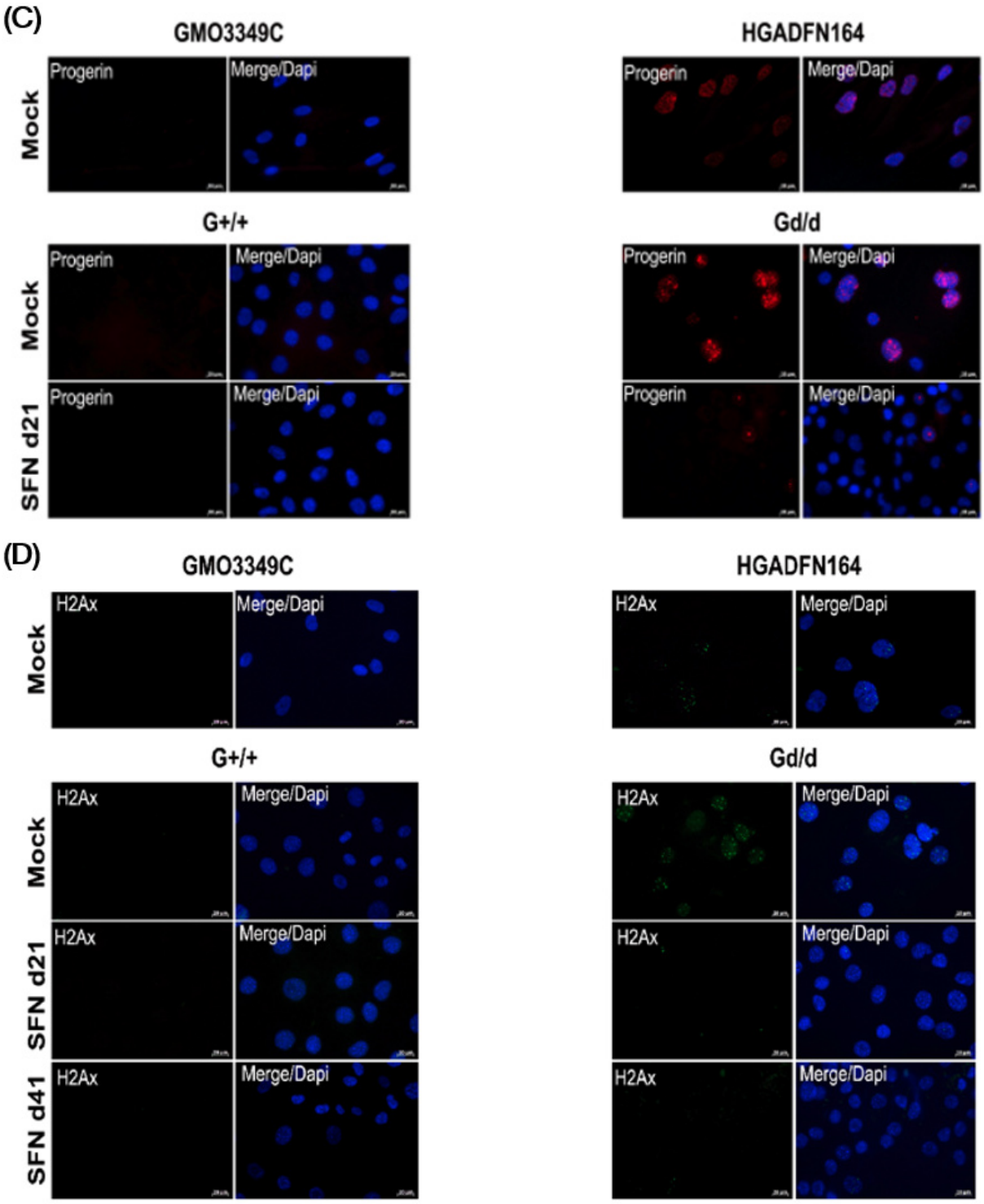

Figure 126: Immunochemistry of mouse fibroblasts after 1 µM SFN. (A) Immunochemistry was performed of the control mouse fibroblasts (G+/+) and HGPS mouse fibroblasts (Gd/d). Human control and HGPS fibroblasts were carried along for comparison reasons. Antibodies directed against indicated proteins were used (lamin A/C, NUP414). Representative images are shown (n=4) Scale bar: 20 µm. (B, C, and D) same cells as in (A) were used to stain with antibodies directed against lamin A, progerin, and γH2A.X (n=4).

The same results as for the SFN treatment described in Chapter 4.4 was observed with 1 µM SFN. Briefly, SFN treatment did not alter the distribution of lamin A/C and the nuclear pores in control cells of human and mouse (Fig. 126 A). In human HGPS and mouse fibroblasts, 1 µM SFN increased the expression of lamin A/C nuclear shape abnormalities were further decreased. The distribution and expression of the nuclear pores were normalized and showed rim-like staining after 41 days.
Staining of lamin A and progerin revealed weaker staining of lamin A in control mouse fibroblasts than in control human fibroblasts (Fig. 126 B, C). Progerin was not detected in both cell lines. After SFN treatment, lamin A levels were increased. Human and mouse HGPS fibroblasts showed progerin accumulation in the most nuclei and lamin A expression was weaker compared to human control cells. Moreover, lamin A was barely detectable in mouse HGPS fibroblasts due to the homozygous mutation. SFN treatment reduced the number of progerin-positive cells and increased the intensity of lamin A.
Next, staining with the DNA damage marker γH2A.X revealed that human and mouse HGPS fibroblasts exhibit elevated levels of DNA DSBs compared to their control counterparts (Fig. 126 D). SFN treatment reduced the levels of DNA damage after 21 days of treatment of human and mouse HGPS fibroblasts.

Finally, mouse fibroblasts and human fibroblasts were compared by Western blot analysis to evaluate potential differences according to their lamin A/C expression (Fig. 127 A-C).

(A)

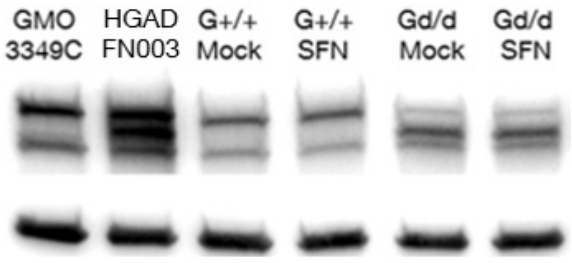

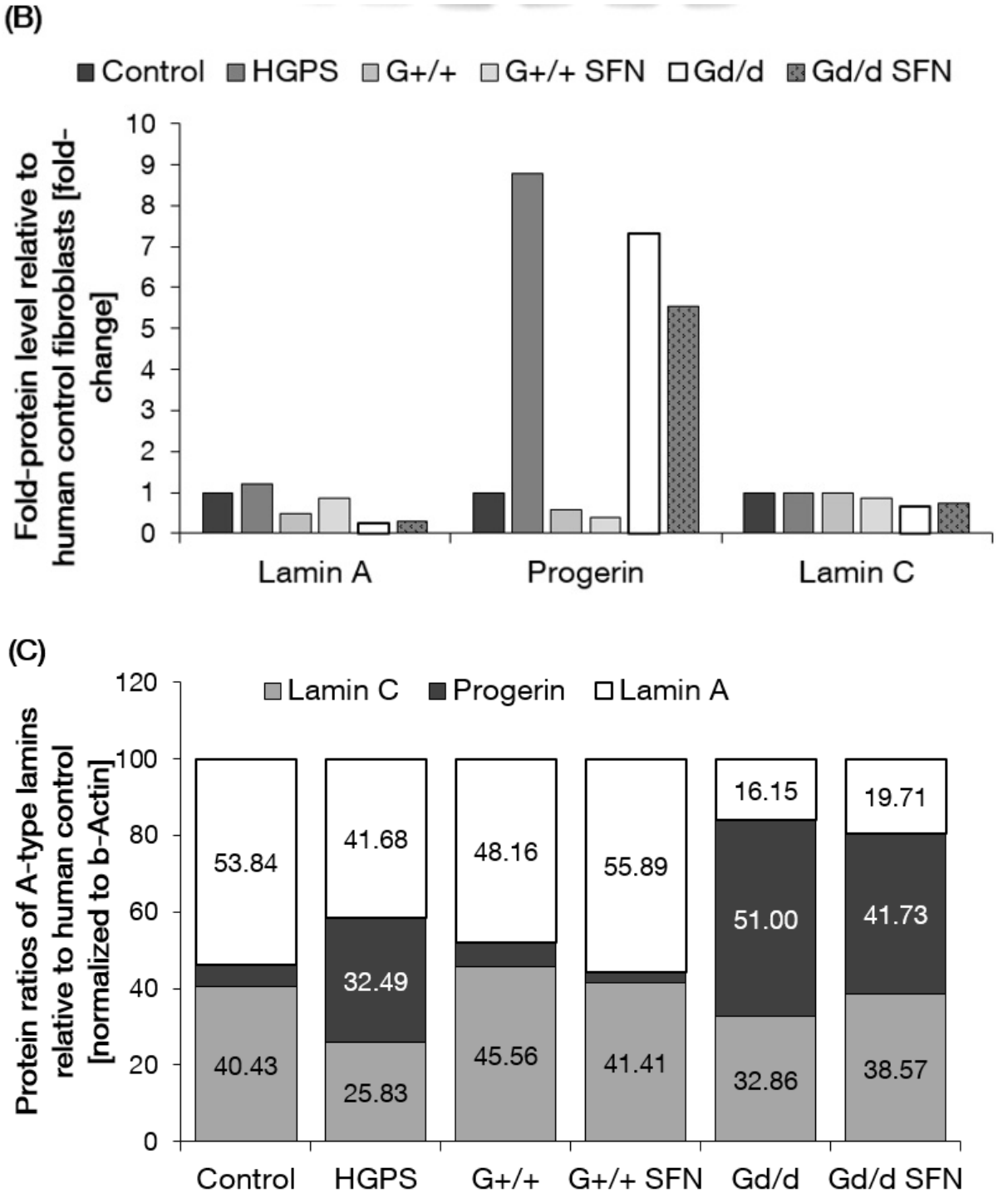

Figure 127: Western blot analysis of human and mouse fibroblasts. (A) Representative Western blot of human control (GMO3349C), human HGPS (HGADFN003), mouse control (G+/+), SFN-treated mouse control (G+/+ SFN), mouse HGPS (Gd/d), and SFN-treated mouse HGPS (Gd/d SFN) fibroblasts. Antibodies against lamin A/C and b-Actin were used (n=2). (B) Analysis of the fold-change of lamin A, progerin, and lamin C levels relative to human control (GMO3349C) and normalized to b-Actin. Same cells as in (A) were used. Data are presents as the fold-change ± S.D. (n=2). (C) Same cells as in (A) were used to quantify the ratios of the A-type lamins (n=2).

As indicated by Western blot, the expression levels of lamin A, progerin, and lamin C vary between human fibroblasts and mouse fibroblasts. While the fold-change of lamin C were only reduced by 10 % in mouse fibroblasts compared to human fibroblasts, lamin A levels were found to be reduced by approximately 40 % in mouse fibroblasts. Protein ratio analysis revealed that progerin levels were 19 % higher in mouse HGPS fibroblasts compared to human HGPS fibroblasts. Levels of lamin A were reduced in mouse HGPS fibroblasts by 25-36 % compared to human fibroblasts. Ratios of control mouse fibroblasts were found to be similar as human control fibroblasts.
In sum, mouse fibroblasts have in general a lower expression of A-type lamins. The ratios of A-type lamins in control mouse fibroblasts were similar as in human controls while the ratios of mouse HGPS fibroblasts exhibited lower lamin A and higher progerin levels.

8.4 SFN in combination with forskolin or Tem

8.4.1 SFN/Tem and SFN/forskolin have no synergistic effects on HGPS cells

In this study, SFN, Fors, and Tem were found to reduce the cellular toxicity of progerin accumulation in HGPS cells by enhancing the activity of the major protein degradation pathways. For this, it was investigated whether Fors or Tem in combination with SFN could exert a synergistic effect to further ameliorate the HGPS cellular phenotype as these drugs target different signaling pathways. Control and HGPS cells were treated either separately with Fors, Tem, and SFN or with Fors/SFN and Tem/SFN for 9 days. To investigate the effects of forskolin or Tem with SFN on the status of A-type lamins, Western blot analyses of total cellular extracts were performed (Fig. 128 A, B).

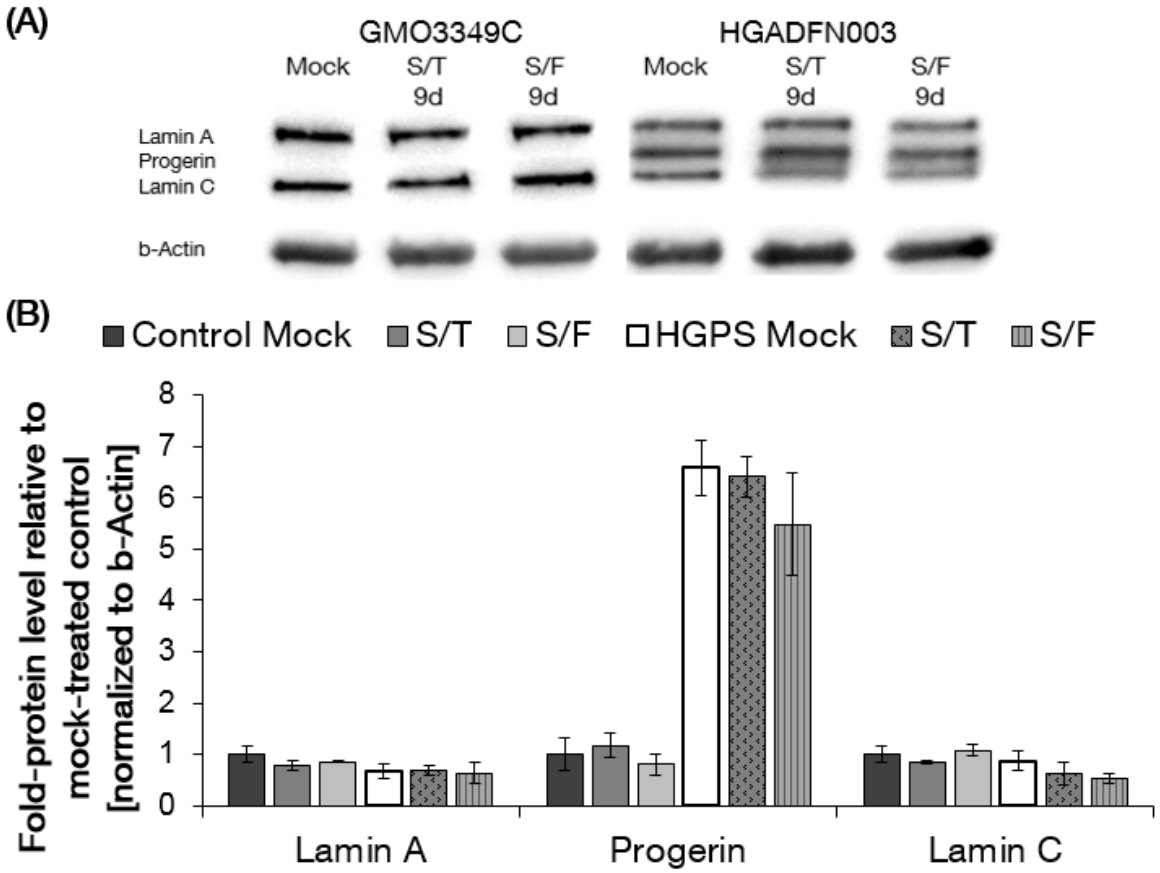

Figure 128: Western blot analyses of SFN/Tem- and SFN/Fors-treated fibroblast cultures. (A) Representative Western blot image of A-type lamins in control and HGPS cells that were mock-treated, SFN/Tem-treated or SFN/Fors-treated for 9 days (n=3). Blots were probed with lamin A/C, and b-actin antibodies. (B) Densitometric analyses of lamin A, progerin, and lamin C signals. Data represent the mean ± S.D. with respect to mock-treated control cells after values were normalized to b-actin signal (*p ≤ 0.05; n=3).

Total lamin A and lamin C levels remained unchanged after drug treatment in control and HGPS cells. Progerin levels were slightly reduced in HGPS cells treated with SFN/Fors. The combination SFN/Tem showed no amelioration of progerin levels. These data indicate that a combination of these drugs are not beneficial.

To analyze the effects of forskolin or Tem in combination with SFN on the nuclear morphology of HGPS cells, immunohistochemistry with anti-lamin A/C, anti-lamin B1, and anti-progerin were performed (Fig. 129).

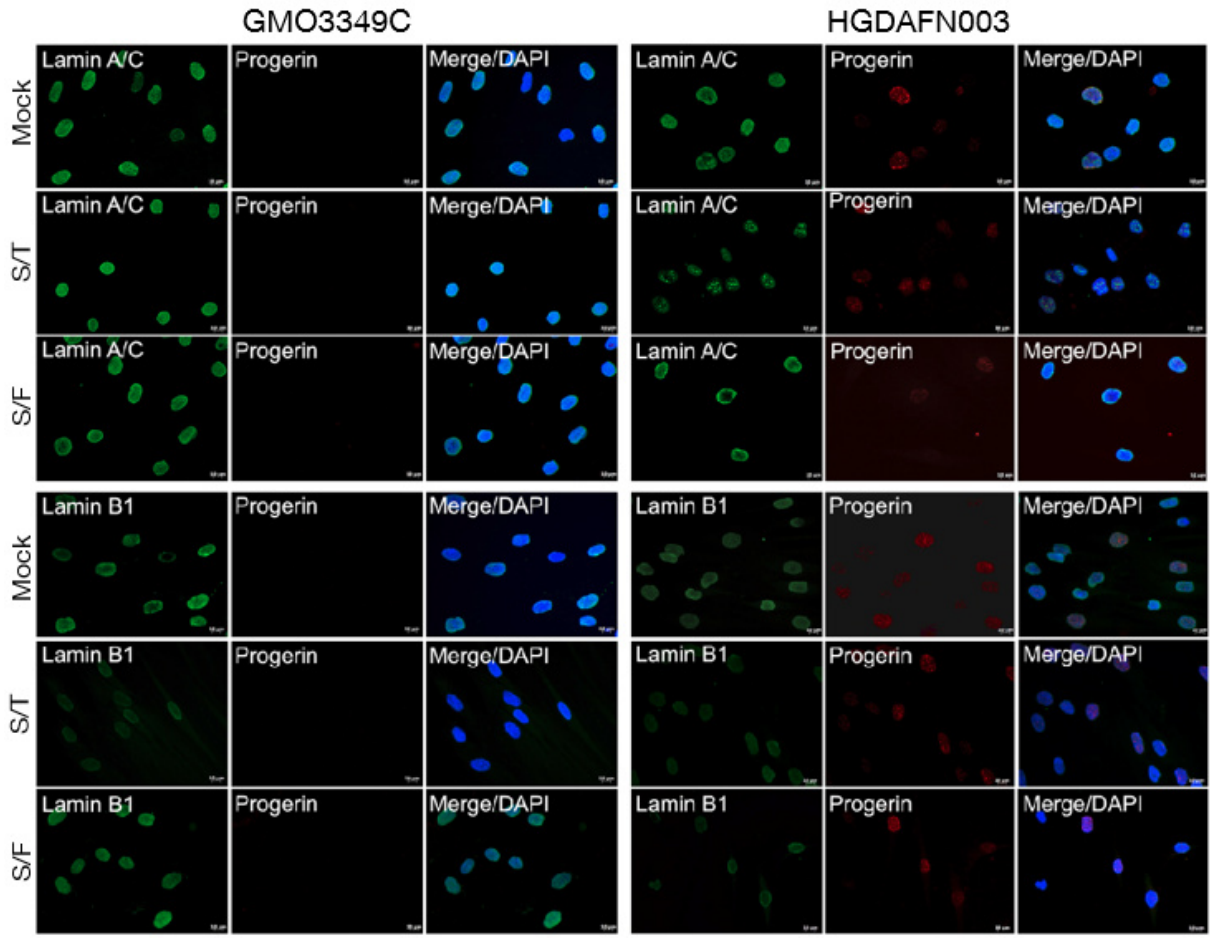

Figure 129: Immunofluorescence of the combination of Tem/SFN or Fors/SFN. Immunochemistry using antibodies directed against lamin A/C, progerin, and lamin B1 was performed on control (GMO3349C) and HGPS (HGADFN003) cells mock-treated or treated with SFN/Tem (A, S/T) or SFN/Fors (B, S/F) for 9 days (n=2). Scale bar: 10 µm.

Control and HGPS cells were treated with 2.5 µM forskolin or 1 µM Tem daily as described previously in combination with 1 µM SFN and fixed after 9 days of treatment. Forskolin or Tem with SFN did not affect the progerin localization in general. The total progerin signals and the frequencies of progerin-positive nuclei were not significantly reduced compared to mock-treated HGPS cells. Nevertheless, a combination of the compounds led to a more ovoid and regular nuclear shape of the HGPS nuclei (Fig. 130).

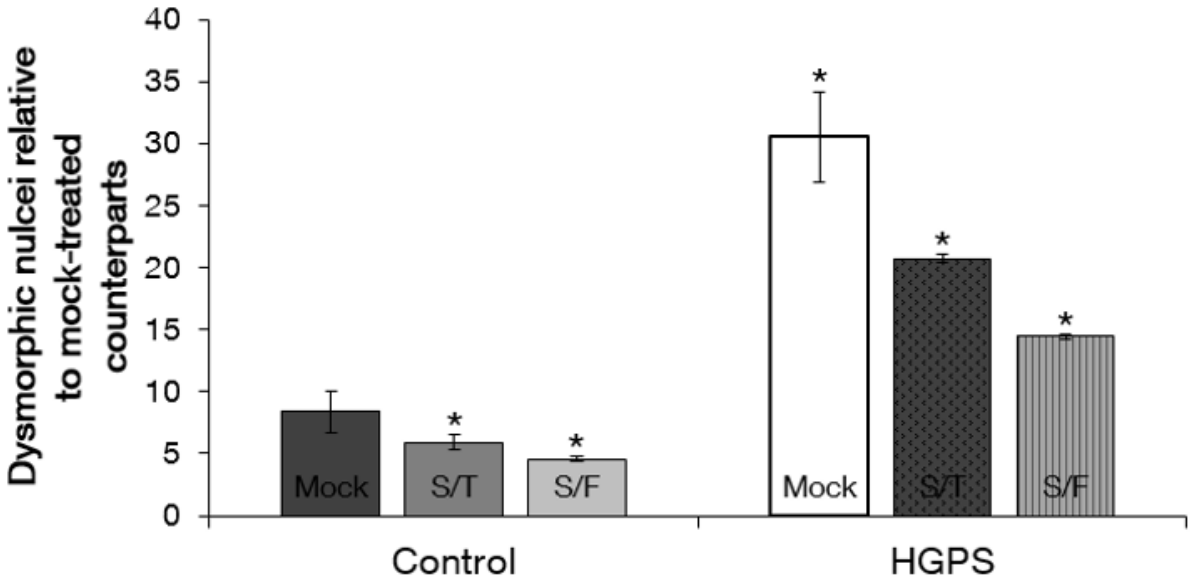

Figure 130: Dysmorphic nuclei after treatment with or without SFN/Tem or SFN/Fors. Frequency of misshapen nuclei (dysmorphic) in 3 control and 3 HGPS fibroblast lines after 4 or 9 days of treatment with either the vehicle or 1 µM SFN/1 µM Tem or 1 µM SFN/2.5 µM Fors. The bars indicate the mean frequency of misshapen nuclei. An average of 800 nuclei were examined for each control and HGPS cell lines and treatment. Data are presented as the mean ± S.D. (*p ≤ 0.05; n=3).

To further investigate the limited rescue of progerin clearance by forskolin or Tem with SFN, the proteasome activity of control and HGPS cells after 9 days treatment was determined (Fig. 131).

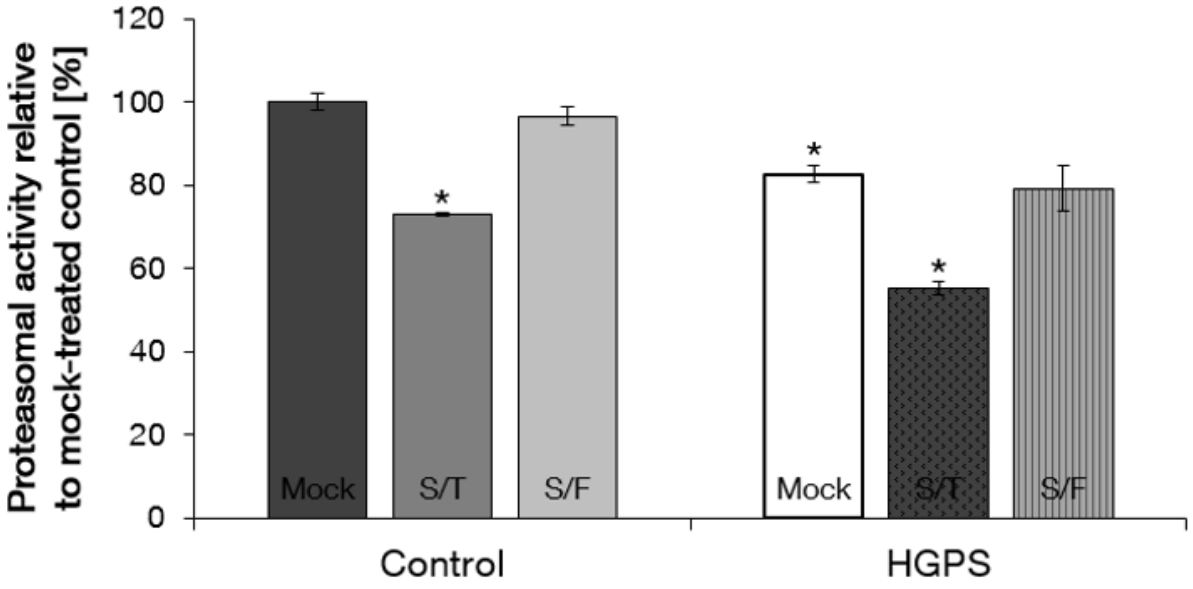

Figure 131: Proteasomal activity of cultures after 9 days of SFN/Tem or SFN/Fors treatment. Proteasome activity was determined by measuring chymotrypsin-like proteasome activity in control (GMO3349C, GMO1582B, GMO1651C, and GMO8398A) and HGPS (HGADFN127, HGADFN003, HGADFN164, and HGADFN155) fibroblasts using Suc-LLVY-AMC as a substrate. Cells were either mock-treated or treated daily with S/T or S/F for a period of 9 days. The percentage of activity was calculated relative to the mock-treated cells. Data are expressed as the mean ± S.D. (*$p \leq 0.05$; n=4).

In accordance to Figure 80, Temsirolimus without or with SFN induced a significant decrease in the proteasomal activity in control and HGPS cells. On contrary to Forskolin and SFN single treatment (Fig. 18, 57), forskolin with SFN had no beneficial effect on the proteasomal activity. Moreover, the positive effect of the drug combinations on autophagy was not superior to treatment with either drug alone (Fig. 132).

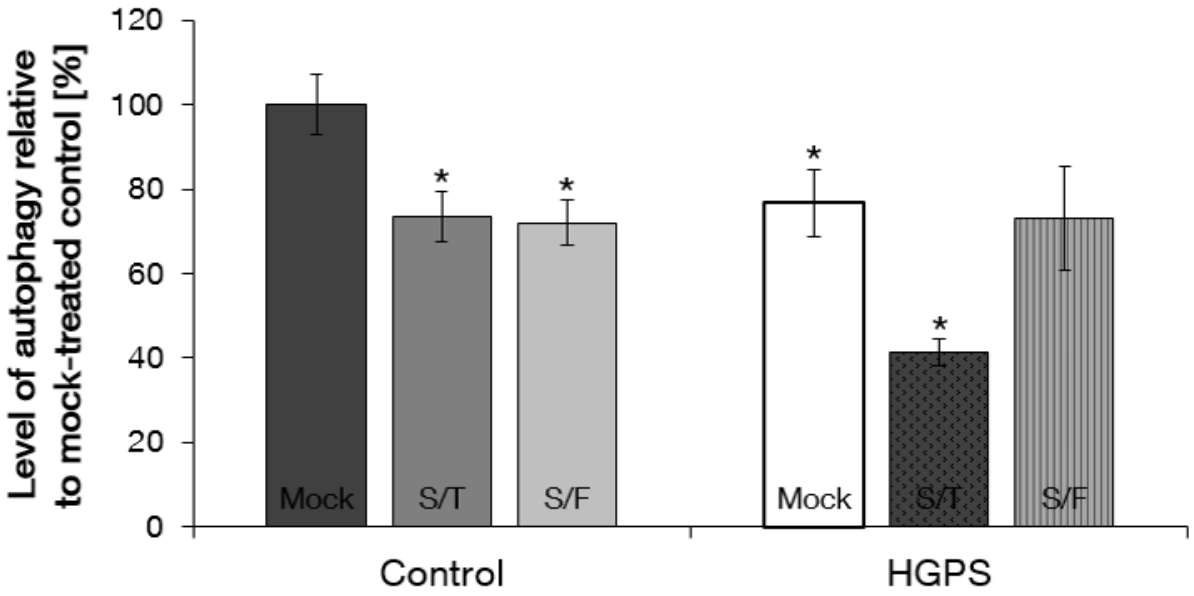

Figure 132: Autophagy levels after 3 and 9 days of SFN/Tem or SFN/Fors treatment. Autophagy was determined in control and HGPS fibroblasts by measuring monodansylcadaverine (MDC) levels with fluorescence photometry. Cells were either mock-treated or treated daily with S/T (SFN/Tem) or S/F (SFN/Fors) for a period of 9 days. The percentage of activity was calculated relative to the mock-treated cells. Data are expressed as the mean ± S.D. (*p ≤ 0.05; n=4).

To dissect why the drug combinations were not synergistically beneficial to control and HGPS cells, the growth properties of the cells after treatment with Forskolin or Tem with SFN were investigated. While forskolin, Tem, and SFN single treatment improved the growth rate of control and HGPS cells, the combination of SFN with forskolin or Tem induced a decrease in the growth potency of control and HGPS cells after 9 days (Fig. 133).

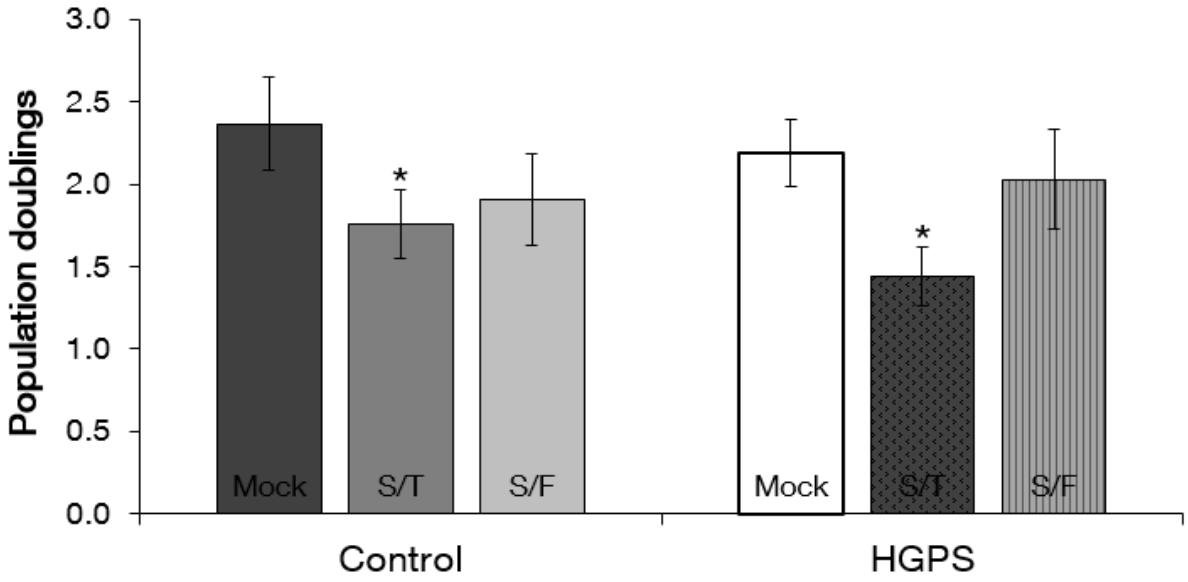

Figure 133: Cell proliferation of cells treated with and without SFN/Tem or SFN/Fors. Population doubling levels were calculated as stated in the Materials and Methods for control and HGPS cells that were mock-treated (vehicle DMSO) or treated daily with 1.0 µM Tem/1 µM SFN or 2.5 µM Fors/1 µM SFN for a period of 9 days. Data are expressed as the mean ± S.D. relative to mock-treated counterparts (*p ≤ 0.05; n=3).

Treatment with a combination of the drugs resulted in a reduction of cell growth in both cell types.

Collectively, these findings indicate that a combination of the drugs with the tested concentrations have no beneficial effect for HGPS cells. Hence, by applying a combination of the drugs the concentrations at which they have a synergistic effect have to be determined. For this, the concentration of single drug treatments at which autophagy levels are still increased were tested. Forskolin were chosen for further investigation with SFN as Fors activating both proteasome and autophagy. In contrast, Tem enhances Autophagy levels but decreases proteasome level to an extent that is lower as mock-treated cells.

8.4.2 Forskolin in combination with SFN at lower concentrations

To further asses a working concentration for the combination of forskolin (Fors) with SFN, different concentrations of these two drugs were tested. Forskolin and SFN were applied as a single treatment for three days in order to assess high levels of autophagy (Fig. 134 A, B).

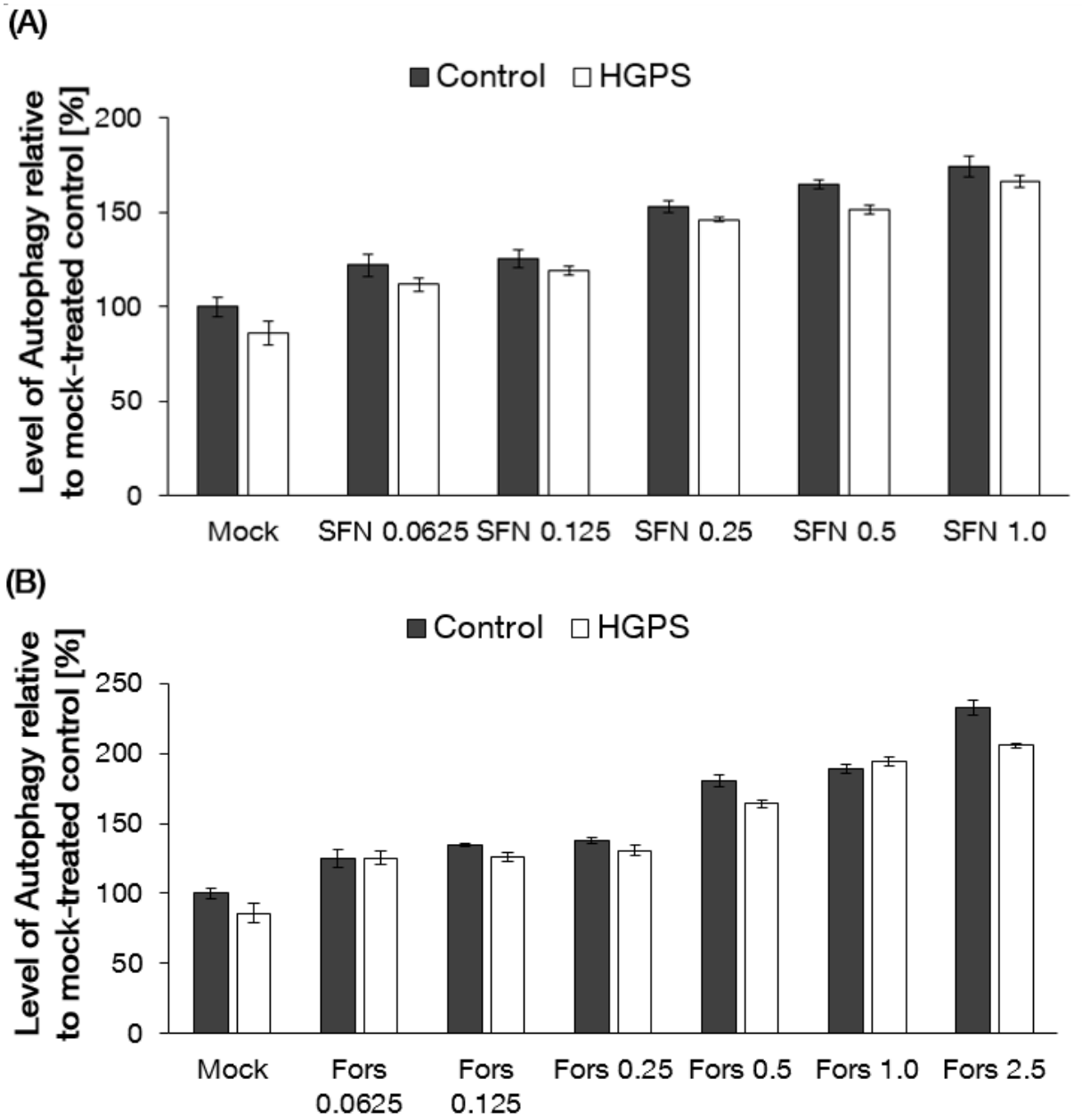

Figure 134: Autophagy levels of different SFN and forskolin concentrations. Autophagy was determined in control and HGPS fibroblasts by measuring monodansylcadaverine (MDC) levels with fluorescence photometry. Cells were either mock-treated or treated daily with different concentrations of SFN (A) and forskolin (B) for 3 days. The percentage of activity was calculated relative to the mock-treated control. Data are expressed as the mean ± S.D. (*p ≤ 0.05; n=4).

Control and HGPS cells show a significant increase of autophagy levels even a concentration of 0.0625 µM SFN. However, autophagy levels were more boosted at a concentration of 0.25 µM SFN. The highest levels if autophagy were reached at 1.0 µM SFN. The same effect was found for forskolin. Autophagy levels were significantly increased at very low concentrations of forskolin and were boosted more at 0.5 µM Forskolin. The highest levels of autophagy were reached after 2.5 µM forskolin treatment.

All tested combination of forskolin and SFN led either to cell death or showed no amelioration when compared to single treatments. For this, the data is only presented in the following without any further comment.

Control and HGPS fibroblasts were treated with 0.25 µM SFN, 0.5 µM forskolin or a combination of both. After 9 days of treatment proliferation rate, autophagy levels, proteasome activity, and the status of the A-type lamins was investigated (Fig. 135 A-D).

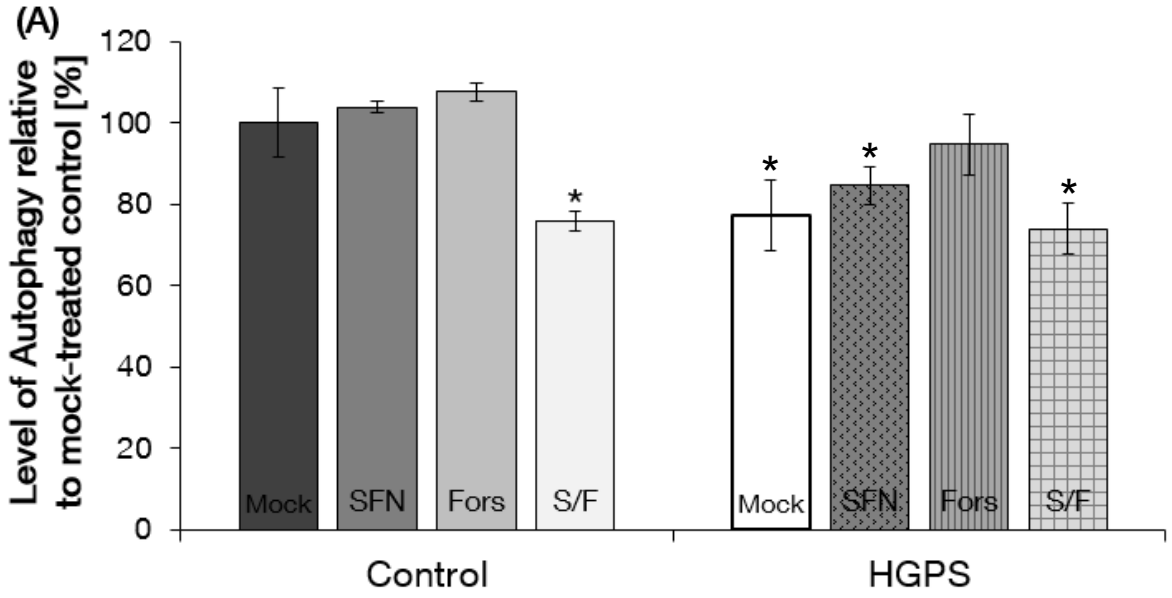

(B)

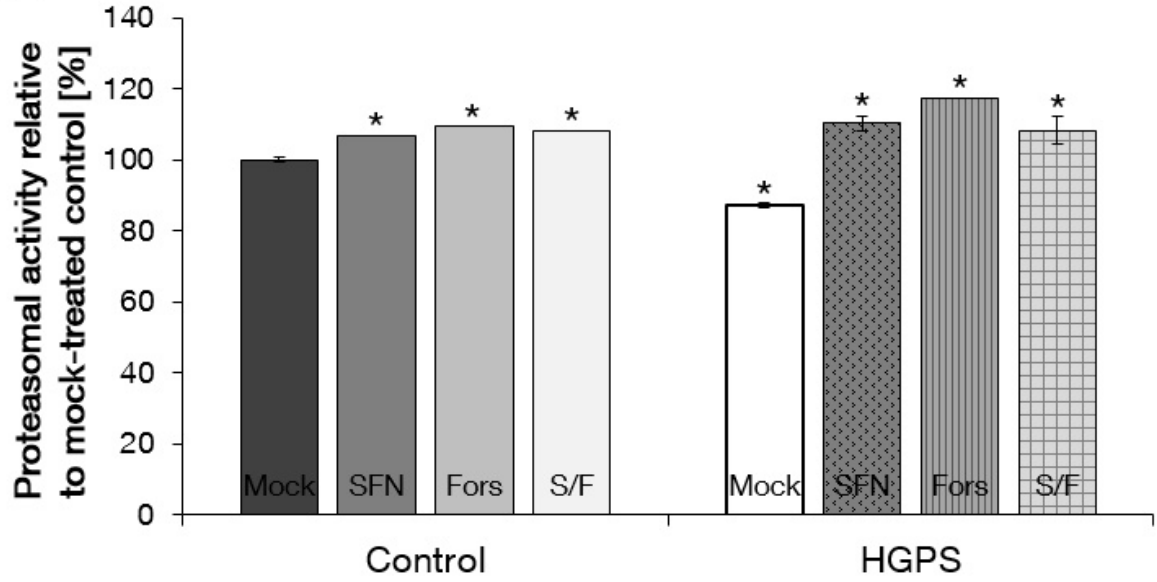
Proteasomal activity relative to mock-treated control [%]
140
120
100
80
60
40
20
0
Mock
SFN
Fors
S/F
Mock
SFN
Fors
S/F
Control
HGPS

(C)

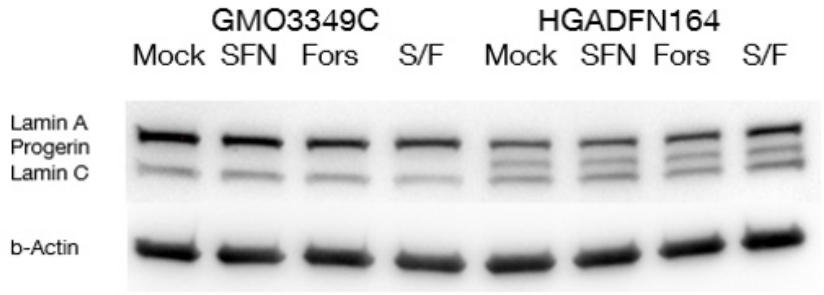
GMO3349C
HGADFN164
Mock SFN Fors S/F Mock SFN Fors S/F
Lamin A
Progerin
Lamin C
b-Actin

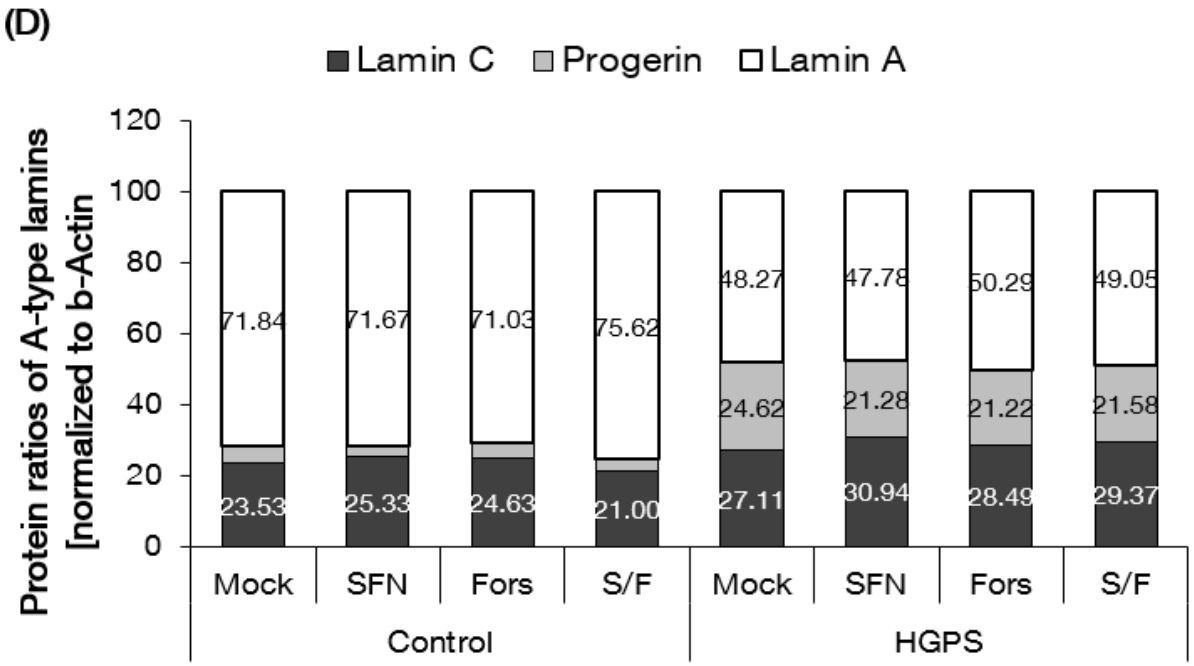

Figure 135: Analysis of the combination of 0.25 µM SFN and 0.5 µM forskolin. (A) Population doubling levels were calculated as stated in the Materials and Methods for control and HGPS cells that were mock-treated (vehicle DMSO) or treated daily with 0.5 µM Fors and 0.25 µM SFN for a period of 9 days. Single treatments were carried along. Data are expressed as the mean ± S.D. (*p ≤ 0.05; n=3). (B) Same cells as in (A) were used to measure autophagy activity. The percentage of activity was calculated relative to the mock-treated control. Data are expressed as the mean ± S.D. (*p ≤ 0.05; n=4). (C) Proteasome activity was determined by measuring chymotrypsin-like proteasome activity of the same cells as in (A using Suc-LLVY-AMC as a substrate. The percentage of activity was calculated relative to the mock-treated cells. Data are presented as the mean ± S.D. (*p ≤ 0.05; n=4). (D) Representative Western blot image of A-type lamins in control and HGPS cells treated as in (A). Blots were probed with lamin A/C, and b-actin antibodies (n=3). (B) Densitometric analyses of lamin A, progerin, and lamin C signals. Data represent the mean ± S.D. with respect to mock-treated control cells after values were normalized to b-actin signal (*p ≤ 0.05; n=3).

As the combination showed no amelioration of the cellular phenotype of HGPS, the concentration of forskolin was raised as it exhibit less cytotoxicity as SFN.

Control and HGPS fibroblasts were treated with 0.25 µM SFN, 1 µM forskolin or a combination of both. After 9 days of treatment proliferation rate, autophagy levels, and the status of the A-type lamins was investigated (Fig. 136 A-D).

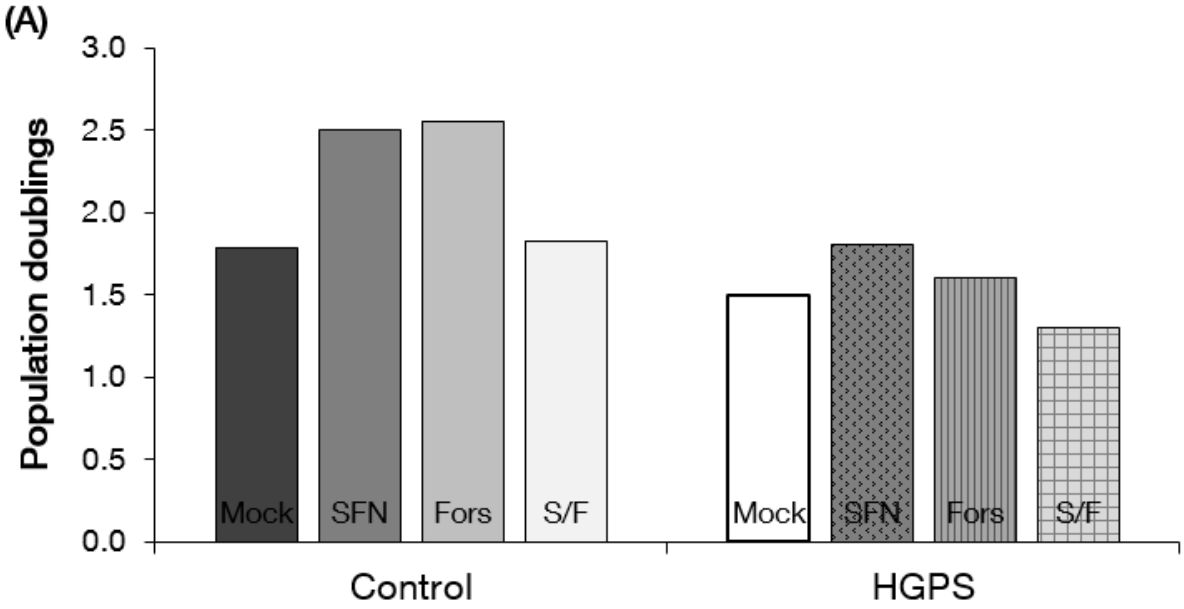
(A)
Population doublings
3.0
2.5
2.0
1.5
1.0
0.5
0.0
Mock
SFN
Fors
S/F
Mock
SFN
Fors
S/F
Control
HGPS

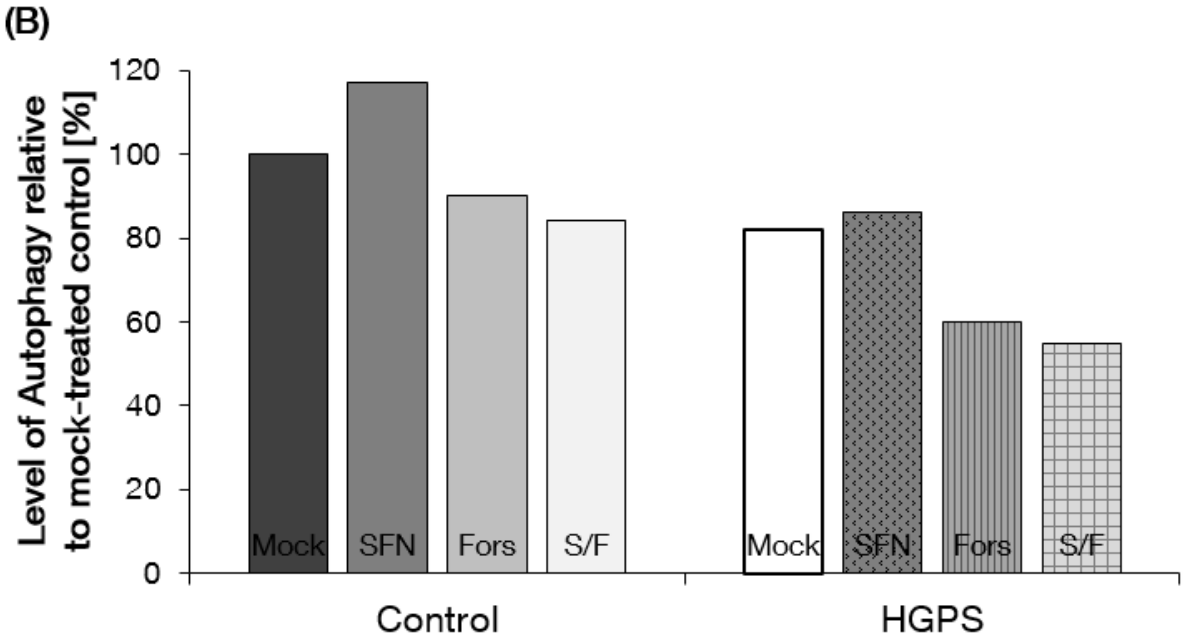
(B)
Level of Autophagy relative to mock-treated control [%]
120
100
80
60
40
20
0
Mock
SFN
Fors
S/F
Mock
SFN
Fors
S/F
Control
HGPS

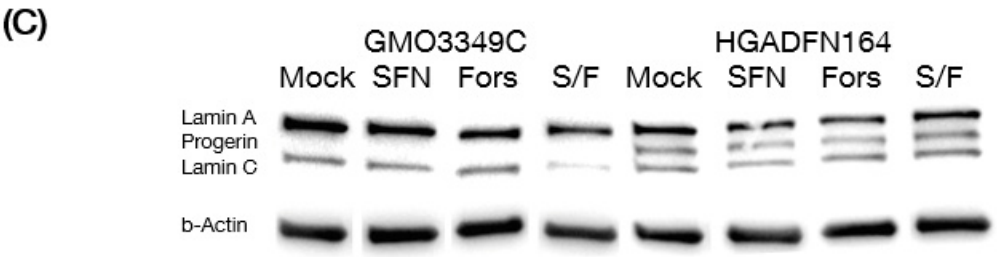
(C)
GMO3349C
HGADFN164
Mock
SFN
Fors
S/F
Mock
SFN
Fors
S/F
Lamin A
Progerin
Lamin C
b-Actin

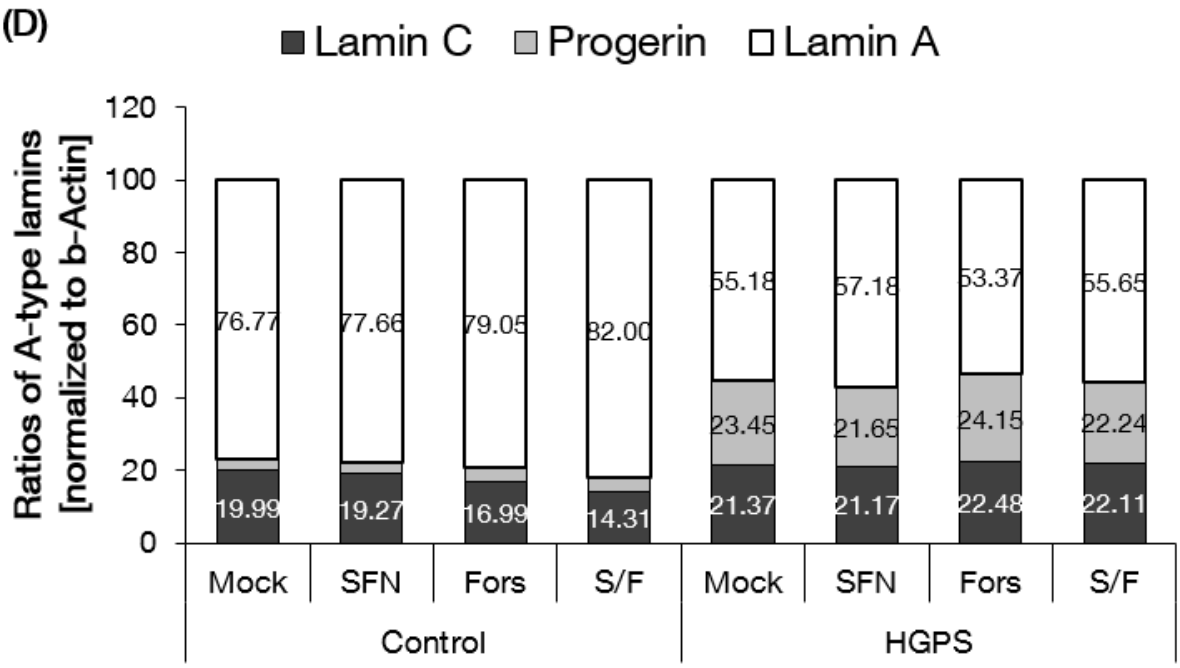

Figure 136: Analysis of the combination of 0.25 µM SFN and 1 µM forskolin. (A) Population doubling levels were calculated as stated in the Materials and Methods for control and HGPS cells that were mock-treated (vehicle DMSO) or treated daily with 1 µM Fors and 0.25 µM SFN for a period of 9 days. Single treatment were carried along. Data are expressed as the mean ± S.D. (*p ≤ 0.05; n=2). (B) Same cells as in (A) were used to measure autophagy activity. The percentage of activity was calculated relative to the mock-treated control. Data are expressed as the mean ± S.D. (*p ≤ 0.05; n=2). (C) Representative Western blot image of A-type lamins in control and HGPS cells treated as in (A) (n=2). Blots were probed with lamin A/C, and b-actin antibodies. (D) Densitometric analyses of lamin A, progerin, and lamin C signals. Data represent the mean ± S.D. with respect to mock-treated control cells after values were normalized to b-actin signal (*p ≤ 0.05; n=2).

The combination of 0.25 µM SFN and 1 µM forskolin showed no increased progerin clearance compared to the single treatments. Furthermore, this combination induced cell death in control and HGPS cells.

Another combination that was testes were 0.25 µM SFN and 1.5 µM forskolin. Population doublings, autophagy, and the ratios of the A-type lamins were analyzed and compared to the mock-treated cells and single treatments (Fig. 137 A-D).

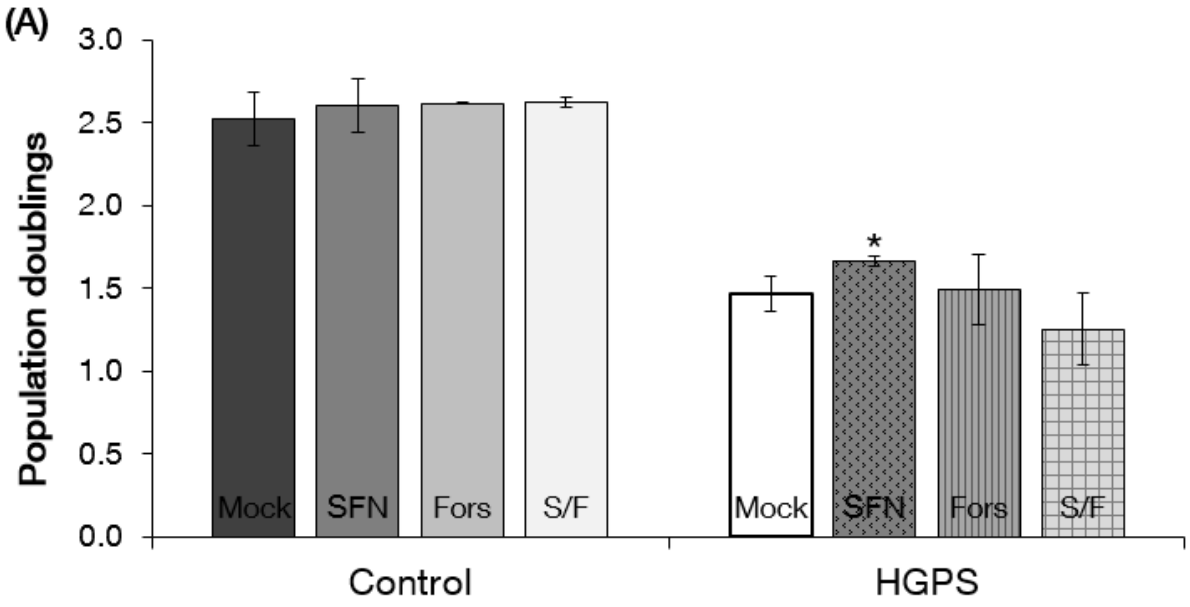
(A)
Population doublings
3.0
2.5
2.0
1.5
1.0
0.5
0.0
Mock
SFN
Fors
S/F
Mock
SFN
Fors
S/F
*
Control
HGPS

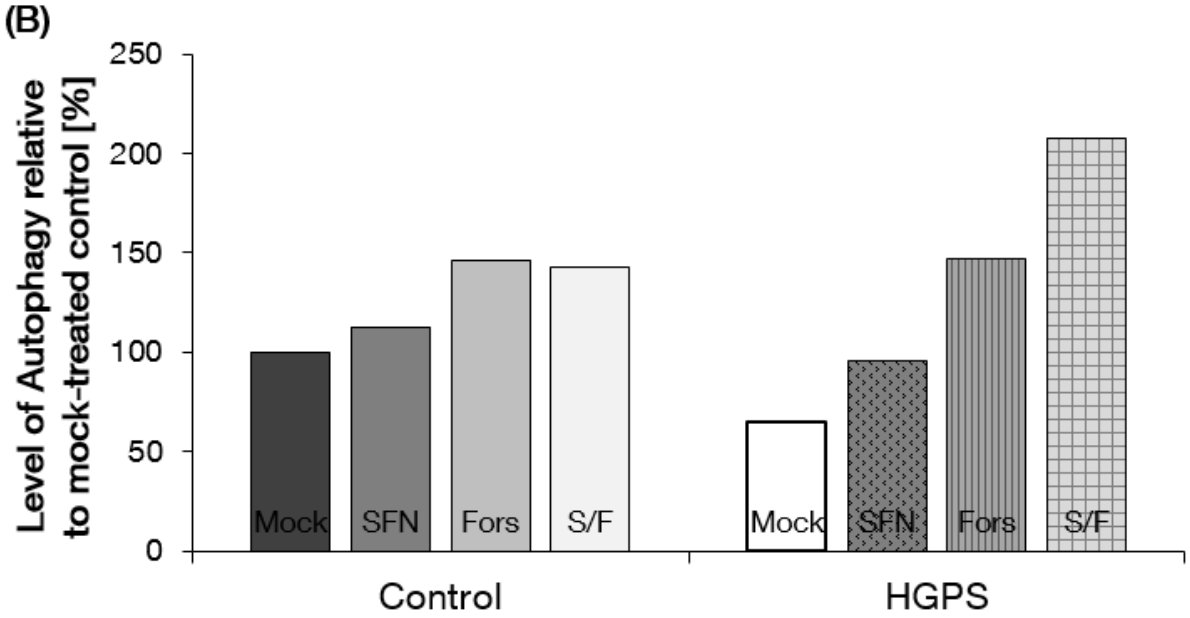
(B)
Level of Autophagy relative to mock-treated control [%]
250
200
150
100
50
0
Mock
SFN
Fors
S/F
Mock
SFN
Fors
S/F
Control
HGPS


(C)
GMO3349C
HGADFN003
Mock
SFN
Fors
S/F
Mock
SFN
Fors
S/F
Lamin A
Progerin
Lamin C
b-Actin

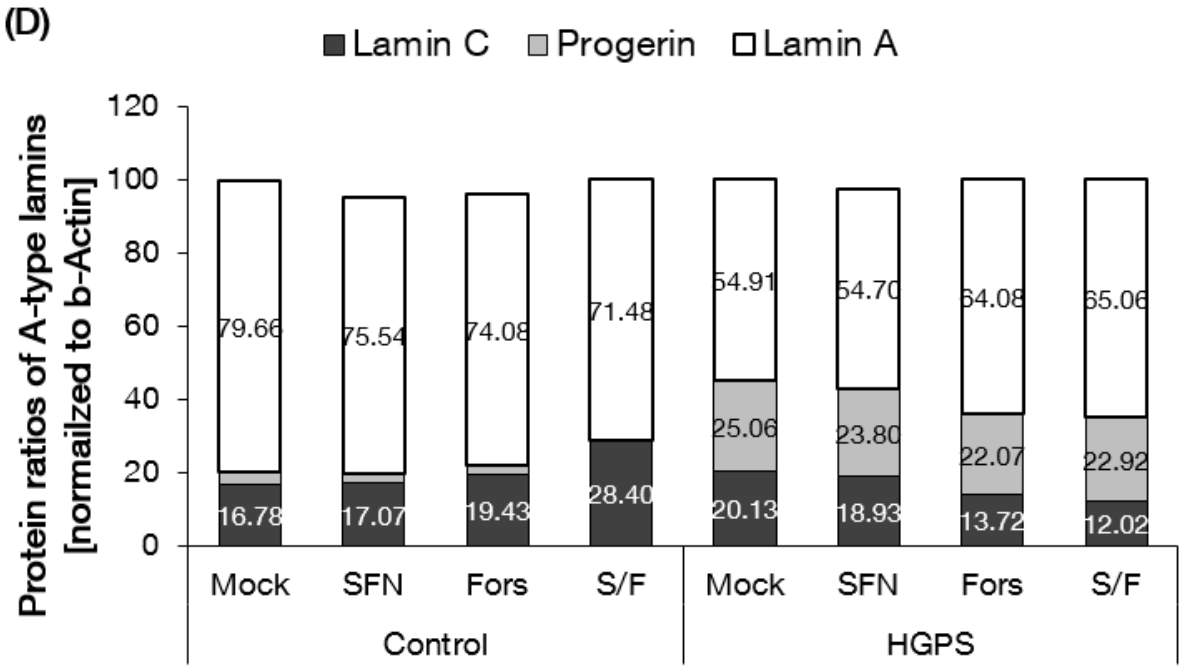

Figure 137: Analysis of the combination of 0.25 µM SFN and 1.5 µM forskolin. (A) Population doubling levels were calculated as stated in the Materials and Methods for control and HGPS cells that were mock-treated (vehicle DMSO) or treated daily with 1 µM Fors and 0.25 µM SFN for a period of 9 days. Single treatment were carried along. Data are expressed as the mean ± S.D. relative to mock-treated counterparts (*p ≤ 0.05; n=2). (B) Same cells as in (A) were used to measure autophagy activity. The percentage of activity was calculated relative to the mock-treated control. Data are expressed as the mean ± S.D. (*p ≤ 0.05; n=2). (C) Representative Western blot image of A-type lamins in control and HGPS cells treated as in (A) (n=2). Blots were probed with lamin A/C, and b-actin antibodies. (D) Densitometric analyses of lamin A, progerin, and lamin C signals. Data represent the mean ± S.D. with respect to mock-treated control cells after values were normalized to b-actin signal (*p ≤ 0.05; n=2).

The combination of 0.25 µM SFN and 1.5 µM forskolin showed no increased progerin clearance compared to the single treatments. The combination enhances autophagy levels over the emending limit. Excessive autophagy levels lead to increased cell death, which probably explains the minor cell growth within the treatment.